

Probing the Role of Sulfenylation in Redox Regulation of Protein Kinases

by

Thu H. Truong

A dissertation submitted in partial fulfillment
of the requirements for the degree of
Doctor of Philosophy
(Chemistry)
in The University of Michigan
2014

Doctoral Committee:

Associate Professor Kate S. Carroll, co-Chair
Professor Anna K. Mapp, co-Chair
Professor Ursula Jakob
Professor David H. Sherman

© Thu H. Truong 2014

All Rights Reserved

For everyone who believed in me.

ACKNOWLEDGEMENTS

I would like to thank my mentor, Dr. Kate S. Carroll, for her support and guidance throughout the course of my graduate career. I am eternally grateful to Kate for taking a chance with me, allowing me to join her lab, and for the countless opportunities over the years. Several years ago when I was mulling over my decision on which graduate school to attend, I knew that I wanted to work on post-translational modifications. Ironically, I had never heard of cysteine oxidation prior to meeting Kate. After our first meeting, she completely sold me on the topic and I immediately knew I had made my decision on what school to attend, and more importantly, who I wanted to work for. Thank you Kate, for introducing me to the wonderful world of redox and opening the doors of science to me. I have benefited immensely from my experience as a "cysteine hunter" in the Carroll lab, and look forward to what comes next.

I would like to thank my committee members Drs. Ursula Jakob, Anna Mapp, and David Sherman for serving on my committee over the years. I am grateful for their valuable feedback and suggestions to improve my research.

I would like to acknowledge and thank all past and present members of the Carroll lab. They have served as an invaluable source over the years to help move my research forward. I would especially like to thank Devayani Bhave, Jiyong Hong, Francisco Garcia, Stephen Leonard, and Candice Paulsen for sharing the experience of being a Carroll lab graduate student with me. Moving across the country in the middle of graduate school was an exciting adventure, and I was fortunate enough to share

this experience with them. I would especially like to thank Candie, who started as my rotation mentor, for working on many projects with me and for making me laugh uncontrollably during experiments. I would also like to thank Pablo Martinez-Acedo for showing me the exciting world of mass spectrometry, and for always giving me a shoulder to lean on.

I would like to thank my friends Heather Rust and Karoline Chiou for everything they have done for me. Heather and I shared some crazy times together in our last years of graduate school, and I always enjoyed bouncing my ideas off her. Karoline was there for me during one of my darkest and difficult times, and I am forever grateful to her for this.

I would like to thank my high school chemistry teacher, Trevor Wildman. He was the one who initially sparked my interest in science and encouraged me to continue my studies in college. I would like to thank my undergraduate research advisor, Dr. Christian Hilty, for giving me my first taste of research. Finally, I would like to thank my undergraduate mentor, Dr. Patricio Santander. He continuously renewed my love for science and taught me that the answers we seek are not always apparent.

I am forever indebted to the late Howard and Nancy Terry for their generous contributions to my college education. I am lucky to call myself a member of the Terry Foundation family.

I would like to thank my parents, Ty and Lan, for their unconditional love and support. I am fortunate to have such selfless parents and am grateful to them for the sacrifices they have made so their children could have a better life. They also gave me the gift of a sister, Kim, who has shared all my ups and downs.

Finally, I would like to thank my partner Jerome who has introduced me to the world of Doctor Who, TexAgs, and college football. There are some days when I feel like I love college football more than J, but I think this is something he is okay with. Most importantly, Jerome served as my inspiration to finish graduate school.

Watching him fight back after his accident to live, learn how to walk again, and come back to finish his degree was the most inspiring thing I have ever witnessed. He motivates me every day and is always, without a doubt, standing right next to me.

PREFACE

This thesis is the compilation of published and unpublished work on probing the role of sulfenylation in redox regulation of protein kinases. Hydrogen peroxide (H_2O_2) functions as a secondary messenger to regulate signal transduction networks, largely through modification of specific cysteine residues in redox-sensitive target proteins. Cysteine sulfenic acid (sulfenylation) is a reversible modification and is the direct product of the reaction between H_2O_2 and a protein thiolate. Sulfenylation has emerged as a central mechanism utilized by proteins to detect changes in the cellular redox balance, and is also correlated with disease states associated with chronic H_2O_2 levels.

In Chapter 1, we present a historical overview of EGFR and signal-mediated production of H_2O_2 as well as the molecular mechanisms involved in redox regulation of this pathway. We begin by highlighting studies linking EGFR activation to endogenous H_2O_2 production and examine the effects of redox modulation on downstream signaling pathways. Finally, we discuss recent examples that identify direct oxidation of EGFR and how these discoveries form the basis for understanding redox-based kinase signaling and development of therapeutic strategies. This work has been published as a review: Truong, T. H. and Carroll, K. S. (2012). "Redox Regulation of Epidermal Growth Factor Receptor Signaling through Cysteine Oxidation." *Biochemistry*. 51 (50), 9954-9965.

In Chapter 2, we present the development and application of an approach that allows relative quantification of sulfenic acids using a pair of light and heavy isotope

labeled probes (DAz-2 and d6-DAz-2) in conjunction with a complementary acid-cleavable linker (Yn-ACL). This method can be used to directly map sites of cysteine oxidation and compare sulfenylation levels in normal and disease states. This work has been published as: Truong, T. H., Garcia, F. J., Seo, Y. H. and Carroll, K. S. (2011). "Isotope-coded chemical reporter and acid-cleavable affinity reagents for monitoring protein sulfenic acids." *Bioorg. Med. Chem. Lett.* 21 (17), 5015-5020.

In Chapter 3, we report the development and application of a new alkyne-based probe (DYn-2) for detection of sulfenic acids. These studies demonstrate EGF-mediated signaling induces endogenous H₂O₂ production and dynamic changes in global protein sulfenylation in A431 cells. Three protein tyrosine phosphatases (SHP2, PTEN, and PTP1B) were observed to undergo ligand-dependent oxidation and exhibit a unique sulfenylation profile in situ. In addition, EGFR was identified as a direct target of signal-derived H₂O₂ at its active site cysteine (Cys797), which enhances its inherent kinase activity. This work has been published as: Paulsen, C. E., Truong, T. H., Garcia, F. J., Homann, A., Gupta V., Leonard, S. E., Carroll, K. S. (2011). "Peroxide-dependent sulfenylation of the EGFR catalytic site enhances kinase activity." *Nat. Chem. Biol.* 8 (1), 57-64.

In Chapter 4, we perform molecular characterization of EGFR sulfenylation to delineate the role of Cys797 and determine its effect on receptor activity. Mutation of this residue abrogates kinase activation, sulfenylation, and decreases its affinity for ATP. Moreover, oxidation affects the propensity of Cys797 to undergo sulfenylation in oncogenic EGFR mutants and affects the potency of inhibitors that target this residue in its reduced thiolate form. Additionally, we explore the possibility that other kinases harboring a structurally homologous cysteine to Cys797 may be subjected to redox-based regulation through this residue. This work is currently in preparation for publication.

In Chapter 5, we report the development of a panel of first-generation nucleophilic

RSOH-targeted inhibitors and evaluate compound potency and selectivity towards Cys797 in response to concomitant EGFR oxidation. We demonstrate our nucleophilic compounds are capable of potent inhibition towards EGFR under oxidizing conditions and occur through partial irreversible mechanisms. Our work provides proof of principle and indicates that the propensity of EGFR Cys797 to undergo sulfenylation can be exploited to develop new classes of inhibitors. This work is current in preparation for publication.

Chapter 6 is a discussion of future directions for the continued study of the molecular mechanisms underlying redox-based regulation of protein kinases and the development of redox-based nucleophilic inhibitors towards EGFR.

Appendix 1 is a collection of protocols that presents a series of methods utilizing the application of sulfenic acid probes for in vitro and in situ detection of sulfenyl modifications. This work has been published as: Truong, T. H. and Carroll, K. S. (2012). "Bioorthogonal Chemical Reporters for Analyzing Protein Sulfenylation in Cells." *Curr. Protoc. Chem. Biol.* 4, 101-122.

Appendix 2 is a comprehensive discussion of the molecular mechanisms involved in redox regulation of protein kinases and downstream signaling pathways. This work has been published as a review: Truong, T. H. and Carroll, K. S. (2013). "Redox Regulation of Protein Kinases." *Crit. Rev. Biochem. Mol. Biol.* 48 (4), 332-356.

TABLE OF CONTENTS

DEDICATION	ii
ACKNOWLEDGEMENTS	iii
PREFACE	vi
LIST OF FIGURES	xiii
LIST OF TABLES	xix
LIST OF SCHEMES	xx
LIST OF APPENDICES	xxi
ABSTRACT	xxii

CHAPTER

I. Redox Regulation of Epidermal Growth Factor Receptor Signaling Through Cysteine Oxidation	1
1.1 Abstract	1
1.2 Redox Regulation of EGFR Signaling Through Cysteine Oxidation	2

1.3	Early Evidence for EGF-Mediated H ₂ O ₂ Production and Redox Regulation of EGFR Signaling	6
1.4	Effect of H ₂ O ₂ on Signaling Networks Downstream of EGFR	8
1.5	Interplay of Reversible Tyrosine Phosphorylation and Redox-Dependent Signaling	10
1.6	Generation and Metabolism of H ₂ O ₂ During EGFR Signaling	13
1.7	Regulation of Intrinsic EGFR Tyrosine Kinase Activity Through Cysteine Oxidation	18
1.8	Future Perspectives	22
1.9	Conclusions	25
1.10	Chapter References	26

II. Isotope-Coded Chemical Reporter and Acid-Cleavable Affinity Reagents for Monitoring Protein Sulfenic Acids 37

2.1	Abstract	37
2.2	Introduction	37
2.3	Results and Discussion	40
2.4	Conclusions	50
2.5	Contributions	50
2.6	Supplementary Methods	50
2.7	Supplementary Figures	59
2.8	Supplementary Tables	64
2.9	Chapter References	66

III. Peroxide-dependent sulfenylation of the EGFR catalytic site enhances kinase activity 69

3.1	Abstract	69
3.2	Introduction	70
3.3	Results	71
3.4	Discussion	82
3.5	Methods	87
3.6	Contributions	90
3.7	Supplementary Methods	90
3.8	Supplementary Figures	100
3.9	Chapter References	111

IV. Characterizing the Role of Cys797 in Redox-Based Regulation of EGFR 116

4.1	Abstract	116
4.2	Introduction	117
4.3	Results	122
4.4	Discussion	139
4.5	Conclusion	142
4.6	Methods	142
4.7	Contributions	152
4.8	Supplemental Figures	153
4.9	Chapter References	162

V. Development and Characterization of Nucleophilic RSOH-Targeted Inhibitors Towards EGFR Cys797 168

5.1	Abstract	168
5.2	Introduction	169
5.3	Results	175
5.4	Discussion	191
5.5	Conclusion	194
5.6	Methods	194
5.7	Contributions	197
5.8	Supplementary Figures	198
5.9	Supplementary Tables	201
5.10	Chapter References	205
 VI. Conclusions		210
6.1	Abstract	210
6.2	Summary	210
6.3	Future Directions	212
6.4	Concluding Remarks	216
6.5	Chapter References	217
 APPENDICES		219

LIST OF FIGURES

1.1	EGFR Timeline	4
1.2	Oxidative modification of cysteine residues by hydrogen peroxide (H ₂ O ₂).	5
1.3	EGFR signaling pathways and general mechanisms for thiol-based redox modulation of signaling proteins.	9
1.4	Redox regulation of peroxiredoxins (Prxs) during EGFR signaling. .	17
1.5	General strategy for detecting protein cysteine sulfenylation (RSOH) in cells	19
1.6	Model for H ₂ O ₂ -dependent regulation of EGFR tyrosine kinase activity	21
1.7	Covalent cysteine-based protein targeting strategies	24
2.1	General strategy for labeling and enrichment of sulfenic acid-modified proteins and peptides	39
2.2	Sulfenic acid modification is detected in model protein C64S C82S Gpx3 using DAz-2 and Yn-ACL	43
2.3	Enrichment and ESI-LC/MS/MS analysis of sulfenic acid-modified C*GFTPQYK peptide from Gpx3 using avidin affinity cartridges . .	45
2.4	Enrichment and ESI-LC/MS/MS analysis of sulfenic acid-modified C*GFTPQYK peptide from Gpx3 using streptavidin-coated mag- netic beads	47

2.5	Relative quantification of Gpx3 sulfenic acid modification	49
2.S1	Sequence coverage obtained from C64S C82S Gpx3 trypsin digestion	59
2.S2	ESI-LC/MS/MS analysis of avidin affinity cartridge enrichment . .	60
2.S3	Comparison of streptavidin-coated magnetic bead elution conditions	61
2.S4	ESI-LC/MS/MS analysis of streptavidin-coated magnetic bead enrichment	62
2.S5	ESI-LC/MS/MS analysis of enriched intact sulfenic acid-modified C*GFTPQYK peptides from ratiometric quantification studies . . .	63
3.1	Cellular redox status affects EGF-mediated signaling.	72
3.2	Development and validation of probes for detecting sulfenic acid. . .	75
3.3	Profiling EGF-mediated ROS production and protein sulfenylation.	77
3.4	Differential sulfenylation of PTPs in EGF-treated cells.	79
3.5	EGF-mediated sulfenylation of EGFR Cys797 in cells.	80
3.6	Model for redox regulation of EGFR signaling.	84
3.S1	EGF-dependent morphological changes in A431 cells.	100
3.S2	Uncut full Western blots	101
3.S3	Effect of inhibitors, antioxidants, and sulfenic acid probes on EGF-mediated signaling.	103
3.S4	DYn-2 detection of Gpx3 sulfenic acid by Western blot and mass spectrometric analysis.	104
3.S5	DYn-2 labeling of protein sulfenic acids in A431 cells.	105
3.S6	DYn-2 treatment of A431 cells does not trigger cell death or oxidative stress.	106
3.S7	EGF-mediated sulfenylation requires EGFR activity and is modulated by cellular redox status in A431 cells.	107
3.S8	Secondary antibody only control in A431 cells.	108

3.S9	Nox2 expression, H ₂ O ₂ -mediated Cys797 oxidation and modulation of recombinant EGFR tyrosine kinase activity.	109
3.S10	Indirect and direct chemical techniques to monitor cysteine oxidation and PTP oxidation/trapping scheme.	110
4.1	Signal-derived H ₂ O ₂ directly targets EGFR and enhances its tyrosine kinase activity upon oxidation	119
4.2	Mutation of Cys797 decreases EGFR tyrosine kinase activity	124
4.3	EGF and H ₂ O ₂ treatment induces autophosphorylation of WT EGFR isolated from immunoprecipitates	125
4.4	EGF-mediated activation of EGFR is affected in C797 mutants <i>in situ</i>	128
4.5	H ₂ O ₂ -mediated activation of EGFR is affected in C797 mutants <i>in situ</i>	128
4.6	H ₂ O ₂ -mediated sulfenylation is decreased in EGFR Cys797 mutants <i>in situ</i>	130
4.7	EGF mediates sulfenylation of EGFR in common oncogenic mutations	131
4.8	EGF mediates sulfenylation ErbB2 in breast cancer cells	132
4.9	Chronic H ₂ O ₂ treatment reduces potency of RSH-targeted irreversible EGFR inhibitors	135
4.10	Bruton's Tyrosine Kinase (BTK) contains a cysteine residue (Cys481) that is structurally homologous to EGFR Cys797	136
4.11	IgM-mediated sulfenylation of BTK in cells	138
4.S1	Sequence alignment of EGFR and nine additional kinases containing a structurally homologous residue to EGFR Cys797	153
4.S2	Chemical Structures of compounds used in this study	154
4.S3	Identification of the MPFGC*L peptide from EGFR labeled with RSH-targeted inhibitors	155
4.S4	Cys797 mutants do not exhibit enhanced autophosphorylation levels in response to EGF or H ₂ O ₂ treatment	156

4.S5	MS/MS spectrum of the precursor ion m/z 821.4 $[M+H]^+$ corresponding to dimedone labeled peptide (MPFGC*L) from recombinant WT EGFR.	157
4.S6	Chronic H_2O_2 treatment reduces potency of PD168393 in common oncogenic mutations	158
4.S7	Chronic H_2O_2 treatment reduces potency of afatinib in common oncogenic mutations	159
4.S8	H_2O_2 treatment mimics IgM-induced activation of BTK	160
4.S9	IgM-mediated ROS production and protein sulfenylation	161
5.1	Development of targeted covalent inhibitors for sulfenyl EGFR	172
5.2	Structures of RSOH-targeted EGFR compounds and blunted controls.	174
5.3	Acute and chronic H_2O_2 treatment increases potency of RSOH-targeted compound 1a	177
5.4	Chronic H_2O_2 treatment reduces potency of RSH-targeted irreversible EGFR inhibitors.	180
5.5	Reductive stress conditions decrease potency of RSOH-targeted EGFR compounds.	181
5.6	Washout effect of RSOH-targeted compounds.	184
5.7	Acute H_2O_2 treatment increases potency of RSOH-targeted EGFR compounds in lung cancer cells	187
5.8	Acute H_2O_2 treatment slightly increases potency of RSOH-targeted EGFR compounds towards ErbB2	188
5.9	RSOH-targeted EGFR compounds decrease EGFR autophosphorylation and sulfenylation levels in xenograft mice models	190
5.S1	Dose-dependence of acute H_2O_2 on EGFR phosphorylation levels.	198
5.S2	Acute H_2O_2 treatment increases potency of RSOH-targeted compounds.	199

5.S3	Human serum albumin (HSA) decreases potency of RSH- and RSOH-targeted compounds.	200
6.1	Sequence alignment of EGFR and nine additional kinases containing a structurally homologous residue to EGFR Cys797.	214
6.2	Structures of 2nd generation RSOH-targeted EGFR compounds . . .	215
A.1	Bioorthogonal detection of protein cysteine oxidation.	224
A.2	Cell-based detection of protein sulfenylation.	227
A.3	Detection of sulfenyl modifications with purified protein in vitro . . .	233
A.4	Detection of EGF-mediated protein sulfenylation in A431 cells . . .	240
A.5	Global changes of protein sulfenylation in HepG2 cells exposed to exogenous H ₂ O ₂	243
A.6	Labeling and detection of protein sulfenylation in adherent A431 and HepG2 cells	254
B.1	Activation of RTKs and downstream signaling cascades	269
B.2	Model for redox-dependent signal transduction	275
B.3	Oxidative modification of cysteine residues by H ₂ O ₂	277
B.4	<i>Trans</i> -activation of PDGFR and EGFR	280
B.5	Isoform-specific roles of Prx during redox-based PDGFR signaling . . .	283
B.6	General strategy for detecting protein sulfenic acids in cells	288
B.7	Model for H ₂ O ₂ -dependent regulation of EGFR activation	291
B.8	Spatial and temporal modulation of VEGFR2 signaling occurs in discrete subcellular compartments	295
B.9	Two proposed models for redoxbased activation of ASK1	305
B.10	Regulation of c-Src	308
B.11	IKK activation of NF- κ B	312

B.12	Abbreviated sequence alignment of EGFR and nine additional kinases that harbor a cysteine residue structurally homologous to EGFR Cys797	317
------	--	-----

LIST OF TABLES

2.S1	Expected and observed m/z of C*GF ^{TPQYK} peptide from Gpx3	64
2.S2	Expected and observed m/z of b and y ions for TFA cleaved C*GF-TPQYK peptide from Gpx3.	65
4.1	Kinetic Parameters of Wild-Type, C797S, and C797A EGFR	123
5.1	IC ₅₀ Values of RSOH-Targeted Compounds and Controls in A431 Cells Treated with Acute H ₂ O ₂	178
5.2	Anti-Proliferative Effects of RSOH-Targeted Compounds and Controls in A431 Cells	185
5.S1	IC ₅₀ Values of H ₂ O ₂ (Acute) in A431 Cells Treated with 1a-5a	201
5.S2	IC ₅₀ Values of RSOH-Targeted Compounds in NCI-H1975 Cells Treated with Acute H ₂ O ₂	202
5.S3	IC ₅₀ Values of RSOH-Targeted Compounds in HCC827 Cells Treated with Acute H ₂ O ₂	203
5.S4	IC ₅₀ Values of RSOH-Targeted Compounds in MDA-MB-453 Cells Treated with Acute H ₂ O ₂	204
B.1	Growth factors that induce ROS production	272
B.2	Example of redox-regulated protein kinases.	313

LIST OF SCHEMES

2.1	Synthesis of deuterated fragment for d_6 -DAz-2	41
2.2	Synthesis of alkyne acid-cleavable linker (Yn-ACL)	41

LIST OF APPENDICES

A.	Bioorthogonal Chemical Reporters for Analyzing Protein Sulfenylation in Cells	220
B.	Redox Regulation of Protein Kinases	265

ABSTRACT

Probing the Role of Sulfenylation in Redox Regulation of Protein Kinases

by

Thu H. Truong

Co-Chairs: Kate S. Carroll and Anna K. Mapp

Hydrogen peroxide (H_2O_2) functions as a secondary messenger to regulate intracellular signaling cascades, largely through the modification of specific cysteine residues within redox-sensitive targets such as protein kinases. Oxidation can influence kinase activity in physiology and pathology, but the molecular mechanisms underlying these events remain largely unknown. In the present study, we present the development and application of chemical tools to detect and quantify changes in sulfenic acid formation (sulfenylation). These tools were used to demonstrate epidermal growth factor (EGF)-mediated signaling induces global and dynamic changes in protein sulfenylation. Three protein tyrosine phosphatases (PTPs) were shown to undergo EGF-dependent oxidation and exhibit a unique sulfenylation profile in cells, suggesting the extent of sulfenylation may be related to differences in subcellular locations of target proteins. In addition, epidermal growth factor receptor (EGFR) was identified as a direct target of signal-derived H_2O_2 at its active site cysteine (Cys797). Sulfenylation of EGFR Cys797 enhances its intrinsic tyrosine kinase activity, and subsequent work has demonstrated mutation of this residue abrogates EGFR autophosphorylation, sulfenylation, and decreases its affinity for ATP. These results highlight the

importance of Cys797 with respect to EGFR function during normal cell signaling. Nine additional kinases harbor a cysteine residue that is structurally homologous to Cys797, and we present evidence that these kinases may be similarly regulated by oxidation of this residue. EGFR is mutated or amplified in a number of human carcinomas, and the proximity of Cys797 in the kinase domain potentially renders it more sensitive to oxidation in oncogenic mutants as shown by our data. Interestingly, EGFR Cys797 serves as a therapeutic target for covalent inhibitors that react with the reduced residue through electrophilic Michael addition. Oxidation of Cys797 alters the potency of current EGFR inhibitors that cannot recognize the kinase in its sulfenyl form. We report the development of a panel of first-generation nucleophilic RSOH-targeted inhibitors and evaluate compound potency towards EGFR Cys797 in response to concomitant oxidation. Collectively, the results of this thesis provide novel insight into how oxidative modification of kinases affects signal transduction pathways and have broad implications for therapeutics in disease states.

CHAPTER I

Redox Regulation of Epidermal Growth Factor Receptor Signaling Through Cysteine Oxidation

1.1 Abstract

Epidermal growth factor receptor (EGFR) exemplifies the family of receptor tyrosine kinases that mediate numerous cellular processes including growth, proliferation and differentiation. Moreover, gene amplification and EGFR mutations have been identified in a number of human malignancies, making this receptor an important target for the development of anticancer drugs. In addition to ligand-dependent activation and concomitant tyrosine phosphorylation, EGFR stimulation results in the localized generation of H_2O_2 by NADPH-dependent oxidases. In turn, H_2O_2 functions as a secondary messenger to regulate intracellular signaling cascades, largely through the modification of specific cysteine residues within redox-sensitive protein targets, including Cys797 in the EGFR active site. In this review, we highlight recent advances in our understanding of the mechanisms that underlie redox regulation of EGFR signaling and how these discoveries may form the basis for development of new therapeutic strategies to target this and other H_2O_2 -modulated pathways.

1.2 Redox Regulation of EGFR Signaling Through Cysteine Oxidation

Activation of receptor tyrosine kinases (RTKs) by their respective extracellular ligands (e.g. growth factors) initiates signaling cascades that regulate cellular proliferation, differentiation, migration, and survival (1). Among the 58 RTKs identified in the human genome, epidermal growth factor (EGF) receptor (EGFR) has served as the quintessential model for understanding RTK biology in physiological signaling and cancer. EGFR, also known as HER1 (or erbB1), is a transmembrane protein grouped into a subfamily that consists of three additional, closely related receptors: HER2 (erbB2), HER3 (erbB3), and HER4 (erbB4). EGFR is comprised of a glycosylated extracellular ligand-binding domain, a transmembrane domain, and an intracellular domain containing its tyrosine kinase core. In response to ligand (e.g. EGF) binding, EGFR forms homo- or heterodimers with other HER family members, followed by autophosphorylation of key tyrosine residues located within the tyrosine kinase domain (2). Once activated, EGFR relays the signal through a variety of downstream intracellular signaling cascades, including the Ras/mitogen activated protein kinase (MAPK) pathway or the phosphatidylinositol 3 kinase (PI3K)/Akt pathway. Since its discovery (3–6), EGFR has been widely studied in regards to its physiologic and pathological settings. In particular, EGFR and related family members have been found to be mutated or amplified in a number of human lung and breast cancers, rendering them an attractive target for the development of therapeutics (7–9).

Beginning in the 1990s, data from several research groups demonstrated that EGF binding to EGFR triggered the production of endogenous hydrogen peroxide (H_2O_2) in cells (Figure 1.1) (10, 11). Moreover, it was also established that other growth factors [FGF (12), PDGF (13), VEGF (14), insulin (15)], cytokines [TNF- α (12, 16), interleukin-1 (16)], and angiotensin II (17) stimulate H_2O_2 generation.

Although chronic exposure to high concentrations of H_2O_2 can lead to a cellular condition known as oxidative stress, cells can also utilize H_2O_2 as a secondary messenger to regulate physiological signal transduction (18–21). H_2O_2 modulates signaling pathways largely through the modification of specific cysteine residues located within redox-sensitive protein targets (Figure 1.2A). The direct product of the reaction between H_2O_2 and a protein thiolate (RS^-) is sulfenic acid (RSOH). Such protein sulfenylation is reversible by thiol-disulfide oxidoreductases of the thioredoxin (Trx) superfamily throughout the intracellular milieu and thus, constitutes a facile switch for modulating protein function, akin to phosphorylation. Associated regulatory redox modifications of cysteine include sulfenamides, nitrosothiols, disulfides, sulfinic, and sulfonic acids (Figure 1.2B). Over the last several years, an increasing number of studies have demonstrated important functional roles for protein sulfenic acids in cell signaling (22–26). In particular, kinases and phosphatases are both known to undergo cysteine-based redox regulation (27, 28) and the collective efforts of many researchers have established that these enzymes are regulated by endogenous H_2O_2 produced during EGF-mediated cell signaling (29).

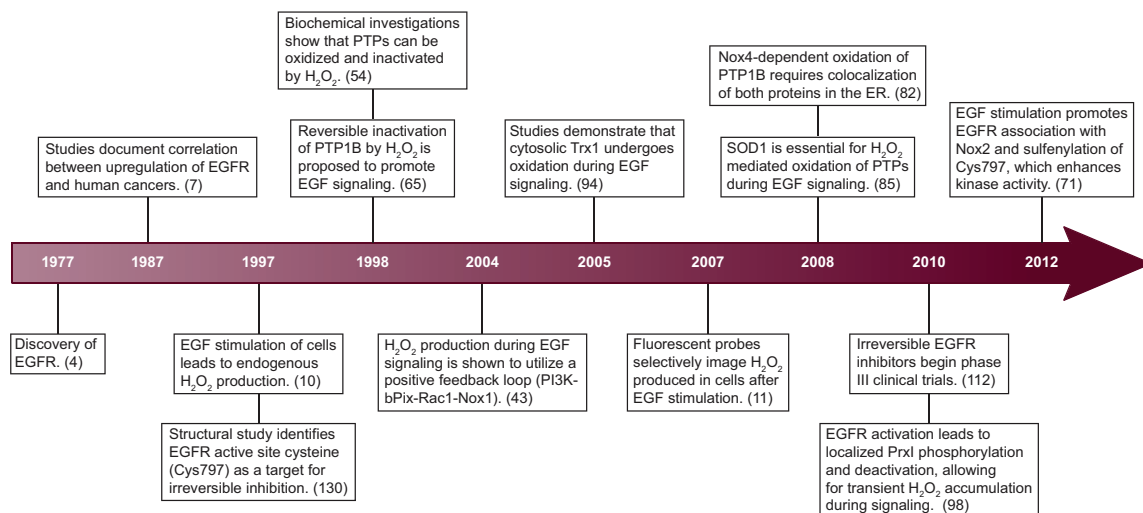


Figure 1.1: **EGFR Timeline.** Timeline outlining key events and discoveries relating to redox regulation of EGFR signaling through cysteine oxidation.

In this review, we present a historical overview of EGFR and ligand-mediated production of H₂O₂ as well as the molecular mechanisms involved in redox regulation of this signaling pathway (Figure 1.1). We begin by highlighting early studies linking EGFR activation to EGF-induced H₂O₂ production. Subsequently, we address the effects of redox modulation on two major pathways downstream of EGFR, Ras/MAPK and PI3K/Akt. Additionally, we discuss the interplay between H₂O₂-mediated inactivation of protein tyrosine phosphatases (PTPs) and kinase activation on net cellular levels of tyrosine (Tyr) phosphorylation. Key enzymes involved in the generation and metabolism of H₂O₂ within EGFR signaling pathways will also be covered. Finally, we focus on recent examples from the literature demonstrating direct oxidation and regulation of EGFR by H₂O₂ and how these discoveries may form the basis for development of new therapeutic strategies to target this and other H₂O₂-modulated pathways.

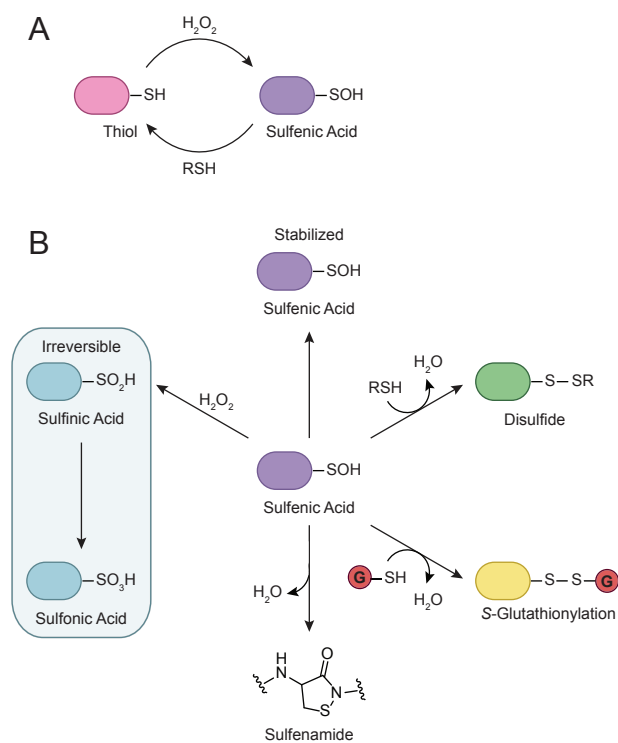


Figure 1.2: **Oxidative modification of cysteine residues by hydrogen peroxide (H_2O_2).** (A) The initial reaction product of a thiolate with H_2O_2 yields sulfenic acid (RSOH). This modification, also known as sulfenylation, is reversible and can be directly reduced back to the thiol form or indirectly through disulfide bond formation. (B) Sulfenic acids can be stabilized by the protein microenvironment and/or undergo subsequent modification. For example, they can condense with a second cysteine in the same or different protein to generate a disulfide bond. Alternatively, reaction with the low molecular weight thiol glutathione (GSH, red circle) affords a mixed disulfide through a process known as *S*-glutathionylation. In a few proteins, such as PTP1B, nucleophilic attack of a backbone amide on RSOH results in sulfenamide formation. Sulfenyl groups can also oxidize further to the sulfinic (RSO₂H) and/or sulfonic (RSO₃H) acid form under conditions of high oxidative stress.

1.3 Early Evidence for EGF-Mediated H₂O₂ Production and Redox Regulation of EGFR Signaling

In 1995, Gamou and Shimizu published the first report to suggest a connection between H₂O₂ and EGFR. In this study, the authors examined the effect of exogenously added H₂O₂ on EGFR phosphorylation (30). EGFR- hyper producing human squamous carcinoma NA cells treated with H₂O₂ (0 - 1 mM) exhibited an increase in the incorporation of [³²P]-phosphate, albeit at half the signal observed for EGF-stimulated cells. On the basis of data obtained from tryptic phosphopeptide mapping, this discrepancy was attributed to the fact that H₂O₂ might preferentially enhance EGFR Tyr phosphorylation, whereas EGF stimulation would trigger both serine/threonine (Ser/Thr) as well as Tyr receptor phosphorylation.

During this same time frame (i.e. the mid-90s), the role of H₂O₂ expanded beyond the traditional view as "toxic byproducts of aerobic metabolism" and began to emerge as secondary messengers in physiological cell signaling. In order for H₂O₂ to serve as a signaling molecule, its concentration must increase rapidly above the steady-state threshold (i.e., high nanomolar to low millimolar) and remain elevated long enough for it to oxidize protein effectors (31). In one of the earliest examples, platelet-derived growth factor (PDGF) was shown to induce endogenous H₂O₂ generation, which is correlated with enhanced Tyr phosphorylation, activation of MAPK pathways, DNA synthesis, and chemotaxis (13). These results suggested that H₂O₂ might act as a signaling molecule generated in response to growth factor stimulation. Soon thereafter, Rhee and colleagues reported that addition of EGF to EGFR-overexpressing human epidermoid carcinoma A431 cells significantly elevated levels of intracellular reactive oxygen species (ROS) (10) as measured by 2,7-dichlorofluorescein diacetate (DCFH-DA) (32). Enzymes such as catalase, peroxiredoxins (Prxs), and glutathione peroxidases (Gpxs) scavenge endogenous H₂O₂ by catalyzing the dismutation (cata-

lase) or reduction (Prxs, Gpxs) of H_2O_2 (33, 34). Introduction of exogenous catalase in EGF-stimulated A431 cells by electroporation attenuated the intracellular build-up of ROS, suggesting that H_2O_2 was the major ROS involved in EGF-dependent signal transduction (10). EGF-induced increases in Tyr phosphorylation levels of PLC- γ 1, a well-characterized physiological substrate of EGFR, were also blunted by catalase incorporation. Although the precise role and/or target(s) of H_2O_2 generated for EGFR signaling were not directly addressed in this study, the authors proposed that inhibition of cysteine-dependent PTPs by H_2O_2 may be required to increase the steady-state level of protein Tyr phosphorylation. This landmark contribution by Rhee and coworkers set the stage for delineating the molecular details underlying redox regulation of EGFR signaling.

In a separate study, Goldkorn et al. reported that exogenous H_2O_2 stimulated EGFR tyrosine kinase activity and increased receptor half-life (35). Experiments performed in A549 human lung adenocarcinoma epithelial cells and isolated membrane fractions showed an increase in EGFR Tyr autophosphorylation levels when treated with H_2O_2 (0-200 μM), and also markedly enhanced receptor activation in conjunction with the native EGF ligand. Pulse-chase experiments with [^{35}S]-methionine revealed that EGFR half-life was 8 h when treated with EGF, whereas H_2O_2 treatment extended receptor half-life to 18 h (combined treatment with EGF and H_2O_2 yielded a half-life of 12 h). Additionally, two-dimensional phosphoamino acid analysis corroborated earlier findings (30) that the phosphorylation site distribution was shifted predominantly towards Tyr after exposure to H_2O_2 . On the basis of these data, the authors of this study postulated that EGF- and H_2O_2 -induced receptor activation may have separate functions and represent an alternate mechanism by which EGFR signaling can be tuned in parallel to treatment with its native ligand.

1.4 Effect of H₂O₂ on Signaling Networks Downstream of EGFR

After ligand binding, EGFR transmits activation signals to prominent downstream cascades, including the Ras/MAPK and PI3K/Akt pathways (Figure 1.3A). In addition to the overall increase in Tyr autophosphorylation of EGFR, the endogenous generation of H₂O₂ also appears to modulate the activity of these two signaling routes. Receptor activation initiates the Ras-Raf-MEK-Erk1/2 signaling module through recruitment of Src homology 2 domain-containing (SHC) adaptor protein, growth factor receptor-bound protein 2 (Grb2), and a guanine nucleotide exchange protein (SOS) to form the SHC-Grb2-SOS complex, a process stimulated by elevated intracellular H₂O₂ (36). Once associated with the receptor, SOS facilitates guanine nucleotide exchange to activate Ras, which subsequently activates a kinase cascade including Raf (MAP3K), MEK (MAP2K), and Erk1/2 (MAPK). Oxidative stress is known to influence the MAPK signaling pathways, but little is known about the molecular mechanisms responsible for such effects (37). For example, Erk1/2 is activated in response to exogenous H₂O₂, which enhances cell survival after oxidant injury (38, 39). On the other hand, it is not known whether the activity of Erk1/2 kinase is directly modulated by ROS.

EGFR also transmits signals through the PI3K/Akt pathway (40). In response to EGF stimulation, PI3K increases the levels of phosphatidylinositol 3,4,5-trisphosphate (PIP₃), which leads to recruitment and activation of serine/threonine kinase, Akt at the plasma membrane (41, 42). Activity of the PI3K/Akt pathway is balanced by action of the opposing lipid phosphatase, PTEN, which will be discussed in later sections of this review. In cells overexpressing the NADPH oxidase isoform Nox1, increased endogenous H₂O₂ production elevates intracellular PIP₃ levels and consequently abrogates the ability of PTEN to promote downstream signaling (43). EGFR-dependent activation of Akt has also been shown to enhance cell survival during oxidative stress-induced apoptosis, analogous to Erk1/2 (44). Interestingly, structural analysis by

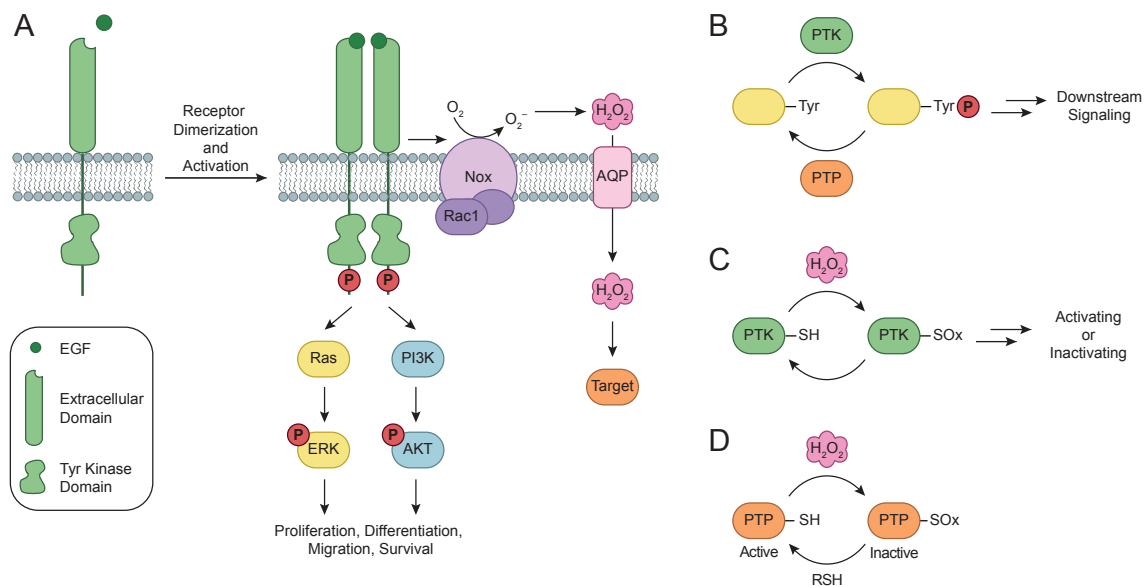


Figure 1.3: EGFR signaling pathways and general mechanisms for thiol-based redox modulation of signaling proteins. (A) Binding of EGF to EGFR induces receptor dimerization, followed by autophosphorylation of tyrosine (Tyr) residues (red circles) within its cytoplasmic domain. In turn, these phosphorylated Tyr residues serve as docking sites for associating proteins to activate a number of downstream signaling cascades. Two such pathways, Ras/ERK and PI3K/AKT, are shown here for simplicity. The EGF-EGFR interaction also triggers the assembly and activation of NADPH oxidase (Nox) complexes, followed by subsequent production of H_2O_2 through spontaneous dismutation or action of SOD. Once formed, endogenous H_2O_2 may pass through specific aquaporin (AQP) channels and/or diffuse across the membrane to reach the intracellular cytosol. Transient increases in H_2O_2 leads to the oxidation of local redox targets. (B) Model for redox-dependent signal transduction. Protein tyrosine kinases (PTKs) catalyze the transfer of γ -phosphoryl groups from ATP to tyrosine hydroxyls of proteins, whereas protein tyrosine phosphatases (PTPs) remove phosphate groups from phosphorylated tyrosine residues. PTPs function in a coordinated manner with PTKs to control signaling pathways to regulate a diverse array of cellular processes. (C) Regulatory cysteines in protein kinases can undergo oxidation/reduction to modulate their function. Depending on the kinase, redox modifications can stimulate or inhibit function. (D) Oxidation of the conserved active site cysteine residue in PTPs inactivates these enzymes, and can be restored by reducing the oxidized residue to its thiol form. SOx: oxidized cysteine.

x-ray crystallography has revealed that Akt2 can form an intramolecular disulfide bond between two cysteines in the activation loop, which inhibits the kinase (45). Overexpression of glutaredoxin (Grx) has been shown to protect Akt against H₂O₂-induced oxidation, resulting in sustained phosphorylation of Akt and inhibition of apoptosis (46). A more recent study is indicative of isoform-specific regulation of Akt by PDGF-induced H₂O₂ (47). In particular, the authors demonstrate that Akt2 Cys124 undergoes sulfenic acid modification during growth factor signaling, which inactivates the kinase.

EGFR activation can also occur through a process known as trans-activation. In this scenario, ligand-inaccessible RTKs may still initiate downstream signaling in lieu of ligand-receptor induced activation. Production of H₂O₂ induced by other ligands such as angiotensin II activates c-Src, a redox-regulated kinase (48). In turn, EGFR undergoes activation through c-Src initiated receptor Tyr phosphorylation to propagate downstream signaling (48–50). Neighboring EGFR kinases may then undergo activation in a lateral-based mechanism. Trans-activation represents another level by which EGFR activity can be modulated by H₂O₂. In addition, other studies have implicated oxidative inactivation of PTPs in promoting EGFR trans-activation (51).

1.5 Interplay of Reversible Tyrosine Phosphorylation and Redox-Dependent Signaling

Regulation of tyrosine phosphorylation depends on the delicate balance between the action of protein kinases and phosphatase (Figure 1.3B, and C). In EGFR signaling, the coordinated regulation of this equilibrium allows for rapid response to changing growth factor levels, whereas dysregulated kinase and phosphatase activity can have severe pathological consequences such as cancer, diabetes, and inflammation (52, 53). Because the balance of these two opposing forces is a central event

in cell signaling, it is not surprising that phosphatase as well as kinase activities are tightly regulated at several levels, including cysteine-based redox modulation. In large part, owing to early studies carried out by Denu and Tanner (54), attention rapidly focused on PTPs as the direct targets of H_2O_2 (Figure 1.3D). The PTP superfamily contains a signature motif, (I/V)HCXXGXXR(S/T), which includes an invariant cysteine residue that functions as a nucleophile in catalysis. The catalytic cysteine of PTPs is characterized by a low pK_a value ranging from 4.6 - 5.5 due to the unique electrostatic environment of the active site, which also renders the enzyme susceptible to inactivation by reversible oxidation (55, 56). Second-order rate constants for oxidation of the PTP cysteine thiolate by H_2O_2 have been measured *in vitro* and range from 10 to 160 $\text{M}^{-1} \text{s}^{-1}$ (54, 57, 58).

Protein tyrosine phosphatase 1B (PTP1B) functions as a negative regulator of the EGFR signaling pathway by directly targeting phosphorylated tyrosine residues that control signaling output (59–62). Given that PTP1B is localized exclusively to the cytoplasmic face of the endoplasmic reticulum (ER), it has been proposed to dephosphorylate activated EGFR at sites of contact between the ER and plasma membranes or upon trafficking of internalized EGFR in close proximity to the ER (63, 64). Studies reported in 1998 provided the first indication that EGF-mediated H_2O_2 production is correlated with oxidation and inactivation of PTP1B (65). Incorporation of radio-labeled iodoacetic acid (IAA) a sulfhydryl-modifying reagent that reacts with active site Cys215 of PTP1B (54) was decreased in PTP1B after EGF stimulation of A431 cells, consistent with oxidation of this essential residue. Conversely, treatment with dithiothreitol (DTT), thioredoxin (Trx), or glutaredoxin (Grx) as reductants readily reversed PTP1B inhibition. Interestingly, assays with recombinant protein indicated that the Trx system functioned more efficiently as an electron donor for PTP1B reactivation, as compared to Grx or glutathione (GSH), suggesting that Trx may function as the physiological reductant (65).

The phosphatase and tensin homologue (PTEN) is another PTP known to maintain a closely intertwined relationship with EGFR. PTEN exhibits dual protein and lipid phosphatase activity and functions as a negative regulator of the PI3K/Akt signaling pathway (66), one of the two major signaling routes downstream of EGFR. PTEN contains five cysteine residues in its catalytic domain and undergoes reversible inactivation by H_2O_2 (67). Site-directed mutagenesis and mass spectrometry indicated that Cys124 was the primary target of H_2O_2 , yielding a sulfenic acid intermediate that condenses with Cys71 to form an intramolecular disulfide bond (68). Cellular studies also point to a connection between growth factor-induced generation of H_2O_2 and reversible inactivation of PTEN. For example, EGF stimulation of cells results in elevated levels of oxidized PTEN in lysates, as indicated by an electrophoretic mobility shift assay that reports on disulfide formation (69). In an alternative approach, protein thiols are alkylated by *N*-ethylmaleimide (NEM) in lysates generated from growth factor stimulated cells. Reversibly oxidized protein thiols are then reduced with DTT and alkylated with biotin-conjugated maleimide. This method was used to examine reversible oxidation of PTEN in response to EGFR activation (69). Together, these studies indicate that EGF-induced activation of PI3K correlates with inactivation of the opposing phosphatase, PTEN. In this way, PTEN inactivation by endogenous H_2O_2 serves as a positive feedback loop to enhance PIP_3 accumulation/Akt activation during EGFR signaling.

SHP2 and DEP-1 represent two additional phosphatases that have been shown to interact with EGFR. SHP2 directly associates with EGFR through its SH2 domains and regulates receptor interactions with downstream signaling components such as Ras (70). Co-localization of SHP2 with EGFR occurs at low nanomolar concentrations (4 ng/ml) of EGF, and was identified as the most sensitive PTP in response to signal-derived H_2O_2 (71). It is unknown if DEP-1 co-localizes with EGFR intracellularly, albeit evidence implicates *in vitro* oxidation of DEP-1 (72).

1.6 Generation and Metabolism of H₂O₂ During EGFR Signaling

The family of NADPH oxidase (Nox) enzymes and their dual oxidase counterparts (Duox) generate superoxide by transferring electrons from cytosolic nicotinamide adenine dinucleotide phosphate (NADPH) to molecular oxygen (73). Once it is generated, superoxide is dismutated spontaneously ($10^5 \text{ M}^{-1} \text{ s}^{-1}$ at pH 7) or enzymatically by superoxide dismutase (SOD; $10^9 \text{ M}^{-1} \text{ s}^{-1}$) to H₂O₂ and molecular O₂ (74, 75). The prototypical Nox isoform, Nox2 (also known as gp91^{phox}) was originally identified and characterized in macrophages and neutrophils, where it functions as an integral part of the innate immune system (76). The active form of Nox2 exists as a multi-subunit complex, consisting of the membrane-bound cytochrome b558 (gp91^{phox} and p22^{phox}), several cytosolic proteins (p47^{phox}, p40^{phox}, p67^{phox}), and the small GTPase Rac1. Since the initial discovery of Nox2, other Nox homologues (Nox 1-5 and Duox 1-2) have been identified in almost every cell type, localized both to the plasma membrane (where they produce superoxide extracellularly) as well as intracellular organelles, and serve as major sources of H₂O₂ for signaling (77–79).

Several Nox isoforms play a critical role in EGFR-mediated signaling cascades. For example, Park *et al.* demonstrated that the PI3K pathway constitutes a positive feedback loop for Nox1 activation in growth factor-stimulated cells (43). This study demonstrated that the Rac-guanine nucleotide exchange factor (GEF) β -Pix is required for and also augments EGF-induced generation of H₂O₂. In this loop, β -Pix and activated Rac1 bind to the C-terminal region of Nox1, relieving auto-inhibitory constraints. Independent studies have also shown that phosphorylation of Nox activator 1 (NOXA1) on Ser282 by Erk1/2 kinases and on Ser172 by protein kinases C and A decreases Rac1 binding to down-regulate Nox1 (80, 81).

Nox4 is an isoform that regulates the activity of internalized EGFR. Keaney and

colleagues report that Nox4 is localized to the ER in vascular endothelial cells where it appears to regulate the activity of PTP1B in a spatially dependent manner (82). Nox4-dependent oxidation of PTP1B required co-localization of both proteins in the ER, as shown by targeting PTP1B to the cytoplasm. Importantly, the study also demonstrated that Nox4-dependent oxidation and inactivation of PTP1B is correlated with reduced phosphorylation of EGFR in proximity to the ER. The significance of co-localization was also verified by ER-targeting of the antioxidant enzyme, catalase. Lastly, EGF-stimulation of A431 cells leads to specific complex formation between Nox2 and EGFR, as demonstrated by co-immunoprecipitation experiments (71).

Superoxide dismutase 1 (SOD1) is another enzyme involved in redox mediation of growth factor signaling. SOD1 is an abundant copper/zinc enzyme located in the cytoplasm and belongs to the SOD family of enzymes. Other members of this family include mitochondrial SOD2 (manganese) and extracellular SOD3 (copper/zinc). Although superoxide can spontaneously dismutate to form H_2O_2 , the second-order rate constant of the reaction is enhanced over 10,000-fold by SOD (74, 75). Indeed, SODs catalyze the conversion of superoxide into H_2O_2 and molecular O_2 to maintain superoxide at low steady-state concentration (10^{-10} M) (83, 84). Inhibition of SOD1 by the tetrathiomolybdate inhibitor, ATN-224, increases the intracellular concentration of superoxide at the expense of H_2O_2 production, thereby attenuating EGFR and Erk1/2 phosphorylation (85).

Membrane transport represents another important mechanism to modulate endogenous H_2O_2 produced during EGFR signaling. Early studies demonstrated that EGF stimulation of cells leads to a rapid increase in the concentration of extracellular H_2O_2 and that the addition of catalase to culture medium was sufficient to inhibit EGFR autophosphorylation (86, 87). These findings raise the question of how extracellularly generated H_2O_2 could mediate intracellular signaling pathways. Although it had been largely assumed that H_2O_2 could diffuse across cellular membranes, more

recent evidence indicates that H_2O_2 may preferentially enter the cell through specific plasma membrane aquaporin channels (88–90). Collectively, these studies suggest that the number or type of aquaporins expressed on the cell surface might modulate the level of intracellular H_2O_2 available for signaling.

Efforts have also focused on delineating mechanisms to regulate intracellular H_2O_2 levels during EGF-mediated signaling. In this regard, superoxide dismutases, catalase, and other peroxidases all function to protect cells against undue oxidative stress. Prxs are a family of thiol-based peroxidases that catalyze the dismutation of H_2O_2 into water and molecular oxygen (91). Prx possesses two cysteines that transiently oxidize to form a disulfide as it metabolizes H_2O_2 . The disulfide in Prx is subsequently reduced by the protein disulfide reductase, Trx, to complete the catalytic cycle. Overexpression of the PrxII isoform reduces EGF-induced intracellular H_2O_2 levels (92). Another study demonstrated that PrxII overexpression is associated with a decrease in EGF-induced cellular PIP_3 , whereas a dominant negative (DN) form of PrxII increased PIP_3 levels, presumably by H_2O_2 modulation of PTEN redox state (69). Similarly, overexpression of another antioxidant enzyme, glutathione peroxidase-1 (Gpx1), decreased Tyr phosphorylation of EGFR, activation of Akt, and cellular proliferation (93). In addition to SODs and peroxidases, cells rely on the glutaredoxin/glutathione (Grx/GSH), Trx/thioredoxin reductase (Trx/TrxR), and glutathione/glutathione reductase (GSH/GSR) buffering systems. For example, EGFR signaling is associated with subcellular compartmental oxidation of Trx1. Jones and colleagues have measured the redox states of cytosolic and nuclear Trx1 and mitochondrial Trx2 using redox Western blot methods during endogenous H_2O_2 production induced by EGF signaling (94). Interestingly, results from this study showed that only the cytoplasmic Trx1 pool undergoes significant oxidation in response to growth factor treatment. Furthermore, the GSH/GSSG redox couple, which was also examined in this study, did not undergo oxidation. This work suggests that

physiological H_2O_2 generation in response to EGF signaling is specifically associated with oxidation of the Trx1 system and not the GSH system. However, whether Trx1 oxidation is part of the signaling mechanism itself or simply results from peroxidase-dependent termination of the redox signal remains an active area of investigation.

The estimated intracellular steady-state concentration of H_2O_2 hovers in the low-nanomolar to low-micromolar range (31). Then again, these estimates assume that H_2O_2 is uniformly distributed throughout the cell. Given that the source of H_2O_2 produced for EGF signaling (e.g. Nox enzymes) are localized to specific regions of the cell, it stands to reason that signal mediated changes in H_2O_2 concentration may not be homogenous throughout the cell. Rather, the oxidant concentration near a source of generation must achieve high local concentrations to function effectively as a second messenger. A growing body of research has focused on delineating the mechanisms that facilitate localized rises in intracellular H_2O_2 during growth factor signaling. Although the cell contains millimolar concentrations of GSH, it reacts too slowly with H_2O_2 to provide much buffering capacity (95). By contrast, Prxs are extremely efficient at H_2O_2 elimination, reducing H_2O_2 at second-order rate constants of 10^5 - $10^8 \text{ M}^{-1}\text{s}^{-1}$ (96, 97). Recent work reported by the Rhee laboratory has shown that membrane localized PrxI can be deactivated by phosphorylation in EGF-stimulated cells and in mice during wound healing (98). Knockdown experiments suggested that c-Src kinase is at least partially responsible for PrxI phosphorylation. RTK activation (e.g. PDGFR) can also lead to overoxidation of the PrxII isoform catalytic cysteine to sulfinic acid, resulting in a transiently inactivated protein (98). Collectively, these studies demonstrate that selective inactivation of PrxI and PrxII allows for transient H_2O_2 accumulation around plasma membranes where signaling components are concentrated, while simultaneously preventing toxic accumulation of ROS elsewhere in the cell during EGF signaling (Figure 1.4). Other mechanisms to modulate localized redox buffering capacity surely await discovery.

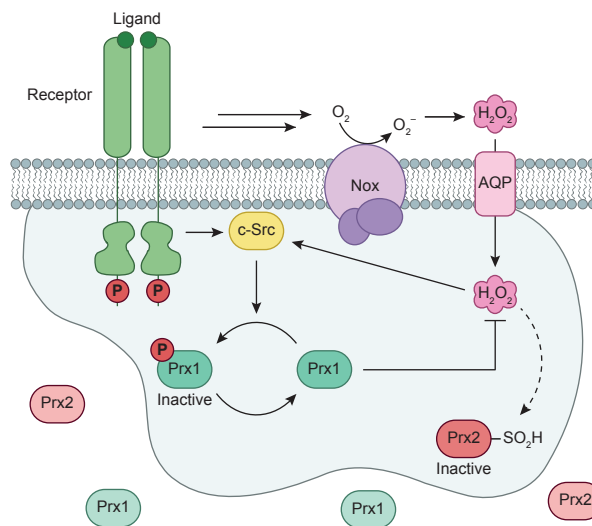


Figure 1.4: **Redox regulation of peroxiredoxins (Prxs) during EGFR signaling.** Receptor activation results in localized phosphorylation and inactivation of peroxiredoxin I (PrxI) by PTKs, such as the redox-regulated cytoplasmic Src (c-Src). Deactivation of PrxI diminishes the redox-buffering capacity adjacent to the cell membrane, allowing for a transient and localized increase in H_2O_2 levels for signal transduction. Additionally, elevated H_2O_2 concentrations can inactivate Prx2 by oxidation of its catalytic cysteine to sulfenic acid.

1.7 Regulation of Intrinsic EGFR Tyrosine Kinase Activity Through Cysteine Oxidation

As outlined above, a growing body of evidence demonstrates that EGFR activity and downstream signaling pathways are regulated by redox-based mechanisms. Up until this point we have only considered downstream events that enhance the overall extent of EGFR activation, such as PTP inactivation. We have also highlighted key regulatory themes in redox signaling, including co-localization of sources/targets of H_2O_2 and modulation of local redox buffering capacity. Until recently, there was scant evidence to indicate that the intrinsic tyrosine kinase activity of EGFR itself might be regulated by endogenous H_2O_2 produced during cell signaling (99–101). In the section below, we recount recent work from our own laboratory, which has demonstrated that EGFR is directly modulated by endogenous H_2O_2 , as well as studies from other groups that hint at the possibility of modification by reactive nitrogen species (RNS).

Previous data from our group demonstrated that breast cancer cells associated with increased expression of EGFR is correlated with a substantial increase in protein sulfenylation (102). Prompted by this observation, we conducted a more detailed investigation of EGF-induced protein sulfenylation in A431 cells (71). Facilitating these studies, we have recently described a new technology that allows for the detection and visualization of sulfenylation proteins within intact cells (103–106), thereby circumventing concerns associated with the analysis of lysates/homogenates including limited spatial-temporal resolution and oxidation artifacts inherent to the lysis procedure (107). Inspired by earlier work demonstrating the selective reaction of 5,5-dimethyl-1,3-cyclohexanedione (commercially known as dimedone) with protein sulfenic acids (108) (Figure 1.5A), we developed a suite of bi-functional probes that contain a membrane-permeable analog of dimedone coupled to an azide or alkyne chemical handle (Figure 1.5B). An orthogonally functionalized biotin or fluorescent

tag can be appended post-cell labeling for detection via the Staudinger ligation (109) or Huisgen [3+2] cycloaddition also known as click chemistry (110). Overall, this general approach provides a facile method for monitoring protein sulfenylation directly in living cells (Figure 1.5C).

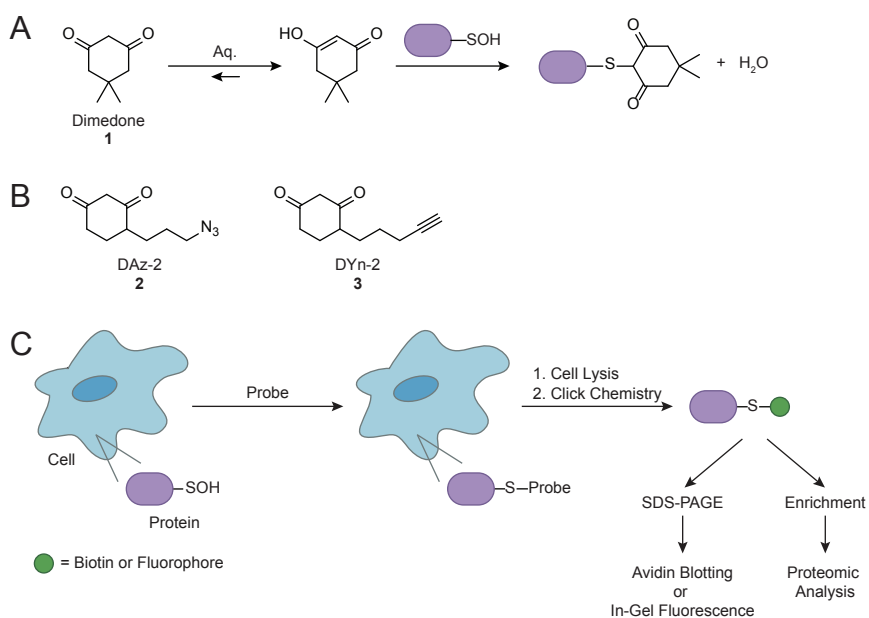


Figure 1.5: **General strategy for detecting protein cysteine sulfenylation (RSOH) in cells.** (A) Chemoselective reaction between sulfenic acid and 5,5-dimethyl-1,3-cyclohexanedione (dimedone, 1). (B) Azide and alkyne-functionalized small-molecule probes for trapping and tagging protein sulfenic acids include DAz-2 (2) and DYn-2 (3). (C) Detection of protein sulfenic acids in living cells. Target cells are incubated with cell-permeable probes to trap and tag protein sulfenic acids *in situ*. In subsequent steps, lysates are prepared and tagged proteins are further elaborated by attachment of biotin or fluorescence labels *via* click chemistry and enables detection by Western blot or in-gel fluorescence. Alternatively, biotinylated proteins may be enriched for proteomic analysis.

Employing this method, we demonstrated that EGFR undergoes sulfenylation in response to EGF addition, even at low-nanomolar concentrations of growth factor (71) (Figure 1.6A). Reciprocal immunoprecipitation analysis also showed that EGFR and Nox2 became associated in an EGF-dependent fashion (71). The intracellular kinase domain of EGFR contains six cysteine residues, one of which (Cys797) is located in the ATP-binding pocket (Figure 1.6B) and is conserved among nine additional receptor and non-receptor tyrosine kinases (Figure 1.6C) (111). Given its active site location and conservation, we hypothesized that Cys797 might be preferentially targeted by endogenous H_2O_2 . Of particular relevance, this residue is selectively targeted by irreversible EGFR inhibitors, such as afatinib, extensively used in basic research and clinical trials for breast and non-small cell lung cancers (112, 113). Consistent with this proposal, pre-treatment of cells with inhibitors that irreversibly modify Cys797 prevented sulfenylation of EGFR. Mass spectrometry was subsequently used to verify Cys797 as the specific site of oxidation. Finally, oxidation of Cys797 increased EGFR kinase activity by approximately five-fold. To put these findings into context, a comparable degree of stimulation is observed for L858R and T790M oncogenic EGFR mutations (114–116). Beyond the A431 cell line model, recent studies in our group also indicate that wild type and several activated mutant EGFR kinases undergo sulfenylation in both lung and breast tumors (T.H.T. and K.S.C., unpublished data). Hence, it appears that oxidation of specific residues in PTPs (catalytic Cys) and EGFR (Cys797) both contribute to an increase in downstream signaling (Figure 1.6A). Current work is directed toward understanding the molecular mechanism by which sulfenylation of EGFR Cys797 enhances kinase activity. The proximity of Cys797 to the ATP ligand as well as the C-helix and activation segment raises the possibility of transition state stabilization and/or destabilization of its auto inhibited conformation (116).

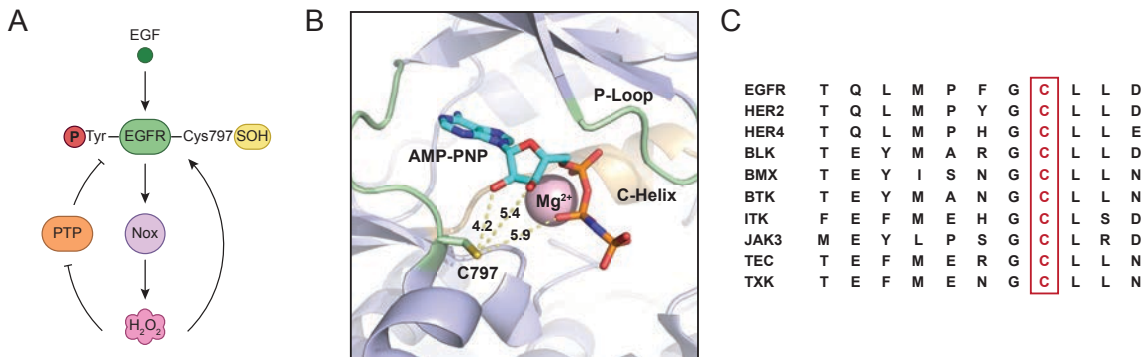


Figure 1.6: **Model for H_2O_2 -dependent regulation of EGFR tyrosine kinase activity.** (A) Binding of EGF induces production of H_2O_2 through Nox2. Nox-derived H_2O_2 directly modifies EGFR cysteine (Cys797) to sulfenic acid in the active site, which enhances its tyrosine kinase activity. Endogenous H_2O_2 can also oxidize and deactivate localized PTPs, leading to a net increase in EGFR phosphorylation. (B) Crystal structure of the EGFR kinase domain (PDB 3GT8) bound to AMP-PNP, a hydrolysis resistant ATP analog, and Mg^{2+} . Dashed yellow lines and accompanying numbers indicate the distance (\AA) between the γ -sulfur atom of Cys797 and key substrate functional groups. Note also that Cys797 can adopt different rotamers and sulfenylation of this residue may enhance its ability to participate in electrostatic and hydrogen-bonding interactions with its substrate. (C) Abbreviated sequence alignment of EGFR and nine other kinases that harbor a cysteine at the structural position that corresponds to Cys797 (adapted from ref. (113)).

We have also applied our chemical biology approach to monitor global changes in EGF-dependent protein sulfenylation (71). Interestingly, growth factor addition led to widespread changes in protein sulfenylation within cells. EGF induced cysteine oxidation in a dose- and time-dependent manner and was accompanied by concomitant fluxes in intracellular H_2O_2 . Additional experiments showed that treatment with cell-permeable PEGylated catalase attenuated EGF associated changes in protein sulfenylation, underscoring the importance of endogenous H_2O_2 . Although sulfenylation of EGFR (and several PTPs) were the focus our recent study (71), many protein targets of EGF-induced endogenous H_2O_2 remain to be identified and will necessitate large-scale proteomic analysis.

Remarkably, a number of studies indicate that EGFR may also undergo modulation by RNS at cysteine residues distinct from Cys797. Reaction of cysteine thiols with RNS, such as nitric oxide (NO), generates nitrosothiols (S-NO). This process, known as S-nitrosylation, is a well-established reversible post-translational cysteine

modification and has been implicated in proliferative and anti-proliferative cellular effects (117). The approach most often used to identify protein nitrosothiols is known as the biotin switch technique (BST) (118). The BST is an indirect method whose success relies heavily on the alkylation of free thiols and the selectivity/efficiency of the ascorbate reducing agent towards nitrosothiols (119, 120). Nonetheless, this method was utilized in two separate studies reporting S-nitrosylation of EGFR. Treatment of several cell types with one millimolar of an exogenous nitric oxide (NO) donor 1,1-diethyl-2-hydroxy-2-nitrosohydrazine (DEA-NO) inhibited EGFR autophosphorylation (121, 122). Serine mutation of EGFR Cys166, located in the extracellular domain, rendered the receptor resistant to NO-induced inhibition. Alternatively, another cysteine residue located at the extracellular EGFR ligand-binding interface undergoes nitrosylation after exposure to one millimolar of exogenous NO donor S-nitroso-L-cysteine (Cys-NO) (123). S-nitrosylation of these residues may inhibit EGFR-mediated signaling by interfering with the ligand interaction site, although this proposal awaits evaluation. By contrast, a more recent study demonstrates that S-nitrosylation induced by the chemical NO donor (Z)-1-[N-(2-aminoethyl)-N-(2-ammonioethyl)amino] diazen-1-ium-1,2-diolate known as DETA-NO can upregulate EGFR signaling and correlates with a transformed breast cancer phenotype (124, 125). An important area for future research is to determine whether EGFR undergoes direct S-nitrosylation in response to physiological stimuli.

1.8 Future Perspectives

Of the 95 receptor and non-receptor PTKs in the human genome, nine additional members harbor a cysteine residue that is structurally homologous to EGFR Cys797 (Figure 1.6C), including two EGFR subfamily members, HER2 and HER4. Although speculative at this time, it is possible that this group of kinases is regulated by oxidation of this residue. EGFR Cys797 and its structural analogues are located at

the N-terminal end of an alpha helix, also known as the N_{cap} position. Interestingly, cysteine is the most sparsely occurring N_{cap} residue in natural proteins, comprising less than 1% of all these positions (126). Interaction of a cysteine located at the N_{cap} position with the helix dipole can drastically lower thiol pK_a and increases its reactivity (127, 128). Of note, the N_{cap} effect has also been attributed to the reactivity of the human PrxI catalytic cysteine (98). Another subfamily of PTKs, which includes cytoplasmic Src and FGFR1, contains a cysteine located within a glycine rich loop that interacts with the γ -phosphate of ATP (129). Oxidation of this residue inhibits the kinase activity of c-Src and FGFR1 in vitro; however neither kinase has been confirmed as a direct target of endogenous H_2O_2 in cells. Over 150 kinases have a cysteine in or around the nucleotide-binding site, some of which may play similar regulatory roles. However, much more work will be required to define the scope and molecular details underlying the redox-regulated kinome.

EGFR is mutated or amplified in a number of human carcinomas including breast and lung cancers, which has motivated the development of selective kinase inhibitors, including analogs that covalently modify Cys797 and are currently in Phase II and III clinical trials (130). The recent finding that EGFR Cys797 undergoes sulfenic acid modification (71) and that elevated EGFR and HER2 in cancer cells correlates with a substantial increase in global protein sulfenylation (102), raises several fundamental questions vis-à-vis cysteine oxidation and thiol-targeted irreversible inhibitors. For example, the acrylamide moiety of irreversible EGFR inhibitors undergoes Michael addition with Cys797 in its thiol form, but these inhibitors would not react with the sulfenic acid or other cysteine chemotypes (Figure 1.7A). Thus, oxidation of Cys797 could affect the potency of these inhibitors, particularly under conditions of oxidative stress often associated with cancer. On the other hand, the sulfenic acid moiety represents an entirely new opportunity in covalent inhibitor design whereby the electrophilic S-atom is targeted using a nucleophilic warhead (Figure 1.7B). In this

approach, the propensity for specific cysteine residues in kinases, and other therapeutically important proteins, to undergo sulfenylation could be exploited for the development of inhibitors that target this unique modification, similar to the proof-of-concept compounds we have recently reported to target oxidized PTPs (131).

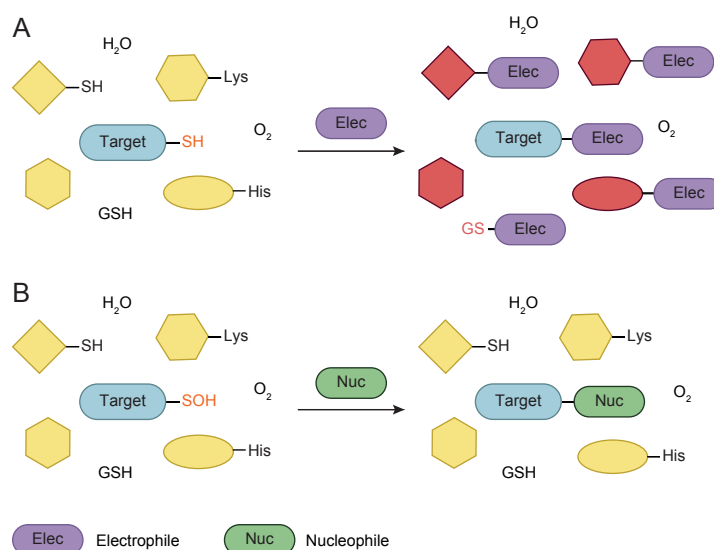


Figure 1.7: **Covalent cysteine-based protein targeting strategies.** (A) Conventional covalent inhibitors of kinases inactivate their target through covalent attachment to the cysteine thiol functional group. However, the electrophilic center (*e.g.*, acrylamide, haloacetamide, vinyl sulfonamide) that reacts with the cysteine can exhibit nonspecific reactivity toward other cellular thiols, including glutathione present at millimolar concentrations inside mammalian cells. The electrophile may also react with other nucleophilic functionalities present in biological systems (amino and imidazole groups of amino acids, various reactive sites in nucleic acid bases, water). (B) Orthogonal strategy as one potential mechanism to address issues associated with employing an electrophilic functional group to target one cysteine among a sea of biological nucleophiles. According to this approach, active site-directed small-molecule inhibitors containing a reactive nucleophilic substituent form a covalent bond with a sulfenic acid-modified cysteine side chain. Such modifications form transiently in specific proteins during H_2O_2 -mediated signal transduction in normal cells, but form constitutively in diseases associated with chronically elevated levels of H_2O_2 , including cancer. In the sulfenic acid oxidation state, the electron-deficient sulfur exhibits enhanced electrophilic character that can be selectively targeted by certain nucleophilic compounds. Because sulfenic acid is a unique chemical moiety in biochemistry, this strategy might decrease the potential for off-target activity while retaining the advantages gained by covalent targeting.

1.9 Conclusions

The perspectives presented here highlight the emerging and rapidly expanding role of redox regulation during EGFR signaling. These studies point to the unique chemistry of reactive cysteine residues within specific target proteins, including EGFR. These redox reactions enable covalent regulation of protein function, much like phosphorylation. The expanding array of modifications that target cysteine suggests that we are just beginning to understand the molecular basis for specificity of redox signaling. One theme that has consistently emerged in numerous studies is the colocalization of the oxidant sources with the redox-regulated target protein. As case in point, ligand activation triggers the association of EGFR and the NADPH oxidase, Nox2. We have also tried to emphasize the value of selective and cell-permeable chemical approaches to elucidate regulatory mechanisms that govern H₂O₂-mediated sulfenylation of proteins. In addition, we are just beginning to appreciate that different biological oxidants may target distinct cysteine residues in the same protein and thus lead to unique regulatory outcomes. Given that aberrant sulfenylation of proteins is linked to aggressive cancer phenotypes and that genetic lesions in H₂O₂-metabolizing enzymes can contribute to tumorigenesis, defining mechanisms that control reversible protein sulfenylation will be vital to understanding both human physiology and disease. Finally, it is hoped that the discovery of EGFR as a direct target of H₂O₂ will lead to a broader examination of the redox-regulated kinome and the development of an orthogonal nucleophilic strategy for covalent inhibition of therapeutically important proteins.

1.10 Chapter References

1. Schlessinger, J. (2000). Cell signaling by receptor tyrosine kinases. *Cell*, *103*(2), 211–25.
2. Schlessinger, J. (2002). Ligand-induced, receptor-mediated dimerization and activation of egf receptor. *Cell*, *110*(6), 669–72.
3. Cohen, S. (1962). Isolation of a mouse submaxillary gland protein accelerating incisor eruption and eyelid opening in the new-born animal. *J Biol Chem*, *237*, 1555–62.
4. Cohen, S., Carpenter, G., & King, J., L. (1980). Epidermal growth factor-receptor-protein kinase interactions. co-purification of receptor and epidermal growth factor-enhanced phosphorylation activity. *J Biol Chem*, *255*(10), 4834–42.
5. Carpenter, G., King, J., L., & Cohen, S. (1978). Epidermal growth factor stimulates phosphorylation in membrane preparations in vitro. *Nature*, *276*(5686), 409–10.
6. Cohen, S. (2008). Origins of growth factors: ngf and egf. *J Biol Chem*, *283*(49), 33793–7.
7. Macias, A., Azavedo, E., Hagerstrom, T., Klintonberg, C., Perez, R., & Skoog, L. (1987). Prognostic significance of the receptor for epidermal growth factor in human mammary carcinomas. *Anticancer Res*, *7*(3 Pt B), 459–64.
8. Yarden, Y. & Sliwkowski, M. X. (2001). Untangling the erbb signalling network. *Nat Rev Mol Cell Biol*, *2*(2), 127–37.
9. Herbst, R. S. (2004). Review of epidermal growth factor receptor biology. *Int J Radiat Oncol Biol Phys*, *59*(2 Suppl), 21–6.
10. Bae, Y. S., Kang, S. W., Seo, M. S., Baines, I. C., Tekle, E., Chock, P. B., & Rhee, S. G. (1997). Epidermal growth factor (egf)-induced generation of hydrogen peroxide. role in egf receptor-mediated tyrosine phosphorylation. *J Biol Chem*, *272*(1), 217–21.
11. Miller, E. W., Tulyathan, O., Isacoff, E. Y., & Chang, C. J. (2007). Molecular imaging of hydrogen peroxide produced for cell signaling. *Nat Chem Biol*, *3*(5), 263–7.
12. Lo, Y. Y. & Cruz, T. F. (1995). Involvement of reactive oxygen species in cytokine and growth factor induction of c-fos expression in chondrocytes. *J Biol Chem*, *270*(20), 11727–30.
13. Sundaresan, M., Yu, Z. X., Ferrans, V. J., Irani, K., & Finkel, T. (1995). Requirement for generation of h₂o₂ for platelet-derived growth factor signal transduction. *Science*, *270*(5234), 296–9.

14. Colavitti, R., Pani, G., Bedogni, B., Anzevino, R., Borrello, S., Waltenberger, J., & Galeotti, T. (2002). Reactive oxygen species as downstream mediators of angiogenic signaling by vascular endothelial growth factor receptor-2/kdr. *J Biol Chem*, *277*(5), 3101–8.
15. May, J. M. & de Haen, C. (1979). Insulin-stimulated intracellular hydrogen peroxide production in rat epididymal fat cells. *J Biol Chem*, *254*(7), 2214–20.
16. Meier, B., Radeke, H. H., Selle, S., Younes, M., Sies, H., Resch, K., & Habermehl, G. G. (1989). Human fibroblasts release reactive oxygen species in response to interleukin-1 or tumour necrosis factor-alpha. *Biochem J*, *263*(2), 539–45.
17. Griendling, K. K., Minieri, C. A., Ollerenshaw, J. D., & Alexander, R. W. (1994). Angiotensin ii stimulates nadh and nadph oxidase activity in cultured vascular smooth muscle cells. *Circ Res*, *74*(6), 1141–8.
18. Rhee, S. G. (2006). Cell signaling. h₂O₂, a necessary evil for cell signaling. *Science*, *312*(5782), 1882–3.
19. D’Autreaux, B. & Toledano, M. B. (2007). Ros as signalling molecules: mechanisms that generate specificity in ros homeostasis. *Nat Rev Mol Cell Biol*, *8*(10), 813–24.
20. Dickinson, B. C. & Chang, C. J. (2011). Chemistry and biology of reactive oxygen species in signaling or stress responses. *Nat Chem Biol*, *7*(8), 504–11.
21. Finkel, T. (2011). Signal transduction by reactive oxygen species. *J Cell Biol*, *194*(1), 7–15.
22. Reddie, K. G. & Carroll, K. S. (2008). Expanding the functional diversity of proteins through cysteine oxidation. *Curr Opin Chem Biol*, *12*(6), 746–54.
23. Paulsen, C. E. & Carroll, K. S. (2010). Orchestrating redox signaling networks through regulatory cysteine switches. *ACS Chem Biol*, *5*(1), 47–62.
24. Jacob, C., Battaglia, E., Burkholz, T., Peng, D., Bagrel, D., & Montenarh, M. (2012). Control of oxidative posttranslational cysteine modifications: from intricate chemistry to widespread biological and medical applications. *Chem Res Toxicol*, *25*(3), 588–604.
25. Zheng, M., Aslund, F., & Storz, G. (1998). Activation of the oxyr transcription factor by reversible disulfide bond formation. *Science*, *279*(5357), 1718–21.
26. Chen, C. Y., Willard, D., & Rudolph, J. (2009). Redox regulation of sh2-domain-containing protein tyrosine phosphatases by two backdoor cysteines. *Biochemistry*, *48*(6), 1399–409.

27. Aslan, M. & Ozben, T. (2003). Oxidants in receptor tyrosine kinase signal transduction pathways. *Antioxid Redox Signal*, 5(6), 781–8.
28. Tonks, N. K. (2005). Redox redux: revisiting ptps and the control of cell signaling. *Cell*, 121(5), 667–70.
29. Finkel, T. (2012). From sulfenylation to sulfhydration: what a thiolate needs to tolerate. *Sci Signal*, 5(215), pe10.
30. Gamou, S. & Shimizu, N. (1995). Hydrogen peroxide preferentially enhances the tyrosine phosphorylation of epidermal growth factor receptor. *FEBS Lett*, 357(2), 161–4.
31. Stone, J. R. & Yang, S. (2006). Hydrogen peroxide: a signaling messenger. *Antioxid Redox Signal*, 8(3-4), 243–70.
32. Bass, D. A., Parce, J. W., Dechatelet, L. R., Szejda, P., Seeds, M. C., & Thomas, M. (1983). Flow cytometric studies of oxidative product formation by neutrophils: a graded response to membrane stimulation. *J Immunol*, 130(4), 1910–7.
33. Giorgio, M., Trinei, M., Migliaccio, E., & Pelicci, P. G. (2007). Hydrogen peroxide: a metabolic by-product or a common mediator of ageing signals? *Nat Rev Mol Cell Biol*, 8(9), 722–8.
34. Halliwell, B. & Gutteridge, J. M. C. (1999). *Free radicals in biology and medicine*. Oxford: Oxford University Press.
35. Goldkorn, T., Balaban, N., Matsukuma, K., Chea, V., Gould, R., Last, J., . . . Chavez, C. (1998). Egf-receptor phosphorylation and signaling are targeted by h2o2 redox stress. *Am J Respir Cell Mol Biol*, 19(5), 786–98.
36. Rao, G. N. (1996). Hydrogen peroxide induces complex formation of shc-grb2-sos with receptor tyrosine kinase and activates ras and extracellular signal-regulated protein kinases group of mitogen-activated protein kinases. *Oncogene*, 13(4), 713–9.
37. McCubrey, J. A., Lahair, M. M., & Franklin, R. A. (2006). Reactive oxygen species-induced activation of the map kinase signaling pathways. *Antioxid Redox Signal*, 8(9-10), 1775–89.
38. Guyton, K. Z., Liu, Y., Gorospe, M., Xu, Q., & Holbrook, N. J. (1996). Activation of mitogen-activated protein kinase by h2o2. role in cell survival following oxidant injury. *J Biol Chem*, 271(8), 4138–42.
39. Wang, X., Martindale, J. L., Liu, Y., & Holbrook, N. J. (1998). The cellular response to oxidative stress: influences of mitogen-activated protein kinase signalling pathways on cell survival. *Biochem J*, 333 (Pt 2), 291–300.

40. Leslie, N. R. (2006). The redox regulation of pi 3-kinase-dependent signaling. *Antioxid Redox Signal*, 8(9-10), 1765–74.
41. Stokoe, D., Stephens, L. R., Copeland, T., Gaffney, P. R., Reese, C. B., Painter, G. F., . . . Hawkins, P. T. (1997). Dual role of phosphatidylinositol-3,4,5-trisphosphate in the activation of protein kinase b. *Science*, 277(5325), 567–70.
42. Franke, T. F., Kaplan, D. R., Cantley, L. C., & Toker, A. (1997). Direct regulation of the akt proto-oncogene product by phosphatidylinositol-3,4-bisphosphate. *Science*, 275(5300), 665–8.
43. Park, H. S., Lee, S. H., Park, D., Lee, J. S., Ryu, S. H., Lee, W. J., . . . Bae, Y. S. (2004). Sequential activation of phosphatidylinositol 3-kinase, beta pix, rac1, and nox1 in growth factor-induced production of h2o2. *Mol Cell Biol*, 24(10), 4384–94.
44. Wang, X., McCullough, K. D., Franke, T. F., & Holbrook, N. J. (2000). Epidermal growth factor receptor-dependent akt activation by oxidative stress enhances cell survival. *J Biol Chem*, 275(19), 14624–31.
45. Huang, X., Begley, M., Morgenstern, K. A., Gu, Y., Rose, P., Zhao, H., & Zhu, X. (2003). Crystal structure of an inactive akt2 kinase domain. *Structure*, 11(1), 21–30.
46. Murata, H., Ihara, Y., Nakamura, H., Yodoi, J., Sumikawa, K., & Kondo, T. (2003). Glutaredoxin exerts an antiapoptotic effect by regulating the redox state of akt. *J Biol Chem*, 278(50), 50226–33.
47. Wani, R., Qian, J., Yin, L., Bechtold, E., King, S. B., Poole, L. B., . . . Furdui, C. M. (2011). Isoform-specific regulation of akt by pdgf-induced reactive oxygen species. *Proc Natl Acad Sci U S A*, 108(26), 10550–5.
48. Ushio-Fukai, M., Alexander, R. W., Akers, M., Yin, Q., Fujio, Y., Walsh, K., & Griending, K. K. (1999). Reactive oxygen species mediate the activation of akt/protein kinase b by angiotensin ii in vascular smooth muscle cells. *J Biol Chem*, 274(32), 22699–704.
49. Chen, K., Vita, J. A., Berk, B. C., & Keaney, J., J. F. (2001). C-jun n-terminal kinase activation by hydrogen peroxide in endothelial cells involves src-dependent epidermal growth factor receptor transactivation. *J Biol Chem*, 276(19), 16045–50.
50. Giannoni, E., Buricchi, F., Grimaldi, G., Parri, M., Cialdai, F., Taddei, M. L., . . . Chiarugi, P. (2008). Redox regulation of anoikis: reactive oxygen species as essential mediators of cell survival. *Cell Death Differ*, 15(5), 867–78.
51. Reynolds, A. R., Tischer, C., Verveer, P. J., Rocks, O., & Bastiaens, P. I. (2003). Egfr activation coupled to inhibition of tyrosine phosphatases causes lateral signal propagation. *Nat Cell Biol*, 5(5), 447–53.

52. Tonks, N. K. (2006). Protein tyrosine phosphatases: from genes, to function, to disease. *Nat Rev Mol Cell Biol*, 7(11), 833–46.
53. Blume-Jensen, P. & Hunter, T. (2001). Oncogenic kinase signalling. *Nature*, 411(6835), 355–65.
54. Denu, J. M. & Tanner, K. G. (1998). Specific and reversible inactivation of protein tyrosine phosphatases by hydrogen peroxide: evidence for a sulfenic acid intermediate and implications for redox regulation. *Biochemistry*, 37(16), 5633–42.
55. Zhang, Z. Y. & Dixon, J. E. (1993). Active site labeling of the yersinia protein tyrosine phosphatase: the determination of the pKa of the active site cysteine and the function of the conserved histidine 402. *Biochemistry*, 32(36), 9340–5.
56. Lohse, D. L., Denu, J. M., Santoro, N., & Dixon, J. E. (1997). Roles of aspartic acid-181 and serine-222 in intermediate formation and hydrolysis of the mammalian protein-tyrosine-phosphatase ptp1. *Biochemistry*, 36(15), 4568–75.
57. Winterbourn, C. C. & Metodiewa, D. (1999). Reactivity of biologically important thiol compounds with superoxide and hydrogen peroxide. *Free Radic Biol Med*, 27(3-4), 322–8.
58. Sohn, J. & Rudolph, J. (2003). Catalytic and chemical competence of regulation of cdc25 phosphatase by oxidation/reduction. *Biochemistry*, 42(34), 10060–70.
59. Flint, A. J., Tiganis, T., Barford, D., & Tonks, N. K. (1997). Development of "substrate-trapping" mutants to identify physiological substrates of protein tyrosine phosphatases. *Proc Natl Acad Sci U S A*, 94(5), 1680–5.
60. Liu, F. & Chernoff, J. (1997). Protein tyrosine phosphatase 1b interacts with and is tyrosine phosphorylated by the epidermal growth factor receptor. *Biochem J*, 327 (Pt 1), 139–45.
61. Wu, Y., Kwon, K. S., & Rhee, S. G. (1998). Probing cellular protein targets of h2o2 with fluorescein-conjugated iodoacetamide and antibodies to fluorescein. *FEBS Lett*, 440(1-2), 111–5.
62. Lou, Y. W., Chen, Y. Y., Hsu, S. F., Chen, R. K., Lee, C. L., Khoo, K. H., ... Meng, T. C. (2008). Redox regulation of the protein tyrosine phosphatase ptp1b in cancer cells. *FEBS Journal*, 275(1), 69–88.
63. Haj, F. G., Markova, B., Klamann, L. D., Bohmer, F. D., & Neel, B. G. (2003). Regulation of receptor tyrosine kinase signaling by protein tyrosine phosphatase-1b. *J Biol Chem*, 278(2), 739–44.
64. Haj, F. G., Verveer, P. J., Squire, A., Neel, B. G., & Bastiaens, P. I. (2002). Imaging sites of receptor dephosphorylation by ptp1b on the surface of the endoplasmic reticulum. *Science*, 295(5560), 1708–11.

65. Lee, S. R., Kwon, K. S., Kim, S. R., & Rhee, S. G. (1998). Reversible inactivation of protein-tyrosine phosphatase 1b in a431 cells stimulated with epidermal growth factor. *J Biol Chem*, *273*(25), 15366–72.
66. Leslie, N. R., Bennett, D., Lindsay, Y. E., Stewart, H., Gray, A., & Downes, C. P. (2003). Redox regulation of pi 3-kinase signalling via inactivation of pten. *EMBO J*, *22*(20), 5501–10.
67. Maehama, T., Taylor, G. S., & Dixon, J. E. (2001). Pten and myotubularin: novel phosphoinositide phosphatases. *Annu Rev Biochem*, *70*, 247–79.
68. Lee, S. R., Yang, K. S., Kwon, J., Lee, C., Jeong, W., & Rhee, S. G. (2002). Reversible inactivation of the tumor suppressor pten by h₂o₂. *J Biol Chem*, *277*(23), 20336–42.
69. Kwon, J., Lee, S. R., Yang, K. S., Ahn, Y., Kim, Y. J., Stadtman, E. R., & Rhee, S. G. (2004). Reversible oxidation and inactivation of the tumor suppressor pten in cells stimulated with peptide growth factors. *Proc Natl Acad Sci U S A*, *101*(47), 16419–24.
70. Agazie, Y. M. & Hayman, M. J. (2003). Molecular mechanism for a role of shp2 in epidermal growth factor receptor signaling. *Mol Cell Biol*, *23*(21), 7875–86.
71. Paulsen, C. E., Truong, T. H., Garcia, F. J., Homann, A., Gupta, V., Leonard, S. E., & Carroll, K. S. (2012). Peroxide-dependent sulfenylation of the egfr catalytic site enhances kinase activity. *Nat Chem Biol*, *8*(1), 57–64.
72. Persson, C., Kappert, K., Engstrom, U., Ostman, A., & Sjoblom, T. (2005). An antibody-based method for monitoring in vivo oxidation of protein tyrosine phosphatases. *Methods*, *35*(1), 37–43.
73. Lambeth, J. D. (2004). Nox enzymes and the biology of reactive oxygen. *Nat Rev Immunol*, *4*(3), 181–9.
74. McCord, J. M. & Fridovich, I. (1969). Superoxide dismutase. an enzymic function for erythrocuprein (hemocuprein). *J Biol Chem*, *244*(22), 6049–55.
75. Hsu, J. L., Hsieh, Y., Tu, C., O'Connor, D., Nick, H. S., & Silverman, D. N. (1996). Catalytic properties of human manganese superoxide dismutase. *J Biol Chem*, *271*(30), 17687–91.
76. Babior, B. M., Lambeth, J. D., & Nauseef, W. (2002). The neutrophil nadph oxidase. *Archives of Biochemistry and Biophysics*, *397*(2), 342–4.
77. Suh, Y. A., Arnold, R. S., Lassegue, B., Shi, J., Xu, X., Sorescu, D., . . . Lambeth, J. D. (1999). Cell transformation by the superoxide-generating oxidase mox1. *Nature*, *401*(6748), 79–82.

78. Cheng, G., Cao, Z., Xu, X., van Meir, E. G., & Lambeth, J. D. (2001). Homologs of gp91phox: cloning and tissue expression of nox3, nox4, and nox5. *Gene*, *269*(1-2), 131–40.
79. De Deken, X., Wang, D., Many, M. C., Costagliola, S., Libert, F., Vassart, G., . . . Miot, F. (2000). Cloning of two human thyroid cdnas encoding new members of the nadph oxidase family. *J Biol Chem*, *275*(30), 23227–33.
80. Oh, H., Jung, H. Y., Kim, J., & Bae, Y. S. (2010). Phosphorylation of serine282 in nadph oxidase activator 1 by erk desensitizes egf-induced ros generation. *Biochem Biophys Res Commun*, *394*(3), 691–6.
81. Kroviarski, Y., Debbabi, M., Bachoual, R., Perianin, A., Gougerot-Pocidalò, M. A., El-Benna, J., & Dang, P. M. (2010). Phosphorylation of nadph oxidase activator 1 (nox1) on serine 282 by map kinases and on serine 172 by protein kinase c and protein kinase a prevents nox1 hyperactivation. *FASEB Journal*, *24*(6), 2077–92.
82. Chen, K., Kirber, M. T., Xiao, H., Yang, Y., & Keaney, J., J. F. (2008). Regulation of ros signal transduction by nadph oxidase 4 localization. *J Cell Biol*, *181*(7), 1129–39.
83. Fridovich, I. (1995). Superoxide radical and superoxide dismutases. *Annu Rev Biochem*, *64*, 97–112.
84. Gardner, P. R., Raineri, I., Epstein, L. B., & White, C. W. (1995). Superoxide radical and iron modulate aconitase activity in mammalian cells. *J Biol Chem*, *270*(22), 13399–405.
85. Juarez, J. C., Manuia, M., Burnett, M. E., Betancourt, O., Boivin, B., Shaw, D. E., . . . Donate, F. (2008). Superoxide dismutase 1 (sod1) is essential for h2o2-mediated oxidation and inactivation of phosphatases in growth factor signaling. *Proc Natl Acad Sci U S A*, *105*(20), 7147–52.
86. DeYulia, J., G. J., Carcamo, J. M., Borquez-Ojeda, O., Shelton, C. C., & Golde, D. W. (2005). Hydrogen peroxide generated extracellularly by receptor-ligand interaction facilitates cell signaling. *Proc Natl Acad Sci U S A*, *102*(14), 5044–9.
87. DeYulia, J., G. J. & Carcamo, J. M. (2005). Egf receptor-ligand interaction generates extracellular hydrogen peroxide that inhibits egfr-associated protein tyrosine phosphatases. *Biochem Biophys Res Commun*, *334*(1), 38–42.
88. Bienert, G. P., Schjoerring, J. K., & Jahn, T. P. (2006). Membrane transport of hydrogen peroxide. *Biochim Biophys Acta*, *1758*(8), 994–1003.
89. Bienert, G. P., Moller, A. L., Kristiansen, K. A., Schulz, A., Moller, I. M., Schjoerring, J. K., & Jahn, T. P. (2007). Specific aquaporins facilitate the diffusion of hydrogen peroxide across membranes. *J Biol Chem*, *282*(2), 1183–92.

90. Miller, E. W., Dickinson, B. C., & Chang, C. J. (2010). Aquaporin-3 mediates hydrogen peroxide uptake to regulate downstream intracellular signaling. *Proc Natl Acad Sci U S A*, *107*(36), 15681–6.
91. Wood, Z. A., Schroder, E., Robin Harris, J., & Poole, L. B. (2003). Structure, mechanism and regulation of peroxiredoxins. *Trends Biochem Sci*, *28*(1), 32–40.
92. Kang, S. W., Chae, H. Z., Seo, M. S., Kim, K., Baines, I. C., & Rhee, S. G. (1998). Mammalian peroxiredoxin isoforms can reduce hydrogen peroxide generated in response to growth factors and tumor necrosis factor- α . *J Biol Chem*, *273*(11), 6297–302.
93. Handy, D. E., Lubos, E., Yang, Y., Galbraith, J. D., Kelly, N., Zhang, Y. Y., . . . Loscalzo, J. (2009). Glutathione peroxidase-1 regulates mitochondrial function to modulate redox-dependent cellular responses. *J Biol Chem*, *284*(18), 11913–21.
94. Halvey, P. J., Watson, W. H., Hansen, J. M., Go, Y. M., Samali, A., & Jones, D. P. (2005). Compartmental oxidation of thiol-disulphide redox couples during epidermal growth factor signalling. *Biochem J*, *386*(Pt 2), 215–9.
95. Winterbourn, C. C. (2008). Reconciling the chemistry and biology of reactive oxygen species. *Nat Chem Biol*, *4*(5), 278–86.
96. Parsonage, D., Karplus, P. A., & Poole, L. B. (2008). Substrate specificity and redox potential of ahpc, a bacterial peroxiredoxin. *Proc Natl Acad Sci U S A*, *105*(24), 8209–14.
97. Peskin, A. V., Low, F. M., Paton, L. N., Maghzal, G. J., Hampton, M. B., & Winterbourn, C. C. (2007). The high reactivity of peroxiredoxin 2 with h(2)o(2) is not reflected in its reaction with other oxidants and thiol reagents. *J Biol Chem*, *282*(16), 11885–92.
98. Woo, H. A., Yim, S. H., Shin, D. H., Kang, D., Yu, D. Y., & Rhee, S. G. (2010). Inactivation of peroxiredoxin i by phosphorylation allows localized h(2)o(2) accumulation for cell signaling. *Cell*, *140*(4), 517–28.
99. Buhrow, S. A., Cohen, S., & Staros, J. V. (1982). Affinity labeling of the protein kinase associated with the epidermal growth factor receptor in membrane vesicles from a431 cells. *J Biol Chem*, *257*(8), 4019–22.
100. Clark, S. & Konstantopoulos, N. (1993). Sulphydryl agents modulate insulin- and epidermal growth factor (egf)-receptor kinase via reaction with intracellular receptor domains: differential effects on basal versus activated receptors. *Biochem J*, *292* (Pt 1), 217–23.
101. Woltjer, R. L. & Staros, J. V. (1997). Effects of sulfhydryl modification reagents on the kinase activity of the epidermal growth factor receptor. *Biochemistry*, *36*(32), 9911–6.

102. Seo, Y. H. & Carroll, K. S. (2009). Facile synthesis and biological evaluation of a cell-permeable probe to detect redox-regulated proteins. *Bioorg Med Chem Lett*, *19*(2), 356–9.
103. Reddie, K. G., Seo, Y. H., Muse Iii, W. B., Leonard, S. E., & Carroll, K. S. (2008). A chemical approach for detecting sulfenic acid-modified proteins in living cells. *Mol Biosyst*, *4*(6), 521–31.
104. Leonard, S. E., Reddie, K. G., & Carroll, K. S. (2009). Mining the thiol proteome for sulfenic acid modifications reveals new targets for oxidation in cells. *ACS Chem Biol*, *4*(9), 783–99.
105. Seo, Y. H. & Carroll, K. S. (2011). Quantification of protein sulfenic acid modifications using isotope-coded dimedone and iododimedone. *Angew Chem Int Ed Engl*, *50*(6), 1342–5.
106. Truong, T. H., Garcia, F. J., Seo, Y. H., & Carroll, K. S. (2011). Isotope-coded chemical reporter and acid-cleavable affinity reagents for monitoring protein sulfenic acids. *Bioorg Med Chem Lett*, *21*(17), 5015–20.
107. Leonard, S. E. & Carroll, K. S. (2011). Chemical 'omics' approaches for understanding protein cysteine oxidation in biology. *Curr Opin Chem Biol*, *15*(1), 88–102.
108. Benitez, L. V. & Allison, W. S. (1974). The inactivation of the acyl phosphatase activity catalyzed by the sulfenic acid form of glyceraldehyde 3-phosphate dehydrogenase by dimedone and olefins. *J Biol Chem*, *249*(19), 6234–43.
109. Saxon, E. & Bertozzi, C. R. (2000). Cell surface engineering by a modified Staudinger reaction. *Science*, *287*(5460), 2007–10.
110. Rostovtsev, V. V., Green, L. G., Fokin, V. V., & Sharpless, K. B. (2002). A step-wise Huisgen cycloaddition process: copper(i)-catalyzed regioselective "ligation" of azides and terminal alkynes. *Angew Chem Int Ed Engl*, *41*(14), 2596–9.
111. Zhang, J., Yang, P. L., & Gray, N. S. (2009). Targeting cancer with small molecule kinase inhibitors. *Nature Reviews. Cancer*, *9*(1), 28–39.
112. Singh, J., Petter, R. C., & Kluge, A. F. (2010). Targeted covalent drugs of the kinase family. *Curr Opin Chem Biol*, *14*(4), 475–80.
113. Singh, J., Petter, R. C., Baillie, T. A., & Whitty, A. (2011). The resurgence of covalent drugs. *Nat Rev Drug Discov*, *10*(4), 307–17.
114. Yun, C.-H., Mengwasser, K. E., Toms, A. V., Woo, M. S., Greulich, H., Wong, K.-K., . . . Eck, M. J. (2008). The T790M mutation in EGFR kinase causes drug resistance by increasing the affinity for ATP. *Proc Natl Acad Sci U S A*, *105*(6), 2070–2075.

115. Yun, C.-H., Boggon, T. J., Li, Y., Woo, M. S., Greulich, H., Meyerson, M., & Eck, M. J. (2007). Structures of lung cancer-derived egfr mutants and inhibitor complexes: mechanism of activation and insights into differential inhibitor sensitivity. *Cancer Cell*, *11*(3), 217–227.
116. Zhang, X., Gureasko, J., Shen, K., Cole, P. A., & Kuriyan, J. (2006). An allosteric mechanism for activation of the kinase domain of epidermal growth factor receptor. *Cell*, *125*(6), 1137–1149.
117. Jaffrey, S. R., Erdjument-Bromage, H., Ferris, C. D., Tempst, P., & Snyder, S. H. (2001). Protein s-nitrosylation: a physiological signal for neuronal nitric oxide. *Nat Cell Biol*, *3*(2), 193–7.
118. Jaffrey, S. R. & Snyder, S. H. (2001). The biotin switch method for the detection of s-nitrosylated proteins. *Sci STKE*, *2001*(86), pl1.
119. Wang, H. & Xian, M. (2011). Chemical methods to detect s-nitrosation. *Curr Opin Chem Biol*, *15*(1), 32–7.
120. Giustarini, D., Dalle-Donne, I., Colombo, R., Milzani, A., & Rossi, R. (2008). Is ascorbate able to reduce disulfide bridges? a cautionary note. *Nitric Oxide*, *19*(3), 252–8.
121. Estrada, C., Gomez, C., Martin-Nieto, J., De Frutos, T., Jimenez, A., & Villalobo, A. (1997). Nitric oxide reversibly inhibits the epidermal growth factor receptor tyrosine kinase. *Biochem J*, *326* (Pt 2), 369–76.
122. Murillo-Carretero, M., Torroglosa, A., Castro, C., Villalobo, A., & Estrada, C. (2009). S-nitrosylation of the epidermal growth factor receptor: a regulatory mechanism of receptor tyrosine kinase activity. *Free Radic Biol Med*, *46*(4), 471–9.
123. Lam, Y. W., Yuan, Y., Isaac, J., Babu, C. V., Meller, J., & Ho, S. M. (2010). Comprehensive identification and modified-site mapping of s-nitrosylated targets in prostate epithelial cells. *PLoS One*, *5*(2), e9075.
124. Glynn, S. A., Boersma, B. J., Dorsey, T. H., Yi, M., Yfantis, H. G., Ridnour, L. A., . . . Ambs, S. (2010). Increased nos2 predicts poor survival in estrogen receptor-negative breast cancer patients. *J Clin Invest*, *120*(11), 3843–54.
125. Switzer, C. H., Glynn, S. A., Cheng, R. Y., Ridnour, L. A., Green, J. E., Ambs, S., & Wink, D. A. (2012). S-nitrosylation of egfr and src activates an oncogenic signaling network in human basal-like breast cancer. *Mol Cancer Res*, *10*(9), 1203–15.
126. Penel, S., Hughes, E., & Doig, A. J. (1999). Side-chain structures in the first turn of the alpha-helix. *J Mol Biol*, *287*(1), 127–43.

127. Anderson, T. A. & Sauer, R. T. (2003). Role of an n(cap) residue in determining the stability and operator-binding affinity of arc repressor. *Biophys Chem*, *100*(1-3), 341–50.
128. Miranda, J. J. (2003). Position-dependent interactions between cysteine residues and the helix dipole. *Protein Sci*, *12*(1), 73–81.
129. Kemble, D. J. & Sun, G. (2009). Direct and specific inactivation of protein tyrosine kinases in the src and fgfr families by reversible cysteine oxidation. *Proc Natl Acad Sci U S A*, *106*(13), 5070–5.
130. Singh, J., Dobrusin, E. M., Fry, D. W., Haske, T., Whitty, A., & McNamara, D. J. (1997). Structure-based design of a potent, selective, and irreversible inhibitor of the catalytic domain of the erbb receptor subfamily of protein tyrosine kinases. *J Med Chem*, *40*(7), 1130–5.
131. Leonard, S. E., Garcia, F. J., Goodsell, D. S., & Carroll, K. S. (2011). Redox-based probes (rbps) for protein tyrosine phosphatases. *Angew Chem Int Ed Engl*, *in press*.

CHAPTER II

Isotope-Coded Chemical Reporter and Acid-Cleavable Affinity Reagents for Monitoring Protein Sulfenic Acids

2.1 Abstract

We have developed an approach that allows relative quantification of protein sulfenic acids using a pair of light and heavy isotope labeled probes, DAz-2 and d_6 -DAz-2. In conjunction with a new complementary acid-cleavable linker, Yn-ACL, we demonstrate that tagged peptides are successfully labeled, enriched, and fully characterized by LC-MS/MS analysis. Overall, this method can be applied to map sites of cysteine oxidation and compare protein sulfenylation in normal and disease states.

2.2 Introduction

Reactive oxygen species (ROS), such as hydrogen peroxide (H_2O_2), were once viewed as the inevitable toxic byproducts of aerobic existence, but increasing evidence indicates that ROS can act as secondary messengers in cellular signaling (1–3). Physiological events mediated by redox-signaling include cellular proliferation, differ-

entiation, and apoptosis, whereas uncontrolled ROS production can lead to pathological events such as cancer and age-associated degenerative disorders (4). Cells can detect changes in ROS homeostasis through selective oxidative modification of the thiol side chain of cysteine residues. These modifications can drastically alter protein structure and function. Of these, reversible modifications include disulfide bonds and sulfenic acids (RSOH). Sulfenic acids are the first oxoform formed as a result of thiolate oxidation. The sulfenic acid product can be stabilized by the protein environment, condense with other protein thiols to form an intra- or intermolecular disulfide bond, or become further oxidized to the sulfinic (RSO₂H) or sulfonic (RSO₃H) acids. Due to their switch-like nature, reversible thiol modifications represent a central mechanism to detect and regulate changes in the cellular redox balance (3, 5).

The discovery of regulatory cysteine switches, particularly sulfenic acids, has stimulated efforts to develop chemical tools to detect these post-translational modifications (6, 7). In large part, current methods are based on the selective reaction between 5,5-dimethyl-1,3-cyclohexanedione (dimedone) and sulfenic acids (8). To facilitate detection and isolation of sulfenylated proteins, we have recently developed bifunctional dimedone-based probes attached to an azide chemical reporter, known as DAz-1 and DAz-2 (**1**; Figure 2.1a) (9–12). After protein labeling, the reporter group is coupled to a biotinylated reagent via bioorthogonal ligation methods, such as the Staudinger ligation or Huisgen [3 + 2] cycloaddition (click chemistry) (13–15). Subsequent selection and enrichment by avidin affinity chromatography followed by streptavidin-HRP immunoblot or LC-MS/MS analysis permits visualization and identification of sulfenylated proteins (10). However, the identification of precise sites of cysteine oxidation and their quantification remains challenging, and is an active area of research.

Current proteomic methods utilize various approaches to profile and quantify cysteine oxidation. The OxICAT method, based on iodoacetamide analogue ICAT

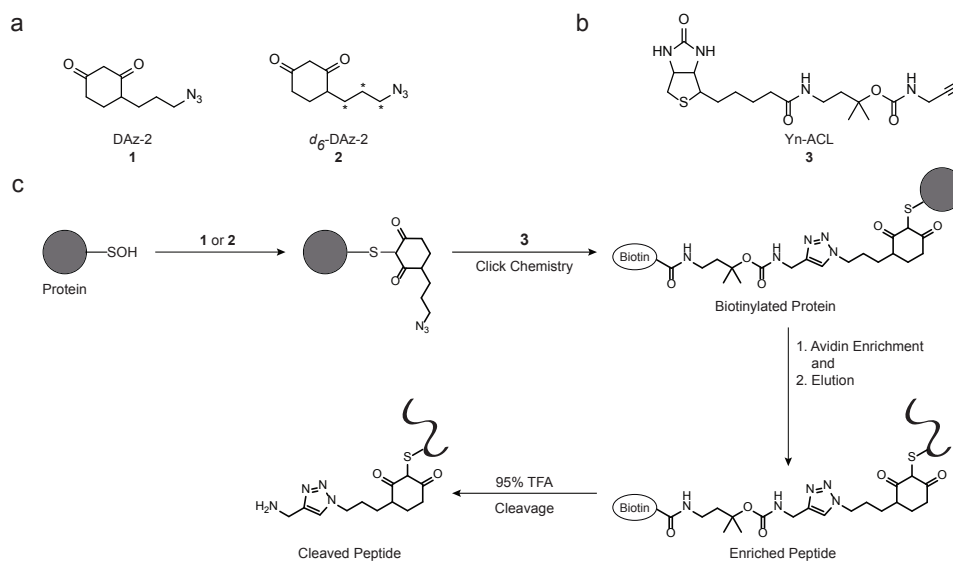


Figure 2.1: General strategy for labeling and enrichment of sulfenic acid-modified proteins and peptides. (a) Structures of DAz-2 (1) and d_6 -DAz-2 (2) azido-probes for detection of protein sulfenylation. (b) Structure of Yn-ACL (3), a biotinylated acid-cleavable linker with an alkyne handle. (c) Method for detection and enrichment. Proteins are labeled with either 1 or 2 and labeled proteins are coupled via click chemistry with 3. Biotinylated labeled samples are then enriched for using either avidin affinity cartridges or streptavidin-coated magnetic beads. Peptides are generated using in-gel or on-resin trypsin digestion. Enriched peptides are then eluted with 30% ACN + 0.4% TFA or guanidine HCl and detected by MS² analysis. Subsequently, enriched peptides are subjected to TFA cleavage to release the biotin moiety and are detected by MS² analysis.

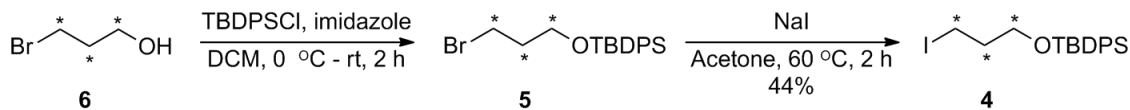
reagents and differential thiol trapping, permits quantification of protein disulfide bonds in cell lysates (16, 17). Weerapana *et al.* reported a method to detect low pKa cysteines using alkyne-functionalized iodoacetamide that can be conjugated to a TEV protease-cleavable affinity tag (18). Strategies based on d_5 -NEM have also been devised to detect cysteine oxidation (19). Despite these advances, none of these techniques are specifically suited to the investigation of sulfenic acid modifications. To address this issue, we have recently reported the ICDID method, which enables quantification of protein sulfenic acid modifications using isotope-labeled dimedone-based probes (20). Herein, we present a complementary strategy for the detection and relative quantification of protein sulfenic acid modifications that couples a new isotope-coded version of DAz-2 (2; Figure 2.1a) with release of the adduct from avidin using an acid-cleavable biotinylated tag (3; Figure 2.1b).

2.3 Results and Discussion

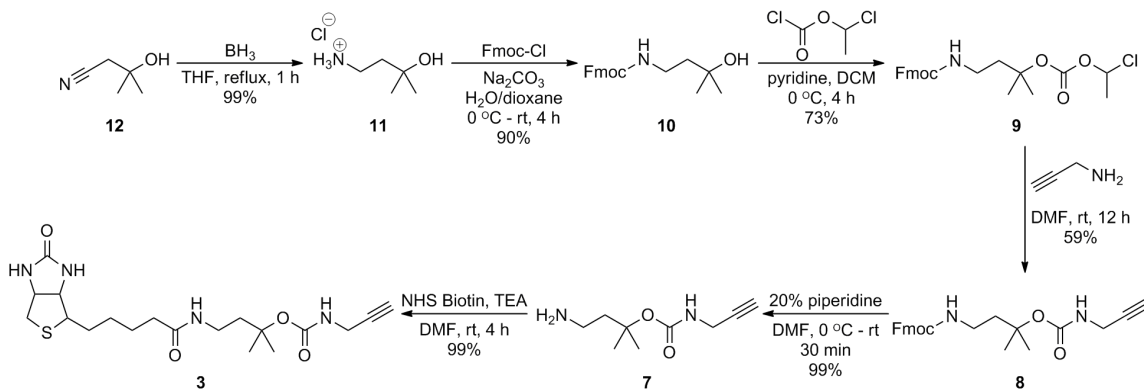
Our general approach for ratiometric quantification of protein sulfenylation follows the strategy outlined in Figure 2.1c: 1) sulfenylated proteins are covalently modified by DAz-2 (**1**) or d_6 -DAz-2 (**2**); 2) labeled proteins are then conjugated via click chemistry to Yn-ACL (**3**), a cleavable biotin conjugate with an alkyne handle; 3) biotinylated proteins or peptides generated via protease cleavage are enriched by avidin affinity cartridge or streptavidin-coated magnetic beads. Both methods yield biotinylated products that can be detected and characterized further by mass spectrometry (MS); 4) The biotin moiety can be cleaved with 95% trifluoroacetic acid (TFA), and the resulting peptides are detected by tandem mass spectrometry (MS²). Overall, this approach allows us to perform quantitative analysis of relative changes in protein sulfenic acid modifications.

The ratiometric method outlined above incorporates a set of isotope-coded ("light and heavy") sulfenic acid-specific probes. DAz-2 was prepared as previously reported (10). d_6 -DAz-2 was generated by coupling deuterated linker **4** (Scheme 2.1) with protected 1,3-cyclohexanedione (10). Compound **4** was synthesized according to known reactions, except that deuterated 3-bromopropanol (**6**) was utilized as the starting material (21). Selective protection of the primary alcohol with TBDPS increased the boiling point of compound **6**, facilitating purification in subsequent steps. Current methods to enrich and identify sulfenylated proteins rely heavily on biotinylated tags in order to enrich for proteins of interest. However, the biotin functional group can complicate the MS² analysis and subsequent database searching, especially for smaller peptides (22, 23). In some cases, particularly in complex peptide mixtures, it is ideal to remove the biotin tag after enrichment of labeled proteins or peptides, prior to MS analysis.

To facilitate large-scale proteomic analysis, a wide variety of cleavable linkers have been reported (24–27). Inspired by these approaches, we designed a cleavable biotiny-



Scheme 2.1: Synthesis of deuterated fragment for d_6 -DAz-2 (**2**)



Scheme 2.2: Synthesis of alkyne acid-cleavable linker (Yn-ACL) (**3**).

lated linker (Scheme 2.2) to use in conjunction with sulfenic acid probes **1** and **2**. The new reagent, termed Yn-ACL (**3**), is composed of three parts: 1) a biotin moiety, 2) a Boc-derivative cleavable by TFA, and 3) an alkyne group for bioorthogonal ligation. Borane reduction of 3-hydroxy-3-methyl butanenitrile (**12**) afforded amine (**11**) in high yield. To prevent undesirable side reactions in future steps, **11** was treated with Fmoc-Cl to give the protected amine (**10**). The hydroxy group in **10** was activated using base-mediated conditions with 1-chloroethyl chloroformate to give activated compound **9**. Subsequently, compound **9** was coupled to propargylamine in DMF to give the resulting carbamate (**8**). Deprotection of the carbamate (**8**) under mild basic conditions gave compound **7**. The final step of the synthesis was achieved by coupling NHS-activated biotin to compound **7** with TEA in DMF to give Yn-ACL (**3**) in 37% yield over 6 steps. Although a biotinylated linker incorporating the Boc group has been previously reported (24), it is important to note that Yn-ACL (**3**) represents an advance in several respects. In particular, the design of Yn-ACL (**3**) allows for a more straightforward synthesis and the spacer between the carbamate cleavage site and alkyne handle of Yn-ACL is minimal, which ensures a small mass tag (249 Da)

post-TFA cleavage to facilitate MS analysis.

C64S C82S Gpx3 (hereafter referred to as Gpx3), a double mutant of recombinant glutathione peroxidase Gpx3 from yeast (28), was selected as the model protein for subsequent studies. Gpx3 contains a catalytic cysteine at Cys36, which is oxidized to a sulfenic acid in the presence of H₂O₂. MS confirmed the intact mass of unmodified mutant Gpx3 as 22738.91 Da (Figure 2.2a). Next, we confirmed the mass of DAz-2-labeled Gpx3. The mutant protein was reacted with H₂O₂ and the oxidized cysteine labeled with DAz-2. Thereafter, azide-tagged protein was coupled to Yn-ACL via click chemistry. Intact MS analysis confirmed that oxidized Gpx3 was successfully labeled by DAz-2 and conjugated to Yn-ACL, corresponding to a molecular weight of 23352.65 Da (Figure 2.2b). Oxidation of Cys36 to sulfinic acid was also observed, as previously reported (20). Next, we evaluated the properties of the cleavable site on Yn-ACL (Figure 2.2c). Mutant Gpx3 was labeled employing the same conditions for intact mass analysis and then subjected to 95% TFA cleavage for 0 - 6 h at 25 °C or 37 °C. Streptavidin-HRP immunoblot analysis of the products showed a robust, DAz-2-dependent signal originating from Yn-ACL-tagged Gpx3. On the other hand, samples that were subjected to 95% TFA exhibited a reduction in signal over time, indicating successful cleavage of the biotin moiety. Complete loss of signal was observed at 4 h for samples subjected to cleavage at 25 °C, compared to 1 h for samples cleaved at 37 °C, demonstrating that cleavage is most efficient at 37 °C.

Having established the orthogonality of the cleavable biotinylation reagent, Yn-ACL, we next evaluated two methods of sample enrichment: 1) avidin affinity cartridge, and 2) streptavidin-coated magnetic beads. For the first approach, Gpx3 was biotinylated as illustrated in Figure 2.1c, subjected to in-gel trypsin digestion, and purified by avidin affinity cartridge. The MS spectrum corresponding to the input peptide sample is complex (Figure 2.3a) and indicates that trypsin digestion effectively covers 83% of the Gpx3 sequence (Figure 2.S1). Tagged Gpx3 peptide

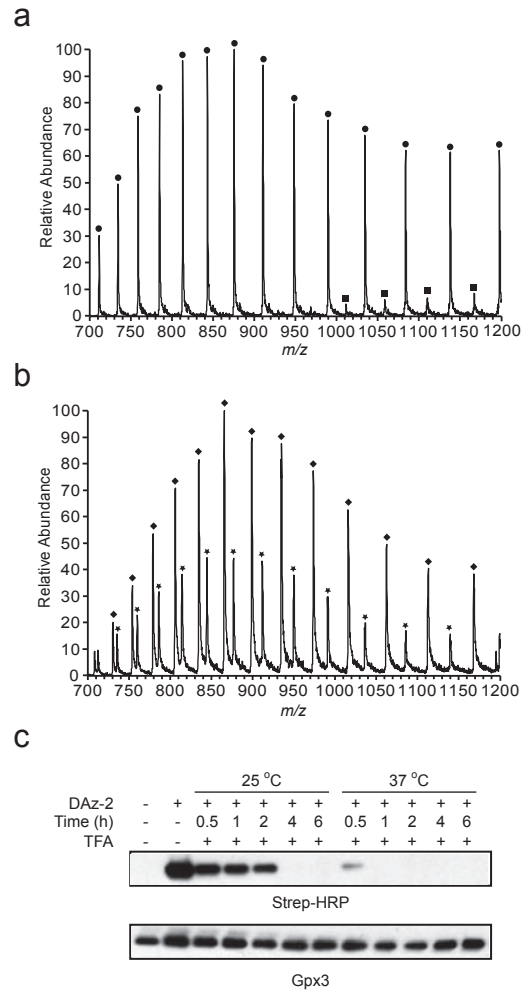


Figure 2.2: **Sulfenic acid modification is detected in model protein C64S C82S Gpx3 using DAz-2 and Yn-ACL.** (a) MS intact mass analysis shows that unmodified Gpx3 (●) corresponds to a molecular weight of 22738.91 Da. Gpx3 dimers (■) are also present. (b) MS intact mass analysis shows that DAz-2 and Yn-ACL labeled Gpx3 (◆) corresponds to a molecular weight of 23352.65 Da. 25 μ M Gpx3 was treated with 37.5 μ M H₂O₂ and labeled with 10 mM DAz-2 for 2 h at 37 °C. Afterwards, labeled protein was coupled via click chemistry with **3**. Over-oxidation of the catalytic cysteine to sulfinic acid (★) is also observed at 22776.79 Da. (c) Comparative analysis of TFA cleavage conditions of Gpx3 labeled protein. Labeled protein was subjected to 95% TFA cleavage for 0 - 6 h at 25 °C or 37 °C. Samples were resolved by SDS-PAGE and visualized by streptavidin-HRP Western blot. Equal protein loading was verified by re-probing with anti His-HRP.

(C*GFTPQYK) was eluted from the avidin column using 30% ACN/0.4% TFA in water (note that the Boc group is stable under these conditions) and analyzed by LC-MS/MS (Figure 2.3b). The molecular ion peak at $m/z = 765.16$ corresponds to peptide labeled by DAz-2 and conjugated to Yn-ACL, with the loss of one water molecule $[M + 2H - H_2O]^{+2}$; other charge states of the tagged peptide were also observed (Table 2.S1, Figure 2.S2a). After treatment of the biotinylated peptide with 95% TFA, the signal at $m/z = 765.16$ disappeared. Instead, a new signal at $m/z = 587.58$ was observed corresponding to the TFA-cleaved peptide, $[M + 2H - H_2O]^{+2}$ (Figure 2.S2b). Collision-induced dissociation (CID) tandem mass spectra of the aforementioned precursor ion confirmed the identity of the tagged peptide (Figure 2.3c, Table 2.S2).

Attempts to cleave biotinylated peptides directly from the avidin affinity cartridge (or streptavidin-coated magnetic beads) using 95% TFA resulted in leaching of avidin subunits into the sample, significantly complicating MS analysis (data not shown).

For the second enrichment method, biotinylated protein was captured on streptavidin-coated magnetic beads, submitted to on-resin trypsin digestion, and biotinylated peptide retained on the beads was eluted. To determine the best conditions for elution from the resin, we first evaluated recovery of biotinylated intact Gpx3 under various conditions via streptavidin-HRP immunoblot analysis (Figure 2.4a). Treatment with 30% ACN/0.4% TFA in water (v/v) at 25 °C or 37 °C afforded moderate recovery of the tagged protein; other temperatures were also explored (Figure 2.S3a), but did not provide satisfactory MS results due to the lack of efficient sample recovery (data not shown). Applied at a concentration of 8 M, guanidine HCl in water showed the best recovery of tagged protein, based on comparison of the input and eluent immunoblot signals. Additional experiments to evaluate the concentration-dependence of guanidine HCl elution show that 8 M affords maximal recovery (Figure 2.S3b). Control experiments showed that biotinylation of Gpx3 was dependent upon DAz-2

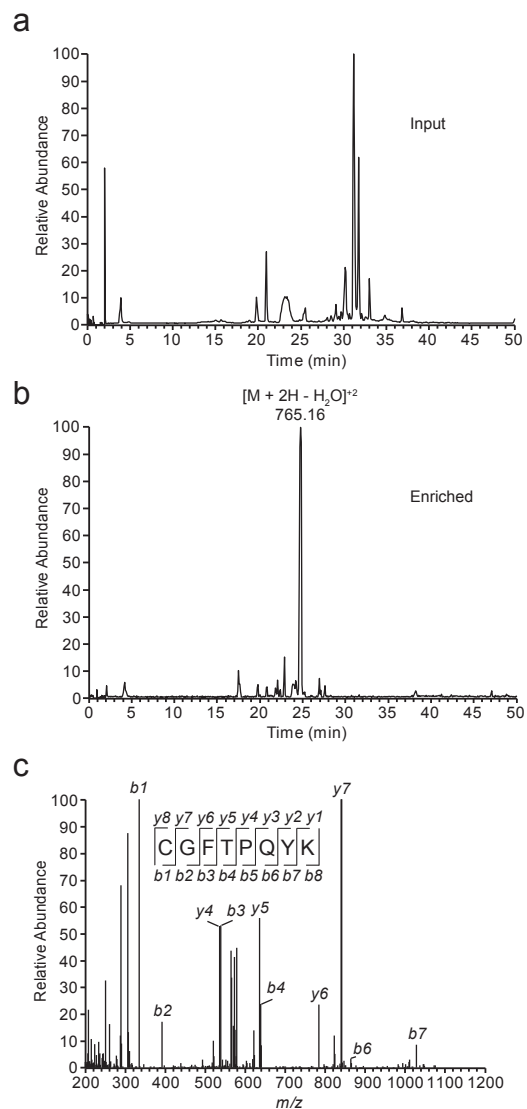


Figure 2.3: **Enrichment and ESI-LC/MS/MS analysis of sulfenic acid-modified C*GFTPQYK peptide from Gpx3 using avidin affinity cartridges.** Samples were generated as in Figure 2.2. After trypsin digestion, biotinylated peptides were enriched for using avidin affinity cartridges. (a) MS scan of input peptides. (b) MS scan of enriched sulfenic acid-modified peptides. m/z 765.16 corresponds to intact sulfenic acid-modified peptides with the loss of water, $[M + 2H - H_2O]^{+2}$. (c) MS² spectra of TFA cleaved sulfenic acid-modified peptides after CID of the precursor ion m/z 587.36 $[M + 2H - H_2O]^{+2}$.

and that the biotin moiety was effectively cleaved by $\geq 10\%$ (v/v) TFA (Figure 2.4a), as indicated by the absence of immunoblot signal. In subsequent experiments, biotin-tagged Gpx3 was enriched on streptavidin-coated magnetic beads and digested on-resin with trypsin. The MS scan of supernatant from the trypsin reaction is complex and demonstrates complete sample digestion (Figure 2.4b). The resin was washed ex-

tensively to remove unbiotinylated products; retained peptides were then eluted with 8 M guanidine HCl and analyzed by MS² (Figure 2.4c). The molecular ion peak at $m/z = 765.11$ corresponds to peptide labeled by DAz-2 and conjugated to Yn-ACL, with the loss of one water molecule $[M + 2H - H_2O]^{+2}$; other charge states of the tagged peptide were also observed (Figure 2.S4a, Table 2.S1). After TFA cleavage, the emergence of a new signal at $m/z = 587.61$ indicates successful cleavage of the biotin moiety (Figure 2.S4b). The MS² spectra of TFA-cleaved peptide after CID shows complete mapping of the expected product (Figure 2.4d, Table 2.S2). Collectively, our characterization of both enrichment methods by LC-MS/MS demonstrates that the biotin-tagged Gpx3 peptide is successfully enriched, eluted, and that the biotin moiety can be separated by TFA treatment. The flexibility of our method provides options for other model systems that may be more ideally suited for one type of enrichment method over the other.

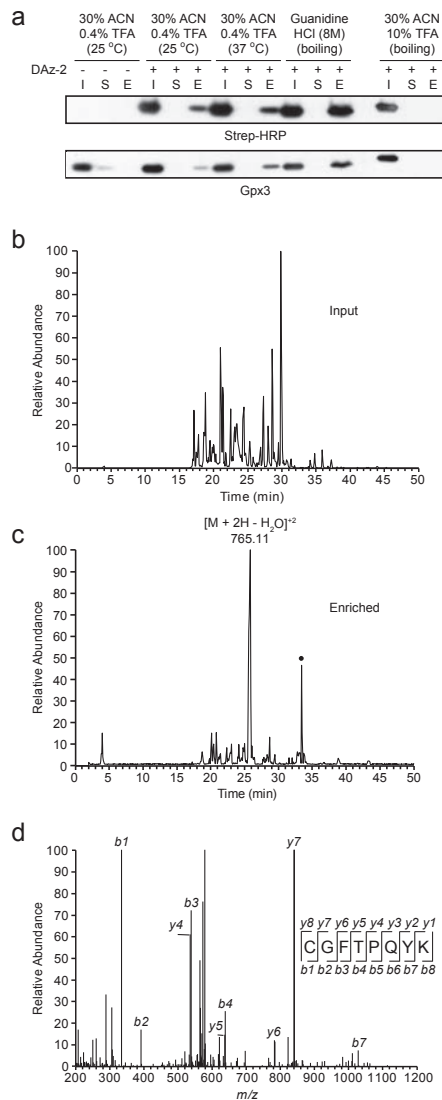


Figure 2.4: **Enrichment and ESI-LC/MS/MS analysis of sulfenic acid-modified C*GFTPQYK peptide from Gpx3 using streptavidin-coated magnetic beads.** Samples were generated as in Figure 2.2. Biotinylated proteins were enriched for using streptavidin-coated magnetic beads and peptides were generated by on-resin trypsin digestion. (a) Comparison of streptavidin-coated magnetic bead elution conditions. Enriched Gpx3 labeled protein was eluted using either 30% ACN + 0.4% TFA at 25 °C or 37 °C, boiling with guanidine HCl (8 M) pH 1.2, or boiling with 30% ACN + 10% TFA for 15 min. I = input, S = supernatant, and E = eluent. (b) MS scan of on-resin trypsin digested supernatant. (c) MS scan of enriched sulfenic acid-modified peptides. m/z 765.11 corresponds to the intact sulfenic acid-modified peptide with the loss of water, $[M + 2H - H_2O]^{+2}$ and m/z 531.38 (•) corresponds to TBTA, $[M + H]^+$. (d) MS² spectra of TFA cleaved sulfenic acid-modified peptides after CID of the precursor ion m/z 587.32 $[M + 2H - H_2O]^{+2}$.

Finally, we applied the strategy outlined in Figure 2.5a to quantify the relative amounts of oxidized Gpx3 in two different samples. In the first sample, Gpx3 was oxidized with 0.1 eq. H_2O_2 and labeled with d_0 -DAz-2 or treated with 1.5 eq. H_2O_2 and labeled with d_6 -DAz-2. In subsequent steps, heavy and light DAz-2 probes were removed with gel filtration spin columns, and the protein samples were combined. Tagged Gpx3 was ligated to Yn-ACL, enriched by avidin affinity cartridge or streptavidin-coated magnetic beads, and peptides were analyzed by LC-MS/MS. Based on our experimental design, we anticipated that the ratio and intensity of d_6 -DAz-2-labeled peptide would be higher relative to the d_0 -DAz-2-treated sample. The resulting data from each enrichment method, represented as extracted ion chromatograms (Figure 2.5b and Figure 2.5d) and single MS scans (Figure 2.5c and Figure 2.5e), are consistent with this expectation and indicate that the ratio of d_0 -DAz-2: d_6 -DAz-2-tagged peptide is 1:2. The molecular ion peak at $m/z = 765$ and 768 correspond to peptides labeled with d_0 or d_6 -DAz-2 and conjugated to Yn-ACL, with the loss of one water molecule $[\text{M} + 2\text{H} - \text{H}_2\text{O}]^{+2}$. The observed difference of 3 Da between these ions represents the expected mass change for the +2 charge state and further MS² analysis was carried out to confirm the identity of these substituents (Figure 2.S5a and Figure 2.S5b). The inset of Figure 2.5e shows the expected decrease in the heavy-light ratio as the concentration of H_2O_2 was increased in d_0 -DAz-2-treated samples.

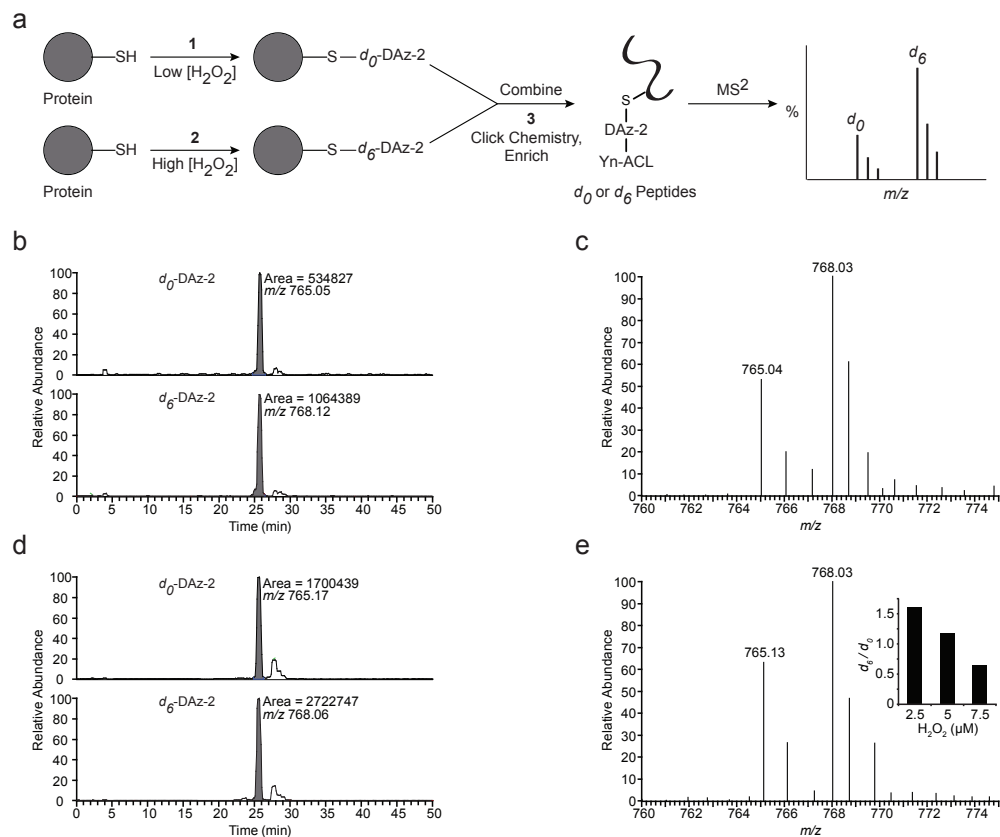


Figure 2.5: Relative quantification of Gpx3 sulfenic acid modification. (a) General scheme for labeling strategy. Parallel samples of 25 μM Gpx3 were treated with low or high concentrations of H_2O_2 and labeled with 10 mM d_0 or d_6 -DAz-2 for 2 h at 37 $^{\circ}C$. Samples were combined and ligated via click chemistry with **3** and enriched with avidin affinity cartridges or streptavidin-coated magnetic beads. The enriched peptides were then subjected to LC-MS/MS analysis. (b) Extracted ion chromatogram and (c) MS scan of avidin affinity cartridge-enriched peptides. (d) Extracted ion chromatogram and (e) MS scan of bead-enriched peptides. The extracted ion chromatograms of m/z 765 and 768 $[M + 2H - H_2O]^{+2}$ correspond to peptides tagged with d_0 or d_6 -DAz-2 and conjugated to Yn-ACL. The observed difference of 3 Da between these ions represents the expected mass change for the +2 charge state. The d_0 -DAz-2: d_6 -DAz-2 ratios, determined by taking the areas under the curves, are 1:2 for avidin affinity cartridge enriched peptides and 1:1.6 for streptavidin-coated magnetic bead enriched peptides. The bar graph inset shows d_6/d_0 ratios for modified peptides stimulated with increasing concentrations of H_2O_2 (2.5, 5, or 7.5 μM) are 1:1.6, 1:1.2, and 1:0.65 respectively.

2.4 Conclusions

To summarize, we have presented a new approach that allows relative quantification of protein sulfenic acid modifications. This method utilizes a set of light and heavy sulfenic acid-specific probes and a complementary acid-cleavable linker to label and enrich tagged peptides. Using the prototype thiol peroxidase, Gpx3, we demonstrate that the biotinylation reagent, Yn-ACL is orthogonal to DAz-2. Biotin-tagged peptides can be enriched via avidin affinity cartridge or streptavidin-coated magnetic beads, cleaved with TFA to remove the biotin moiety, and subjected to LC-MS/MS analysis. A key feature of this approach is that it facilitates mapping the specific site of cysteine oxidation. Additionally, we show that the isotope probe pair, d_0 -DAz-2 and d_6 -DAz-2, can be used to monitor relative changes in protein oxidation. Together, these studies set the stage for global profiling of sulfenic acid formation in H_2O_2 -mediated signaling pathways and disease states associated with oxidative stress.

2.5 Contributions

T.H.T. and Y.H.S. performed synthetic experiments. T.H.T. performed biological experiments. F.J.G. performed mass spectrometry experiments. K.S.C., T.H.T., F.J.G., and Y.H.S. designed experimental strategies.

2.6 Supplementary Methods

General Experimental. All reactions were performed under an argon atmosphere in oven-dried glassware. Methylene chloride was distilled over calcium hydride and tetrahydrofuran was distilled over sodium hydride prior to use. Reagents and solvents were purchased from Sigma or other commercial sources and were used without further purification. Analytical thin layer chromatography (TLC) was carried

out using Analtech Uniplate silica gel plates and visualized using a combination of UV, ceric ammonium molybdate, ninhydrin, and potassium permanganate staining. Flash chromatography was performed using silica gel (32-63 μM , 60 \AA pore size) from Sorbent Technologies Incorporated. NMR spectra were obtained on a Bruker Avance 400 (400 MHz for ^1H ; 100 MHz for ^{13}C). ^1H and ^{13}C NMR chemical shifts are reported in parts per million (ppm) referenced to the residual solvent peak. Low-resolution electrospray ionization (ESI) mass spectra were obtained with an Agilent 6120 Single Quadrupole LC/MS.

Experimental Procedures and Spectroscopic Data

Synthesis of Deuterated Fragment for $d_6\text{-DAz-2}$. Compound **4** was synthesized according to established literature procedures, except deuterated 3-bromopropanol was used; physical properties were consistent with previously reported values (21).

Synthesis of Alkyne Acid-Cleavable Linker (Yn-ACL). Compound **11**. In an oven-dried round bottom flask purged with argon, 3-hydroxy-3-methyl-butanenitrile (1.24 mL, 12.00 mmol) was dissolved in THF (30 mL). 1M $\text{BH}_3\text{-THF}$ complex (36.00 mL, 36.00 mmol) was added to the reaction at 0 $^\circ\text{C}$. The resulting solution was heated to reflux for 1 h, cooled to 0 $^\circ\text{C}$, and quenched with MeOH. 1M HCl (36 mL) was added to the reaction mixture, refluxed for 1 h, and the solution was concentrated *in vacuo* to provide compound **11** (1660 mg, 11.89 mmol) in 99% yield as a white solid. ^1H NMR (MeOD, 400 MHz): δ 3.06 (t, $J = 7.2$ Hz, 2H), 1.77 (t, $J = 7.2$ Hz, 2H), 1.25 (s, 6H). ^{13}C NMR (MeOD, 100 MHz): δ 70.66, 40.63, 37.45, 29.45.

Compound **10**. Compound **11** (1700 mg, 12.2 mmol) was added to a solution of Na_2CO_3 (3879 mg, 36.6 mmol) dissolved in H_2O (40 mL) and 1,4-dioxane (30 mL) and cooled to 0 $^\circ\text{C}$ with an ice bath. To the resulting solution, Fmoc-Cl (3492 mg, 13.5 mmol) in 1,4-dioxane (10 mL) was added dropwise. The temperature was slowly brought up to rt and the reaction was allowed to stir for 4 h. After completion of the reaction, the reaction mixture was extracted with DCM (3 x 50 mL), washed with

brine (50 mL), dried over MgSO_4 , and concentrated *in vacuo*. The crude residue was purified by silica gel chromatography, eluting with 1:9 ethyl acetate: dichloromethane to yield compound **10** (3569 mg, 11.0 mmol) in 90% yield as a white solid. R_f : 0.13 (1:9 ethyl acetate: dichloromethane). ^1H NMR (CDCl_3 , 400 MHz): δ 7.77 (d, $J = 7.6$ Hz, 2H), 7.61 (d, $J = 7.6$ Hz, 2H), 7.40 (t, $J = 7.6$ Hz, 2H), 7.31 (td, $J = 7.6$ Hz, 1.2 Hz, 2H), 4.40 (d, $J = 4.4$ Hz, 2H), 4.22 (t, $J = 6.8$ Hz, 1H), 3.36 (t, $J = 6.0$ Hz, 2H), 1.69 (t, $J = 6.8$ Hz, 2H), 1.26 (s, 6H). ^{13}C NMR (CDCl_3 , 100 MHz): δ 156.56, 144.06, 141.32, 127.65, 127.04, 125.08, 119.96, 70.87, 66.59, 47.34, 42.18, 37.43, 29.71. ESI-LRMS calcd. for $\text{C}_{20}\text{H}_{23}\text{NO}_3$ (M+H) 326.4, found 326.2.

Compound **9**. In an oven dried round bottom flask, compound **10** (1000 mg, 3.08 mmol) was dissolved in DCM (40 mL). 1-chloroethyl chloroformate (0.43 mL, 4.00 mmol) was added dropwise and the reaction mixture was cooled to 0 °C. To the resulting solution, dry pyridine (0.37 mL, 4.63 mmol) was added dropwise slowly and the reaction was allowed to stir at 0 °C for 4 h. After completion of the reaction, 0.5M HCl (50 mL) was added and the reaction mixture was extracted with DCM (3 x 30 mL). The organic layers were combined, washed with brine (30 mL), dried over MgSO_4 , and concentrated *in vacuo*. The crude residue was purified by silica gel chromatography, eluting with 1:2 ethyl acetate: hexane to yield compound **9** (968 mg, 2.24 mmol) in 73% yield as a white solid. R_f : 0.43 (1:2 ethyl acetate: hexane). ^1H NMR (CDCl_3 , 400 MHz): δ 7.77 (d, $J = 7.6$ Hz, 2H), 7.60 (d, $J = 7.6$ Hz, 2H), 7.40 (t, $J = 7.6$ Hz, 2H), 7.32 (t, $J = 7.6$ Hz, 2H), 6.39 (q, $J = 5.6$ Hz, 1H), 4.41 (d, $J = 6.8$ Hz, 2H), 4.21 (t, $J = 6.8$ Hz, 1H), 3.32 (q, $J = 6.8$ Hz, 2H), 2.03 (t, $J = 7.2$ Hz, 2H), 1.81 (d, $J = 6.0$ Hz, 2H), 1.54 (s, 6H). ^{13}C NMR (CDCl_3 , 100 MHz): δ 156.32, 150.82, 143.95, 141.33, 127.69, 127.05, 125.04, 119.99, 84.88, 84.14, 66.65, 47.29, 40.32, 36.60, 25.67, 25.17. ESI-LRMS calcd. for $\text{C}_{23}\text{H}_{26}\text{ClNO}_5$ (M+Na⁺) 454.9, found 454.1.

Compound **8**. In a round bottom flask, compound **9** (500 mg, 1.16 mmol) was

dissolved in dry DMF (19 mL). In a separate flask, propargyl amine (0.15 mL, 2.32 mmol) was dissolved in dry DMF (1 mL) and then added dropwise to the reaction mixture. The resulting solution was allowed to stir at rt for 12 h. After completion of the reaction, EtOAc (50 mL) was added and the reaction mixture was extracted with H₂O (5 x 20 mL). The organic layer was washed with brine (20 mL), dried with MgSO₄, filtered, and concentrated *in vacuo* to yield a clear orange oil. The crude residue was purified by silica gel chromatography, eluting with 1:3 ethyl acetate: hexane to yield compound **8** (277 mg, 0.68 mmol) in 59% yield as a pale yellow solid. R_f: 0.10 (1:3 ethyl acetate: hexane). ¹H NMR (CDCl₃, 400 MHz): δ 7.77 (d, *J* = 7.6 Hz, 2H), 7.60 (d, *J* = 7.2 Hz, 2H), 7.40 (t, *J* = 7.6 Hz, 2H), 7.32 (t, *J* = 7.6 Hz, 2H), 4.41 (d, *J* = 6.8 Hz, 2H), 4.21 (t, *J* = 6.8 Hz, 1H), 3.89 (s, 2H), 3.31-3.29 (m, 2H), 2.20 (t, *J* = 2.4 Hz, 1H), 2.01 (t, *J* = 6.4 Hz, 2H), 1.48 (s, 6H). ¹³C NMR (CDCl₃, 100 MHz): δ 156.35, 155.10, 143.98, 141.34, 127.68, 127.04, 125.02, 119.98, 80.98, 79.89, 71.44, 66.56, 47.31, 40.64, 36.78, 30.43, 26.53. ESI-LRMS calcd. for C₂₄H₂₆N₂O₄ (M+Na⁺) 429.4, found 429.2.

Compound **7**. In a round bottom flask, compound **8** (200 mg, 0.49 mmol) was dissolved in dry DMF (2 mL) and cooled to 0 °C. Piperidine (0.5 mL) was added to the reaction and the resulting solution was brought up to rt and allowed to stir for 30 min. After completion of the reaction, the reaction mixture was concentrated *in vacuo* to yield compound **7** (90 mg, 0.49 mmol) in 99% yield. ESI-LRMS calcd. for C₉H₁₆N₂O₂ (M+Na⁺) 207.4, found 207.1.

Alkyne Acid-Cleavable Linker (Yn-ACL) **3**. In a round bottom flask, a mixture of compound **7** (90 mg, 0.49 mmol) and NHS biotin (201 mg, 0.59 mmol) was dissolved in DMF (5 mL). TEA (0.20 mL, 1.47 mmol) was added to the reaction and the resulting solution was stirred at rt for 4 h. After completion of the reaction, the reaction mixture was concentrated *in vacuo*. The crude residue was purified by silica gel chromatography, eluting with 1:9 methanol: ethyl acetate to yield compound **3**

(200 mg, 0.49 mmol) in 99% yield as a golden brown solid. R_f : 0.09 (1:9 methanol: ethyl acetate). ^1H NMR (CDCl_3 , 400 MHz): δ 4.49-4.46 (m, 1H), 4.29-4.26 (m, 1H), 3.85 (s, 2H), 3.49 (dt, $J = 53.2$ Hz, 5.2 Hz, 1H), 3.29-3.27 (m, 2H), 3.13-3.08 (m, 1H), 2.85 (dd, $J = 12.8$ Hz, 4.8 Hz, 1H), 2.72 (d, $J = 9.2$ Hz, 1H), 2.15 (dt, $J = 64.4$ Hz, 7.6 Hz, 2H), 1.95-1.92 (m, 2H), 1.72-1.67 (m, 2H), 1.65-1.57 (m, 2H), 1.53-1.48 (m, 2H), 1.39 (s, 6H). ^{13}C NMR (CDCl_3 , 100 MHz): δ 171.38, 164.46, 155.54, 81.01, 80.24, 71.28, 62.10, 60.25, 55.59, 40.58, 36.30, 35.99, 32.90, 28.50, 28.07, 26.70, 25.69, 24.50. ESI-LRMS calcd. for $\text{C}_{19}\text{H}_{30}\text{N}_4\text{O}_4\text{S}$ ($\text{M}+\text{Na}^+$) 433.5, found 433.3.

Stock Solutions. DAz-2 and d_6 -DAz-2 stocks were made up to a final concentration of 250 mM in a 70:30 mixture of DMSO and 500 mM Bis-Tris HCl pH 7.4. Yn-ACL stock was made up to a final concentration of 5 mM in DMSO. All reagents were added directly to purified protein samples.

Cloning, Expression, and Purification of Recombinant Gpx3. Recombinant C64S C82S Gpx3 protein was expressed and purified as described previously (28).

DAz-2 Labeling of C64S C82S Gpx3. C64S C82S Gpx3 (hereafter referred to as Gpx3) was previously stored in 50 mM Tris HCl pH 7.4, 300 mM NaCl, 10% glycerol, and 5 mM DTT. DTT was removed from Gpx3 *via* spin filtration using P-30 micro BioSpin columns (BioRad) buffer exchanged into Gpx3 buffer (50 mM Tris HCl pH 7.4, 300 mM NaCl). 25 μM Gpx3 was labeled with 10 mM DAz-2 and treated with 37.5 μM H_2O_2 for 2 h at 37 $^\circ\text{C}$ while rocking. Small molecules were removed by passing the reactions through two consecutive P-30 columns.

Detection of DAz-2 Labeled Proteins Using Click Chemistry. Probe modified proteins were detected *via* bioorthogonal Huisgen [3 + 2] cycloaddition (click chemistry). The protein samples were buffer exchanged into click labeling buffer (50 mM triethanolamine pH 7.4, 1% SDS). The samples were incubated with Yn-ACL (100 μM), TCEP (1 mM), TBTA (100 μM), and CuSO_4 (1 mM) and allowed to react for 1 h at rt while rocking. Click chemistry reactions were passed through two

consecutive P-30 columns to remove small molecules.

ESI-LC/MS Analysis of Intact Gpx3 Labeled with DAz-2 and Yn-ACL. Gpx3 was labeled with DAz-2 and Yn-ACL as previously described above. The intact protein sample was analyzed on an electrospray linear ion trap mass spectrometer (LTQ-XL, Thermo Scientific) after separation on an Agilent Eclipse XDB-C8 2.1 mm x 15 mm trap with mobile phases A (0.1% formic acid in water) and B (0.1% formic acid in acetonitrile) which was used to trap, desalt, and elute proteins onto a Varian 2.1 mm x 50 mm 5 μ m PLRP-S C18 column with a gradient of 5% to 100% B in 14 min at a flow rate of 200 μ L/min.

TFA Cleavage Conditions of Yn-ACL Labeled Proteins. The biotin moiety of Yn-ACL was cleaved from biotinylated protein samples using a cleavage cocktail (95% TFA, 2% TIS). The samples were subjected to cleavage conditions for 0 - 6 h at rt or 37 °C while rocking. Afterwards, the cleavage cocktail was removed *via* vacuum centrifugation. The samples were analyzed by immunoblot as described below.

Immunoblot. Protein samples were resuspended in SDS protein loading buffer containing 10% 2- β ME. The samples were separated by SDS-PAGE using Mini-Protean TGX 4-15% Tris-Glycine gels (BioRad) and transferred to a polyvinylidene difluoride (PVDF) membrane (BioRad). After transfer, the PVDF membrane was blocked with 3% BSA for 1 h at rt. The membrane was washed with TBST (2 x 10 min) and then incubated with 1:80,000 streptavidin-HRP (GE Healthcare). PVDF membrane was washed with TBST (2 x 10 min) and then developed with chemiluminescence (GE Healthcare ECL Plus Western Blot Detection System) and imaged by film. To verify equal protein loading, His-tag of Gpx3 protein was probed with 1:100,000 His-HRP (Thermo Scientific). Membranes were routinely stained with Ponceau S to assess quality of protein transfer and loading.

In-Gel Trypsin Digestion of Biotinylated Labeled Proteins. Gpx3 was labeled with DAz-2 and Yn-ACL as described above and exchanged into 25 mM

ammonium bicarbonate, pH 8.3 (Ambic). The samples were concentrated *via* vacuum centrifugation and separated by SDS-PAGE. The SDS-PAGE gel was rinsed with H₂O and then stained with SimplyBlue SafeStain (Invitrogen). After staining, the gels were washed with H₂O and bands of interest were excised. The excised bands were dehydrated in 2:1 ACN: 25 mM Ambic, and subsequently rehydrated with 25 mM Ambic twice prior to reducing with 10 mM DTT for 1 h at 56 °C. DTT was removed, and the samples were alkylated with 55 mM iodoacetamide for 45 min at rt in the dark. Iodoacetamide was removed, and the excised bands were washed with 25 mM Ambic and then dehydrated and rehydrated two additional times. Sequencing grade modified trypsin (Promega), at a ratio of 1: 25 (w/w), was added to the excised bands and incubated overnight at 37 °C. Peptides were extracted from the gel by collecting the supernatant and by dehydrating and rehydrating the excised bands. Peptide samples were concentrated *via* vacuum centrifugation.

Avidin Affinity Cartridge Enrichment of Biotinylated Labeled Peptides. Biotinylated labeled peptides generated from the in-gel trypsin digestion described above were enriched for using the Cleavable ICAT Reagent Kit for Protein Labeling (Applied Biosystems) according to the manufacturer's instructions.

ESI-LC/MS/MS Analysis of Gpx3 Peptides Labeled with DAz-2 and Yn-ACL. Gpx3 peptides were labeled with DAz-2 and Yn-ACL, and enriched for using avidin affinity cartridges as previously described or streptavidin-coated magnetic beads as described below. The peptide samples were analyzed on an electrospray linear ion trap mass spectrometer (LTQ-XL, Thermo Scientific) after separation on an Agilent Eclipse XDB-C8 2.1 mm x 15 mm trap with mobile phases A (0.1% formic acid in water) and B (0.1% formic acid in acetonitrile) which was used to trap, desalt, and elute proteins onto a Vydac Everest reverse-phase C18 monomeric column (2.1 mm x 150 mm, 300 Å, 5 μm) with a gradient of 5% to 60% B in 60 min at a flow rate of 200 μL/min.

TFA Cleavage of Biotinylated Peptide Samples for MS Analysis. The biotin moiety of Yn-ACL was cleaved from biotinylated peptide samples using a cleavage cocktail (95% TFA, 2% TIS). The samples were subjected to cleavage conditions for 1 h at 37 °C while rocking. Afterwards, the cleavage cocktail was removed *via* vacuum centrifugation. Cleaved peptide samples were resuspended in 0.1% formic acid and subjected to MS analysis.

Streptavidin-Coated Magnetic Bead Enrichment of Biotinylated Labeled Proteins. Gpx3 was labeled with DAZ-2 and Yn-ACL as described above and exchanged into phosphate buffered saline (PBS). Protein samples were enriched for using MagnaBind Streptavidin (Thermo Scientific) magnetic beads. Samples were incubated with the beads for 1 h at rt with rocking. After enrichment, the beads were washed three times with PBS (500 μ l, 5 min)

Elution Conditions for Streptavidin-Coated Magnetic Beads Elution Comparison. Biotinylated labeled Gpx3 was enriched using streptavidin-coated magnetic beads as described above. Enriched protein was eluted with 30% ACN/0.4% TFA in water for 15 min at 25 °C or 37 °C, boiling with 30% ACN/10% TFA in water, or boiling with 8M guanidine HCl in water. Samples were analyzed by immunoblot as described above.

Elution Conditions for Temperature-Dependent Study of 30% ACN Elution for Streptavidin-Coated Magnetic Beads. Biotinylated labeled Gpx3 was enriched using streptavidin-coated magnetic beads as described above. Enriched protein was eluted with 30% ACN/0.4% TFA in water for 15 min at 37 °C, 60 °C, or boiling. Samples were analyzed by immunoblot as described above.

Elution Conditions for Concentration-Dependent Study of Guanidine HCl Elution for Streptavidin-Coated Magnetic Beads. Biotinylated labeled Gpx3 was enriched using streptavidin-coated magnetic beads as described above. Enriched protein was eluted by boiling with 1, 4, or 8M guanidine HCl. Samples

were analyzed by immunoblot as described above.

On-Resin Trypsin Digestion of Enriched Biotinylated Labeled Proteins. Biotinylated Gpx3 was enriched using streptavidin-coated magnetic beads as described above. After enrichment, the beads were washed three times with PBS (500 μ l, 5 min) and resuspended in 2M urea in 25 mM Ambic pH 8.3. Sequencing grade modified trypsin (Promega), at a ratio of 1: 25 (w/w), was added to the beads and incubated overnight at 37 °C. The next day, the beads were washed three times with 2M urea in 25 mM Ambic pH 8.3 and three times with 25 mM Ambic pH 8.3 (500 μ l, 5 min). The enriched peptides were eluted by boiling with 8M guanidine HCl for 15 min. The peptide samples were de-salted by passing through a MacroSpin C18 column (Nest Group), concentrated *via* vacuum centrifugation, resuspended in 0.1% formic acid, and subjected to MS analysis.

Ratiometric Quantification of Sulfenic Acid Modifications Using DAz-2 and d_6 -DAz-2. Parallel samples of Gpx3 were subjected to two labeling conditions: (1) 25 μ M Gpx3 treated with 10 mM d_6 -DAz-2 and 37.5 μ M H₂O₂ or (2) 25 μ M Gpx3 treated with 10 mM d_0 -DAz-2 and 2.5 μ M H₂O₂ for 2 h at 37 °C. The samples were passed through two consecutive P-30 columns to remove excess small molecules. The d_0 -DAz-2 and d_6 -DAz-2 labeled samples were combined and then subjected to click chemistry with Yn-ACL as described above. The biotinylated labeled samples were enriched using either the avidin affinity cartridge or the streptavidin-coated magnetic beads as described above. The resulting peptides were then analyzed by ESI-LC/MS/MS.

2.7 Supplementary Figures

```
1  MRGSHHHHHH GMASMTGGQQ MGRDLYDDDD KDRWGSMSSEF YKLAPVDKKG
51 QPFQDQLKG KVVLIVNVAS KCGFTPQYKE LEALYKRYKD EGFTIIGFPS
101 NQFGHQEPGS DEEIAQFSQL NYGVTFPIMK KIDVNGGNET PVYKFLKSQK
151 SGMLGLRGIK WNFEKFLVDK KGKVVYERYSS LTKPSSLSET IEELLKEVE
                                     83% Sequence Coverage
                                     22 Peptides Identified
```

Figure 2.S1: Sequence coverage obtained from C64S C82S Gpx3 trypsin digestion. Underlined sequence corresponds to the additional sequence from the vector.

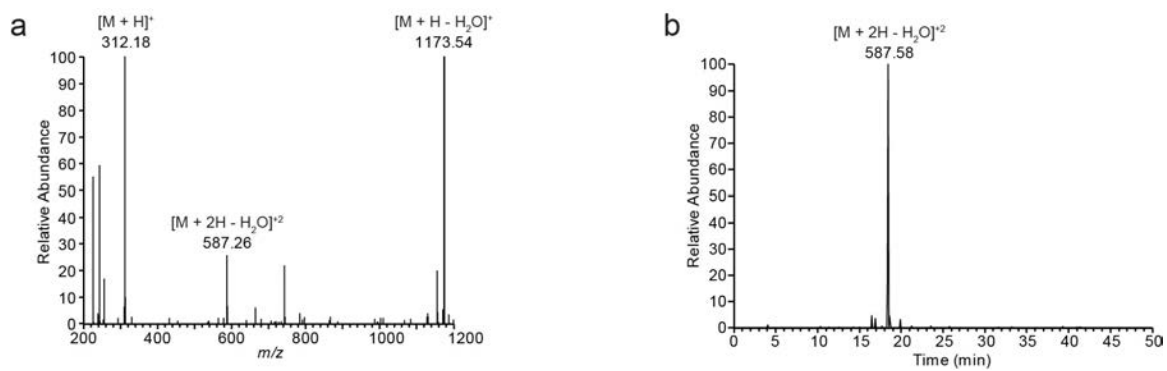


Figure 2.S2: ESI-LC/MS/MS analysis of avidin affinity cartridge enrichment. (a) MS² of m/z 765.16 produces the biotinylated fragment m/z 312.18 $[M + H]^+$, fragmented enriched sulfenic acid-modified peptide with loss of water, m/z 587.26 $[M + 2H - H_2O]^{+2}$, and m/z 1173.54 $[M + H - H_2O]^+$. (b) Extracted ion chromatogram of TFA cleaved peptide m/z 587.58 $[M + 2H - H_2O]^{+2}$.

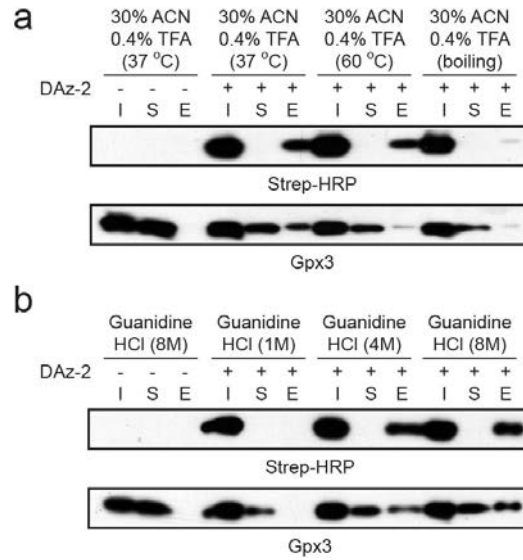


Figure 2.S3: Comparison of streptavidin-coated magnetic bead elution conditions 30% ACN + 0.4% TFA or guanidine HCl. Samples were generated as in Figure 2.2. I = input, S = supernatant, and E = eluent. (a) Temperature-dependent study of 30% ACN + 0.4% TFA elution conditions. Enriched Gpx3 labeled protein was eluted using 30% ACN + 0.4% TFA at 37 °C, 60 °C, or boiling for 15 min. (b) Concentration-dependent study of guanidine HCl elution conditions. Enriched Gpx3 labeled protein was eluted using guanidine HCl (1, 4, or 8 M) pH 1.2 for 15 min.

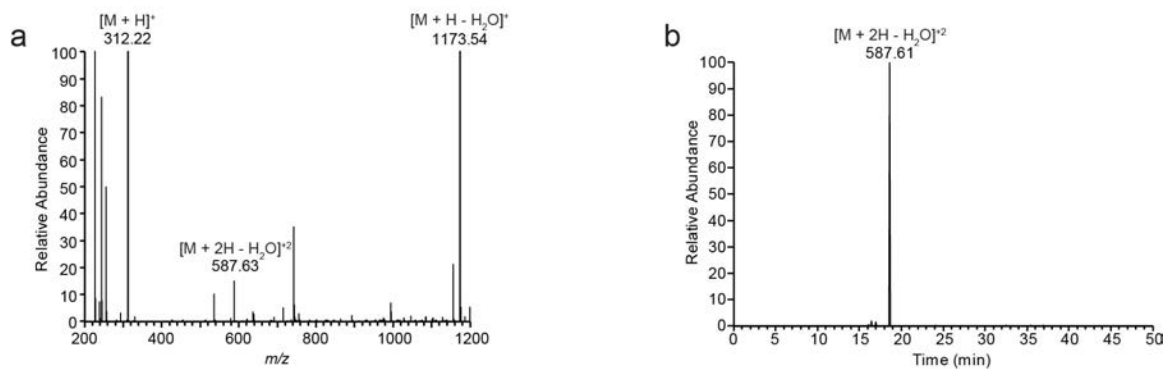


Figure 2.S4: ESI-LC/MS/MS analysis of streptavidin-coated magnetic bead enrichment. (a) MS² of m/z 765.11 $[M + 2H - H_2O]^{+2}$ produces fragmentation of the intact sulfenic acid-modified peptide to give the biotinylated fragment m/z 312.22 $[M + H]^+$, fragmented sulfenic acid-modified peptide m/z 587.63 $[M + 2H - H_2O]^{+2}$, and m/z 1173.54 $[M + H - H_2O]^+$. (b) Extracted ion chromatogram of TFA cleaved peptide m/z 587.61 $[M + 2H - H_2O]^{+2}$.

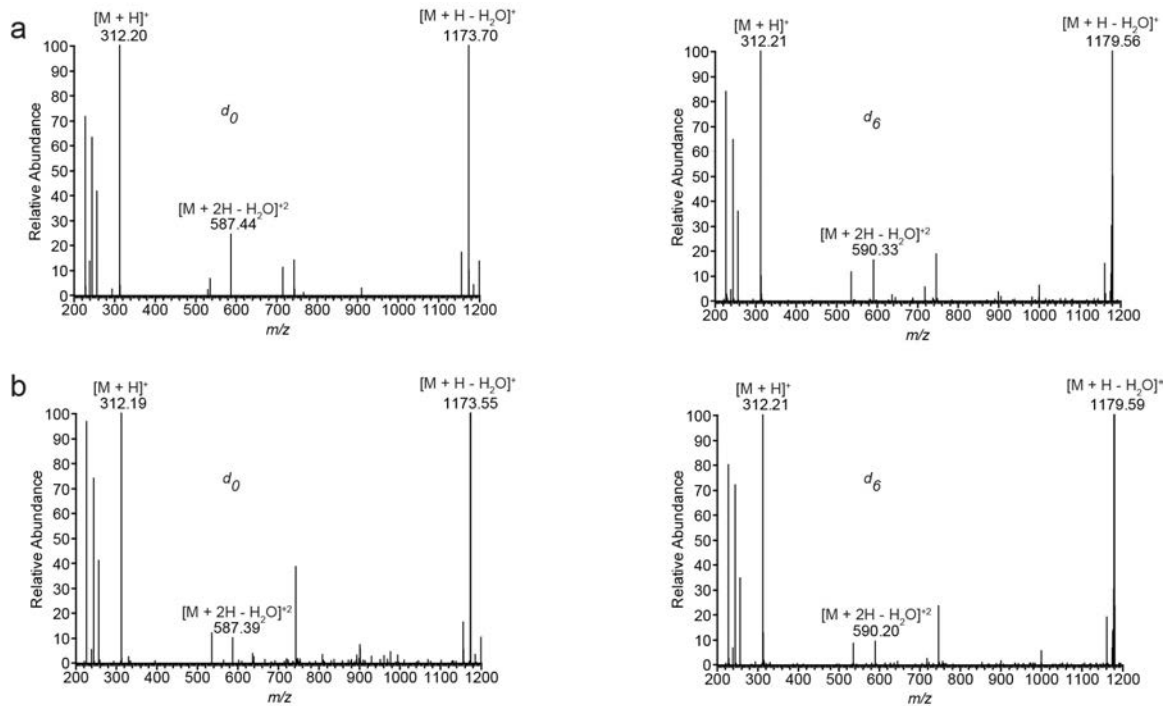


Figure 2.S5: ESI-LC/MS/MS analysis of enriched intact sulfenic acid-modified C*GFTPQYK peptides from ratiometric quantification studies. (a) Avidin affinity cartridge enriched peptides. (b) Streptavidin-coated magnetic beads enriched peptides. MS² spectra shows the biotin fragment m/z 312 $[M + H]^+$, fragmented sulfenic acid-modified peptides m/z 587 (d_0) and 590 (d_6) $[M + 2H - H_2O]^{+2}$, and m/z 1173 (d_0) and 1179 (d_6) $[M + H - H_2O]^+$.

2.8 Supplementary Tables

Table 2.S1: Expected and observed m/z of C*GFTPQYK peptide from Gpx3

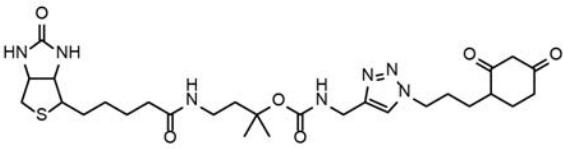
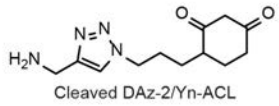
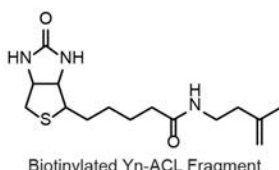
CGFTPQYK Modification	Expected m/z	Observed m/z	z	Adduct
 <p>Intact DAz-2/Yn-ACL</p>	1546.72	N/A	+1	[M + H] ⁺¹
	773.86	774.05	+2	[M + 2H] ⁺²
	516.24	516.84	+3	[M + 3H] ⁺³
	1528.70	1528.64	+1	[M + H - H ₂ O] ⁺¹
	764.85	765.07	+2	[M + 2H - H ₂ O] ⁺²
	510.23	510.64	+3	[M + 3H - H ₂ O] ⁺³
 <p>Cleaved DAz-2/Yn-ACL</p>	1191.56	1191.50	+1	[M + H] ⁺¹
	596.28	596.37	+2	[M + 2H] ⁺²
	1173.54	1173.57	+1	[M + H - H ₂ O] ⁺¹
	587.27	587.45	+2	[M + 2H - H ₂ O] ⁺²
 <p>Biotinylated Yn-ACL Fragment</p>	312.17	312.20	+1	[M + H] ⁺¹

Table 2.S2: Expected and observed m/z of b and y ions for TFA cleaved C*GFTPQYK peptide from Gpx3.

<div style="text-align: center;"> y_8 y_7 y_6 y_5 y_4 y_3 y_2 y_1 C G F T P Q Y K b_1 b_2 b_3 b_4 b_5 b_6 b_7 b_8 </div>						
Sequence	#	Expected b	Observed b	#	Expected y	Observed y
C	8	352.14	334.21	1	1191.56	N/A
G	7	409.16	391.20	2	840.42	840.47
F	6	556.23	538.47	3	783.40	783.45
T	5	657.28	639.31	4	636.28	636.34
P	4	754.33	N/A	5	535.28	535.30
Q	3	882.39	N/A	6	438.23	N/A
Y	2	1045.45	1044.47	7	310.17	N/A
K	1	1173.55	1173.70	8	147.11	N/A

2.9 Chapter References

1. Rhee, S. G. (2006). Cell signaling. H_2O_2 , a necessary evil for cell signaling. *Science*, *312*(5782), 1882–3.
2. D’Autreaux, B. & Toledano, M. B. (2007). Ros as signalling molecules: mechanisms that generate specificity in ros homeostasis. *Nat Rev Mol Cell Biol*, *8*(10), 813–24.
3. Paulsen, C. E. & Carroll, K. S. (2010). Orchestrating redox signaling networks through regulatory cysteine switches. *ACS Chem Biol*, *5*(1), 47–62.
4. Giorgio, M., Trinei, M., Migliaccio, E., & Pelicci, P. G. (2007). Hydrogen peroxide: a metabolic by-product or a common mediator of ageing signals? *Nat Rev Mol Cell Biol*, *8*(9), 722–8.
5. Sivaramakrishnan, S., Cummings, A. H., & Gates, K. S. (2010). Protection of a single-cysteine redox switch from oxidative destruction: on the functional role of sulfenyl amide formation in the redox-regulated enzyme ptp1b. *Bioorg Med Chem Lett*, *20*(2), 444–7.
6. Kettenhofen, N. J. & Wood, M. J. (2010). Formation, reactivity, and detection of protein sulfenic acids. *Chem Res Toxicol*, *23*(11), 1633–46.
7. Leonard, S. E. & Carroll, K. S. (2011). Chemical ‘omics’ approaches for understanding protein cysteine oxidation in biology. *Curr Opin Chem Biol*, *15*(1), 88–102.
8. Benitez, L. V. & Allison, W. S. (1974). The inactivation of the acyl phosphatase activity catalyzed by the sulfenic acid form of glyceraldehyde 3-phosphate dehydrogenase by dimedone and olefins. *J Biol Chem*, *249*(19), 6234–43.
9. Reddie, K. G., Seo, Y. H., Muse Iii, W. B., Leonard, S. E., & Carroll, K. S. (2008). A chemical approach for detecting sulfenic acid-modified proteins in living cells. *Mol Biosyst*, *4*(6), 521–31.
10. Leonard, S. E., Reddie, K. G., & Carroll, K. S. (2009). Mining the thiol proteome for sulfenic acid modifications reveals new targets for oxidation in cells. *ACS Chem Biol*, *4*(9), 783–99.
11. Seo, Y. H. & Carroll, K. S. (2009). Facile synthesis and biological evaluation of a cell-permeable probe to detect redox-regulated proteins. *Bioorg Med Chem Lett*, *19*(2), 356–9.
12. Leonard, S. E., Garcia, F. J., Goodsell, D. S., & Carroll, K. S. (2011). Redox-based probes (rbps) for protein tyrosine phosphatases. *Angew Chem Int Ed Engl*, *in press*.

13. Saxon, E. & Bertozzi, C. R. (2000). Cell surface engineering by a modified Staudinger reaction. *Science*, *287*(5460), 2007–10.
14. Rostovtsev, V. V., Green, L. G., Fokin, V. V., & Sharpless, K. B. (2002). A step-wise Huisgen cycloaddition process: copper(I)-catalyzed regioselective "ligation" of azides and terminal alkynes. *Angew Chem Int Ed Engl*, *41*(14), 2596–9.
15. Raghavan, A., Charron, G., Flexner, J., & Hang, H. C. (2008). Chemical probes for profiling fatty acid-associated proteins in living cells. *Bioorg Med Chem Lett*, *18*(22), 5982–6.
16. Sethuraman, M., McComb, M. E., Heibeck, T., Costello, C. E., & Cohen, R. A. (2004). Isotope-coded affinity tag approach to identify and quantify oxidant-sensitive protein thiols. *Mol Cell Proteomics*, *3*(3), 273–8.
17. Leichert, L. I., Gehrke, F., Gudiseva, H. V., Blackwell, T., Ilbert, M., Walker, A. K., ... Jakob, U. (2008). Quantifying changes in the thiol redox proteome upon oxidative stress in vivo. *Proc Natl Acad Sci U S A*, *105*(24), 8197–202.
18. Weerapana, E., Wang, C., Simon, G. M., Richter, F., Khare, S., Dillon, M. B., ... Cravatt, B. F. (2010). Quantitative reactivity profiling predicts functional cysteines in proteomes. *Nature*, *468*(7325), 790–5.
19. Danielson, S. R., Held, J. M., Oo, M., Riley, R., Gibson, B. W., & Andersen, J. K. (2011). Quantitative mapping of reversible mitochondrial complex I cysteine oxidation in a Parkinson disease mouse model. *J Biol Chem*, *286*(9), 7601–7608.
20. Seo, Y. H. & Carroll, K. S. (2011). Quantification of protein sulfenic acid modifications using isotope-coded dimedone and iododimedone. *Angew Chem Int Ed Engl*, *50*(6), 1342–5.
21. El Fangour, S., Balas, L., Rossi, J. C., Fedenyuk, A., Gretskeya, N., Bobrov, M., ... Durand, T. (2003). Hemisynthesis and preliminary evaluation of novel endocannabinoid analogues. *Bioorg Med Chem Lett*, *13*(12), 1977–80.
22. Qiu, Y., Sousa, E. A., Hewick, R. M., & Wang, J. H. (2002). Acid-labile isotope-coded extractants: a class of reagents for quantitative mass spectrometric analysis of complex protein mixtures. *Anal Chem*, *74*(19), 4969–79.
23. Borisov, O. V., Goshe, M. B., Conrads, T. P., Rakov, V. S., Veenstra, T. D., & Smith, R. D. (2002). Low-energy collision-induced dissociation fragmentation analysis of cysteinyl-modified peptides. *Anal Chem*, *74*(10), 2284–92.
24. Fauq, A. H., Kache, R., Khan, M. A., & Vega, I. E. (2006). Synthesis of acid-cleavable light isotope-coded affinity tags (icat-1) for potential use in proteomic expression profiling analysis. *Bioconjug Chem*, *17*(1), 248–54.

25. Szychowski, J., Mahdavi, A., Hodas, J. J., Bagert, J. D., Ngo, J. T., Landgraf, P., . . . Tirrell, D. A. (2010). Cleavable biotin probes for labeling of biomolecules via azide-alkyne cycloaddition. *J Am Chem Soc*, *132*(51), 18351–60.
26. Yang, Y. Y., Grammel, M., Raghavan, A. S., Charron, G., & Hang, H. C. (2010). Comparative analysis of cleavable azobenzene-based affinity tags for bioorthogonal chemical proteomics. *Chem Biol*, *17*(11), 1212–22.
27. Park, K. D., Liu, R., & Kohn, H. (2009). Useful tools for biomolecule isolation, detection, and identification: acylhydrazone-based cleavable linkers. *Chem Biol*, *16*(7), 763–72.
28. Paulsen, C. E. & Carroll, K. S. (2009). Chemical dissection of an essential redox switch in yeast. *Chem Biol*, *16*(2), 217–25.

CHAPTER III

Peroxide-dependent sulfenylation of the EGFR catalytic site enhances kinase activity

3.1 Abstract

Protein sulfenylation (SOH) is a post-translational modification of emerging importance in higher eukaryotes. However, investigation of its diverse roles remains challenging, particularly within a native cellular environment. Herein we report the development and application of DYn-2, a new chemoselective probe for detecting sulfenylated proteins in cells. These studies show that epidermal growth factor receptor (EGFR)-mediated signaling results in hydrogen peroxide (H_2O_2) production and oxidation of downstream proteins. In addition, we demonstrate that DYn-2 has the ability to detect differences in sulfenylation rates within the cell, which are associated with differences in target protein localization. Finally, we show that EGFR is directly modified by H_2O_2 at a critical active site cysteine (Cys797), which enhances its tyrosine kinase activity. Collectively, our findings highlight sulfenylation as a global signaling mechanism akin to phosphorylation, with regulatory implications for other receptor tyrosine kinases and irreversible inhibitors that target oxidant-sensitive cysteines in proteins.

3.2 Introduction

Hydrogen peroxide (H_2O_2) is a source of oxidative stress, but also acts as an essential second messenger in signal transduction networks of normal healthy cells, wherein growth factors, cytokines and a variety of other ligands trigger its production through activation of their corresponding receptors (1, 2). Indeed, H_2O_2 has been demonstrated to regulate many basic cellular processes including proliferation, differentiation, growth, migration, and survival. For example, binding of epidermal growth factor (EGF) to the extracellular domain of the EGF receptor (EGFR) results in the assembly and activation of NADPH oxidase (Nox) complexes, which generate H_2O_2 (3, 4) (Figure 3.1a). Once formed, H_2O_2 modulates signaling cascades by reaction with specific biomolecular targets.

There is now a wealth of evidence indicating that protein cysteine residues are sensitive targets of H_2O_2 , both by direct oxidation and vis-à-vis thiol peroxidases (5, 6). The product of the reaction between H_2O_2 and a thiolate is sulfenic acid (SOH). Also known as sulfenylation, this modification is reversible (either directly or indirectly by disulfide formation) and provides a mechanism by which changes in cellular redox state can be exploited to regulate protein function, analogous to phosphorylation (7, 8). Recent studies shed new light on the role of sulfenic acid and expand the repertoire of proteins that can undergo sulfenylation (9–13), hinting at the regulatory potential and significance of these modifications. Nonetheless, the scope of sulfenylation in biological processes, particularly in eukaryotic signal transduction, remains virtually unknown.

Investigating the role of sulfenylation remains challenging, particularly in the context of the native cellular environment (14). We now present the development and application of DYn-2, a chemoselective probe for detecting sulfenylated proteins directly in cells with improved sensitivity. These studies show that DYn-2 is capable of monitoring global changes in protein sulfenylation generated by Nox-mediated growth

factor signaling. In addition, we demonstrate that DYn-2 has the ability to detect differences in sulfenylation rates within the cell, due to differences in target protein localization. Finally, we show that EGFR is modified by H_2O_2 at a critical cysteine (Cys797) in its catalytic site that stimulates its kinase activity, thereby demonstrating that sulfenylation, as well as phosphorylation, can regulate receptor tyrosine kinase (RTK) function.

3.3 Results

EGF modulates cell morphology and EGFR trafficking. To investigate events after the interaction of EGF with its receptor we used the human epidermoid carcinoma A431 cell line, which naturally expresses high levels of EGFR. As shown by phase contrast microscopy, EGF stimulation induced rapid changes in cell shape (Supplementary Results, Supplementary Figure 3.S1). Additionally, we used immunofluorescence to determine whether EGF-dependent changes in morphology coincided with receptor mobilization (Figure 3.S1b). EGFR localized to the plasma membrane without EGF stimulation and concentrated at sites of membrane ruffling within two minutes of mitogen treatment. At 30 minutes, the majority of EGFR had accumulated in punctate foci throughout the peripheral cytoplasm, and after one hour, internalized receptors had recycled back to the cell surface. These data show that EGF stimulation dramatically changes cell morphology and receptor localization, setting the stage to probe oxidant-mediated signal transduction.

Cellular redox balance affects EGF-mediated signaling. Next, we examined the relationship between EGFR signaling and reactive oxygen species (ROS) in A431 cells. Intracellular generation of ROS was measured via the conversion of 2,7-dihydro-dichlorofluorescein diacetate ($\text{H}_2\text{DCF-DA}$) to fluorescent product dichlorofluorescein (DCF). Coincident with membrane ruffling, EGF-stimulated cells exhibited an increase in DCF fluorescence intensity (Figure 3.1c). Moreover, reversible

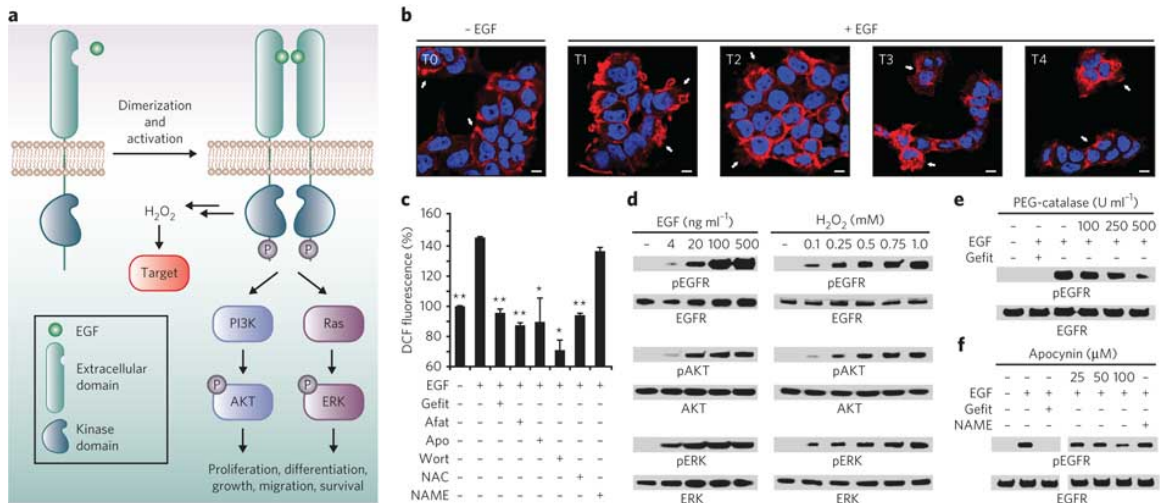


Figure 3.1: Cellular redox status affects EGF-mediated signaling. (a) EGF binding to EGFR and subsequent dimerization induces receptor auto-phosphorylation on specific tyrosine residues within the cytoplasmic domain. The newly phosphorylated sites serve as interaction platforms for proteins involved in key prosurvival pathways, such as PI3K/ AKT and Ras/ERK. Receptor-ligand interaction also stimulates the production of ROS and oxidation of intracellular biomolecules, leading to modulation of the signaling cascade. (b) Confocal fluorescence images of EGFR localization in A431 cells before (T0) and after 100 ng/ml EGF stimulation for 2, 15, 30, and 60 min (T1, T2, T3, and T4, respectively). Cells were stained with rabbit anti-EGFR followed by Alexa594-conjugated goat anti-rabbit (red). White arrows highlight changes in receptor localization (T0, plasma membrane; T1, membrane ruffles; T2, cell stretching and migration; T3, perinuclear and endosomal membranes; T4, cell surface and ruffles). Nuclei were counterstained with DAPI (blue). Scale bar, 10 μ m. (c) EGF-induced ROS generation in A431 cells as revealed by DCF fluorescence. Data are representative of three independent readings, were normalized to the vehicle control and error bars show \pm s.e.m. **indicates that $P < 0.001$, *indicates that $P < 0.05$ when compared against EGF-only treated cells. (d-f) Western blots showing phosphorylated (p) and total EGFR, AKT, and/or ERK. A431 cells were stimulated with the indicated concentrations of EGF, H₂O₂ or vehicle for 5 min (d), or with 100 ng/ml EGF or vehicle for 5 min (e,f). Where specified, cells were treated with the indicated concentrations of PEG-catalase (e), apocynin (f), or gefitinib (g), prior to EGF stimulation.

and irreversible inhibitors of EGFR (gefitinib and afatinib, respectively), Nox (apocynin), phosphatidylinositol-3-OH kinase (PI3K, wortmannin), and the antioxidant, N-acetyl cysteine (NAC) attenuated EGF-dependent ROS generation. Control experiments with an NO synthase inhibitor (L-NAME) had no significant impact on ROS levels, as expected (Figure 3.1c). These experiments support and extend previous observations (3, 15) that EGF-mediated ROS production requires both EGFR and Nox activation.

We then investigated the effect of exogenous H_2O_2 on phosphorylation of EGFR and downstream kinases, AKT and ERK. In the absence of EGF, treatment with H_2O_2 was sufficient to trigger a dose-dependent increase in phosphorylation of each kinase (Figure 3.1d and Supplementary Figure 3.S2 for all uncut gel images in this study). Control experiments showed that each protein became phosphorylated in response to EGF and that EGFR or PI3K inhibitors attenuated this effect, as expected (Figure 3.1d and Supplementary Figure 3.S3a). Subsequently, we examined the role of H_2O_2 produced by EGF stimulation (i.e., endogenous H_2O_2) on pathway activation. Scavenging of growth factor-induced H_2O_2 with PEG-catalase or NAC suppressed EGFR phosphorylation (Figure 3.1e), global tyrosine phosphorylation, and AKT/ERK activation (Supplementary Figure 3.S3b-e). Additionally, Nox inhibitors, apocynin and diphenyleneiodium (DPI), blunted protein phosphorylation, whereas L-NAME had no apparent effect (Figure 3.1f and Supplementary Figure 3.S3f,g). Collectively, these data underscore the importance of endogenous H_2O_2 for EGFR signaling as a result of Nox activation.

The requirement for protein sulfenylation in yeast H_2O_2 sensing (16) and T-cell activation (17) has been shown through inhibition with 5,5-dimethyl-1,3-cyclohexadione (dimedone), a small-molecule that reacts selectively with sulfenic acid under aqueous conditions (18–20) (Figure 3.2a). Along these lines, treatment of cells with dimedone, prior to EGF stimulation, inhibited EGFR, AKT, and ERK phosphorylation (Supplementary Figure 3.S3h), consistent with an essential role for protein sulfenylation in EGFR signaling.

Synthesis and evaluation of DYn-1 and DYn-2. Chemical probes directly conjugated to biotin or a fluorophore often have limited cell permeability due to their bulky detection tag. Accordingly, protocols involving such reagents typically involve homogenization of cells prior to labeling, which disrupts the native environment, including redox balance. To address this issue, we have developed a strategy for

detecting protein sulfenic acids directly in cells (11, 20, 21), wherein the dimedone warhead is functionalized with a small azide chemical handle that does not impede membrane permeability (DAz-1 and DAz-2, Figure 3.2b). An alkyne-functionalized detection tag is then appended post-homogenation using the Staudinger ligation or click chemistry.

Recent studies demonstrate that alkynyl-chemical reporters, in combination with azide-bearing detection tags, offer superior sensitivity relative to the reverse orientation (22). In light of this observation, we designed and synthesized the alkyne-modified analogs, DYn-1 (1) and DYn-2 (2) (Figure 3.2b,c and Supplementary Methods). The synthesis began with ethyl protection of the reactive diketone. Alkylation of 3-ethoxy-cyclohex-2-enone with 3-bromopropyne to afford DYn-1 proceeded smoothly; however, low yields were obtained in analogous reactions for 5-iodopent-1-yne. As a result, we examined monoalkylation of the dianion of 1,3-cyclohexadione. Using this strategy, DYn-2 was prepared without protecting groups in a single step from commercially available materials in 96% yield (Figure 3.2c).

With DYn-1 and DYn-2 in hand, we performed comparative studies to determine their utility for detecting protein sulfenic acid modifications alongside DAz-2. To this end, we used a recombinant thiol peroxidase from budding yeast, known as Gpx3, with an active site cysteine (Cys36) that is readily oxidized to sulfenic acid (16). Analysis of these reactions by Western blot revealed robust, H_2O_2 -dependent labeling of Gpx3 by DYn-2, with increased intensity relative to DAz-2 (Figure 3.2d). Control reactions, performed in the absence of probe, showed no detectable signal by Western blot (Figure 3.2d). Conversely, DYn-1 exhibited a marked reduction in sulfenic acid labeling compared to DYn-2 (Supplementary Figure 3.S4a). Therefore, DYn-1 was not pursued further.

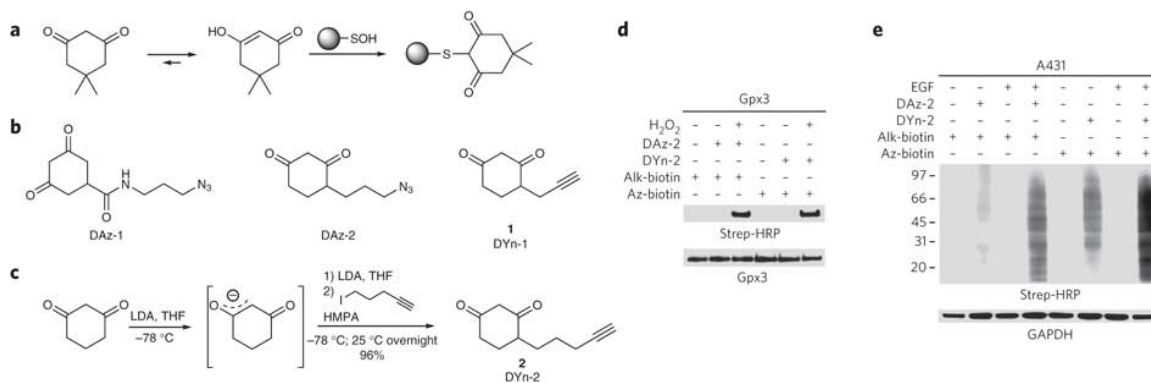


Figure 3.2: Development and validation of probes for detecting sulfenic acid. (a) Selective reaction between sulfenic acid and dimedone. (b) Chemical structures of chemical reporters for sulfenic acid. (c) Design and synthesis of DYn-2 (2). LDA, lithium diisopropylamide; HMPA, hexamethyl phosphoramide; 5-iodopent-1-yne. (d) Comparison of DAz-2 and DYn-2 detection of sulfenic acid in recombinant Gpx3. 50 μ M protein was untreated or exposed to 100 μ M H₂O₂ and incubated in presence or absence of 1 mM probe for 15 min at 37 °C. Labeled proteins were detected by streptavidin-HRP Western blot. Comparable protein loading was confirmed by reprobng the blot with anti-His tag antibody. (e) Western blots showing DAz-2 and DYn-2 detection of protein sulfenic acids and total GAPDH in A431 cells. Cells were stimulated with 100 ng/ml EGF or vehicle for 5 min, washed, collected as described in Methods, and then incubated with 5 mM probe or vehicle for 1 h at 37 °C.

Next, we verified the nature of the covalent adduct formed between oxidized Gpx3 and DYn-2 by electrospray ionization mass spectrometry (ESI-MS) (Supplementary Figure 3.S4b,c). Analysis of the intact protein afforded a single major species with a molecular weight of 22916.39 Da, consistent with a single DYn-2 adduct. Detailed examination of trypsin cleavage products confirmed Cys36 as the site of modification from the doubly-charged peptide ion at m/z 551.52 corresponding to H₂N-C-(2)GFTPQYK-OH and the series of b and y-type ions observed in the MS/MS spectrum. Overall, Western blot and MS analyses establish that DYn-2 selectively targets protein sulfenic acid modifications.

We then evaluated DYn-2 for detecting sulfenic acids in cells using the strategy outlined in Supplementary Figure 3.S5a. Analysis of probe labeling by Western blot revealed sulfenylated proteins in both A431 and HeLa cells (Figure 3.2e and Supplementary Figure 3.S5b,c). The qualitative profile of DYn-2 labeling was similar to DAz-2, suggesting that the probes reacted with the same protein targets. Notably, the total signal from DYn-2 labeling was greater than DAz-2 under identical conditions,

and the signal ratio of EGF-stimulated and unstimulated A431 cells was almost 40% greater for DYn-2. Detection of sulfenylated proteins by DYn-2 was also dependent on probe dose and time of incubation (Supplementary Figure 3.S5d,e). Controls performed with or without catalase in lysis buffer further confirmed that DYn-2 labeling did not occur after cell homogenization (Supplementary Figure 3.S5f). Addition of DYn-2, before or after EGF treatment, did not affect phosphorylation of EGFR or downstream targets (Supplementary Figure 3.S3h and Supplementary Figure 3.S5g), likely due to the decrease in reactivity inherent to many dimedone analogs. Lastly, probe-treated cells showed no loss of viability and maintained redox balance (Supplementary Figure 3.S6). Collectively, these results validate DYn-2 as a robust chemical reporter for protein sulfenylation in cells and our general approach of tagging oxidized proteins *in situ*.

Dynamic, global protein sulfenylation in response to EGF. The preceding studies reveal EGF-dependent changes in protein sulfenylation. This observation is the first of its kind and, thus we investigated this discovery in greater detail. Addition of EGF to A431 cells increased intracellular ROS (Figure 3.3a) and protein sulfenylation (Figure 3.3b,c) in a dose-dependent manner. The maximal increase in sulfenic acid modification was apparent at 100 ng/ml EGF, which fell to the basal level at 500 ng/ml. ROS generation (Figure 3.3d) and protein sulfenylation (Figure 3.3e,f) were also dynamic temporal events, peaking 5 min after EGF stimulation (100 ng/ml) and declining thereafter. Furthermore, pharmacological studies indicated that EGF-dependent changes in protein sulfenylation required EGFR, PI3K, and Nox activation, as well as intracellular H₂O₂ (Supplementary Figure 3.S7).

Fluorescence microscopy with antibodies against the protein-dimedone adduct (21) further highlighted the dynamic nature of EGF-mediated protein sulfenylation (Figure 3.3g). Relative to unstimulated cells, EGF treatment markedly increased signal intensity with a peak at 6 min, whereas control samples omitting primary antibody

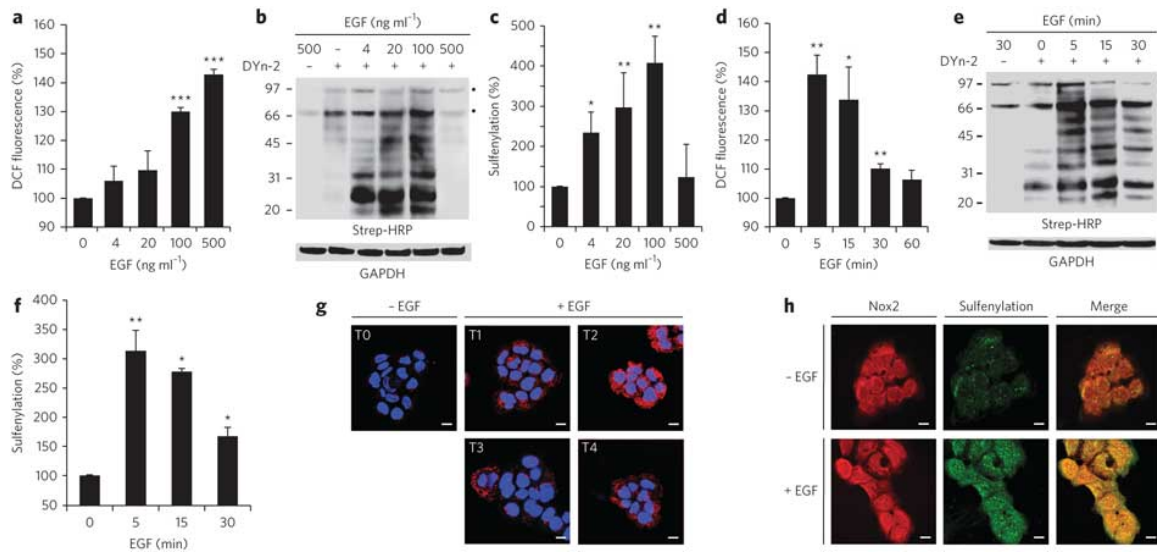


Figure 3.3: Profiling EGF-mediated ROS production and protein sulfenylation. A431 cells were incubated with EGF at the indicated concentrations (a, b) or the indicated times (d,e). In (a), A431 cells were stimulated with EGF or vehicle for 5 min, and ROS was measured by DCF fluorescence. In (b), A431 cells were stimulated with EGF or vehicle for 2 min and sulfenic acids were detected by Western blot as in Figure 3.2e. (c) Densitometric quantification of each lane in b. In (d), A431 cells were stimulated with 500 ng/ml EGF or vehicle and ROS was measured by DCF fluorescence. In (e), A431 cells were stimulated with 100 ng/ml EGF or vehicle and sulfenic acids detected as in b. (f) Densitometric quantification of each lane in f. Western blots were reprobed for GAPDH as a loading control. Data are representative of four independent experiments for Western blots and three independent readings for ROS measurements and represent the mean \pm s.e.m. **indicates that $P < 0.001$, *indicates that $P < 0.05$ compared to vehicle control. (g) Fluorescence images of sulfenylation (red) in A431 cells before (T0) and after stimulation with 100 ng/mL EGF for 0.5, 1, 1.5, or 2 min, then treated with 5 mM dimedone for 5 min at 37 °C in EGF-containing media; total EGF exposure was 5.5, 6, 6.5 and 7 min (T1, T2, T3, and T4, respectively). Nuclei were counterstained with DAPI (blue). Scale bar, 10 μ m. In (h), A431 cells were stimulated with 100 ng/mL EGF or vehicle for 0.5 min and treated with dimedone as in g. Cells were stained for the dimedone-protein adduct (red) and Nox2 (green). The merged image reveals partial co-localization (yellow). Scale bar, 10 μ m.

showed no signal (Supplementary Figure 3.S8). The slight difference in sulfenylation peak times observed by Western blot (and ROS levels by DCF) and immunofluorescence analyses is most likely due to variations in sample handling inherent to each procedure.

There are seven isoforms of nonphagocytic NADPH oxidase (Nox1-5 and Duox1 and 2) that exhibit unique activation mechanisms and tissue-specific expression (23). Western blot and immunofluorescence analyses revealed that Nox2 is a major isoform in A431 cells (Supplementary Figure 3.S9a,b). Because proteins in the vicinity

of Nox are prime targets for oxidation, we wondered whether Nox2 might colocalize with sites of protein sulfenylation. Immunofluorescence analysis indicated the distribution of Nox2 at the plasma membrane and perinuclear area (Figure 3.3h and Supplementary Figure 3.S9c). Remarkably, the merged image of Nox2 and protein sulfenylation revealed a significant degree of colocalization (Figure 3.3h). Together, these data show that EGF-stimulation results in dynamic changes of protein sulfenylation, whose distribution in cells overlaps with Nox2.

Differential oxidation of phosphatases. We next sought to identify targets of H_2O_2 within the EGFR pathway. Growth factor-induced ROS generation is commonly attributed to oxidation and inactivation of an essential active site cysteine residue in protein tyrosine phosphatases (PTPs). While the analysis of cysteine oxidation in cell extracts indicates that PTP inhibition promotes kinase signaling (17, 24, 25), rates of these reactions are orders of magnitude slower relative to H_2O_2 -metabolizing enzymes, raising the specter of physiological relevance (26). Because direct evidence of PTP oxidation in cells has not yet been reported, we used DYn-2 to investigate sulfenylation in three signaling phosphatases: PTEN, PTP1B and SHP2. PTEN is predominantly cytoplasmic and functions reciprocal to PI3K, PTP1B down-regulates endocytosed receptors within the endoplasmic reticulum (ER), while SHP2 interacts directly with EGFR at the plasma membrane through its SH2 domains where it serves to mediate interactions with downstream components.

Western blot analysis of immunoprecipitated PTPs showed that each protein underwent EGF-dependent sulfenylation in A431 cells (Figure 3.4a-c). Moreover, each PTP displayed a distinct oxidation profile with respect to growth factor concentration (Figure 3.4a-c): SHP2 sulfenylation peaked at a relatively low level of EGF (20 ng/ml), followed by PTEN (500 ng/ml), and finally PTP1B (750 ng/ml). Subsequently, we investigated PTP localization in cells before and after EGF treatment. Immunofluorescence staining showed that SHP2 underwent a dramatic change in lo-

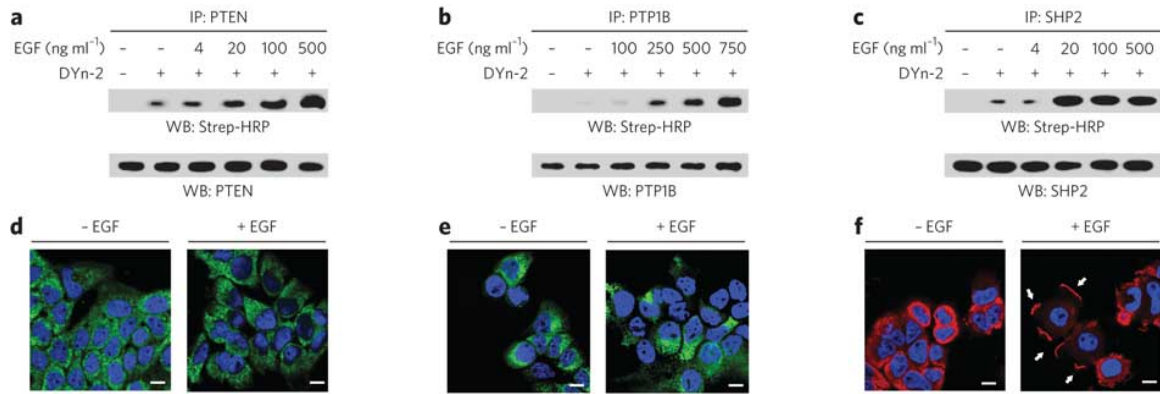


Figure 3.4: **Differential sulfenylation of PTPs in EGF-treated cells.** (a-c) Western blots showing sulfenylated and total immunoprecipitated PTEN, PTP1B, and SHP2. A431 cells were stimulated with EGF or vehicle for 2 min at the indicated concentrations, washed, collected, and then incubated with 5 mM DYn-2 or vehicle for 1 h at 37 °C. Following treatment, lysates were immunoprecipitated with mouse anti-PTEN (a), mouse anti-PTP1B (b), or rabbit anti-SHP2 (c) and recovered with protein A or G coated beads. Sulfenylation of PTPs was detected by streptavidin-HRP Western blot. To verify equivalent recovery of immunoprecipitated protein, Western blots were reprobed for total PTP as indicated. (d-f) Confocal fluorescence images of A431 cells stimulated with vehicle or 100 ng/ml EGF for 5 min. Cells were fixed and stained with anti-PTEN (d), anti-PTP1B (e), or anti-SHP2 (f), followed by Alexa488-conjugated goat anti-mouse (green, d,e) or Alexa594-conjugated goat anti-rabbit (red, f). Nuclei were counterstained with DAPI (blue). Scale bar, 10 μ m. The white arrows in (f) highlight the change in subcellular localization of SHP2 after stimulation with EGF.

calization, concentrating at sites of plasma membrane ruffling, whereas EGF had no apparent effect on PTEN or PTP1B (Figure 3.4d-f). Overall, these data demonstrate that PTPs undergo EGF-dependent oxidation and suggest that the extent of sulfenylation in the cell may be related to differences in target protein localization.

Identification of EGFR as a sensitive target of H₂O₂. The overall level of EGFR autophosphorylation reflects the balance between kinase and phosphatase activities. H₂O₂-induced PTP inhibition would shift the balance toward phosphorylation; however, the increase in EGFR phosphorylation could similarly be accounted for by H₂O₂-mediated enhancement of intrinsic kinase activity. To examine this possibility, we first tested whether EGFR was a target of H₂O₂ in cells. Strikingly, these studies revealed that EGF stimulation led to robust sulfenic acid modification of EGFR (Figure 3.5a), a finding that was recapitulated with exogenous H₂O₂ (Figure 3.5b). EGFR sulfenylation peaked at the lowest concentration of EGF employed in this study

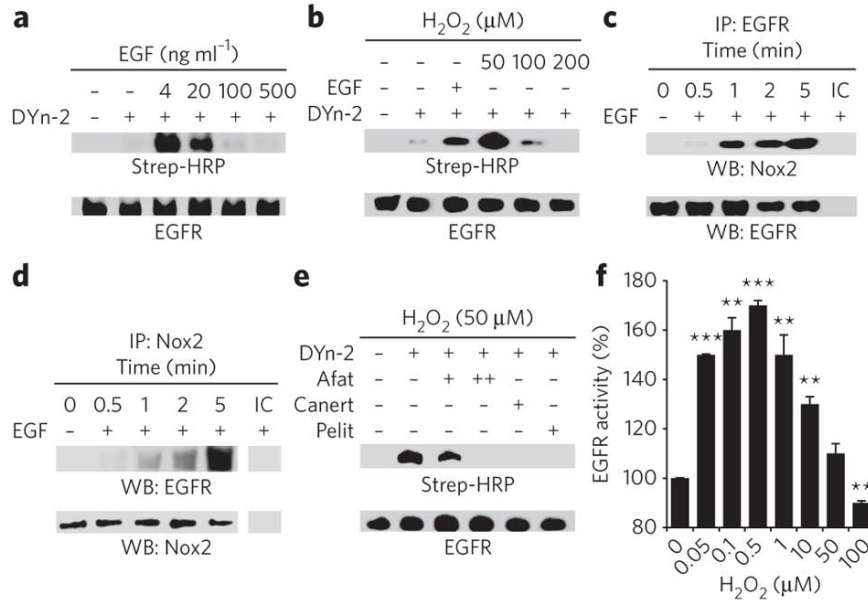


Figure 3.5: **EGF-mediated sulfenylation of EGFR Cys797 in cells.** (a,b) Western blots showing sulfenylated and total EGFR. A431 cells were stimulated with EGF at the indicated concentrations or vehicle for 2 min (a) or H_2O_2 for 10 min (b) and sulfenic acids were detected by streptavidin-HRP Western blot as in Figure 3.4a-c, except that rabbit anti-EGFR was used for immunoprecipitation. (c,d) Western blots showing coimmunoprecipitation of Nox2 and EGFR. A431 cells were stimulated with 100 ng/ml EGF or vehicle for the indicated times, harvested in native lysis buffer to preserve protein-protein interactions, and immunoprecipitated using goat anti-EGFR (c) or rabbit anti-Nox2 (d). (c) The presence of Nox2 was evaluated using goat anti-Nox2 and comparable recovery of immunoprecipitated EGFR was confirmed by probing the blot with rabbit anti-EGFR. IC, isotype control. (d) The presence of EGFR was evaluated using rabbit anti-EGFR and comparable recovery of immunoprecipitated Nox2 was confirmed by probing the blot with goat anti-Nox2. (e) Western blot showing sulfenylated and total EGFR. A431 cells were incubated with 1 or 5 μM afatinib (+ and ++, respectively), 10 μM canertinib, 1 μM pelitinib or vehicle before treatment with H_2O_2 and sulfenylation was detected as in b. (f) Measurement of EGFR tyrosine kinase activity in vitro. Recombinant EGFR kinase was untreated or exposed to H_2O_2 at the indicated concentrations and then assayed for activity. Data are representative of three independent readings and represent the mean \pm s.e.m. ***indicates that $P < 0.001$, **indicates that $P < 0.01$, and *indicates that $P < 0.05$ compared to vehicle control.

(4 ng/ml) and at $\sim 10 \mu M$ exogenous H_2O_2 (Supplementary Figure 3.S9d). Given the marked increase in EGFR oxidation at low EGF concentrations, we wondered whether the receptor might form a complex with Nox2. This proposal was confirmed by co-immunoprecipitation, which demonstrated EGF- and time-dependent association of Nox2 with EGFR and visa versa (Figure 3.5c,d). In addition, we found that the EGFR/Nox complex co-immunoprecipitated SHP2, consistent with its propensity for oxidation in cells (Supplementary Figure 3.S9e).

Oxidation of EGFR active site modulates kinase activity. The kinase domain of EGFR contains six cysteine residues. Of these, a conserved cysteine within the ATP binding site (Cys797, Supplementary Figure 3.S9f) is a major target for irreversible inhibitors in cancer clinical trials (27, 28). On this basis, we hypothesized that Cys797 might be the site of oxidation. This proposal was supported by studies with irreversible inhibitors, which blocked exogenous H₂O₂-mediated EGFR sulfenylation (Figure 3.5e). Next, we mapped the site of EGF-induced oxidation in cells using dimedone. ESI-LC/MS/MS analysis of pepsin-digested EGFR confirmed Cys797 as the site of covalent modification from the doubly-charged peptide ion at m/z 402.80 corresponding to H₂N-MPFGC*L-OH and the series of b- and y-type ions observed in the MS/MS spectrum (Supplementary Figure 3.S9g). The reduced EGFR peptide was also detected and the ratio of peak areas of the dimedone-modified peptide ion relative to the unmodified version was approximately 6:1 (Supplementary Figure 3.S9h).

Given the proximity of Cys797 to the ATP binding site (Supplementary Figure 3.S9f) it is plausible that oxidation of this residue modulates enzymatic activity. To test this hypothesis, we performed activity assays using the recombinant EGFR kinase domain. First, we verified that enzyme activity increased as a function of EGFR concentration and decreased with inhibitor treatment (Supplementary Figure 3.S9i-k). Subsequent studies revealed that tyrosine kinase activity was enhanced, relative to the untreated control, by moderate H₂O₂ concentrations (0.05-10 μ M), followed by a decline at levels greater than 50 μ M (Figure 3.5f). Incubation with the reducing agent, dithiothreitol (DTT) mitigated inhibition by H₂O₂ (Supplementary Figure 3.S9l), indicating that the decline in EGFR activity at high oxidant concentrations involves reversible thiol oxidation. Control experiments also showed that H₂O₂ had no significant effect on other components of the assay system (Supplementary Figure 3.S9m). Collectively, these data demonstrate that EGFR Cys797

is a direct target of endogenous H_2O_2 , ostensibly through its association with Nox2, and that signaling levels of this oxidant enhance EGFR kinase activity.

3.4 Discussion

Historically, protein cysteine oxidative has been investigated using indirect methods of detection (14) (Supplementary Figure 3.S10a,b). As these approaches require comprehensive blocking of free thiols at the outset of the procedure, their application is restricted to the analysis of oxidation within purified proteins or cell lysates. Alternatively, oxidative cysteine modifications can be detected on the basis of their distinct chemical attributes using selective probes (Supplementary Figure 3.S10c), which enable cysteine oxidation to be detected directly in cells. This is not a trivial consideration since redox potentials differ markedly among subcellular compartments (29) and, when the redox balance of the cell is disrupted during lysis, proteins undergo a massive amount of artifactual oxidation. This fundamental, but often ignored issue, increases the challenge involved in detecting modifications in low-abundance proteins and for interpreting biological significance.

With the development of DYn-2, we have expanded the chemical toolbox with which to probe protein sulfenic acid formation in cells. The discovery that protein sulfenylation is a dynamic process during EGFR-mediated signaling likely has broader implications for other receptor-mediated processes. Consistent with this proposal, alterations in protein sulfenic acid modifications have been observed in lysates generated from HEK293 cells treated with the cytokine $\text{TNF}\alpha$ (30) and CD8+ T cells stimulated with CD3/CD28 antibodies (17). While the changes in global protein sulfenylation observed in our study generally showed a strong positive correlation with ROS levels, cells treated with 500 ng/ml EGF were an exception to this rule. Interestingly, the apparent lack of sulfenylation is consistent with the absence of global disulfide bond formation in A431 cells under these conditions (31), and may reflect ox-

oxidation of sulfenic to sulfinic acid, upregulation of efflux transporters, dissociation of EGFR clusters from lipid rafts, and/or activation of alternate pathways that function independent of cysteine oxidation.

Each protein analyzed in this study exhibited a unique sulfenylation profile in cells (Figure 3.6a,b). For PTPs, differential susceptibility to oxidation is particularly notable because their active site cysteines are deprotonated at physiological pH and their reaction rates with H_2O_2 are almost identical in biochemical studies (32, 33). One possible explanation for this apparent paradox is that the proximity of target proteins to the source of ROS (e.g., Nox) has a significant influence on rates of oxidation within the cell. Consistent with this model, we observed that EGFR and SHP2 form a complex with Nox2. On the other hand, oxidation of PTP1B, an ER-resident phosphatase, was not observed until much higher EGF levels. Along these lines, a recent study in aortic endothelial cells showed that PTP1B oxidation by Nox4 requires ER localization of both proteins (34). Alternatively, the absence of PTP1B oxidation at lower EGF concentrations might result from sulfenyl amide formation outcompeting the DYn-2 trap (Supplementary Figure 3.S10d). However, this scenario seems unlikely as sulfenyl amide condensation in PTP1B is expected to be at least 100-fold slower than intramolecular disulfide formation in PTEN and SHP2 (35, 36).

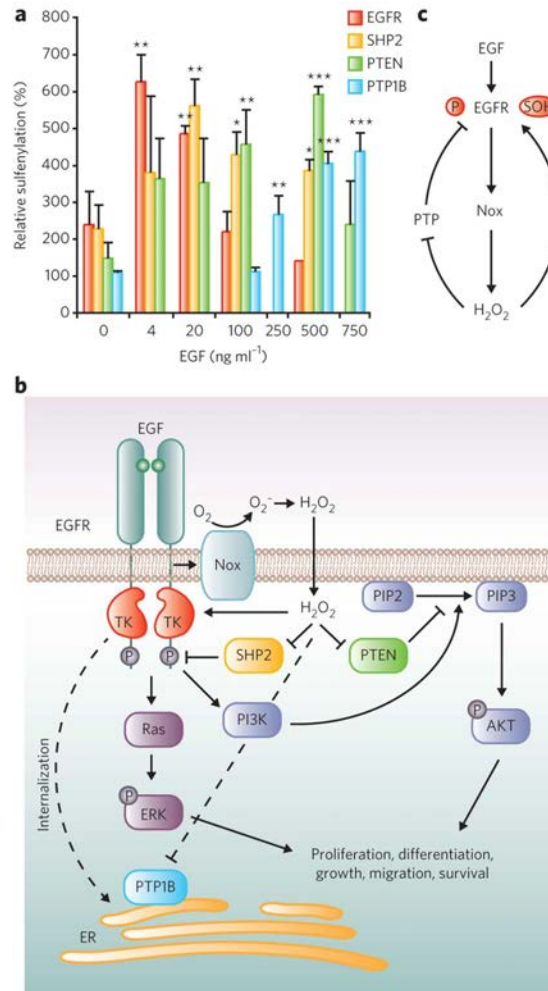


Figure 3.6: **Model for redox regulation of EGFR signaling.** (a) Densitometric quantification of EGFR and PTP sulfenylation from blots in Figure 3.4a-c and Figure 3.5a. Data are representative of four independent experiments and represent the mean \pm s.e.m. for each protein. *** indicates that $P < 0.001$, ** indicates that $P < 0.01$ and * indicates that $P < 0.05$ when compared against vehicle control. (b) The mitogen EGF binds to EGFR and induces the production of ROS in A431 cells via Nox2. The proximity of target proteins to Nox2 impacts the rate of cysteine oxidation within the cell. Dashed lines are relevant to EGFR internalization. (c) Model for H_2O_2 -mediated increase in EGFR kinase activity. Nox-generated H_2O_2 directly modifies EGFR at a critical cysteine (Cys797) in the active site, which enhances its tyrosine kinase activity. Endogenous H_2O_2 also oxidizes and deactivates PTPs, which serves to maintain EGFR phosphorylation. Collectively, these events lead to an increase in receptor autophosphorylation, which promotes signaling through downstream pathways.

Another central finding of this study is that EGFR becomes sulfenylated at Cys797 in EGF-stimulated cells and this modification enhances its intrinsic tyrosine kinase activity (Figure 3.6c). Interestingly, the decline in EGFR activity at higher H₂O₂ concentrations may reflect disulfide bond formation with another cysteine in the kinase domain, however future studies will be required to fully address this possibility. The biphasic response of recombinant EGFR kinase activity with H₂O₂ paralleled that of receptor sulfenic acid modification in cells; however, the peroxide concentration required for maximal rate enhancement was approximately 20-fold lower relative to sulfenylation in cells. One likely explanation for this difference is that antioxidant enzymes and other biomolecular targets consume the H₂O₂ applied to cells. Another noteworthy aspect of this behavior is that cellular sulfenylation and kinase activity decreased above 50 μ M H₂O₂, whereas EGFR phosphorylation continued to increase at peroxide levels above 500 μ M. These findings suggest a complex interplay between EGFR kinase activity and PTP inhibition at different concentrations of H₂O₂, wherein low levels stimulate catalysis, an effect that may be lost at higher doses, but is compensated for by PTP inactivation. Additionally, oxidation of Cys797 could positively regulate other aspects of EGFR function, including protein-protein interactions.

It is intriguing to consider the possibility that cysteine oxidation may serve as a general mechanism to regulate RTK activity. Of the 95 receptor and non-receptor protein tyrosine kinases (PTKs) in the human genome, nine additional members harbor a cysteine residue at the structural position that corresponds to Cys797, including two additional EGFR family members, Her2 and Her4 (28). Another subfamily of PTKs, which includes cytoplasmic Src as well as FGFR1, have a cysteine residue within a conserved glycine rich loop that interacts with the γ -phosphate of ATP. Interestingly, cellular studies implicate cysteine oxidation in Src regulation (37–39), albeit with apparently contradictory results. Furthermore, biochemical analysis of

Src shows that the glycine loop cysteine is reactive and that addition of DTT to recombinant FGFR1 stimulates kinase activity (40). To date, however, it has not been ascertained whether Src is a direct target of signaling-mediated H₂O₂ in cells; nor has the reaction of peroxide with FGFR1 been reported.

EGFR is mutated or amplified in a number of human carcinomas including breast and lung cancers, which has motivated the development of inhibitors, including analogs that covalently modify Cys797, which are currently under evaluation in clinical trials (27, 28). Recently, we have reported that overexpression of EGFR and Her2 in breast cancer cell lines correlates with elevated H₂O₂ and global protein sulfenylation (21). Coupled with the discovery that EGFR Cys797 undergoes sulfenic acid modification, these findings raise several fundamental questions vis-à-vis cysteine oxidation and thiol-targeted irreversible inhibitors. For example, the acrylamide moiety of the aforementioned EGFR inhibitors undergoes Michael addition with Cys797 in its thiol form, but does not undergo facile reaction with the sulfenic acid or disulfide states, which could influence the potency of these drugs. In addition, can the propensity for a particular cysteine residue to undergo oxidation be exploited in the design of irreversible inhibitors with a nucleophilic warhead targeting the sulfenylated protein, as has recently been reported for PTPs (41)? Taking this one step further, could this strategy be exploited to selectively target proteins in cells under oxidative stress, a condition that is associated with cancer, diabetes, and neurodegeneration? These topics represent new and exciting avenues for future research.

In summary, we have developed the new chemoselective probe, DYn-2, for detecting sulfenylated proteins in cells. Using this reagent, we have shown that growth factor-mediated signal transduction leads to oxidation of key signaling proteins, including EGFR. From a broader perspective, our findings highlight sulfenylation as a signaling mechanism analogous to phosphorylation and allude to new redox-based strategies for therapy development. In conjunction with new tools for ROS detec-

tion (2, 42, 43) and quantitative proteomic analysis (41, 44–46), these results presage a bright future ahead in the dissection of the regulatory mechanisms that underlie redox-regulation of cell signaling.

3.5 Methods

DYn-2 (2). Lithium diisopropylamide (LDA) was prepared by the dropwise addition of 2.5 M solution of n-BuLi (15.7 ml, 39.2 mmol) to a solution of diisopropylamine (3.97 g, 39.2 mmol) in THF (40 ml) and the resulting pale yellow mixture was stirred at -78 °C for 30 min in a 250 ml flask equipped with a magnetic stir bar under N₂ pressure. A solution of 1,3-cyclohexadione (2.0 g, 17.8 mmol) in THF (20 ml) and HMPA (10 ml) was added dropwise to the LDA solution at -78 °C. The resulting mixture was allowed to stir at -78 °C for 1.5 h. The temperature was increased to 0 °C briefly to facilitate the stirring, and then cooled again to -78 °C. To this dianion slurry, a solution of 5-iodopent-1-yne (3.81 g, 19.6 mmol) in THF (20 ml) was added dropwise at -78 °C. The reaction was stirred and allowed to warm to 25 °C over 2 h. The mixture was then neutralized with 1.0 M HCl (22 ml) and concentrated under reduced pressure. The residue was diluted with H₂O and extracted with ethyl acetate (3 x 50 ml). The organic phase was then washed with brine, dried over anhydrous MgSO₄, and concentrated. Purification by column chromatography (gradient: dichloromethane/methanol from 100:0 to 98:2) afforded compound **2** as a mixture of the keto and enol forms (3.0 g, 96% yield). The product was further purified by reversed-phase preparative HPLC (Varian Polaris 5 C18-A 150 × 21.2 mm column) using a gradient of water/acetonitrile from 95:5 to 5:95 over 30 min. ¹H-NMR (400 MHz, CDCl₃): δ 5.42 (s, 1H), 3.41 (d, *J* = 4.0 Hz, 2H), 2.75 - 1.72 (m, 16H), 1.68 - 1.45 (m, 6H). ¹³C-NMR (100 MHz, CDCl₃): δ 204.9, 204.4, 197.0, 189.2, 104.2, 84.4, 84.1, 69.1, 68.9, 58.5, 49.1, 41.8, 39.9, 30.1, 29.6, 28.5, 26.4, 26.2, 26.1, 24.7, 18.8, 18.7. ESI-MS: *m/z* for C₁₁H₁₄O₂ calculated: 178.23; observed: 179.1 [M+H]⁺.

Cell culture. HeLa cells were cultured as previously described (11). A431 cells (American Type Culture Collection) were maintained at 37 °C in a 5% CO₂ humidified atmosphere. Unless indicated otherwise, cells were cultured in high-glucose DMEM medium (Invitrogen) containing 10% FBS (Invitrogen), 1% GlutaMax (Invitrogen), 1% MEM nonessential amino acids (Invitrogen), and 1% penicillin-streptomycin (Invitrogen). For EGF treatment, cells were cultured until 80-90% confluent, rinsed with PBS, and placed in high-glucose DMEM medium without serum for 16-18 h. Following serum-deprivation, cells were treated with the indicated concentration of EGF for the indicated time period. EGF treatment was stopped by the removal of the medium and washing with PBS.

Sulfenic acid labeling in cells. HeLa cells were labeled as previously described (11). A431 cells were lifted with 0.25% trypsin-EDTA, harvested by centrifugation at 1500g for 2 min, washed, and resuspended in serum-free DMEM at a density of $3-4 \times 10^6$ cells/ml. Intact cells in suspension were incubated with DMSO vehicle (2% v/v) or the indicated concentration of sulfenic acid probe (DYn-2, DAz-2, or dimedone) at 37 °C in a 5% CO₂ humidified atmosphere with periodic gentle agitation. Following treatment for the indicated time, cells were collected, and washed with PBS. The resulting cells were routinely counted using a hemocytometer and uniformly displayed greater than 90% viability by trypan blue exclusion.

Click chemistry. Cell lysate (200 μ g, 1 mg/ml) was pretreated with 75 μ l NeutrAvidin-agarose (Pierce) to remove endogenously biotinylated proteins. The pre-cleared lysate was incubated with 100 μ M azide- or alkyne-biotin, 1 mM TCEP-HCl, 100 μ M TBTA ligand, and 1 mM CuSO₄ for 1 h at 25 °C with gentle rocking (final reaction volume of 200 μ l). The reaction was quenched by 40 mM EDTA, followed by methanol precipitation of the proteins. The resulting protein precipitate was then resolubilized in Laemmli sample buffer containing 5% of SDS in PBS. To analyze immunoprecipitated proteins, the resin was treated with 20 μ l click chemistry mix

(100 μ M azide-biotin, 1 mM TCEP, 100 μ M TBTA, 1 mM CuSO_4 in PBS) as above; reactions were quenched by boiling with 20 μ l Laemmli sample buffer for 10 min.

Immunostaining and fluorescence imaging. A431 cells were seeded on collagen-coated coverslips (BD Biosciences) and cultured as described above. The cells were then fixed with 4% paraformaldehyde in PBS for 15 min, washed three times with PBS, followed by blocking in 5% horse serum, 0.1% Triton X-100 in PBS for 30 min at 25 °C (blocking solution). The cells were then treated with rabbit anti-EGFR (1005, Santa Cruz Biotechnology), mouse anti-PTEN (A2B1, Santa Cruz Biotechnology), mouse anti-PTP1B (FG6, Calbiochem), or rabbit anti-SHP2 (Santa Cruz Biotechnology), at 2 μ g/ml in blocking solution for 1 h at 25 °C. Control cells were treated with PBS only. The cells were washed three times in PBS and incubated with Alexa594-conjugated goat anti-rabbit (Invitrogen), Alexa488-conjugated goat anti-rabbit (Invitrogen), or Alexa488-conjugated goat anti-mouse (Invitrogen) secondary antibodies diluted to 1:1000 in blocking solution for 1 h at 25 °C in the dark. For experiments involving dimedone, cells were fixed in cold methanol:acetone (1:1), blocked, and treated with rabbit anti-2-thiodimedone (1:3000) as previously described. The cells were then washed three times with PBS and stained by Alexa594-conjugated goat anti-rabbit secondary antibody (1:1000) for 1 h at 25 °C in the dark. To visualize Nox2, cells were double stained with rabbit anti-2-thiodimedone antibody (1:3000) and PE-conjugated mouse anti-Nox2 antibody (7D5, MBL International, 1:1000), followed by Alexa488-conjugated goat anti-rabbit secondary antibody (1:1000). Cells were then washed three times with blocking solution, counterstained with 0.1 mg/ml DAPI, washed with PBS, and mounted with Fluoromount G (Southern Biotech). Confocal fluorescence imaging studies on A431 cells were performed with an Olympus FV1000 microscope and an x100 oil-immersion objective lens. Excitation of Alexa488-conjugate was carried out with an argon laser and emission was collected using a 488-nm to 515-nm filter set. Excitation of Alexa594- or PE-conjugate was

carried out with a HeNe laser, and emission was collected using a 548-nm to 644-nm filter set.

3.6 Contributions

C.E.P., T.H.T. and A.H. performed cell culture and immunostaining experiments. F.J.G. performed mass spectrometry experiments. V.G. and S.E.L. performed synthetic experiments. K.S.C. designed experimental strategies with help from C.E.P. and V.G.

3.7 Supplementary Methods

Synthetic Materials and Methods. All reactions were performed under a nitrogen atmosphere in oven-dried glassware. Tetrahydrofuran was distilled over sodium hydride prior to use. All other reagents and solvents were purchased from Sigma in the highest available purity and were used without further purification. Analytical thin layer chromatography (TLC) was carried out using Analtech Uniplate silica gel plates and visualized using a combination of UV and potassium permanganate staining. Flash chromatography was performed using silica gel (32-63 μM , 60 Å pore size) from Sorbent Technologies Incorporated. NMR spectra were obtained on a Bruker Avance 400 (400 MHz for ^1H ; 100 MHz for ^{13}C) in CDCl_3 (Cambridge Isotope Laboratories). ^1H and ^{13}C NMR chemical shifts are reported in parts per million (ppm) referenced to the residual CHCl_3 . Low-resolution electrospray ionization (ESI) mass spectra were obtained with an Agilent 6120 Single Quadrupole LC/MS.

3-ethoxy-6-(prop-2-yn-1-yl)cyclohex-2-enone. To a lithium diisopropylamide (LDA) solution, prepared from diisopropylamine (1.66 ml, 12 mmol) and *n*-BuLi (4.8 ml of a 2.5 M solution in hexanes, 12 mmol) in anhydrous THF (45 ml) at -78 °C under argon, was added 3-ethoxycyclohex-2-enone (1.4 g, 10 mmol) in THF (20 ml),

dropwise over 0.5 h. The reaction was stirred for an additional 2 h at -78 °C. Stirring was followed by the dropwise addition of propargyl bromide (1.3 ml, 12 mmol). The reaction was allowed to warm to rt and stirred for 8 h. The reaction was quenched with water (20 ml) and sat. NH₄Cl (20 ml). The aqueous phase was extracted with DCM (3x50 ml), and the organic phases were combined, washed with brine (20 ml), dried over Na₂SO₄, and concentrated. The resulting syrup was purified with silica gel column chromatography using 6:4 Hexanes: ethyl acetate resulting in a yellow oil **3** (1.6 g, 8.99 mmol) in 89% yield. R_f: 0.6 (1:1 hexanes: ethyl acetate). ¹H NMR (400 MHz, CDCl₃) 5.31 (s, 1H), 3.98 - 3.78 (m, 2H), 2.76 (dt, *J* = 16.6, 3.2 Hz, 1H), 2.59 - 2.41 (m, 2H), 2.41 - 2.20 (m, 4H), 1.95 (q, *J* = 2.3 Hz, 1H), 1.82 (dtd, *J* = 16.8, 11.5, 5.1 Hz, 1H), 1.45 - 1.27 (m, 3H). ESI-MS: *m/z* for C₁₁H₁₄O₂ calculated 178.10; observed 179.1 [M+H]⁺.

4-(prop-2-yn-1-yl)cyclohexane-1,3-dione (1). To a solution of 3-ethoxy-6-(prop-2-yn-1-yl)cyclohex-2-enone (0.05 g, 0.29 mmol) in acetonitrile (2 ml) and water (2 ml) was added CAN (0.015 g, 0.028 mmol). The solution was heated to reflux for 2 hr. The reaction mixture was then diluted with brine (20 ml), and extracted with EtOAc (3x20 ml). The organic phases were combined, washed with brine (30 ml), dried over Na₂SO₄, and concentrated *in vacuo*. The resulting orange solid was purified by silica gel column chromatography using 1:1 Hexanes:EtOAc to give compound **1** as a pale yellow solid (0.042 g, 0.28 mmol) in 96% yield. R_f: 0.3 (1:1 Hexanes:EtOAc). ¹H NMR (400 MHz, dms_o-d₆) δ 11.05 (s, 1H), 5.25 (s, 1H), 3.43 - 3.14 (m, 1H), 2.76 (d, *J* = 24.8 Hz, 1H), 2.37 - 2.16 (m, 4H), 2.04 (dt, *J* = 28.7, 11.9 Hz, 1H), 1.81 - 1.57 (m, 1H). ¹³C NMR (100 MHz, dms_o-d₆) δ 103.4, 82.7, 72.2, 25.7, 18.9. ESI-MS: *m/z* for C₉H₁₀O₂ calculated: 150.07; observed: 151.1 [M+H]⁺.

Synthesis of 5-iodopent-1-yne, alkyne-biotin and azide-biotin. 5-iodopent-1-yne was synthesized according established literature procedures (47). Alkyne-biotin was synthesized according to established literature procedures (48). Azide-biotin was

synthesized according to established literature procedures (49). In all cases, ESI-MS, ^1H and ^{13}C NMR spectra matched literature values (47–49).

Reagent Source, Purity and Stock Solutions. All stocks were stored at -20°C , unless otherwise indicated. The EGF (BD Biosciences) solution was prepared at $30\ \mu\text{g}/\text{ml}$ in ddH_2O . H_2O_2 was purchased from Sigma and lower concentrations were made by dilution of the stock solution with ddH_2O . Gefitinib (1 mM, Santa Cruz Biotechnology, $>99\%$ purity), Afatinib (100 μM and 500 μM , Chemietek, $>99\%$ purity), Canertinib (1 mM, Chemietek, $>99\%$ purity), Pelitinib (100 μM , Santa Cruz Biotechnology, 98% purity), Apocynin (10 mM, Calbiochem, $\geq 98\%$ purity), and Wortmannin (10 mM, Cayman Chemicals, $\geq 98\%$ purity) stocks were prepared in DMSO at the indicated concentrations. DAz-2 was synthesized and purified ($\geq 99\%$ purity) as previously described (11). DAz-2, DYn-1 ($\geq 98\%$ purity) and DYn-2 ($\geq 99\%$ purity) were prepared in DMSO at 250 mM. Dimedone (Sigma, $\geq 99\%$ purity) was prepared as a 50:50 mixture of DMSO and 0.5 M Bis-Tris HCl (pH 7.0) at 250 mM. Catalase (20,000 U/ml, Sigma) included in lysis buffers and PEG-catalase (100,000 U/ml, Sigma) were prepared in 50 mM Tris-HCl (pH 7.4) and stored at -80°C or made up fresh, respectively. L-NAME (10 mM, Calbiochem, $\geq 98\%$ purity) and NAC (1 M, Research Products International, $>99\%$ purity) were freshly prepared in serum-free DMEM at the indicated concentrations. DPI (2.5 mM, 5 mM, and 10 mM, Sigma, $\geq 98\%$ purity) stocks were made in DMSO. Azide- or alkyne-biotin were prepared at 5 mM in DMSO, TBTA ligand was prepared at 2 mM stock in 4:1 DMSO:tBuOH, and TCEP-HCl (Sigma) and CuSO_4 (Sigma) were freshly prepared at 50 mM in ddH_2O .

Expression, purification, and labeling of sulfenylated Gpx3. Recombinant Cys82Ser Gpx3 and Cys64Ser Cys82Ser Gpx3 were expressed and purified as previously described (16). Cys82Ser Gpx3 and Cys64Ser Cys82Ser Gpx3 were previously stored in 50 mM Tris HCl pH 7.4, 300 mM NaCl, 10% glycerol, and 5 mM DTT. DTT was removed from Gpx3 mutants via spin filtration using P-30 micro BioSpin

columns (BioRad) pre-equilibrated with Gpx3 buffer (50 mM Tris HCl pH 7.4, 300 mM NaCl). 50 μ M Cys82Ser Gpx3 was treated with 1 mM DAz-2, 1 mM DYn-1, 1 mM DYn-2 or vehicle in the presence or absence of 100 μ M H₂O₂ for 15 min at 37 °C. Excess probe was removed by spin filtration, and azide- or alkyne-modified Cys82Ser Gpx3 was biotinylated and analyzed as described in Methods. After click chemistry, the reactions were quenched by addition of an equal volume of Laemmli sample buffer. To verify the DYn-2 adduct by mass spectrometry, Cys64Ser Cys82Ser Gpx3 was incubated with H₂O₂ and 10 mM DYn-2 for 1 h at 37 °C with gentle rocking. The concentrations of Cys64Ser Cys82Ser Gpx3 and H₂O₂ used are indicated in the figure legends. Excess reagent was removed by spin filtration as described above.

Lysate preparation. Cells were harvested in modified RIPA lysis buffer [50 mM triethanolamine, pH 7.4, 150 mM NaCl, 1% NP-40, 1% sodium deoxycholate, 0.1% SDS, 1x EDTA-free complete mini protease inhibitors (Roche), 200 U/ml catalase (Sigma)]. After 20 min incubation on ice with frequent mixing, unlysed cell fragments were removed by centrifugation at 14000g for 15 min at 4 °C, and protein concentration was determined by BCA assay (Pierce). For analysis of protein phosphorylation, cells were harvested in phosphorylation lysis buffer [50 mM triethanolamine, pH 7.4, 150 mM NaCl, 1% NP-40, 1% sodium deoxycholate, 0.1% SDS, 5 mM sodium pyrophosphate, 50 mM sodium fluoride, 10 μ M β -glycerophosphate, 1 mM sodium orthovanadate, 0.5 mM DTT, and 1x complete mini protease inhibitors (Roche)]. For co-immunoprecipitation of Nox2 with EGFR, cells were harvested by gentle scraping with a rubber policeman in native lysis buffer A (50 mM Tris-HCl, pH 7.4, 150 mM NaCl, 0.1% Triton X-100, 0.1% NP-40, 4 mM EDTA, 1 mM sodium orthovanadate, 2.5 mM sodium pyrophosphate, 1 mM β -glycerophosphate and 1x complete mini protease inhibitors) and lysed with gentle rotation at 4 °C for 1 h. Coimmunoprecipitation of EGFR with Nox2 was performed as described above, except in native lysis buffer B (50 mM Tris-HCl, pH 7.4, 150 mM NaCl, 3 mM EDTA, 0.5% NP-40,

20 mM β -glycerophosphate, 1 mM sodium orthovanadate, 1x complete mini protease inhibitors).

Western blot. Protein samples were separated by SDS-PAGE using Mini-Protean TGX 4-15% Tris-Glycine gels (BioRad) and transferred to a polyvinylidene difluoride (PVDF) membrane (BioRad). After transfer, the membrane was blocked with 3% BSA or 5% milk (pAKT/AKT blotting) in TBST for 1 h at 25 °C. The membrane was washed with TBST and immunoblotting was performed with the following primary and secondary antibodies at the indicated dilutions in TBST, unless otherwise noted: phospho-EGFR (pY1068, Abcam, 1:1000), EGFR (1005, Santa Cruz Biotechnology, 1:200), phospho-AKT (pS473 XP, Cell Signaling Technology, 1:2000 or pT308, Cell Signaling Technology, 1:1000), AKT (Cell Signaling Technology, 1:2000), phospho-ERK (pT185/pY187, Invitrogen, 1:1000), ERK (Invitrogen, 1:1000), streptavidin-HRP (GE Healthcare, 1:8000 - 1:80000), His-HRP (Pierce, 1:50000), GAPDH (Santa Cruz Biotechnology, 1:200), PTEN (A2B1, Santa Cruz Biotechnology, 1:200), PTP1B (Calbiochem, 1:1000), SHP2 (Santa Cruz Biotechnology, 1:200), Nox2 (ab31092, Abcam, or Santa Cruz Biotechnology, 1:500 - 1:1000 in PBST), Nox1 (ab55831, Abcam, 1:500 in PBST), phospho-Tyrosine (Millipore, 1:1000), goat anti-rabbit IgG-HRP (Calbiochem, 1:2000 - 1:50000), rabbit anti-mouse IgG-HRP (Invitrogen, 1:30000), and donkey anti-goat IgG-HRP (Santa Cruz Biotechnology, 1:30000 in PBST). PVDF membrane was developed with chemiluminescence (GE Healthcare ECL Plus Western Blot Detection System) and imaged by film. Data was quantified by densitometry with ImageJ (Wayne Rasband, US National Institutes of Health, <http://rsbweb.nih.gov/ij/>). PVDF membranes were stripped using mild stripping buffer (200 mM glycine pH 2.2, 0.1% SDS, 1% Tween-20) according to established protocol (www.abcam.com) before reprobing.

Immunoprecipitation. EGFR was immunoprecipitated from 500 μ g cell lysate (1 mg/ml) with 1 μ g of anti-EGFR antibody. PTPs were immunoprecipitated from

1 mg lysate prepared from A431 cells cultured in low-glucose DMEM with 1 μ g anti-PTEN antibody, anti-PTP1B antibody (BD Transduction Laboratories), or anti-SHP2 antibody overnight at 4 °C with gentle rocking. The immunocomplexes were isolated by incubating 20 μ l protein A sepharose (EGFR and SHP2; GE Healthcare) or protein G agarose (PTEN and PTP1B; Roche) for an additional 2 h at 4 °C with rocking. The resin was collected by centrifugation at 100g for 2 min at 25 °C, washed three times with cold RIPA buffer (Boston BioProducts), subjected to click chemistry as described in Methods, and proteins were eluted by boiling with Laemmli sample buffer for 10 min. Nox2 and SHP2 were co-immunoprecipitated with EGFR from 500 μ g of lysate with 20 μ l goat anti-EGFR antibody-conjugated agarose (Santa Cruz Biotechnology) or isotype control (normal goat IgG) in a total volume of 500 μ l for 4 h at 4 °C with gentle rocking. The resin was collected as above and washed three times with cold native lysis buffer, and eluted as above. EGFR was coimmunoprecipitated with Nox2 as above, except using 20 μ l rabbit anti-Nox2 antibody-conjugated agarose (Santa Cruz Biotechnology) or normal rabbit IgG as an isotype control. For ESI-MS analysis in Supplementary Figure 3.S4c, A431 cells were stimulated with 4 ng/ml EGF for 2 min, harvested by trypsinization, and treated with dimedone as in Methods. Following treatment, EGFR was immunoprecipitated from 6 mg cell lysate as described above. The EGFR was eluted by boiling for 10 min in 10% SDS in ddH₂O and then precipitated by acetone. The resulting protein precipitate was resuspended in Laemmli sample buffer, and resolved by SDS-PAGE.

Intracellular ROS detection. Intracellular ROS were measured in a 96-well plate using the fluorescent probe DCF (the intracellular product of H₂-DCF diacetate that fluoresces in the presence of ROS, including H₂O₂). A431 cells were seeded at 1.5×10^4 per well, grown and stimulated with EGF as described in Methods. Inhibitors/scavengers were added to culture medium prior to treatment for the period of time indicated in figure legends. Following stimulation, cells were washed

twice with PBS, and incubated in the dark for 30 min at 25 °C with 10 μ M 2',7'-dichlorodihydrofluorescein diacetate (H₂DCF-DA, Sigma) in PBS. H₂DCF-DA is a cell permeable indicator for ROS that is a nonfluorescent compound that can enter cells and is trapped by intracellular esterase cleavage of the diacetate group. H₂DCF is converted into a fluorescent product upon interaction with intracellular ROS. After incubation, the intensity of fluorescence was measured at 488 nm (excitation) and 525 nm (emission) using a SpectraMax M5 microplate reader (Molecular Devices). To examine the effect of DYn-2 on intracellular ROS, serum-deprived A431 cells were washed three times with PBS and then harvested by 0.25 % trypsin/EDTA. The trypsin was neutralized with DMEM and cells were collected by centrifugation at 1500g for 2 min. Cells were aliquoted at 6×10^5 cells per microcentrifuge tube and treated with 5 mM DYn-2 or DMSO vehicle (2% v/v) for 1 h at 37 °C. Following treatment, the cells were washed three times with PBS, seeded into 96-well plates at 1×10^5 cells/well in triplicate, and analyzed for DCF fluorescence as described above.

Cell viability. Serum-deprived A431 cells were labeled with 5 mM DYn-2 or DMSO vehicle (2% v/v) as described in Methods. After labeling, the cells were washed three times with PBS and resuspended in 500 μ l PBS with an equal volume of trypan blue solution (0.4 % w/v). The mixture was incubated at 25 °C for 3 min, and 10 μ l of the cell suspension was loaded onto a hemocytometer and counted under a microscope.

Quantification of glutathione in A431 Cells. Serum-deprived A431 cells were treated with 5 mM DYn-2 or DMSO vehicle (2% v/v) as described in Methods. After labeling, the cells were washed three times with PBS and lysed in 1x GSH MES buffer (Cayman Chemicals). Levels of total, reduced, and oxidized glutathione were measured using the Glutathione Assay kit (Cayman Chemicals) according to the manufacturers instructions.

Quantification of peroxiredoxin SO₃ in A431 Cells. Serum-deprived A431

cells were treated with 5 mM DYN-2 or 2% (v/v) DMSO as described in Methods. After labeling, cells were lysed in modified RIPA lysis buffer, resolved by SDS-PAGE, and analyzed by anti-Peroxiredoxin-SO3 (Abcam, 1:1000) Western blot.

In-gel trypsin digestion of Gpx3. DYN-2 labeled Gpx3 was resolved by SDS-PAGE and stained with SimplyBlue SafeStain (Invitrogen). After staining, the gels were washed with H₂O and bands of interest were excised. The excised bands were dehydrated in 2:1 ACN: 25 mM ammonium bicarbonate (Ambic), pH 8.0 and subsequently rehydrated with 25 mM Ambic pH 8.0 twice prior to reducing with 10 mM DTT for 1 h at 56 °C. DTT was removed and the samples were alkylated with 55 mM iodoacetamide for 45 minutes at 25 °C in the dark. Iodoacetamide was removed and the excised bands were washed with 25 mM Ambic pH 8.0 then dehydrated and rehydrated two additional times. Sequencing grade modified trypsin (Promega) was added to the excised bands at a ratio of 1:25 (w/w), and the samples were incubated overnight at 37 °C. Peptides were extracted from the gel by collecting the supernatant and by dehydrating and rehydrating the excised bands. Peptide samples were concentrated via vacuum centrifugation and analyzed by ESI-LC-MS/MS.

In-gel pepsin digestion of immunoprecipitated EGFR. The band corresponding to EGFR was excised and the gel slice was processed as above with the following modifications. After iodoacetamide removal, the excised bands were washed with 75 mM K₂HPO₄/75 mM KH₂PO₄ pH 2.5 then dehydrated and rehydrated two additional times with 2:1 ACN: 75 mM K₂HPO₄/75 mM KH₂PO₄ pH 2.5 and 75 mM K₂HPO₄/75 mM KH₂PO₄ pH 2.5, respectively. Sequencing grade pepsin (Princeton Separations) was added to excised bands at 20 ng/ μ L and incubated overnight at 37 °C.

ESI-LC/MS/MS Analysis. Protein and peptides were analyzed on an electrospray linear ion trap mass spectrometer (LTQ-XL, Thermo Scientific) after separation on an Agilent Eclipse XDB-C8 2.1 mm x 15 mm trap with mobile phases A (0.1%

formic acid in water) and B (0.1% formic acid in acetonitrile) which was used to trap, desalt, and elute peptides onto a Vydac Everest reverse-phase C18 monomeric column (2.1 mm x 150 mm, 300 Å, 5 μm) with a gradient of 5% to 60% B in 60 min at a flow rate of 200 μL/min. Peptide and protein identification were performed using Mascot (<http://www.matrixscience.com>). Mass lists, in the form of Mascot generic files, were created automatically and used as the input for Mascot MS/MS Ion searches against a database containing the full sequence of EGFR. The search parameters were as follows: The enzyme specificity was Pepsin A with one missed cleavage permitted. The variable modifications included Carbamidomethyl (C-SH), Dimedone (C-SOH), and Oxidation (M). The mass tolerance for the precursor ions obtained from the ESI-TRAP was set to ± 2 Da and the fragment mass tolerance was set to ± 2 Da. The maximum expectation value (p) for accepting individual MS/MS spectra was set at 0.05.

***In vitro* EGFR kinase assay.** The tyrosine kinase activity of recombinant human EGFR kinase domain (Promega) was assayed using the ADP-Glo™ Kinase Assay (Promega) according to the manufacturers protocol (www.promega.com), except that DTT was not included in the reaction buffer. In brief, the ADP-Glo™ Kinase Assay is a luminescent assay that measures ADP formed from the EGFR kinase reaction; ADP is converted into ATP, which is a substrate in a reaction catalyzed by Ultra-Glo™ Luciferase that produces light. The luminescent signal positively correlates with ADP amount and kinase activity. Poly (4:1 Glu, Tyr) (Promega) was used as a peptide substrate. When present, EGFR inhibitors, H₂O₂ or DTT were added to the reaction mixture for the period of time indicated in figure legends.

Statistical analysis. Each graph represents the mean values for the corresponding experiment ± s.e.m. Where appropriate, statistical significances were determined from unnormalized data using the two-tailed Student's t-test, which is a variation of the ANOVA test appropriate for small sample sizes. Each statistically-characterized

Western blot experiment is representative of four independent trials and each ROS, glutathione, or recombinant EGFR experiment is representative of three independent readings. p-values smaller than 0.05 were deemed statistically significant and ranges are provided in the figure legends. The full p-values for each experiment in order from left to right are: Figure 3.1c, calculated with respect to the EGF-only sample: 7.30×10^{-8} , 1.73×10^{-6} , 2.38×10^{-8} , 0.02, 0.003, 0.0016; Figure 3.3a, calculated with respect to the vehicle only control: 3.83×10^{-7} , 1.02×10^{-7} ; Figure 3.3c: 0.02, 0.0016, 4.00×10^{-3} ; Figure 3.3d, calculated with respect to the vehicle only control: 0.003, 0.04, 0.005; Figure 3.3f, calculated with respect to the vehicle only control: 0.0012, 0.018; 0.025; Figure 3.5h, calculated with respect to the 0 μ M H₂O₂ control: 0.00014, 0.003, 3.00×10^{-5} , 0.002, 0.002, 0.008; Figure 3.6a, calculated with respect to the corresponding vehicle only control for each protein: EGFR, 0.002, 0.007; SHP2, 0.002, 0.016, 0.017; PTEN, 0.0100, 1.634×10^{-5} ; PTP1B, 0.003, 7.248×10^{-6} , 5.626×10^{-5} .

3.8 Supplementary Figures

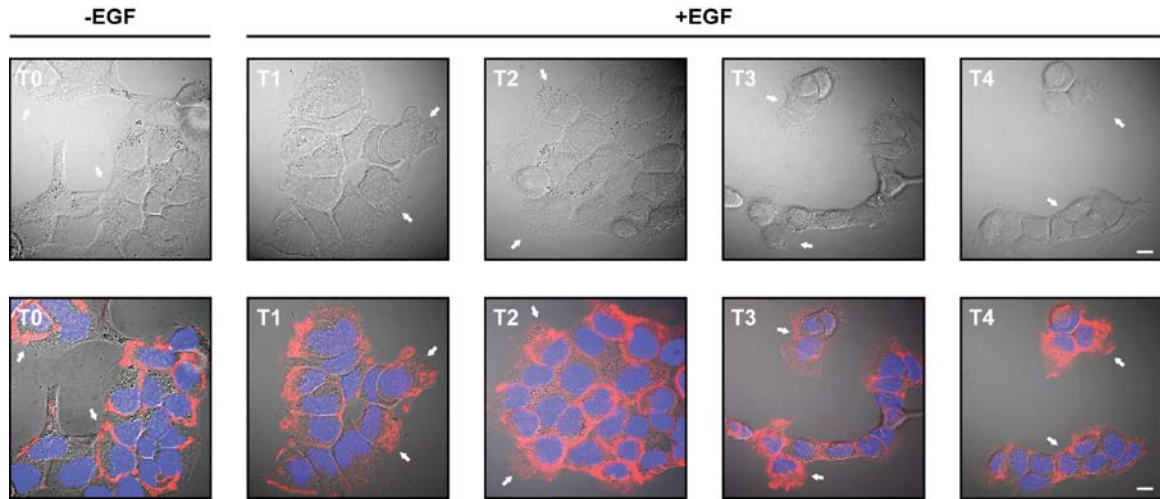


Figure 3.S1: **EGF-dependent morphological changes in A431 cells.** Top images: Bright-field images of A431 cells before (T0) and after 100 ng/ml EGF stimulation for 2, 15, 30, and 60 min (labeled as T1, T2, T3, and T4, respectively). Bottom images: Combined bright-field and confocal fluorescence image of A431 cells (Figure 3.1b depicts the confocal fluorescence image alone). Cells were fixed and stained as described in Methods with rabbit anti-EGFR antibody (2 $\mu\text{g}/\text{ml}$) followed by Alexa594-conjugated (red) goat anti-rabbit secondary antibody (1:1000). White arrows highlight changes in receptor localization (T0, plasma membrane; T1, membrane ruffles; T2, regions of cell stretching and migration; T3, perinuclear and endosomal membranes; T4, plasma membrane and ruffles). Nuclei were counterstained with DAPI (blue). Scale bar, 10 μm .

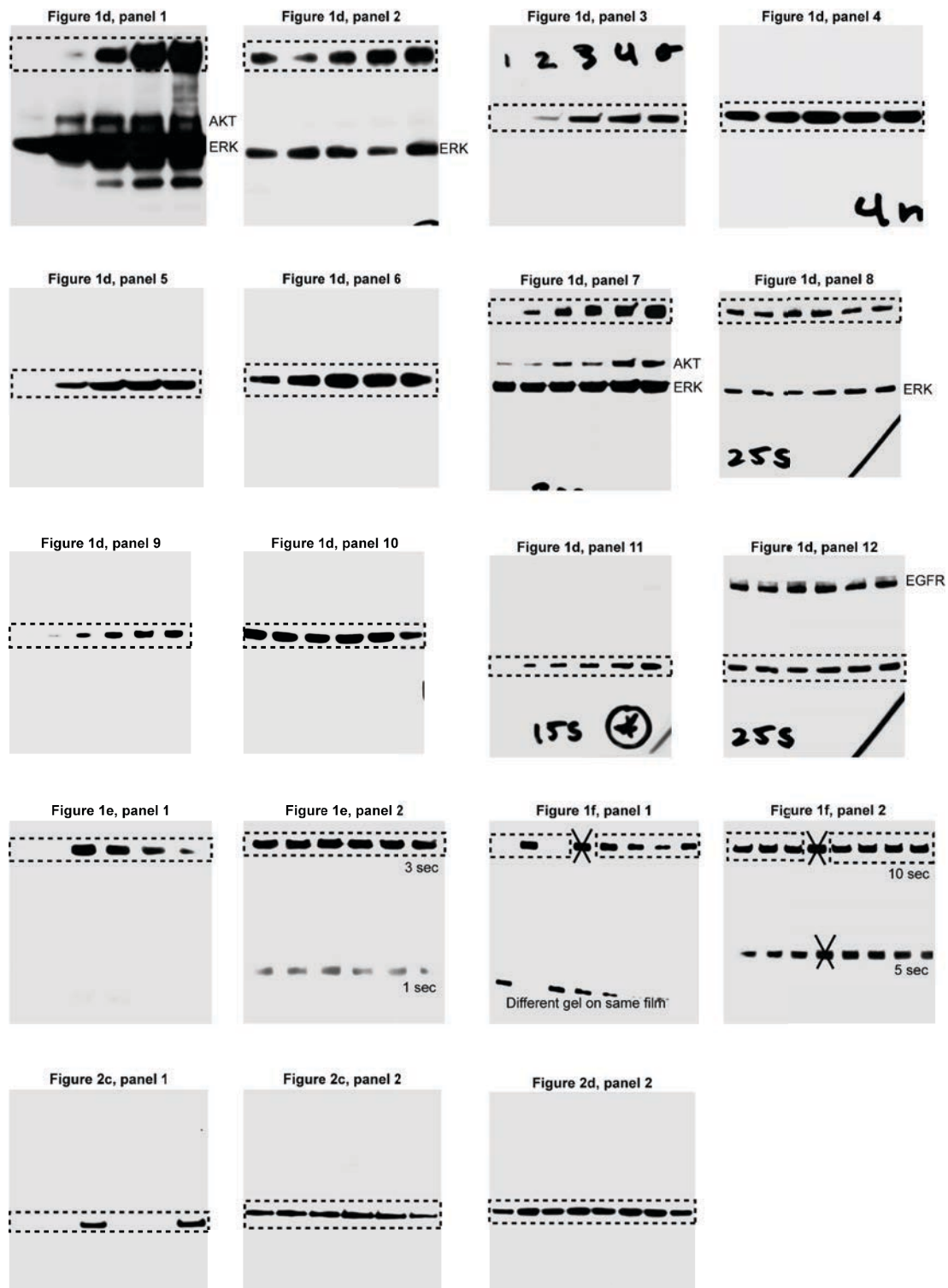
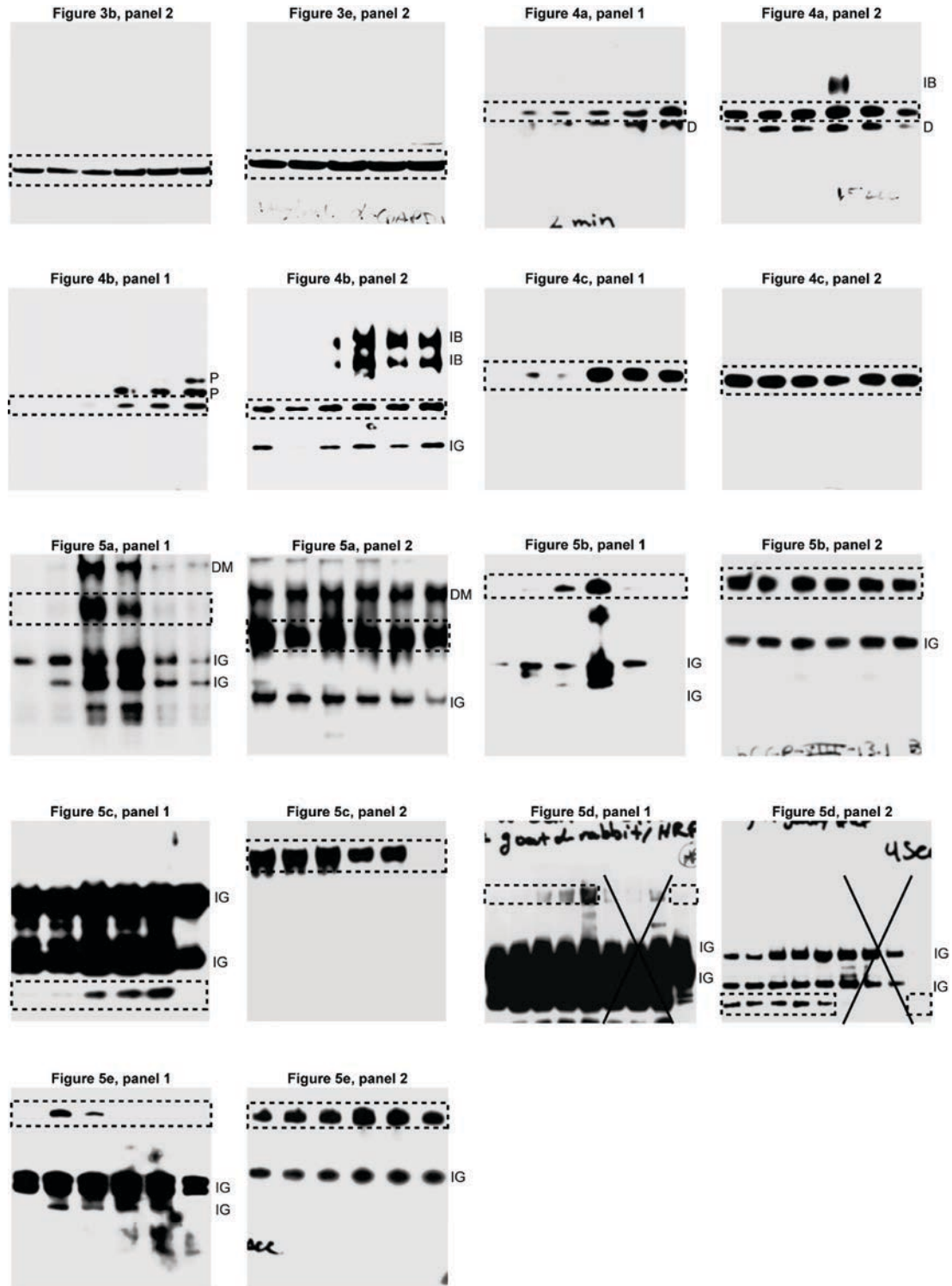


Figure 3.S2: Uncut full Western blots shown (part 1) in Figure 3.1d-f, Figure 3.2c,d, Figure 3.3b,e, Figure 3.4a-c, and Figure 3.5a-e. The regions surrounded by dashed lines represent the panels in the respective figures. IG, immunoglobulin; IB, nonspecific immunoreactive band non-specific band; D, degradation; P, phosphorylated; DM, dimer.



Uncut full Western blots shown (part 2) in Figure 3.1d-f, Figure 3.2c,d, Figure 3.3b,e, Figure 3.4a-c, and Figure 3.5a-e. The regions surrounded by dashed lines represent the panels in the respective figures. IG, immunoglobulin; IB, nonspecific immunoreactive band non-specific band; D, degradation; P, phosphorylated; DM, dimer.

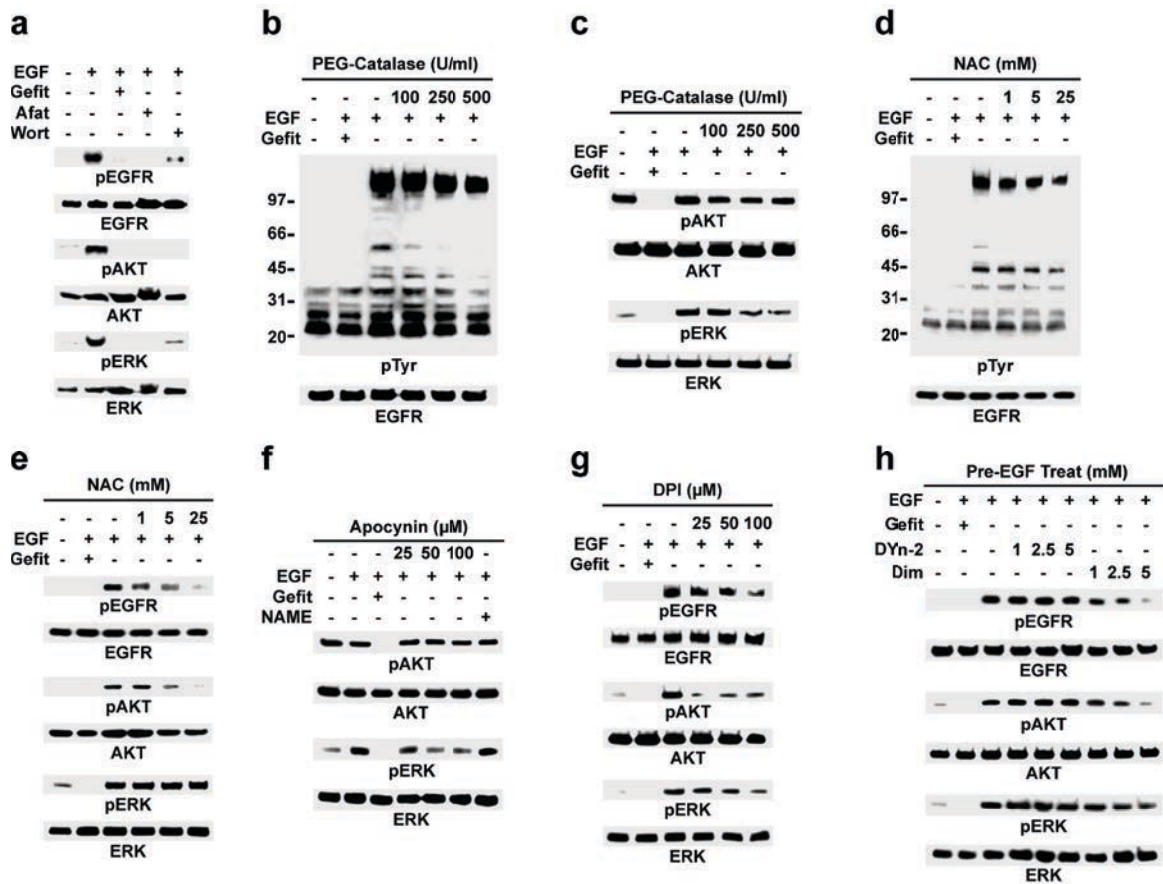


Figure 3.S3: **Effect of inhibitors, antioxidants, and sulfenic acid probes on EGF-mediated signaling.** (a-h) Western blots showing global tyrosine phosphorylation (pTyr) or phosphorylated (p) EGFR, AKT and/or ERK and total EGFR, AKT, and/or ERK as loading controls. (a) A431 cells were stimulated with 100 ng/ml EGF or vehicle for 5 min. Where indicated, A431 cells were pretreated with 10 μ M gefitinib, 100 μ M afatinib or 100 μ M wortmannin for 25 min. (b,c) A431 cells were treated with the indicated concentrations of PEG-catalase for 5 min (b) or 30 min (c) and then stimulated with 100 ng/ml EGF or vehicle for 5 min. Gefitinib treatment was as in a. (d,e) A431 cells were stimulated with 100 ng/ml EGF or vehicle for 5 min in the presence of the indicated concentrations of NAC. Gefitinib treatment was as in a. (f) A431 cells were stimulated with 100 ng/ml EGF or vehicle for 5 min. Where indicated, A431 cells were pretreated with the indicated concentrations of apocynin for 25 min before stimulation. (g) A431 cells were stimulated with 100 ng/ml EGF or vehicle for 5 min. Where indicated, A431 cells were pretreated with the indicated concentrations of DPI for 5 min before stimulation. (h) A431 cells were stimulated with 100 ng/ml EGF or vehicle for 5 min. Where indicated, A431 cells were pretreated with the indicated concentrations of DYn-2 or dimedone for 25 min before stimulation.

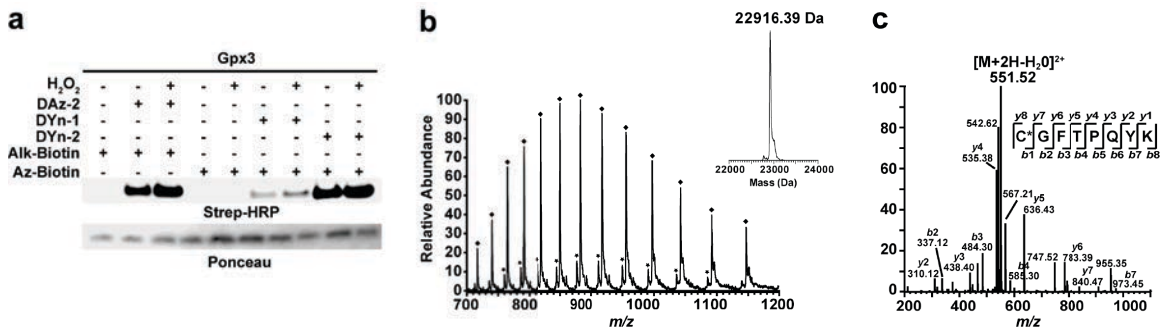


Figure 3.S4: **DYn-2 detection of Gpx3 sulfenic acid by Western blot and mass spectrometric analysis.** (a) Comparison of DAz-2, DYn-1 and DYn-2 detection of sulfenic acid in recombinant Gpx3. 50 μ M protein was untreated or exposed to 100 μ M H₂O₂ and incubated in presence or absence of 1 mM probe for 15 min at 37 °C. Labeled proteins were then conjugated to azide-biotin (Az-Biotin) or alkyne-biotin (Alk-biotin) via copper(I)-catalyzed azide-alkyne [3+2] cycloaddition (click chemistry), separated by SDS-PAGE, and detected by streptavidin-HRP Western blot, as described in Methods. Comparable protein loading was confirmed by Ponceau stain. (b) ESI-LC/MS intact mass analysis shows the covalent attachment of a single DYn-2 molecule to Gpx3 (\blacklozenge , 22916.39 Da). The inset shows the deconvoluted mass spectrum. The observed mass shift is 177.48 Da, whereas the expected mass shift for a single DYn-2 adduct is 176.08 Da. The slight discrepancy is well within range of the mass accuracy for the LTQ-XL instrument (100 ppm or \pm 2.29 Da at 22916.39). Over-oxidation of the catalytic cysteine to sulfenic acid (SO₂H) is also observed (\blackstar , 22776.36 Da). 25 μ M Gpx3 was treated with 37.5 μ M H₂O₂ and labeled with 10 mM DAz-2 for 1 h at 37 °C. (c) ESI-LC/MS/MS analysis of the reaction from a using collision-induced dissociation (CID) of the precursor ion m/z 551.52 [M + 2H - H₂O]⁺² corresponding to DYn-2-tagged peptide (C(2)GFTPQYK-OH) derived from trypsin digest of Gpx3.

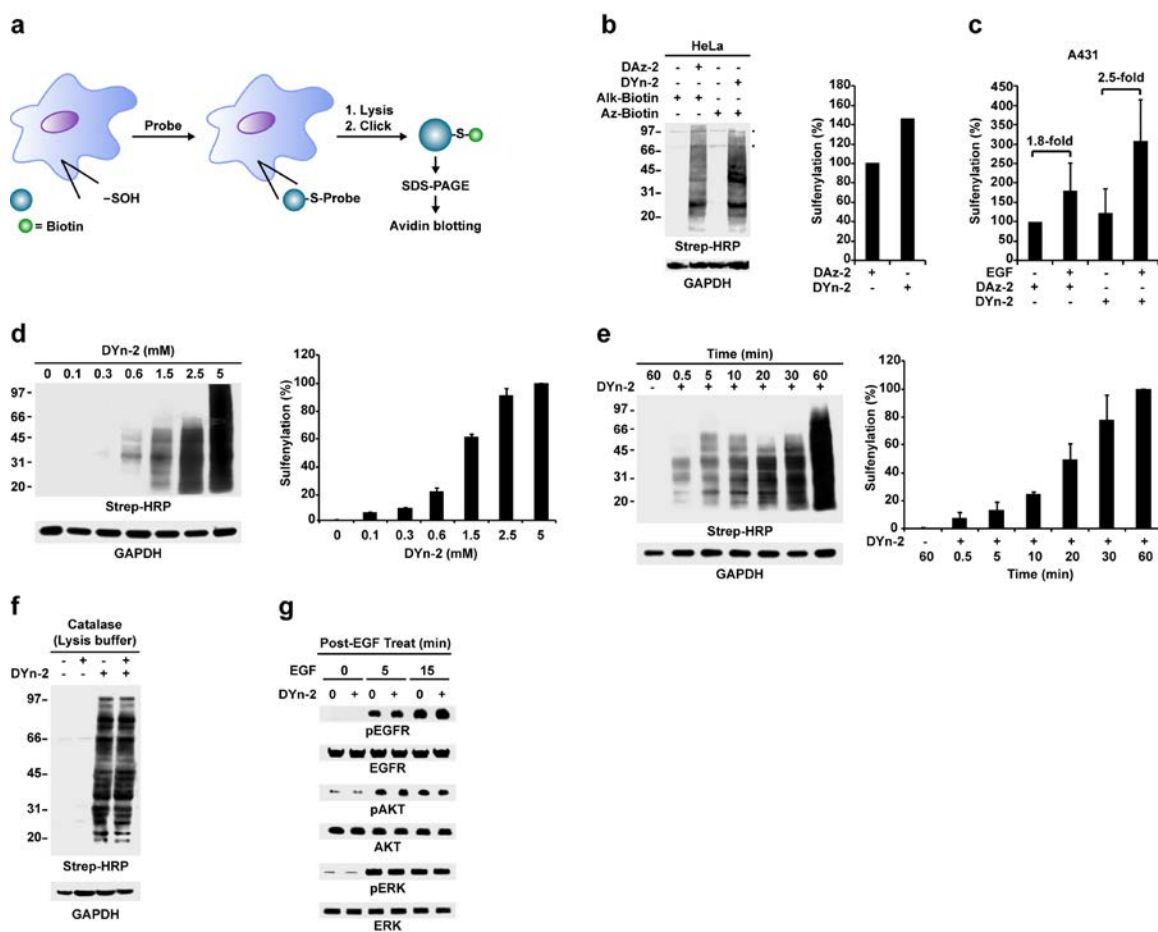


Figure 3.S5: **DYn-2 labeling of protein sulfenic acids in A431 cells.** (a) Bioorthogonal chemical reporter strategy to label sulfenylated proteins in cells and their subsequent detection using click chemistry and streptavidin-HRP Western blot. (c) Western blot showing DAz-2 and DYn-2 detection of protein sulfenic acids and total GAPDH in HeLa cells incubated with 5 mM probe or vehicle for 2 h at 37 °C. (right panel b,c) Densitometric quantification of electrophoretic lanes from c and Figure 3.2d. (c) The numbers situated above indicate the fold-increase in sulfenylation signal between unstimulated and EGF-treated cells. (d,e) Western blot showing dose- and time-dependent detection of protein sulfenic acids in A431 cells and total GAPDH as loading controls. A431 cells were stimulated with 100 ng/ml EGF for 5 min, washed, lifted as described in Methods and then treated with vehicle or the indicated concentrations of DYn-2 for 1 h at 37 °C (d), or with 5 mM DYn-2 for the indicated times (e), and protein sulfenic acids were detected by streptavidin-HRP Western blot as in Figure 3.2e. Densitometric quantification of each electrophoretic lane from dose (d) and time (e) dependencies are shown at the right of their respective Western blots and data were normalized to the maximal signal observed in each case. (f) A431 cells were treated with 5 mM DYn-2 or vehicle for 1 h at 37 °C, washed, harvested in the presence or absence of 200 U/ml catalase, and protein sulfenic acids were detected by streptavidin-HRP Western blot as in Figure 3.2d. Data for all graphs are representative of four independent experiments and represent the mean \pm s.e.m. (g) A431 cells were stimulated with 100 ng/ml EGF or vehicle for the indicated times, washed, harvested, resuspended in serum-free DMEM, and incubated with 5 mM DYn-2 or DMSO vehicle (2% v/v) for 15 min at 37 °C as described in Methods.

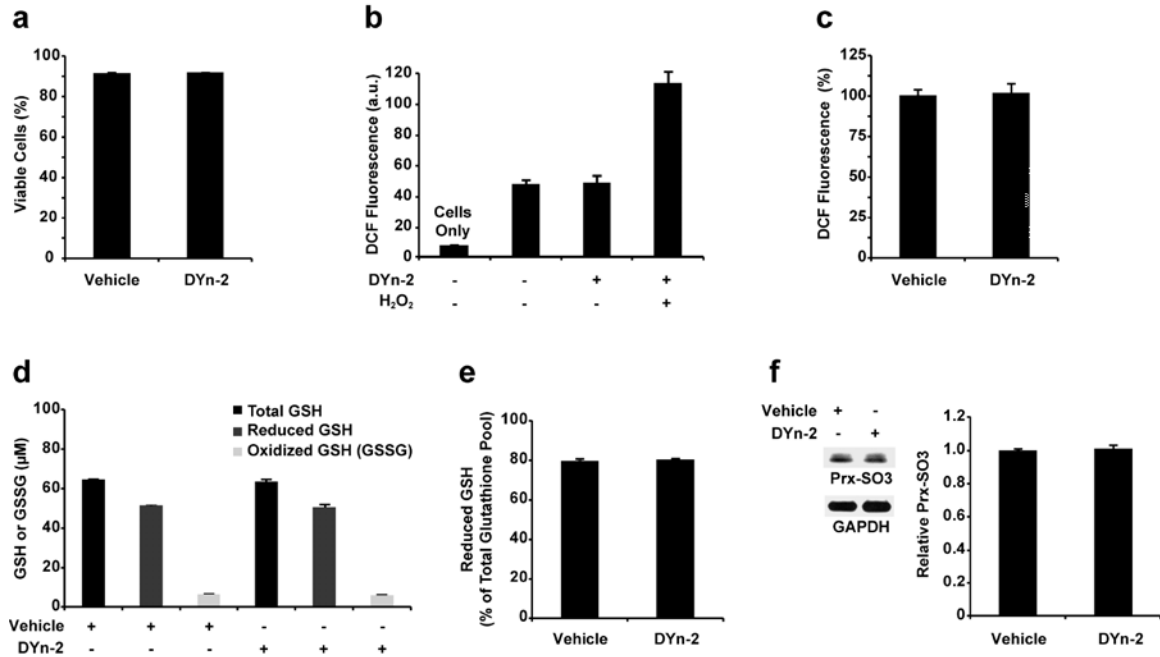


Figure 3.S6: DYn-2 treatment of A431 cells does not trigger cell death or oxidative stress. A431 cells were stimulated with 100 ng/ml EGF for 5 min, washed, and incubated with 5 mM DYn-2 or vehicle for 1 h at 37 °C as described in Methods. Following treatment: (a) A431 cell viability was evaluated by cell counting using trypan blue exclusion after DYn-2 or vehicle treatment and results were expressed as the percentage of viable cells. (b,c) Production of intracellular ROS was measured by DCF fluorescence as described in Supplementary Methods. Where indicated, H₂O₂ was added at a final concentration of 400 μM. In (c), data were normalized to vehicle control as 100% DCF fluorescence. (d) Reduced glutathione (GSH) and oxidized glutathione (GSSG) levels were measured in DYn-2 and vehicle-treated samples as described in Supplementary Methods. (e) GSH represented as a percentage of total glutathione pool. (f) Samples were resolved by SDS-PAGE and analyzed by anti-Prx-SO₃ Western blot (left). Comparable protein loading was confirmed by anti-GAPDH Western blot. Prx-SO₃ signal was quantified by densitometry, and normalized to the vehicle control (right). Data for all graphs are representative of three independent readings and represent mean ± s.e.m.

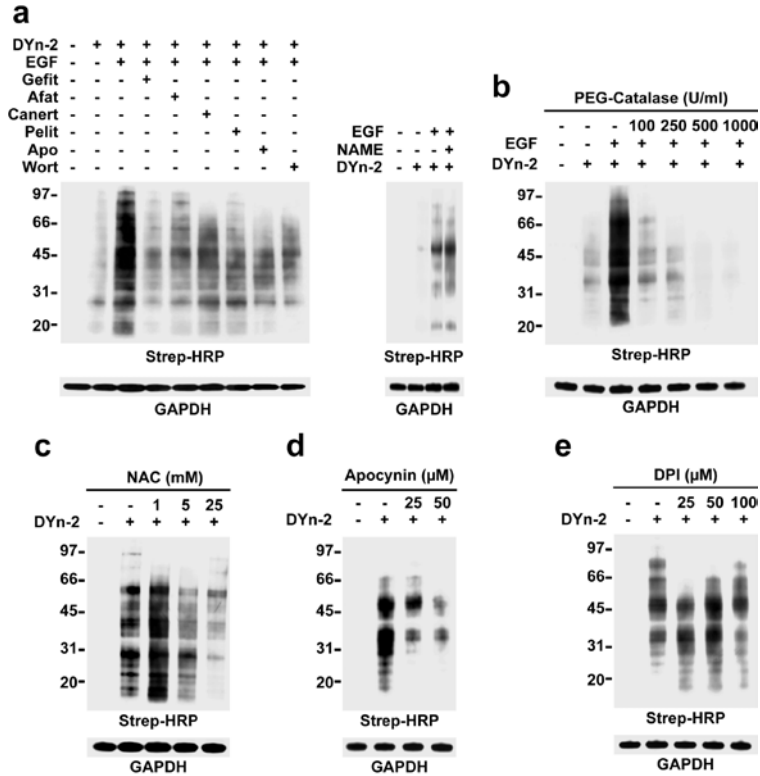


Figure 3.S7: **EGF-mediated sulfenylation requires EGFR activity and is modulated by cellular redox status in A431 cells.** Western blots showing protein sulfenic acids in A431 cells and total GAPDH. (a) A431 cells were stimulated with 100 ng/ml EGF for 2 min after pretreatment with 10 μ M gefitinib, 1 μ M afatinib, 10 μ M canertinib, 1 μ M pelitinib, 100 μ M apocynin, 100 μ M wortmannin, 100 μ M L-NAME or vehicle for 25 min. In (b), A431 cells were stimulated with 100 ng/ml EGF for 2 min after pretreatment with PEG-catalase at the indicated concentration for 5 min. In (c), A431 cells were stimulated with 100 ng/ml EGF for 5 min after pretreatment with NAC at the indicated concentration for 5 min. In (d), A431 cells were stimulated with 100 ng/ml EGF for 2 min after pretreatment with apocynin at the indicated concentration for 5 min (d). In (e) A431 cells were stimulated with 100 ng/ml EGF for 5 min after pretreatment with DPI at the indicated concentration for 5 min. Following treatment, cells were incubated with DYn-2 or vehicle for 1 h (a) or 15 min (b-e) at 37 °C and sulfenic acids were detected by streptavidin-HRP Western blot as in Figure 3.2e. When applied at 25 μ M, DPI decreased sulfenic acid modification of proteins; however, higher doses were associated with an increase in sulfenylation relative to control samples. This observation is most likely due to DPI-mediated inhibition of the thioredoxin-thioredoxin reductase system that reduces oxidized cysteines to their reduced state.

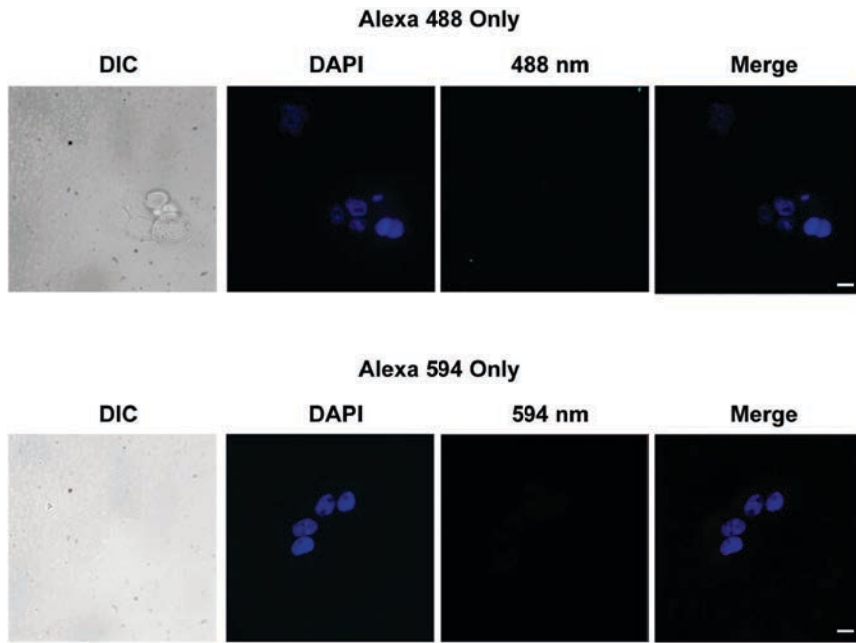


Figure 3.S8: **Secondary antibody only control in A431 cells.** Confocal fluorescence images of A431 cells labeled with secondary antibody only. Cells were fixed and stained as described in Methods with Alexa488-conjugated (green) goat anti-rabbit secondary or Alexa594-conjugated (red) goat anti-rabbit secondary antibodies (1:1000). Nuclei were counterstained with DAPI (blue). Scale bar, 10 μm .

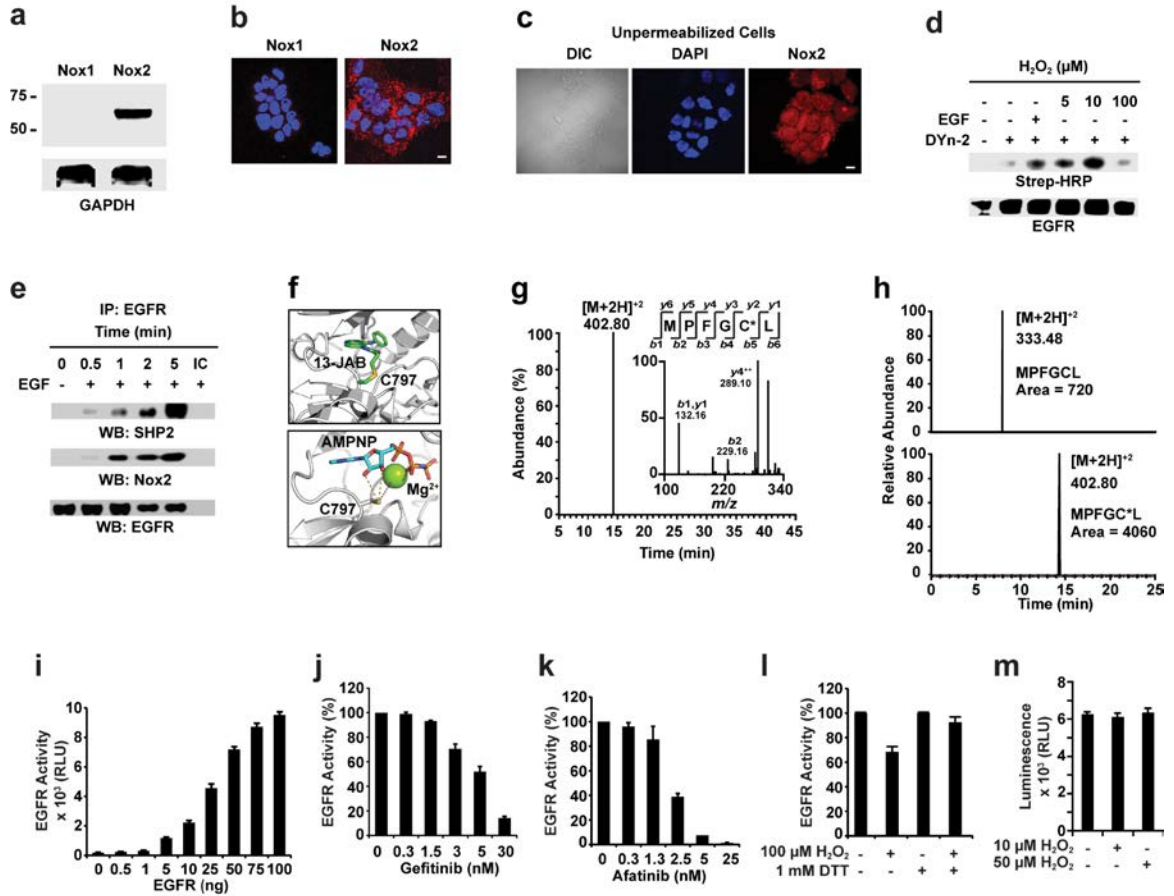


Figure 3.S9: Nox2 expression, H_2O_2 -mediated Cys797 oxidation and modulation of recombinant EGFR tyrosine kinase activity. (a, b) Expression of Nox1 and Nox2 in A431 cells was analyzed by Western blot with rabbit anti-Nox1 and rabbit anti-Nox2, with GAPDH as a loading control (a) or immunofluorescence microscopy (b). In (b), cells were fixed and stained with rabbit anti-Nox1 or rabbit anti-Nox2 antibodies at 2 μ g/ml, followed by Alexa594-conjugated goat anti-rabbit (red) secondary antibodies (1:1000). Nuclei were counterstained with DAPI (blue). Scale bar, 10 μ m. (c) A431 cells were fixed but not permeabilized and stained with PE-conjugated (red) mouse anti-Nox2 antibody. Nuclei were counterstained with DAPI (blue). Scale bar, 10 μ m. (d) Western blot showing sulfenylated and total EGFR. A431 cells were stimulated with H_2O_2 at the indicated concentrations for 10 min and sulfenic acids were detected by streptavidin-HRP Western blot as in Figure 3.5b. (e) Western blot showing coimmunoprecipitation of SHP2, EGFR, and Nox2. A431 cells were stimulated with 100 ng/ml EGF or vehicle for the indicated times and samples were processed as in Figure 3.5c. The presence of SHP2 was evaluated using a rabbit anti-SHP2 antibody and comparable recovery of immunoprecipitated EGFR was confirmed by probing the Western blot with rabbit anti-EGFR antibody. IC, isotype control. (f) Crystal structure of EGFR kinase domain with irreversible inhibitor, 13-JAB bound covalently to Cys797 (top panel; PDB 2J5E) or non-covalently associated with the ATP analog, AMPNP and Mg^{2+} (bottom panel; PDB 3GT8). Molecular images were generated with the ATP analog, AMPNP and Mg^{2+} (bottom panel; PDB 3GT8). Molecular images were generated with PyMOL (<http://pymol.sourceforge.net>). (g) Extracted ion (ion current at m/z 402.80) chromatogram (left) and MS/MS spectrum (right) of the precursor ion m/z of 402.80 $[M+2H]^{+2}$ corresponding to dimedone-tagged peptide (MPFGC*L) from native EGFR. A431 cells were stimulated with 4 ng/ml EGF for 2 min, washed, incubated with 5 mM dimedone for 1 h at 37 $^{\circ}$ C, immunoprecipitated with anti-EGFR antibody as in Figure 3.5a, and resolved by SDS-PAGE. The band corresponding to EGFR (\sim 170 kDa) was excised, digested with pepsin, and analyzed by ESI-LC/MS/MS as described in Supplementary Methods. (h) Top spectrum: Extracted ion (ion current at m/z 333.48 $[M+2H]^{+2}$) chromatogram corresponding to the unmodified peptide (MPFGCL) from native EGFR. Bottom spectrum: The extracted ion (ion current at m/z 402.80 $[M+2H]^{+2}$) chromatogram corresponding to the dimedone-tagged peptide (MPFGC*L) from native EGFR. The ratio of dimedone-modified to unmodified peptide was determined by taking the areas under the curves and was determined to be approximately 6:1. Samples were generated as in g. (i-k) Measurement of EGFR tyrosine kinase activity in vitro as described in Supplementary Methods. (i) Recombinant EGFR (rEGFR) kinase activity titration. (j,k) rEGFR was incubated with gefitinib (j) or afatinib (k) at the indicated concentrations and assayed for kinase activity. (l) rEGFR was incubated with H_2O_2 or vehicle for 15 min, and then 1 mM DTT or vehicle was added for an additional 10 min and assayed for kinase activity. (m) The ATP-regenerating system from the EGFR kinase activity assay was untreated or co-incubated with the indicated concentrations of H_2O_2 and assayed for kinase activity. Data for all graphs are representative of three independent readings and represent the mean \pm s.e.m.

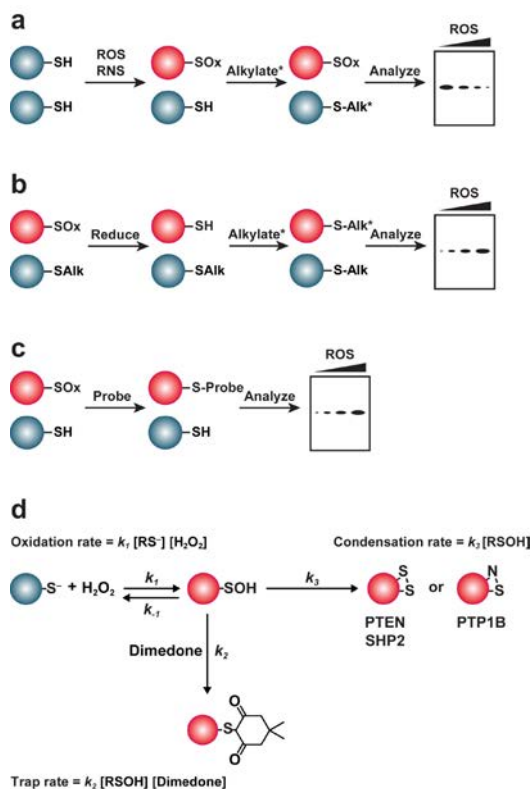


Figure 3.S10: Indirect and direct chemical techniques to monitor cysteine oxidation and PTP oxidation/trapping scheme. (a) Loss of reactivity with thiol-modifying reagents indirectly monitors cysteine oxidation. ROS and RNS oxidize reactive protein thiols (red protein). Addition of a thiol-specific alkylating agent such as NEM or IAM derivatized with a detection handle covalently modifies free thiols. Increased cysteine oxidation exhibits a decrease in probe signal. (b) Restoration of thiol-labeling by reducing agents indirectly monitors cysteine oxidation. Initially samples are incubated with NEM or IAM to irreversibly alkylate free thiols. Next a reducing agent returns oxidized cysteines to free thiols. Addition of NEM or IAM derivatized with a detection handle covalently modifies nascent thiols. Increased cysteine oxidation exhibits an increase in probe signal. (c) Direct detection of specific cysteine oxoforms. Samples are incubated with a chemoselective alkylating agent for a specific cysteine oxoform (i.e. nitrosothiols and sulfenic acids) derivatized with a detection handle. Visualization of probe incorporation results in an increase in signal with increased oxidation. (d) Reaction of H_2O_2 with the catalytic cysteine thiolate of PTPs generates sulfenic acid (second order reaction). Once formed, the sulfenic acid can condense with a backbone amide to form a sulfenamide in PTP1B, or with a second cysteine residue to form an intramolecular disulfide in PTEN and SHP2 (first order reaction). Alternatively, the sulfenic acid intermediate can be trapped by dimedone or DYn-2 (second order reaction). The amount of sulfenic acid detected is a function of the: (i) rate of oxidation ($\sim 2\text{-}10 \text{ M}^{-1}\text{s}^{-1}$) (32, 33), (ii) rate of dimedone/DYn-2 trap ($\sim 10^3 \text{ M}^{-1}\text{s}^{-1}$) (19, 50), and (iii) rate of intramolecular condensation ($\sim 10^{-3} \text{ s}^{-1}$ for sulfenamide (36) and $\sim 10 \text{ s}^{-1}$ for intramolecular disulfide) (35). Note: the aforementioned rates were measured in vitro with recombinant proteins. In some cases, the sulfenic acid may be directly reduced back to the thiol.

3.9 Chapter References

1. Finkel, T. (2011). Signal transduction by reactive oxygen species. *J Cell Biol*, *194*(1), 7–15.
2. Dickinson, B. C. [B. C.] & Chang, C. J. (2011). Chemistry and biology of reactive oxygen species in signaling or stress responses. *Nat Chem Biol*, *7*(8), 504–11.
3. Miller, E. W., Tulyathan, O., Isacoff, E. Y., & Chang, C. J. (2007). Molecular imaging of hydrogen peroxide produced for cell signaling. *Nat Chem Biol*, *3*(5), 263–7.
4. Woo, H. A., Yim, S. H., Shin, D. H., Kang, D., Yu, D. Y., & Rhee, S. G. (2010). Inactivation of peroxiredoxin i by phosphorylation allows localized h(2)o(2) accumulation for cell signaling. *Cell*, *140*(4), 517–28.
5. Paulsen, C. E. & Carroll, K. S. (2010). Orchestrating redox signaling networks through regulatory cysteine switches. *ACS Chem Biol*, *5*(1), 47–62.
6. Winterbourn, C. C. (2008). Reconciling the chemistry and biology of reactive oxygen species. *Nat Chem Biol*, *4*(5), 278–86.
7. Reddie, K. G. & Carroll, K. S. (2008). Expanding the functional diversity of proteins through cysteine oxidation. *Curr Opin Chem Biol*, *12*(6), 746–54.
8. Roos, G. & Messens, J. (2011). Protein sulfenic acid formation: from cellular damage to redox regulation. *Free Radic Biol Med*, *51*(2), 314–326.
9. Charles, R. L., Schroder, E., May, G., Free, P., Gaffney, P. R. J., Wait, R., . . . Eaton, P. (2007). Protein sulfenation as a redox sensor: proteomics studies using a novel biotinylated dimedone analogue. *Mol Cell Proteomics*, *6*(9), 1473–1484.
10. Depuydt, M., Leonard, S. E., Vertommen, D., Denoncin, K., Morsomme, P., Wahni, K., . . . Collet, J.-F. (2009). A periplasmic reducing system protects single cysteine residues from oxidation. *Science*, *326*(5956), 1109–1111.
11. Leonard, S. E., Reddie, K. G., & Carroll, K. S. (2009). Mining the thiol proteome for sulfenic acid modifications reveals new targets for oxidation in cells. *ACS Chem Biol*, *4*(9), 783–99.
12. Takanishi, C. L. & Wood, M. J. (2011). A genetically encoded probe for the identification of proteins that form sulfenic acid in response to h2o2 in *saccharomyces cerevisiae*. *J Proteome Res*, *10*(6), 2715–2724.
13. Wani, R., Qian, J., Yin, L., Bechtold, E., King, S. B., Poole, L. B., . . . Furdui, C. M. (2011). Isoform-specific regulation of akt by pdgf-induced reactive oxygen species. *Proc Natl Acad Sci U S A*, *108*(26), 10550–5.

14. Leonard, S. E. & Carroll, K. S. (2011). Chemical 'omics' approaches for understanding protein cysteine oxidation in biology. *Curr Opin Chem Biol*, 15(1), 88–102.
15. Bae, Y. S., Kang, S. W., Seo, M. S., Baines, I. C., Tekle, E., Chock, P. B., & Rhee, S. G. (1997). Epidermal growth factor (egf)-induced generation of hydrogen peroxide. role in egf receptor-mediated tyrosine phosphorylation. *J Biol Chem*, 272(1), 217–21.
16. Paulsen, C. E. & Carroll, K. S. (2009). Chemical dissection of an essential redox switch in yeast. *Chem Biol*, 16(2), 217–25.
17. Michalek, R. D., Nelson, K. J., Holbrook, B. C., Yi, J. S., Stridiron, D., Daniel, L. W., . . . Grayson, J. M. (2007). The requirement of reversible cysteine sulfenic acid formation for t cell activation and function. *J Immunol*, 179(10), 6456–6467.
18. Benitez, L. V. & Allison, W. S. (1974). The inactivation of the acyl phosphatase activity catalyzed by the sulfenic acid form of glyceraldehyde 3-phosphate dehydrogenase by dimedone and olefins. *J Biol Chem*, 249(19), 6234–43.
19. Poole, L. B., Klomsiri, C., Knaggs, S. A., Furdui, C. M., Nelson, K. J., Thomas, M. J., . . . King, S. B. (2007). Fluorescent and affinity-based tools to detect cysteine sulfenic acid formation in proteins. *Bioconjug Chem*, 18(6), 2004–17.
20. Reddie, K. G., Seo, Y. H., Muse Iii, W. B., Leonard, S. E., & Carroll, K. S. (2008). A chemical approach for detecting sulfenic acid-modified proteins in living cells. *Mol Biosyst*, 4(6), 521–31.
21. Seo, Y. H. & Carroll, K. S. (2009). Facile synthesis and biological evaluation of a cell-permeable probe to detect redox-regulated proteins. *Bioorg Med Chem Lett*, 19(2), 356–9.
22. Charron, G., Zhang, M. M., Yount, J. S., Wilson, J., Raghavan, A. S., Shamir, E., & Hang, H. C. (2009). Robust fluorescent detection of protein fatty-acylation with chemical reporters. *J Am Chem Soc*, 131(13), 4967–4975.
23. Bedard, K. & Krause, K.-H. (2007). The nox family of ros-generating nadph oxidases: physiology and pathophysiology. *Physiol Rev*, 87(1), 245–313.
24. Lee, S. R., Kwon, K. S., Kim, S. R., & Rhee, S. G. (1998). Reversible inactivation of protein-tyrosine phosphatase 1b in a431 cells stimulated with epidermal growth factor. *J Biol Chem*, 273(25), 15366–72.
25. Meng, T.-C., Fukada, T., & Tonks, N. K. (2002). Reversible oxidation and inactivation of protein tyrosine phosphatases in vivo. *Mol Cell*, 9(2), 387–399.

26. Tanner, J. J., Parsons, Z. D., Cummings, A. H., Zhou, H., & Gates, K. S. (2011). Redox regulation of protein tyrosine phosphatases: structural and chemical aspects. *Antioxid Redox Signal*, *15*(1), 77–97.
27. Singh, J., Petter, R. C., Baillie, T. A., & Whitty, A. (2011). The resurgence of covalent drugs. *Nat Rev Drug Discov*, *10*(4), 307–17.
28. Singh, J., Petter, R. C., & Kluge, A. F. (2010). Targeted covalent drugs of the kinase family. *Curr Opin Chem Biol*, *14*(4), 475–80.
29. Go, Y.-M. & Jones, D. P. (2008). Redox compartmentalization in eukaryotic cells. *Biochim Biophys Acta*, *1780*(11), 1273–1290.
30. Nelson, K. J., Klomsiri, C., Codreanu, S. G., Soito, L., Liebler, D. C., Rogers, L. C., . . . Poole, L. B. (2010). Use of dimedone-based chemical probes for sulfenic acid detection methods to visualize and identify labeled proteins. *Methods Enzymol*, *473*, 95–115.
31. Cuddihy, S. L., Winterbourn, C. C., & Hampton, M. B. (2011). Assessment of redox changes to hydrogen peroxide-sensitive proteins during egf signaling. *Antioxid Redox Signal*, *15*(1), 167–74.
32. Chen, C. Y., Willard, D., & Rudolph, J. (2009). Redox regulation of sh2-domain-containing protein tyrosine phosphatases by two backdoor cysteines. *Biochemistry*, *48*(6), 1399–409.
33. Denu, J. M. & Tanner, K. G. (1998). Specific and reversible inactivation of protein tyrosine phosphatases by hydrogen peroxide: evidence for a sulfenic acid intermediate and implications for redox regulation. *Biochemistry*, *37*(16), 5633–42.
34. Chen, K., Kirber, M. T., Xiao, H., Yang, Y., & Keaney, J., J. F. (2008). Regulation of ros signal transduction by nadph oxidase 4 localization. *J Cell Biol*, *181*(7), 1129–39.
35. Lee, C., Lee, S. M., Mukhopadhyay, P., Kim, S. J., Lee, S. C., Ahn, W.-S., . . . Ryu, S. E. (2004). Redox regulation of oxyr requires specific disulfide bond formation involving a rapid kinetic reaction path. *Nat Struct Mol Biol*, *11*(12), 1179–1185.
36. Lee, J.-W., Soonsanga, S., & Helmann, J. D. (2007). A complex thiolate switch regulates the bacillus subtilis organic peroxide sensor ohrr. *Proc Natl Acad Sci U S A*, *104*(21), 8743–8748.
37. Giannoni, E., Buricchi, F., Raugei, G., Ramponi, G., & Chiarugi, P. (2005). Intracellular reactive oxygen species activate src tyrosine kinase during cell adhesion and anchorage-dependent cell growth. *Mol Cell Biol*, *25*(15), 6391–6403.

38. Tang, H., Hao, Q., Rutherford, S. A., Low, B., & Zhao, Z. J. (2005). Inactivation of src family tyrosine kinases by reactive oxygen species in vivo. *J Biol Chem*, *280*(25), 23918–23925.
39. Cunnick, J. M., Dorsey, J. F., Standley, T., Turkson, J., Kraker, A. J., Fry, D. W., ... Wu, J. (1998). Role of tyrosine kinase activity of epidermal growth factor receptor in the lysophosphatidic acid-stimulated mitogen-activated protein kinase pathway. *J Biol Chem*, *273*(23), 14468–14475.
40. Kemble, D. J. & Sun, G. (2009). Direct and specific inactivation of protein tyrosine kinases in the src and fgfr families by reversible cysteine oxidation. *Proc Natl Acad Sci U S A*, *106*(13), 5070–5.
41. Leonard, S. E., Garcia, F. J., Goodsell, D. S., & Carroll, K. S. (2011). Redox-based probes (rbps) for protein tyrosine phosphatases. *Angew Chem Int Ed Engl*, *in press*.
42. Dickinson, B. C. [Bryan C.], Huynh, C., & Chang, C. J. (2010). A palette of fluorescent probes with varying emission colors for imaging hydrogen peroxide signaling in living cells. *J Am Chem Soc*, *132*(16), 5906–5915.
43. Dickinson, B. C. [Bryan C.], Peltier, J., Stone, D., Schaffer, D. V., & Chang, C. J. (2011). Nox2 redox signaling maintains essential cell populations in the brain. *Nat Chem Biol*, *7*(2), 106–112.
44. Truong, T. H., Garcia, F. J., Seo, Y. H., & Carroll, K. S. (2011). Isotope-coded chemical reporter and acid-cleavable affinity reagents for monitoring protein sulfenic acids. *Bioorg Med Chem Lett*, *21*(17), 5015–20.
45. Weerapana, E., Wang, C., Simon, G. M., Richter, F., Khare, S., Dillon, M. B., ... Cravatt, B. F. (2010). Quantitative reactivity profiling predicts functional cysteines in proteomes. *Nature*, *468*(7325), 790–5.
46. Seo, Y. H. & Carroll, K. S. (2011). Quantification of protein sulfenic acid modifications using isotope-coded dimedone and iododimedone. *Angew Chem Int Ed Engl*, *50*(6), 1342–5.
47. Zhao, X. Z., Semenova, E. A., Liao, C., Nicklaus, M., Pommier, Y., & Burke, T. R., Jr. (2006, December). Biotinylated biphenyl ketone-containing 2,4-dioxobutanoic acids designed as hiv-1 integrase photoaffinity ligands. *Bioorg Med Chem*, *14*(23), 7816–7825. doi:10.1016/j.bmc.2006.07.064
48. Lin, P.-C., Ueng, S.-H., Tseng, M.-C., Ko, J.-L., Huang, K.-T., Yu, S.-C., ... Lin, C.-C. (2006, June). Site-specific protein modification through cu(i)-catalyzed 1,2,3-triazole formation and its implementation in protein microarray fabrication. *Angew Chem Int Ed Engl*, *45*(26), 4286–4290. doi:10.1002/anie.200600756

49. Jackson, P., Moody, C., & Shah, P. (1990). Preparation and diels-alter reactivity of thieno[2,3-c]-and thioeno[3,2-c]-pyran-3-one. *J Chem Soc Perkin Trans*, 11, 2909–2918.
50. Klomsiri, C., Nelson, K. J., Bechtold, E., Soito, L., Johnson, L. C., Lowther, W. T., ... Poole, L. B. (2010). Use of dimedone-based chemical probes for sulfenic acid detection evaluation of conditions affecting probe incorporation into redox-sensitive proteins. *Methods Enzymol*, 473, 77–94. doi:10.1016/S0076-6879(10)73003-2

CHAPTER IV

Characterizing the Role of Cys797 in Redox-Based Regulation of EGFR

4.1 Abstract

EGF-mediated signaling results in H₂O₂ production and sulfenylation of downstream target proteins. EGFR has been identified as a target of signal-derived H₂O₂ and is directly modified at its critical active site cysteine (Cys797), resulting in enhanced tyrosine kinase activity. To further characterize the importance of this residue in physiologic signaling events, we generated cysteine mutants (C797S and C797A) to dissect the effect of Cys797 sulfenylation on EGFR kinase activity. *In vitro* and cellular studies demonstrate mutation of Cys797 decreases affinity for ATP and abrogates kinase activation and sulfenylation levels. Additionally, we examine the impact of common oncogenic EGFR mutations on the ability of Cys797 to undergo redox-based modification. We demonstrate Cys797 oxidation reduces potency of thiol-targeted EGFR inhibitors, suggesting alternative approaches for inhibitor development should be explored. Finally, we demonstrate cysteine oxidation may serve as a general mechanism to regulate kinase activity in two structural homologues of EGFR. Taken together, our results demonstrate the role of Cys797 in redox-based EGFR regulation and highlight the importance of defining the mechanisms that control reversible pro-

tein sulfenylation to understand human physiology and pathology.

4.2 Introduction

Epidermal growth factor receptor (EGFR) is one of the most studied receptor tyrosine kinases (RTK) and serves as a quintessential model for understanding the biological function of RTKs in physiological signaling and disease states (1). Activation of RTKs by their respective extracellular ligands (i.e. growth factors) initiates downstream signaling networks to regulate a number of processes which include cellular proliferation, differentiation, metabolism, and survival. Growth factor-dependent stimulation can also mediate localized production of hydrogen peroxide (H_2O_2) (2, 3), which serves as a second messenger in signal transduction cascades (4–6). In particular, binding of epidermal growth factor (EGF) to EGFR triggers the assembly and activation of NADPH oxidase (Nox) complexes to generate H_2O_2 (7, 8), which reacts with redox-sensitive protein targets largely through modification of specific cysteine residues. The direct product of the reaction between H_2O_2 and a protein thiolate (RS^-) is sulfenic acid (RSOH), also referred to as sulfenylation. Cysteine oxidation represents a biologically important mechanism for regulation of protein activity and to detect changes in the cellular redox balance (9, 10).

Utilizing chemical probes selective for sulfenic acid (DYn-2), we recently demonstrated EGF-mediated signaling induces dynamic changes in global protein sulfenylation in downstream pathways (11). EGFR and Nox2 become associated in an EGF-dependent fashion to induce endogenous production of H_2O_2 , which subsequently modulates target proteins (Figure 4.1A). Three protein tyrosine phosphatases (PTPs) (SHP2, PTEN, PTP1B) were found to undergo ligand-dependent oxidation and exhibit a unique sulfenylation profile in cells due to differences in their subcellular location. A central finding of this study demonstrates EGFR undergoes sulfenylation at its active site cysteine Cys797 in response to EGF and enhances its tyrosine ki-

nase activity. The EGFR intracellular kinase domain contains six cysteine residues, only one of which (Cys797) is located in the ATP-binding pocket. Given its active site location and proximity to the ATP ligand, sulfenylation of Cys797 may enhance kinase ability to participate in electrostatic and hydrogen-bonding interactions with its substrate (Figure 4.1B). Furthermore, the location of this residue with respect to the C-helix and activation segment also raises the possibility of transition-state stabilization and/or destabilization of its auto-inhibitory conformation (12). EGFR Cys797 is located at the N-terminal end of an α -helix, also referred to as the Ncap position. Cysteine residues are the most sparsely occurring Ncap residue in native proteins, and comprises <1% of all these positions (13). The interaction of cysteines located at the Ncap position with the helix dipole can drastically lower the thiol pKa and increase its susceptibility to oxidation (14, 15). To note, the Ncap effect has been attributed to the reactivity of the catalytic cysteine in human peroxiredoxin I (8). Interestingly, Cys797 is conserved among nine additional receptor and non-receptor kinases (Supplementary Figure 4.S1) and it is possible that activity of these structural homologues may be affected by oxidation of this residue.

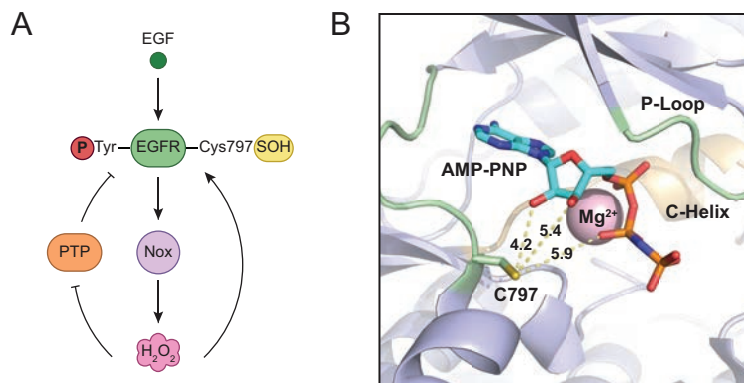


Figure 4.1: **Signal-derived H_2O_2 directly targets EGFR and enhances its tyrosine kinase activity upon oxidation.** (A) Binding of EGF induces production of H_2O_2 through Nox2. Nox-derived H_2O_2 directly modifies EGFR cysteine (Cys797) to sulfenic acid in the active site, which enhances its tyrosine kinase activity. Endogenous H_2O_2 can also oxidize and deactivate localized PTPs, leading to a net increase in EGFR phosphorylation. (B) Crystal structure of the EGFR kinase domain (PDB 3GT8) bound to AMP-PNP, a hydrolysis resistant ATP analog, and Mg^{2+} . Dashed yellow lines and accompanying numbers indicate the distance (\AA) between the γ -sulfur atom of Cys797 and key substrate functional groups. Note also that Cys797 can adopt different rotamers and sulfenylation of this residue may enhance its ability to participate in electrostatic and hydrogen-bonding interactions with its substrate.

Perturbation of physiologic kinase signaling due to mutations and other genetic alterations is a hallmark of many disease states and can result in aberrant kinase activity and malignant transformation (16). EGFR is mutated or amplified in a number of human carcinomas (i.e. breast and lung cancers), which has motivated the development of reversible ATP-competitive inhibitors (17). This class of inhibitors, which include gefitinib (18) and erlotinib (19), achieve selectivity by recognizing unique features of the EGFR ATP-binding domain and have proven successful in clinical trials. Somatic mutations in the EGFR kinase domain have been identified as a cause of non-small cell lung cancer (NSCLC) (20, 21), and the two most frequent mutations are the exon 19 point mutation (L858R) and exon 19 deletion ($\Delta 746-750$) (22, 23). L858R is the single most common mutation (approximately 40%) and lies within the kinase activation loop. This point mutation is 50-fold more active than wild-type EGFR and constitutively activates the kinase by destabilizing its auto-inhibitory conformation, which is normally maintained in the absence of ligand stimulation (12, 24). Cells bearing these oncogenic EGFR mutations exhibit decreased affinity for ATP and are, in

general, more sensitive to reversible ATP-competitive inhibitors than cells expressing wild-type kinase (25–27).

Lung cancer patients expressing these common mutations (L858R and Δ 746-750) eventually relapse after 12-18 months of treatment (28). In approximately 50% of cases, drug resistance to ATP-competitive inhibitors is due to a second site mutation (T790M) of the gatekeeper residue (29). This residue is located at the entrance of the hydrophobic pocket in the back of the ATP binding pocket, and makes it an important determinant of inhibitor specificity. Studies provided evidence that the T790M mutation induces drug resistance by restoring ATP affinity to comparable levels as wild-type EGFR, thereby increasing the concentration of ATP-competitive inhibitor required to maintain efficacy (30). Moreover, L858R/T790M mutants remain sensitive to covalent irreversible inhibitors which can be utilized to overcome clinical resistance to reversible ATP-competitive treatments (31–33).

In physiologic signaling, H_2O_2 levels are maintained through pro- and anti-oxidant enzymes and buffering systems to promote cellular growth and survival. On the contrary, chronic H_2O_2 levels can ultimately result in cell death and are prevalent in pathologic conditions (34, 35). Oxidation of H_2O_2 -sensitive cysteine residues form transiently in specific proteins to mediate redox-based signal transduction, but can undergo malignant transformation in disease states associated with high oxidative stress. Previous data from our group demonstrates that elevated expression levels of EGFR and HER2 (member of EGFR subfamily) are correlated to increased protein oxidation and global sulfenylation in breast cancer cells (36). When coupled to the recent discovery that EGFR Cys797 undergoes sulfenic acid modification, these findings raise several fundamental questions regarding the function of cysteine oxidation with respect to EGFR signaling in normal and disease states. For example, what are the molecular mechanisms underlying the role of Cys797 oxidation? How, and to what extent, does oxidation of EGFR Cys797 ultimately affect kinase activity?

Additionally, can cysteine oxidation serve as a general mechanism to regulate kinase activity, specifically in structural homologues of EGFR?

In order to gain a better understanding of physiologic EGFR signaling, the scope and molecular details by which Cys797 affects redox-based regulation of EGFR must be delineated. Interestingly, EGFR Cys797 is also the target residue of a number of covalent irreversible inhibitors currently under evaluation in clinical trials: EKB-569 (pelitinib), HKI-272 (neratinib), and BIBW 2992 (afatinib) (31, 32, 37). These compounds contain an electrophilic acrylamide moiety that reacts with the EGFR Cys797 thiolate through Michael addition to achieve irreversible binding. Pre-treatment of A431 cells with these covalent inhibitors prevents formation of sulfenyl EGFR and highlights the dual role of this kinase regarding its importance in kinase signaling and as a direct drug target (11). Given the proximity of EGFR Cys797 to the ATP-binding pocket and because thiol (RSH)-targeted acrylamide inhibitors do not recognize the kinase in its sulfenic acid form, we postulate that Cys797 oxidation can alter the potency of irreversible EGFR inhibitors. Chronically high levels of H_2O_2 affiliated with cancers can lead to aberrant levels of oxidized EGFR Cys797 and decrease the thiol form available for covalent modification by RSH-targeted inhibitors, thereby reducing drug efficacy. Additionally, the location of oncogenic EGFR mutations with respect to Cys797 may induce conformational changes and/or alter its sensitivity to H_2O_2 .

To address these questions, we generated cysteine mutants (C797S and C797A) to probe the effect of this mutation with respect to EGFR kinase activity. We characterized the kinetic parameters of wild-type (WT) and mutant kinases *in vitro*. We demonstrate that cysteine mutants are less active than wild-type EGFR and have decreased affinity for ATP, suggesting Cys797 may play a role in substrate interaction. Full-length EGFR kinase isolated from cells and activity assays revealed moderate H_2O_2 treatment enhanced tyrosine kinase activity for wild-type, but not for cysteine mutants. Additionally, EGFR autophosphorylation and sulfenylation levels for

cysteine mutants are abrogated in response to H₂O₂ stimulation *in situ*. Using thiol-targeted inhibitors, we examine the effect of EGFR Cys797 oxidation with respect to compound potency. EGFR undergoes sulfenylation in two common oncogenic mutants (L858R/T790M and Δ 746-750) in response to EGF and provides some insight regarding the effect of oxidation in disease states. EGF-mediated ErbB2 sulfenylation was also explored, and indicates EGFR family members are subject to growth factor-induced oxidation. Finally, we demonstrate cysteine oxidation may serve as a general mechanism to modulate kinase activity in a structural homologue of EGFR. Collectively, these studies highlight the importance of EGFR Cys797 oxidation in physiologic kinase signaling and have broad implications for the development of new redox-based strategies to target H₂O₂ cysteines in therapeutically important proteins.

4.3 Results

Mutation of EGFR Cys797 affects kinase activity *in vitro*

To investigate the role of EGFR Cys797, we generated two cysteine mutants: C797S and C797A. Serine and alanine are both used as replacements for cysteine in the literature. Although serine can make it a closer match to cysteine due to its size, alanine substitutions can remove the effect of side chains and help deduce the involvement of side chain interactions. Therefore, we chose to characterize the behavior of both substitutions in order to evaluate the full extent of the mutation.

Due to its active site location and proximity to the ATP ligand, we characterized the catalytic activity of wild-type and mutant enzymes. Kinetic characterization was performed with recombinant protein expressing the kinase domain (696-1022). The kinetic parameters for ATP and peptide substrate poly [Glu4:Tyr1] were determined using a continuous, colorimetric *in vitro* kinase assay (adapted from (24, 30)) and are summarized in Table 4.1. Fold activity (k_{cat}) and rate plots of wild-type and

mutant kinases for ATP (Figure 4.2A, B) and peptide (Figure 4.2C, D) are shown as well. On average, C797S and C797A mutants are 2-fold less active than wild-type as determined from their calculated k_{cat} values. Decreased catalytic activity of these mutants, as compared to wild-type, is likely due to disruption of substrate binding interactions although structural data would be needed to support this. Affinity for ATP (K_m values) is decreased by 2.6- and 3-fold for mutants, respectively. Additionally, affinity for peptide substrate is decreased 2-fold for both C797S and C797A. The increases in K_m values for the C797S and C797A are modest, but suggest this mutation induces structural changes in the ATP-binding pocket. The kinetic parameters we determined for wild-type EGFR are comparable to those previously reported using similar and different assay systems (24, 30, 38). Covalent EGFR irreversible inhibitors afatinib and PD168393 (Supplementary Figure 4.S2) were used to validate the fraction of catalytically competent EGFR. MS/MS analyses of wild-type EGFR confirmed labeling with these ATP-competitive compounds and ensure our kinetic parameters are based on competent enzyme (Supplementary Figure 4.S3A, B).

Table 4.1: Kinetic Parameters of Wild-Type, C797S, and C797A EGFR

	ATP ^a			Peptide ^b		
	K_m (μM)	k_{cat} (s^{-1})	k_{cat}/K_m	K_m (μM)	k_{cat} (s^{-1})	k_{cat}/K_m
WT	7.45 ± 0.36	$0.00542 \pm 3.40 \text{ E-4}$	7.28 E-4	906 ± 48	$0.0175 \pm 3.46 \text{ E-4}$	1.93 E-5
C797S	19.62 ± 0.84	$0.00320 \pm 1.36 \text{ E-4}$	1.63 E-4	1911 ± 119	$0.00845 \pm 7.00 \text{ E-4}$	4.42 E-6
C797A	21.72 ± 1.12	$0.00281 \pm 9.77 \text{ E-4}$	1.29 E-4	2134 ± 129	$0.00637 \pm 2.19 \text{ E-4}$	2.99 E-6

^a Parameters for ATP were determined using a consensus peptide with the sequence RAHEEIYHFFFAKKK.

^b Parameters for peptide were determined using poly [Glu4Tyr1] as the peptide substrate.

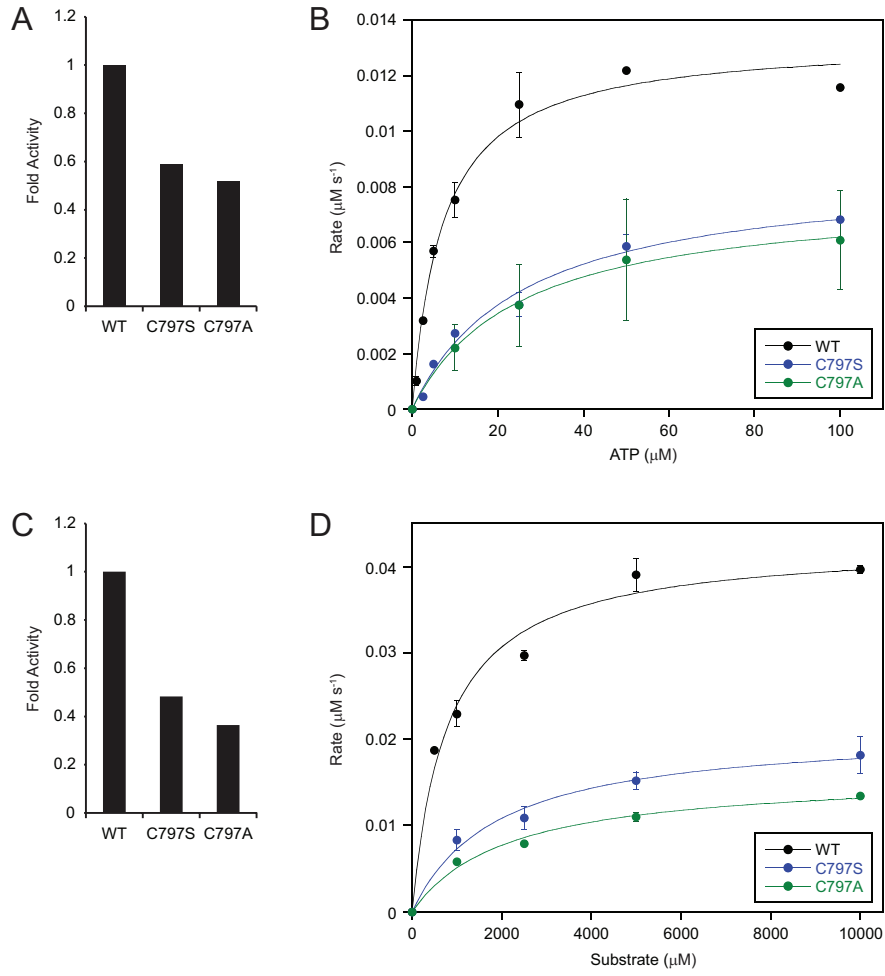


Figure 4.2: **Mutation of Cys797 decreases EGFR tyrosine kinase activity.** (A) Fold activity of WT, C797S, and C797A kinases with respect to ATP. The fold activity of WT and mutant enzymes was calculated by determining the k_{cat} for each protein with ATP and saturating peptide substrate (RAHEEIYHFFAKKK) and dividing by the k_{cat} for WT enzyme. (B) Rate plot of WT and C797 mutant kinases with respect to ATP. (C) Fold activity of WT, C797S, and C797A kinases with respect to substrate. The fold activity of WT and mutant enzymes was calculated by determining the k_{cat} for each protein with saturating ATP and poly [Glu4Tyr1] as peptide substrate and dividing by the k_{cat} for WT enzyme. (D) Rate plot of WT and C797 mutant kinases with respect to peptide substrate.

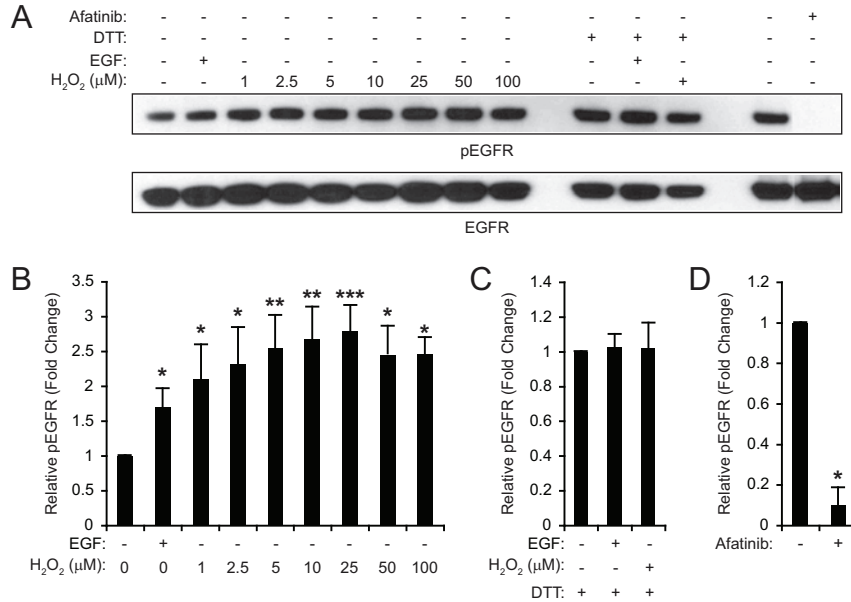


Figure 4.3: EGF and H₂O₂ treatment induces autophosphorylation of WT EGFR isolated from immunoprecipitates. (A) Full length native WT EGFR was immunoprecipitated from A431 cell lysate, assayed for tyrosine kinase activity with ATP, and stimulated with EGF (3.3 ng/μl) or H₂O₂ (0-100 μM). Western blot shows phosphorylated (p) and total EGFR. (B) Densitometric quantification of A. EGF and H₂O₂ treatment increases kinase activity in EGFR immunoprecipitates. (C) DTT reverses EGF and H₂O₂-mediated EGFR autophosphorylation. To assess the reversibility of H₂O₂-induced kinase activation, immunoprecipitated EGFR was pre-incubated with H₂O₂ (5 μM) followed by addition of DTT simultaneous with ATP. (D) Afatinib blocks inherent EGFR kinase activity. To verify that EGFR autophosphorylation was due to enhanced kinase activity, immunoprecipitated EGFR was pre-incubated with afatinib (1 μM). Data are representative of three independent readings and represent the mean ± s.e.m. **p* < 0.05, ***p* < 0.01, ****p* < 0.001 compared to untreated control.

We also investigated the *in vitro* effect of EGFR Cys797 mutation on kinase activity using full-length receptor. Although we have previously demonstrated H₂O₂ treatment enhances tyrosine kinase activity of wild-type EGFR, these results were generated with recombinant protein expressing the kinase domain. Therefore, this approach allows us to investigate the behavior of wild-type and mutant EGFR in its complete form. For our studies, we used the human epidermoid carcinoma A431 cell line naturally expresses high concentrations of EGFR and serves as an effective model to study the wild-type kinase (39). Full-length native WT EGFR was isolated from A431 cell lysate and assayed for tyrosine kinase activity with ATP. Upon EGF or dose-dependent H₂O₂ treatment, autophosphorylation levels are increased

by up to 3-fold compared to the unstimulated control (Figure 4.3A, B). To assess the reversibility of H₂O₂-induced kinase activation, immunoprecipitated EGFR was pre-incubated with H₂O₂ followed by addition of DTT simultaneous with ATP. DTT blocks EGF and H₂O₂-mediated increases in EGFR autophosphorylation, and confirms H₂O₂-dependent activation occurs through a reversible mechanism (Figure 4.3A, C). In addition, pre-incubation with afatinib completely abolishes EGFR autophosphorylation (Figure 4.3D) and verifies that the observed changes (Figure 4.3B) are due to enhanced kinase activity. These results demonstrate H₂O₂ treatment enhances wild-type EGFR activity *in vitro* using full-length receptor, and confirm our earlier findings observed with the kinase domain.

Using the above approach, we transiently transfected C797S and C797A into HeLa cells to evaluate the effect of this mutation in its fully-expressed form *in vitro*. Wild-type EGFR was also transfected and served as a control to adjust for any potential changes occurring from the transfection process. Wild-type EGFR autophosphorylation was increased 8-fold and 12-fold upon EGF and H₂O₂ treatment, respectively in immunoprecipitates isolated from HeLa-transfected cell lysate (Supplementary Figure 4.S4A, B). On the contrary, C797s and C797A did not exhibit drastic changes in autophosphorylation levels upon EGF and H₂O₂ treatment. On average, C797S was determined to exhibit a 2-fold increase in phosphorylation but these changes may be a result of the serine side-chain interaction or reversion of the serine mutation back to its original residue. The fold change for C797A could not be calculated because detection of autophosphorylation was completely abrogated. Collectively these results highlight the functional role of EGFR Cys797 with respect to kinase activity in its kinase domain and its full-length form *in vitro*.

Mutation of EGFR Cys797 affects autophosphorylation and sulfenylation level *in situ*

To place our findings in a more relevant signaling context, we explored the behavior of wild-type and EGFR cysteine mutants *in situ* in response to EGF and H₂O₂ treatment. Wild-type, C797S, and C797A were transiently transfected into HeLa cells, stimulated with EGF or H₂O₂, and analyzed for changes in autophosphorylation levels. EGF treatment induces a strong dose-dependent increase in wild-type phosphorylation (Figure 4.4A, B), and is decreased in both cysteine mutants (Figure 4.4A, B). This decrease is more pronounced in the C797A mutant, which agrees with our earlier *in vitro* kinase assays. Similarly, H₂O₂-mediated activation of EGFR is reduced in C797 mutants compared to wild-type kinase (Figure 4.5A, B). Phosphorylation levels are completely abrogated in the C797A mutant, whereas C797S mutant still exhibits a detectable amount of activity equivalent to its corresponding untreated control. At higher H₂O₂ concentrations (500 μ M), activation of C797S increases to comparable levels to wild-type EGFR and may be due to concomitant inhibition of PTPs (Figure 4.5B).

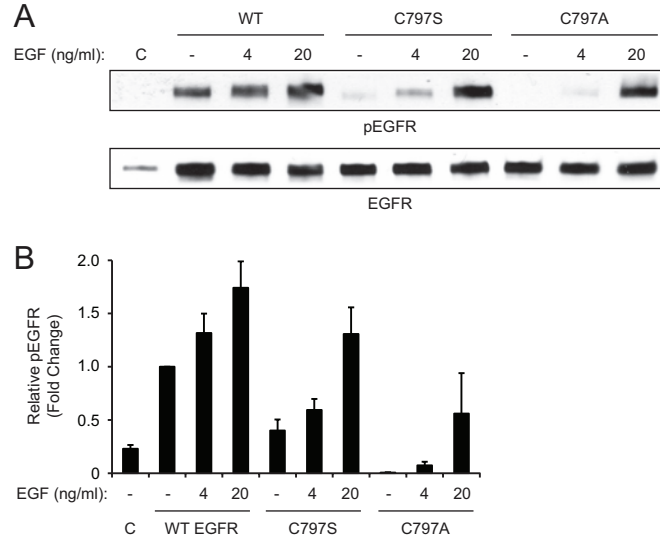


Figure 4.4: **EGF-mediated activation of EGFR is affected in C797 mutants *in situ*.** (A) WT, C797S, and C797A EGFR were transfected into HeLa cells and stimulated with EGF at the indicated concentrations for 5 min. Western blot shows phosphorylated (p) and total EGFR. Both mutants exhibit decreased autophosphorylation levels when compared to WT enzyme. (B) Densitometric quantification of A. Data are representative of three independent readings and represent the mean \pm s.e.m.

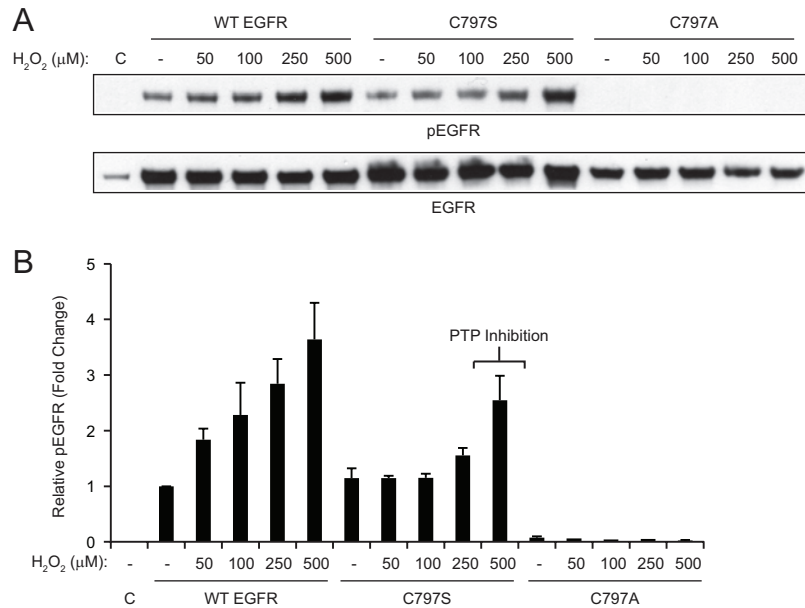


Figure 4.5: **H₂O₂-mediated activation of EGFR is affected in C797 mutants *in situ*.** (A) WT, C797S, and C797A EGFR were transfected into HeLa cells and stimulated with H₂O₂ at the indicated concentrations for 5 min. Western blot shows phosphorylated (p) and total EGFR. Both mutants exhibit decreased autophosphorylation levels when compared to WT enzyme. (B) Densitometric quantification of A. At higher H₂O₂ concentrations (500 μM), C797S phosphorylation levels increase and may be due to inhibition of protein tyrosine phosphatases (PTPs). Data are representative of three independent readings and represent the mean \pm s.e.m.

Next, we investigated the effect of H₂O₂-mediated sulfenylation in wild-type, C797S, and C797A. Dimedone and its derivatives are the prototypical sulfenic acid probes and have been shown extensively to specifically react with sulfenyl groups *in vitro* and *in situ* (40). These small molecules are used to trap and tag sulfenic acids, and labeled proteins can subsequently be detected by specific antibodies (36) or through attachment of biotin or fluorescent reporter (11, 41–43). HeLa cells were transfected with wild-type or cysteine mutants and labeled with DYn-2 following H₂O₂ stimulation. Upon treatment, EGFR sulfenylation is decreased in both cysteine mutants compared to sulfenyl wild-type levels (Figure 4.6A, B). In particular, sulfenylation levels of C797A are completely abolished whereas the C797S mutant does not exhibit as drastic of an effect. The behavioral differences of these mutants is similar to those observed with *in situ* phosphorylation experiments (Figure 4.5), and may be due to structural changes induced by these substitutions. We also attempted to investigate the effect of EGF-mediated sulfenylation in wild-type and mutant kinases, but did not obtain successful results. We suspect this is because Nox2 is not expressed at high levels in HeLa cells (data not shown), and therefore do not contain the cellular components necessary to generate endogenous H₂O₂ in response to growth factor stimulation. MS/MS analysis of dimedone-labeled wild-type EGFR confirms Cys797 as the site of modification in response to H₂O₂ treatment (Supplementary Figure 4.S5). This was the only dimedone-labeled cysteine identified in our MS studies. Collectively these results demonstrate mutation of Cys797 decreases EGFR autophosphorylation and sulfenylation, and confirm H₂O₂-mediated sulfenylation occurs at the EGFR active site residue Cys797.

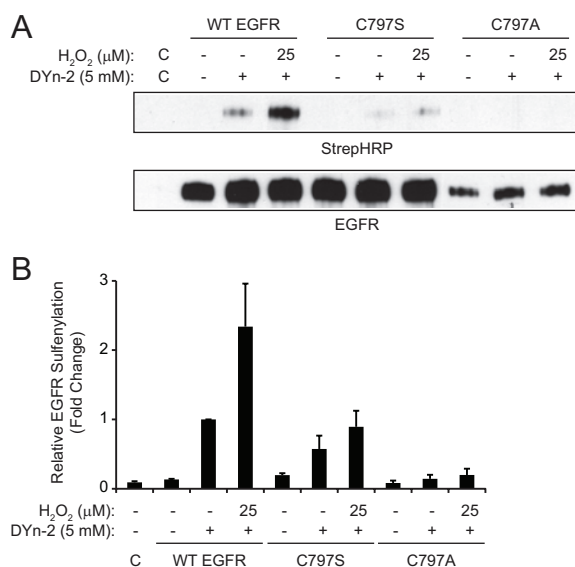


Figure 4.6: **H₂O₂-mediated sulfenylation is decreased in EGFR Cys797 mutants *in situ*.** (A) WT, C797S, and C797A EGFR were transfected into HeLa cells and stimulated with H₂O₂ (25 μM) for 5 min. Sulfenic acids were detected by Strep-HRP western blot. Both mutants exhibit decreased EGFR sulfenylation when compared to WT enzyme. (B) Densitometric quantification of A. Data are representative of three independent readings and represent the mean ± s.e.m.

EGFR is sulfenylated in common oncogenic kinase mutations

As discussed earlier in the introduction, somatic mutations in the EGFR kinase domain have been identified as a cause of NSCLC. In particular, two of the most frequently occurring mutations (L858R and Δ746-750) confer increased sensitivity to ATP-competitive inhibitors (i.e. gefitinib and erlotinib) by decreasing kinase affinity for ATP (25–27). T790M is a second site mutation that accounts for half of the cases wherein lung cancer patients undergoing treatment eventually relapse (28, 29). Given the proximity of EGFR Cys797 to the substrate binding pocket, we speculate oxidation of Cys797 may be affected in these oncogenic mutants. To investigate this, we used two lung cancer cell lines harboring these somatic mutations: NCI-H1875 (L858R, T790M) and HCC827 (Δ746-750) (44). Cells were stimulated with growth factor in a dose-dependent manner, and labeled with DYn-2 to detect formation of sulfenic acids. EGF-mediated sulfenylation of EGFR was detected in both oncogenic mutants (Figure 4.7A, B). The fold-change of sulfenylation is higher in the

L858R/T790M mutant compared to Δ 746-750, and suggests that the propensity of the cysteine to undergo oxidative modification may be increased with respect to this mutant (Figure 4.7C). Increased H₂O₂ sensitivity of Cys797 may be due to structural changes induced by the L858R/T790M mutant, but further studies would be necessary to dissect the separate contributions of each mutation. Moreover, chronic levels of H₂O₂ associated with cancers expressing these mutations may provide an oxidizing environment that favors the sulfenyl EGFR form. Therefore, understanding the role of EGFR sulfenylation in pathologic states may provide a platform to develop effective treatments targeting this kinase.

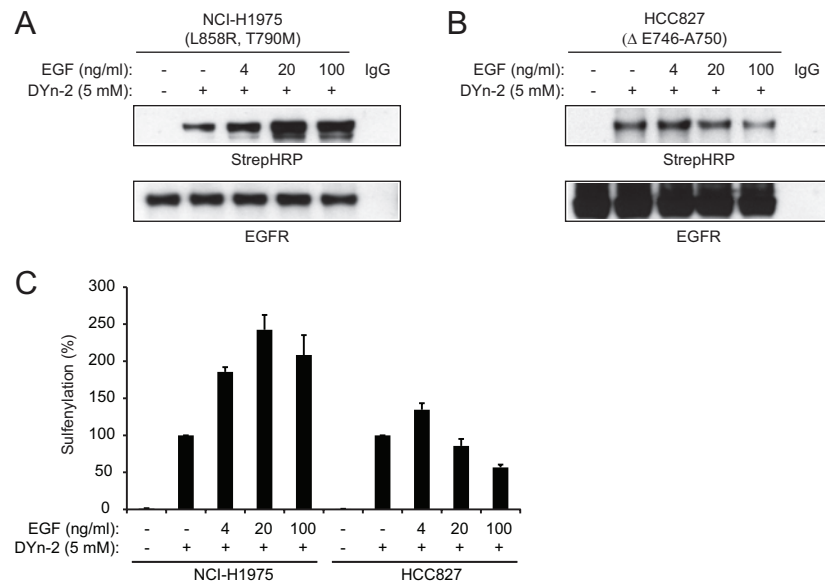


Figure 4.7: **EGF mediates sulfenylation of EGFR in common oncogenic mutations.** (A, B) Western blots showing sulfenylated and total EGFR. Lung cancer cell lines expressing common EGFR mutations, (A) NCI-H1975 (L858R, T790M) and (B) HCC827 (Δ E746-A750), were stimulated with EGF at the indicated concentrations or vehicle for 2 min and sulfenic acids were detected by Strep-HRP western blot. (C) Densitometric quantification of A and B. Data are representative of three independent readings and represent the mean \pm s.e.m.

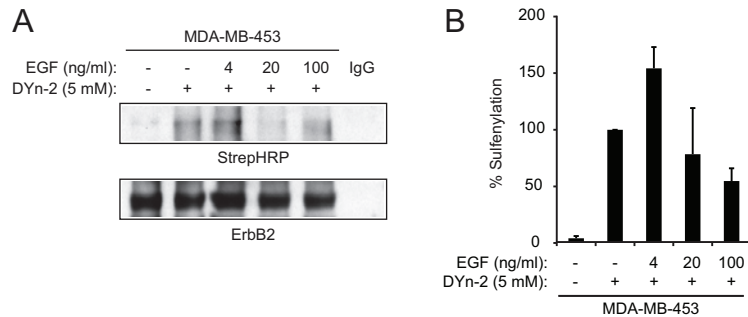


Figure 4.8: **EGF mediates sulfenylation ErbB2 in breast cancer cells.** (A) Western blot showing sulfenylated and total ErbB2. MDA-MB-453 cells were stimulated with EGF at the indicated concentrations or vehicle for 2 min and sulfenic acids were detected by Strep-HRP western blot. (B) Densitometric quantification of A. Data are representative of three independent readings and represent the mean \pm s.e.m.

EGFR is part of a subfamily that consists of three additional closely related receptors: HER2 (ErbB2), HER3 (ErbB3), and HER4 (ErbB4). Two of these receptors, HER2 and HER4, contain a structurally homologous residue to EGFR Cys797. In particular, overexpression of HER2 has been shown to play an important role in the development and progression of breast cancer. Additionally, increased protein oxidation and global sulfenylation has been observed in breast cancer cells with high HER2 expression levels (36). We sought to investigate if HER2 undergoes EGF-mediated sulfenylation similar to EGFR. For these studies, we used the metastatic breast carcinoma MDA-MB-453, which expresses high levels of HER2. EGF treatment of these cells induces oxidation of HER2 in a dose-dependent manner and peaks at 4 ng/ml (Figure 4.8A, B). These results demonstrate EGFR subfamily members exhibit detectable trends in sulfenylation similar to EGFR and its oncogenic mutations, and highlight the importance of understanding the mechanisms underlying kinase redox-regulation.

Chronic H₂O₂ treatment reduces potency of irreversible thiol (RSH)-targeted EGFR inhibitors

A number of covalent EGFR inhibitors achieve irreversible binding with an electrophilic acrylamide moiety that reacts with the EGFR Cys797 thiolate through Michael addition (45, 46). These compounds also utilize the 4-anilinoquinazoline scaffold, identified by structure-based design, to direct them to the ATP-binding domain and facilitate reaction with Cys797 (47). Oxidation of Cys797 to its sulfenyl form prevents recognition of EGFR by these targeted covalent inhibitors, and can potentially affect compound potency given its active site location. Furthermore, elevated H₂O₂ levels affiliated with cancers can generate increased levels of sulfenyl EGFR and simultaneously lower the available amount of reduced kinase.

To investigate the effect of EGFR oxidation on inhibitor potency, we used two 4-anilinoquinazoline inhibitors: afatinib (32) and PD168393 (45). Afatinib is a successful irreversible inhibitor currently undergoing clinical trials. PD168393 is also a potent compound, but did not make it to clinical trials due to low bioavailability stemming from solubility issues. A431 cells were subjected to chronic H₂O₂ conditions using glucose oxidase (GO) prior to inhibitor incubation. GO is an oxidoreductase that catalyzes the oxidation of glucose to steadily produce H₂O₂ (48). This enzyme can be used to mimic the chronic H₂O₂ levels typically associated with disease states through H₂O₂ production over prolonged treatment. Following H₂O₂ and compound treatment, cells were stimulated with EGF and analyzed for changes in autophosphorylation levels. As a technical issue, we point out that treating cells with H₂O₂ or other biological oxidants increases the fraction of sulfenyl EGFR but also results in kinase activation and PTP inhibition. Therefore, the EGF-stimulation step was included as a control to reflect the net increase mediated by EGF and H₂O₂ in these phosphorylation assays.

EGFR phosphorylation levels were increased (up to 40%) under chronic H₂O₂

conditions at higher concentrations of inhibitor compared to their respective EGF-control for both compounds (Figure 4.9A, C). Afatinib and PD169383 achieve nearly complete covalent inhibition of wild-type EGFR at 0.1 μM and higher in the EGF-control, but the potency of these compounds are reversed at these concentrations when cells are subjected to conditions of oxidative stress (Figure 4.9B, D). These results demonstrate oxidizing conditions (chronic H_2O_2) reduces the potency of RSH-targeted EGFR inhibitors by modifying the kinase into a different form. Additionally, we also probed the effect of oxidation on inhibitor potency in oncogenic EGFR mutations (L858R/T790M and $\Delta 746-750$) to determine if these mutant kinases exhibited results to wild-type kinase. For L858R/T790M, chronic oxidizing conditions induce slight increases in EGFR autophosphorylation levels, but the effect is not as pronounced as we observed in wild-type EGFR (Supplementary Figure 4.S6A, Figure 4.S7A). Therefore, sulfenylation does decrease the potency of afatinib and PD168393 in the L858R/T790M mutation, but to a smaller degree when compared to wild-type kinase (Supplementary Figure 4.S6B, Figure 4.S7B). In the $\Delta 746-750$ deletion mutant, EGFR autophosphorylation levels are increased significantly under chronic H_2O_2 conditions (Supplementary Figure 4.S6C, Figure 4.S7C). The potency of both inhibitors is reversed at concentrations of 0.01 μM and higher under oxidizing conditions when compared to its EGF control (Supplementary Figure 4.S6D, Figure 4.S7D). However, it is important to note that afatinib and PD168393 are unable to achieve complete irreversible inhibition in the $\Delta 746-750$ deletion mutant. This may indicate that this mutant has inherent resistance to these compounds, which is further enhanced by Cys797 sulfenylation. Taken together, these data confirm EGFR Cys797 sulfenylation reduces the potency of current RSH-targeted irreversible inhibitors.

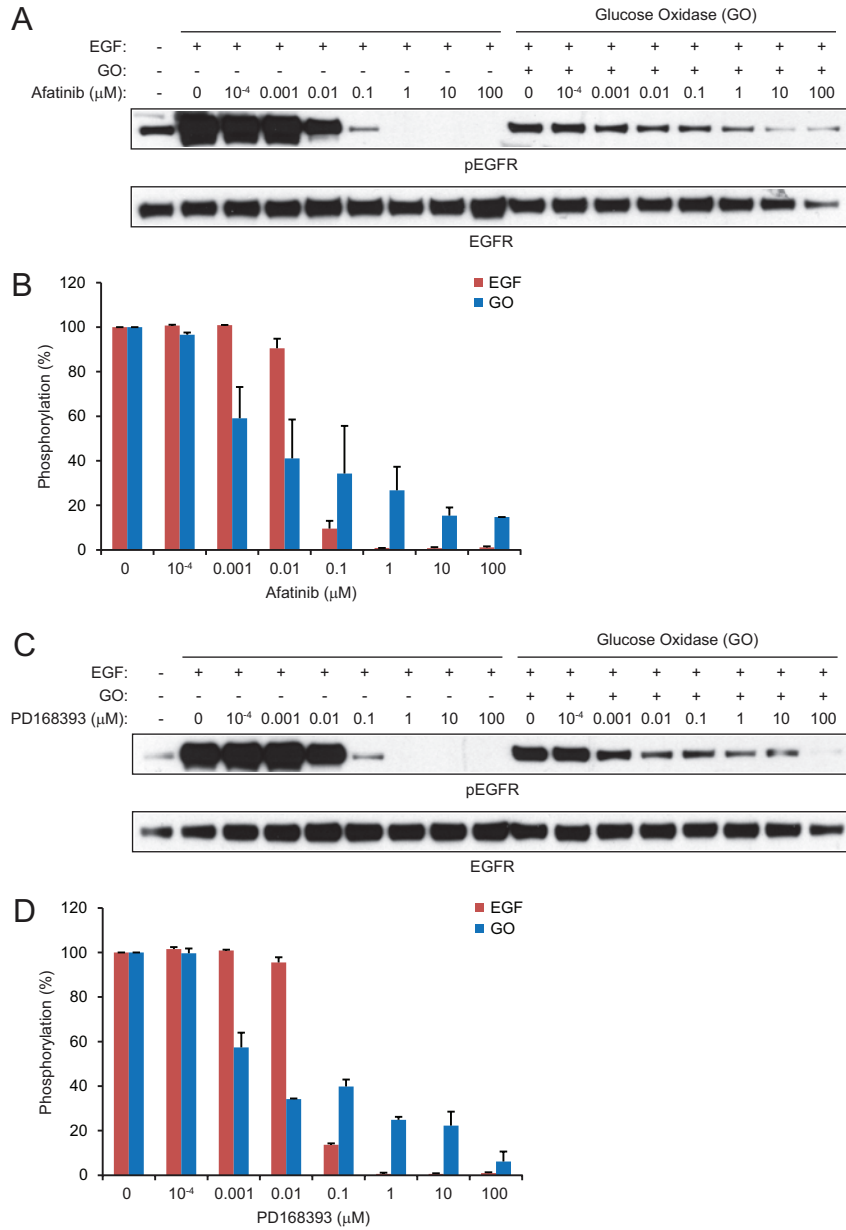


Figure 4.9: Chronic H_2O_2 treatment reduces potency of RSH-targeted irreversible EGFR inhibitors. A431 cells were incubated with glucose oxidase (2 u/ml) for 3 h to induce chronic H_2O_2 conditions, treated with the indicated concentrations of (A) afatinib or (C) PD168393 for 1 h, and subsequently stimulated with EGF (100 ng/ml) for 5 min. Western blots show phosphorylated (p) and total EGFR. The potency of both inhibitors was reduced in the presence of chronic H_2O_2 . (B, D) Densitometric quantification of A (afatinib) and C (PD168393), respectively. At higher inhibitor concentrations, phosphorylation levels (%) for chronic H_2O_2 -treated samples are higher when compared to their EGF-treated counterpart. Data are representative of two independent readings and represent the mean \pm s.e.m.

Structural homologue BTK may contain a redox-sensitive cysteine

There are nine other kinases that harbor a cysteine residue that is structurally homologous to EGFR Cys797 as mentioned previously (Supplementary Figure 4.S1). We postulate that this group of kinases could potentially be regulated by oxidation of this residue, which may serve as a general mechanism for redox-based kinase signaling. To investigate this, we decided to begin with Bruton's tyrosine kinase (BTK), a non-receptor kinase that plays an essential role in regulation calcium signaling during B-cell receptor (BCR) activation (49). We chose BTK as our starting point because it is the only other kinase besides EGFR (and HER2) that currently has inhibitors undergoing clinical trials (46). BTK Cys481 is located in the kinase active site near the beginning of an alpha helix similar to EGFR Cys797 (Figure 4.10A). In addition, BTK contains a second cysteine residue (Cys527) that is approximately 8.1 Å from Cys481 which could possibly undergo redox-mediated disulfide bond formation. Cys481 is also near the ATP binding site adjacent to the activation loop containing Tyr551, which is the phosphorylation site that enables full activation of BTK (Figure 4.10B).

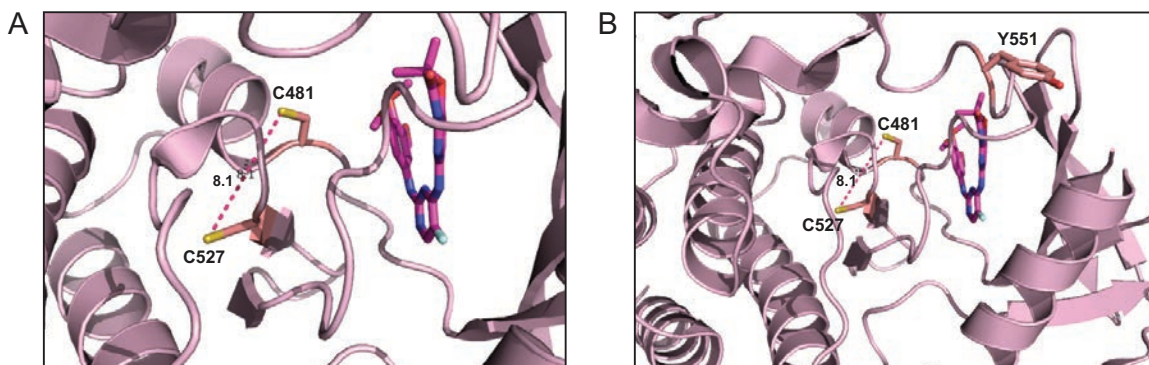


Figure 4.10: **Bruton's Tyrosine Kinase (BTK) contains a cysteine residue (Cys481) that is structurally homologous to EGFR Cys797.** (A) BTK Cys481 is located in the enzyme active site near the beginning of an alpha helix similar to EGFR Cys797. In addition, BTK contains a second cysteine residue (Cys527) that is 8.1 Å from Cys481 which could undergo redox-mediated disulfide bond formation. (B) BTK Cys481 is located near the substrate binding site, which is adjacent to the activation loop containing Tyr551.

To explore redox-based modulation of BTK activity *in situ*, we used the human B-cell lymphoma Ramos cells. First, we investigated the effect of exogenous H₂O₂ on phosphorylation of BTK. H₂O₂ treatment triggers a dose- and time-dependent increase in kinase phosphorylation levels (Supplementary Figure 4.S8C, D), and recapitulates IgM-induced activation of BTK (Supplementary Figure 4.S8A, B). These results suggest H₂O₂ mediates changes in BTK phosphorylation levels, similar to what we have observed for EGFR. To place these findings into context, we then examined if IgM treatment was capable of inducing sulfenic acid formation. Upon IgM stimulation, Ramos cells exhibited increased intracellular reactive oxygen species (ROS) levels and global protein sulfenylation in a dose-dependent manner (Supplementary Figure 4.S9A, B). The maximal increase in sulfenylation was apparently at 2.5 $\mu\text{g}/\text{ml}$ IgM, and gradually fell to basal levels at higher ligand concentrations. ROS generation and protein sulfenylation were also dynamic temporal events peaking at 2 min after IgM stimulation, and decreased thereafter (Supplementary Figure 4.S9C, D). Together, these data demonstrate H₂O₂ mimics the effects of IgM stimulation and provide the foundation to probe redox-based modulation of BTK.

We next sought to determine if BTK is a direct target of H₂O₂ in cells. Following IgM stimulation and DYn-2 labeling, BTK was immunoprecipitated and analyzed for changes in protein sulfenylation. These studies revealed that IgM stimulation leads to sulfenic acid modification of BTK, peaking at 2.5 $\mu\text{g}/\text{ml}$ IgM (Figure 4.11A). Interestingly, this is the same concentration that induces maximal protein sulfenylation levels in our global studies (Supplementary Figure 4.S9B). BTK sulfenylation is also a temporal event, peaking at 2 min following IgM stimulation (Figure 4.11B). Given these findings, we hypothesized that BTK Cys481 is the site of oxidation due to its structural homology to EGFR Cys797. To test this, we pre-incubated Ramos cells with PCI-32765 to evaluate its effect on BTK sulfenylation. PCI-32765 is an irreversible and potent inhibitor of BTK (Supplementary Figure 4.S2), and utilizes

the same electrophilic acrylamide moiety as EGFR inhibitors to covalently modify its target residue Cys481 (50, 51). Pre-treatment with PCI-32765 induced decreased IgM-mediated sulfenylation of BTK (Figure 4.11C). The sulfenyl signal was not completely abolished, suggesting additional mechanisms may be involved in modulating the oxidation status of Cys481. It is possible that the second cysteine residue (Cys527) located in the kinase active site may participate in redox-mediated disulfide bond formation with Cys481 (Figure 4.10A). Additional mass spectrometry and mutational studies would be necessary to test these propositions and are currently underway. Collectively, these results present strong evidence to indicate BTK is a direct target of H₂O₂ and undergoes sulfenic acid modification at Cys481.

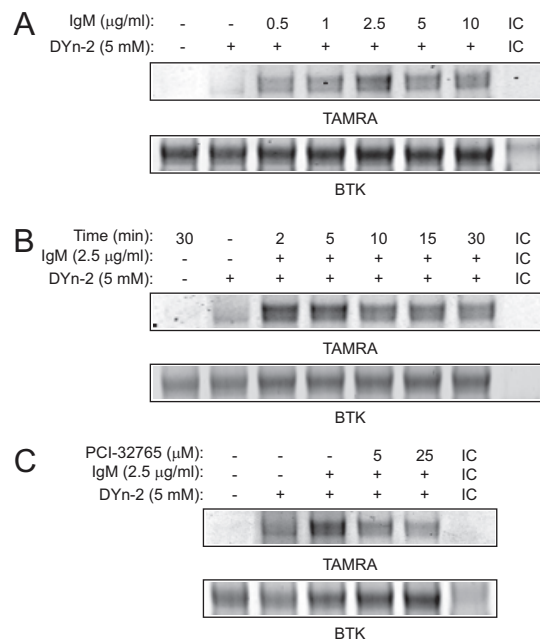


Figure 4.11: **IgM-mediated sulfenylation of BTK in cells.** (A) Dose and (B) time-dependence of BTK sulfenylation in Ramos cells. Cells were stimulated with IgM at the indicated concentrations (A) or times (B), and sulfenic acids were detected by in-gel fluorescence. (C) PCI-32765 (irreversible BTK inhibitor) treatment decreases BTK sulfenylation. Ramos cells were incubated with PCI-32765 at the indicated concentrations or vehicle before IgM stimulation and sulfenylation was detected by in-gel fluorescence.

4.4 Discussion

Sulfenic acid modifications have proven to have significant impacts on kinase activity during cellular signaling events (52, 53). In particular, recent studies have demonstrated EGFR undergoes sulfenylation at its active site cysteine in response to EGF and enhances its tyrosine kinase activity (11). Given its location and proximity to the ATP ligand, structural changes induced by Cys797 sulfenylation may enhance kinase ability to participate in electrostatic and hydrogen-bonding interactions with its substrate. Therefore, delineating the molecular mechanisms and function of cysteine oxidation in EGFR signaling may lead to a better understanding of the role of sulfenic acid during physiologic kinase-mediated events.

We generated two cysteine mutants (C797S and C797A) expressing the kinase domain and also its full-length receptor form to investigate the role of EGFR Cys797 *in vitro*. We first performed kinetic characterization to look for any changes stemming from residue mutation. Kinase activity assays revealed that these cysteine mutants exhibited decreased catalytic activity and lowered affinity for ATP when compared to wild-type enzyme (Table 4.1, Figure 4.2). Autophosphorylation assays with full-length receptor corroborated these findings and provided strong evidence that Cys797 mutation has a detrimental effect with respect to kinase activity *in vitro* (Figure 4.3, Supplementary Figure 4.S4). Additionally, EGFR autophosphorylation and sulfenylation levels are completely abrogated in response to EGF or H₂O₂ stimulation in cells (Figure 4.4, Figure 4.5, Figure 4.6). The behavior of these cysteine mutants *in vitro* and *in situ* suggest Cys797 participates in binding interactions with the substrate, which are dissolved upon residue mutation (Figure 4.1B). This series of studies collectively demonstrate EGFR Cys797 plays an important role in EGF-mediated activation, and occur through redox-based modification of this residue during normal cell signaling.

A number of EGFR mutations have been identified as a cause of human carcino-

mas. Commonly occurring oncogenic mutations (L858R/T790M and Δ 746-750) have been of particular interest because these mutations induce changes in the kinetic parameters of EGFR (24, 30), which subsequently affects sensitivity of the kinase in response to reversible and irreversible inhibitor treatment. These mutations are located in the activation loop near the ATP-binding pocket. Coupled with the active site location of Cys797, we speculated that these mutations may affect oxidation of Cys797. Analysis of EGFR Cys797 sulfenylation in these mutants revealed discernible trends and suggest the L858R/T790M mutation increases the propensity of Cys797 to undergo oxidation modification compared to the Δ 746-750 mutant (Figure 4.7). This has huge implications because deregulation of EGFR signaling in human cancers has motivated the development of inhibitors to specifically target EGFR Cys797 in its thiol form (46, 54–56). Disease states such as cancer are often correlated with chronic levels of H_2O_2 and can lead to enhanced levels of protein sulfenylation (36). These conditions favor oxidation and can shift the fraction of EGFR towards its sulfenyl form. Interestingly, the potency of afatinib and PD168393 (irreversible thiol-targeted inhibitors) was decreased under chronic H_2O_2 in wild-type and oncogenic mutant EGFR (Figure 4.9, Supplementary Figure 4.S6, Figure 4.S7). These results suggest alternate mechanisms to target sulfenyl EGFR must be developed to overcome the potential shortcomings of thiol-targeted inhibitors introduced upon oxidation and may afford additional means of achieve selectivity. The sulfenic acid modification is a unique chemical moiety and therefore represents a new opportunity in covalent inhibitor design. Nucleophilic warheads (i.e. dimedone-based derivatives) can be utilized to target the electrophilic sulfur in sulfenyl proteins. In this approach, the propensity of H_2O_2 -sensitive cysteines in kinases and other therapeutically relevant proteins (i.e. phosphatases) can be exploited to develop a new class of inhibitors similar to the proof-of-concept compounds recently reported by our group to target PTP oxidation (57). Following this study, we have developed a panel of first-generation

RSOH-targeted inhibitors and evaluated compound selectivity towards EGFR Cys797 in response to concomitant kinase oxidation. To date, our compounds induce inhibition towards EGFR under oxidizing conditions and demonstrate proof of principle for our nucleophilic approach (T. Truong, V. Gupta, and K. Carroll, unpublished results).

Protein kinases containing structurally homologous cysteine to EGFR Cys797 represent another exciting area of research (Supplementary Figure 4.1). This group contains receptor and non-receptor kinases, including two EGFR subfamily members HER2 and HER4. We speculated that oxidation of this residue may act as a general mechanism to regulate this group of kinases. In particular, we explored the possibility of two of these structural homologues to undergo sulfenylation in our studies, HER2 and BTK. Both kinases have irreversible inhibitors currently in clinical trials and represent therapeutically important targets (56). Not surprisingly, HER2 was shown to undergo EGF-mediated sulfenylation (Figure 4.8). HER2 can form a heterodimer with EGFR upon stimulation, and oxidation of HER2 may be facilitated by receptor dimerization (58). Our preliminary work with BTK demonstrates that it is a direct target of H_2O_2 and undergoes sulfenic acid modification at Cys481 (Figure 4.11). The enzyme active site contains a second cysteine residue (Cys527) that can potentially undergo redox-mediated disulfide bond formation with Cys481 (Figure 4.10). Recent studies have demonstrated ROS production is induced in response to BCR activation in human B-cells (59), and is mediated in part by sulfenic acid formation (60). Moreover, BTK has been shown to negatively regulate ROS production in human neutrophils (61). Further work is needed to define the scope of BTK oxidation, and represents an intriguing area of research. Another subfamily of protein tyrosine kinases, which includes cytoplasmic Src and FGFR1, contains a cysteine residue located within its glycine rich loop and interacts with the γ -phosphate of ATP (62). Oxidation of this residue inhibits kinase activity of c-Src and FGFR1 *in vitro*, but

neither of these kinases has been confirmed as a direct target of H₂O₂ in situ. In the physiologic context, more than 150 kinases contain a cysteine in or around the nucleotide-binding site and may play similar regulatory roles. However, a broader examination will be required to define the scope and molecular details underlying the redox-regulated kinome.

4.5 Conclusion

EGFR Cys797 sulfenylation plays a significant role in EGF-mediated cellular events, and the continued effort to define these redox-based mechanisms may provide a better general understanding of kinase signal transduction and in pathologic states associated with increased oxidative stress. Our efforts have demonstrated the physiologic importance of Cys797, and have huge implications for the development of new therapeutics whereby the sulfenic acid moiety can be exploited as an alternate target by covalent inhibitors.

4.6 Methods

Cloning of EGFR C797 mutants. EGFR in pCMV6-XL4 was obtained from Origene. EGFR C797S was generated by site-directed PCR mutagenesis with the following primers: 5-CATGCCCTTCGGCTCGCTCCTGGACTATG-3 and 3-CAT-AGTCCAGGAGCGAGCCGAAGGGCATG-5. EGFR C797A was generated with the following primers: 5-CATGCCCTTCGGCGCCCTCCTGGACTATG-3 and 3-CATAGTCCAGGAGGGCGCCGAAGGGCATG-5.

Cloning, expression, and purification of EGFR kinase domain (696-1022). EGFR (696-1022) in pFastBac was obtained from Blue Sky BioServices. EGFR C797S (696-1022) was generated by site-directed PCR mutagenesis with the following primers: 5- CATGCCGTTTCGGTTCGTTGTTGGACTACG-3 and 3- CGT-

AGTCCAACAACGAACCGAACGGCATG-5. EGFR C797A (696-1022) was generated with the following primers: 5- CATGCCGTTTCGGTGCCTTGTTGGACTACG-3 and 3- CGTAGTCCAACAAGGCACCGAACGGCATG-5. The three EGFR kinase domain constructs (WT, C797S, and C797A) were expressed and purified using a baculovirus/insect cell system by Blue Sky BioServices. The protein was concentrated to 5 mg/ml and stored in 50 mM Tris HCl pH 7.5, 150 mM NaCl, 2 mM DTT, and 20% glycerol.

Reagent source, purity, and stock solutions. All stocks were stored at -20 °C, unless otherwise indicated. EGF (30 μ g/ml, BD Biosciences) was prepared in ddH₂O. Serial dilutions of H₂O₂ (Sigma) were prepared in ddH₂O. DYn-2 (\geq 99% purity) was synthesized and purified as previously described (11). DYn-2 (250 mM) was prepared in DMSO. Dimedone (250 mM, Sigma) was prepared in 70% DMSO/30% Bis-Tris (500 mM, pH 7.4). Catalase (20,000 U/ml, Sigma) included in lysis buffers was prepared in 50 mM Tris-HCl pH 7.4 and stored at -80 °C or made up fresh, respectively. Glucose oxidase (500 U/ml, Sigma) was prepared fresh in 50 mM Tris-HCl pH 7.4. Azide biotin (5 mM, Invitrogen) and TAMRA azide (5 mM, Invitrogen) were prepared in DMSO. BTTP (100 mM, Peng Wu) was prepared in DMSO, and lower concentrations were made by dilution of stock solution with ddH₂O. Sodium L-ascorbate (Sigma) and CuSO₄ (Sigma) were prepared fresh in ddH₂O. Afatinib (10 mM, ChemieTek, \geq 99% purity), PD168393 (10 mM, Santa Cruz Biotechnology, \geq 95% purity), LFM-A13 (10 mM, Cayman Chemicals, \geq 99% purity), and PCI-32765 (10 mM, Selleckchem, \geq 98% purity) stocks were prepared in DMSO at the indicated concentrations.

Enzyme kinetic assays and data analysis. Steady-state EGFR kinetic parameters were determined in triplicate by using the ATP/NADH coupled enzyme assay system in a 384-well format (63). The reaction mixture contained 0.5 mg/ml BSA, 2 mM MnCl₂, 1 mM phospho(enol) pyruvic acid (PEP; Sigma Aldrich, # P7002), 1 mM TCEP (Sigma Aldrich), 0.1 M MOPS pH 7.5, 1/50 of the final reaction mixture vol-

ume of pyruvate kinase/lactic dehydrogenase enzymes from rabbit muscle (PK/LDH; Sigma Aldrich, # P-0294), 0.5 mM NADH (Sigma Aldrich), fixed (to determined ATP kinetic parameters) or varied (to determine peptide kinetic parameters) concentrations of peptide substrate, and 2.5 μ M EGFR kinase. ATP was added last to initiate the reaction. The two substrate kinase reaction was simplified to two one-substrate reactions to determine ATP and peptide kinetic parameters separately. When determining ATP kinetic parameters, the peptide concentration was kept the same and in excess (more than five times the K_m value). When determining peptide kinetic parameters, the ATP concentration was kept the same and in excess (more than five times the K_m value). Steady-state initial velocity data was drawn from the slopes of the A_{340} curves and fit to the Michaelis-Menten equation to determine V_{max} and K_m values. The peptide substrate was either a consensus peptide with the sequence (RAHEEIYHFFFAKKK) (38, 64) or the widely used tyrosine kinase substrate poly [Glu4Tyr1] (Sigma Aldrich, # P7244) as indicated in Table 4.1. Due to the limited solubility of the consensus peptide in the ATP/NADH coupled enzyme assay system, poly [Glu4Tyr1] was used as the peptide substrate to determine peptide kinetic parameters. To verify that our derived kcat parameters reflected concentrations of active enzyme, parallel aliquots of wild-type and mutant kinases were treated with the EGFR-specific irreversible inhibitor afatinib to determine the fraction of catalytically active molecules. Mass spectrometry analysis demonstrated complete labeling with this ATP-competitive compound, and assured that our values were based from active enzyme.

Cell culture. Mammalian cell lines (American Type Culture Collection) were maintained at 37 °C in a 5% CO₂ humidified atmosphere. A431, HeLa, and MDA-MB-453 cells were cultured in high glucose DMEM media (Invitrogen) containing 10% FBS (Invitrogen), 1% GlutaMax (Invitrogen), 1% MEM nonessential amino acids (Invitrogen), and 1% penicillin-streptomycin (Invitrogen). NCI-H1975, HCC827, and

Ramos cells were cultured in RPMI 1640 media with glutamine (Invitrogen) containing 10% FBS (Invitrogen), 1% MEM nonessential amino acids (Invitrogen), and 1% penicillin-streptomycin (Invitrogen). For EGF and H₂O₂ treatment, cells were cultured until 80-85% confluency, washed with PBS, and placed in culture media without serum (serum-starved) for 16 h. After serum deprivation, cells were treated with the indicated concentration of EGF or H₂O₂ for the indicated time period. Treatment was stopped by removing the media and washing with PBS. For glucose oxidase treatment, cells were cultured until 80-85% confluency, washed with PBS, and serum-starved for 16 h. After serum deprivation, cells were treated with the indicated concentration of glucose oxidase for the indicated time period to induce chronic H₂O₂. Cells were then incubated with the indicated concentration of inhibitor for the indicated time period, washed with PBS, and treated with the indicated concentration of EGF for the indicated time period. Treatment was stopped by removing the media and washing with PBS. For goat anti-human IgM (Jackson ImmunoResearch) treatment, cells were cultured until 80-85% confluency, washed with PBS, and placed in culture media without serum (serum-starved) for 16 h. After serum deprivation, cells were treated with the indicated concentration of IgM for the indicated time period. Treatment was stopped by removing the media and washing with PBS.

Transfection of EGFR. HeLa cells were transfected at 80-85% confluency with EGFR, EGFR C797S, EGFR C797A, or empty vector (pCMV6-XL4) using Lipofectamine 2000 (Invitrogen) according to manufacturer guidelines for 24 h. For EGF and H₂O₂ treatment, cells were washed with PBS after transfection and serum-starved for 2 h. After serum deprivation, cells were treated with the indicated concentration of EGF or H₂O₂ for the indicated time period. Treatment was stopped by removing the media and washing with PBS.

Sulfenic acid labeling in cells. Mammalian cells were lifted with 0.25% trypsin-EDTA, harvested by centrifugation at 1000 rpm for 2 min, washed, and resuspended

in serum-free media at a density of $3\text{-}4 \times 10^6$ cells/ml. Intact cells in suspension were incubated with vehicle (DMSO, 2% v/v) or the indicated concentration of sulfenic acid probe (DYn-2) at 37 °C in a 5% CO₂ humidified atmosphere with periodic gentle agitation for 15 min unless indicated otherwise. Following treatment for the indicated time, cells were collected by centrifugation (1000 rpm) and washed with PBS. The resulting cells were routinely counted using a hemocytometer and uniformly showed greater than 90% viability by trypan blue exclusion.

Cell lysate preparation. Cells were harvested in HEPES lysis buffer [50 mM HEPES pH 7.4, 150 mM NaCl, 1% NP-40, 0.1% SDS, 1× EDTA-free complete mini protease inhibitors (Roche), and 200 U/ml catalase (Sigma)]. After 15 min incubation on ice with frequent mixing, cell debris was removed by centrifugation at 14,000 rpm for 15 min at 4 °C. Protein concentration was determined by BCA assay (Pierce). For analysis of protein phosphorylation, cells were harvested in phosphorylation lysis buffer [50 mM HEPES pH 7.4, 150 mM NaCl, 1% NP-40, 0.1% SDS, 5 mM sodium pyrophosphate, 50 mM sodium fluoride, 10 μM β-glycerophosphate, 1 mM sodium orthovanadate, 0.5 mM DTT, and 1× complete mini protease inhibitors (Roche)]. For immunoprecipitated EGFR kinase assays, cells were harvested in RIPA B buffer [20 mM HEPES, pH 7.0, 150 mM NaCl, 0.2 mM MgCl₂, 1% Triton X-100, 1× complete mini protease inhibitors (Roche)].

Click chemistry. For global sulfenylation analyses, cell lysate (100 μg, 1 mg/ml) was pre-incubated with NeutrAvidin agarose resin (50 μl, Pierce) to remove endogenously biotinylated proteins. The pre-cleared lysate was incubated with azide biotin (100 μM), CuSO₄ (250 μM), BTTP (500 μM), and sodium L-ascorbate (2.5 mM) for 1 h at rt with gentle rocking (final reaction volume, 100 μl). The reaction was quenched with 1 mM EDTA, and the sample was subjected to methanol precipitation. The resulting protein precipitate was then resolubilized in LDS sample buffer (Invitrogen). For immunoprecipitated protein analyses, the resin was treated with 20

μ l click chemistry mix [azide biotin (100 μ M), CuSO₄ (250 μ M), BTTP (500 μ M), and sodium L-ascorbate (2.5 mM) in PBS] for 1 h at rt with gentle rocking. The reaction was quenched with 1 mM EDTA, and the samples were boiled with LDS sample buffer. For in-gel fluorescence, TAMRA azide (100 μ M) was used in place of azide biotin.

Western blot. Protein samples were separated by SDS-PAGE using NuPAGE Novex 4-12% Bis-Tris Midi gels (Invitrogen) and transferred to a polyvinylidene difluoride (PVDF) membrane (BioRad). After transfer, the membrane was blocked with 3% BSA or 5% milk in TBST (ErbB2) for 1 h at rt. The membrane was washed with TBST and immunoblotting was performed with the following primary and secondary antibodies at the indicated dilutions in TBST, unless otherwise noted: phospho-EGFR (pY1068, Abcam, 1:1000), EGFR (1005, Santa Cruz Biotechnology, 1:200), ErbB2 (Neu C-18, Santa Cruz Biotechnology, 1:200), phospho-BTK (pY223, Abcam, 1:1000), BTK (C-20, Santa Cruz Biotechnology, 1: 200), streptavidin-HRP (GE Healthcare, 1:8000 - 1:80000), GAPDH (Santa Cruz Biotechnology, 1:200), goat anti-rabbit IgG-HRP (Calbiochem, 1:30000 - 1:50000), and rabbit anti-mouse IgG-HRP (Invitrogen, 1:30000 - 1:50000). PVDF membrane was developed with chemiluminescence (Pierce) and imaged by film. Data was quantified by densitometry with ImageJ (Wayne Rasband, US National Institutes of Health, <http://rsbweb.nih.gov/ij/>).

In-gel fluorescence. Protein samples were separated by SDS-PAGE using NuPAGE Novex 4-12% Bis-Tris Midi gels. The gel was destained 2X (40% methanol, 10% acetic acid, 50% H₂O) and 1X with water for 10 min at rt to remove any background fluorescence from excess reagents. Afterwards, the gel was analyzed using a Typhoon 9400 variable mode imager (Amersham Biosciences). The following wavelengths (excitation/emission) were used: 550/580 nm (TAMRA), and 280 or 450/610 nm (SYPRO ruby protein stain, Lonza).

Immunoprecipitation. EGFR was immunoprecipitated from 500 μ g cell lysate

(1 mg/ml) with goat anti-EGFR conjugated agarose (Santa Cruz Biotechnology) or isotype control (normal goat IgG) overnight at 4 °C with gentle rocking. ErbB2 was immunoprecipitated from 500 μ g cell lysate (1 mg/ml) with 1 μ g of anti-ErbB2 antibody or isotype control for 2 h at 4 °C with gentle rocking. The immunocomplexes were isolated by incubating with Protein A/G Plus Agarose (20 μ l, Santa Cruz Biotechnology) overnight at 4 °C with rocking. BTK was immunoprecipitated from 750 μ g cell lysate (1 mg/ml) with 2 μ g of anti-BTK antibody or isotype control for 2 h at 4 °C with gentle rocking. The immunocomplexes were isolated by incubating with Protein A/G Plus Agarose (20 μ l, Santa Cruz Biotechnology) overnight at 4 °C with rocking. The resin was collected by centrifugation at 100g for 2 min at rt, and washed with cold RIPA buffer (1X) and cold PBS buffer (2X). The resin was subjected to click chemistry as described earlier in Methods, and the bound proteins were eluted by boiling with LDS sample buffer for 10 min, and resolved by SDS-PAGE and analyzed by Western blot.

Immunoprecipitated EGFR kinase assays. To assess EGF and H₂O₂-induced WT EGFR autophosphorylation activity, A431 cells were cultured until 80-85% confluency, washed with PBS, and serum-starved for 2 h. After serum-deprivation, cells were washed with cold PBS (2X) and lysed in RIPA B buffer as previously described. EGFR was immunoprecipitated from 1000 μ g (1 mg/ml) with goat anti-EGFR conjugated agarose (40 μ l) for 30 min at 4 °C with gentle rocking. The resin was collected by centrifugation at 100g for 2 min at rt, washed with cold RIPA B buffer (3X), and resuspended in 40 mM HEPES, pH 7.4 (100 μ l). EGFR kinase activity was assayed with full-length native receptor immunoprecipitated from 30-50 μ g lysate in 10 μ l reactions containing 20 mM HEPES pH 7.4, 6 mM MnCl₂, 100 μ M NaVO₄ (New England Biolabs), 1 μ M ATP (Promega) and supplemented with EGF (3.3 ng/ μ l) or H₂O₂ (0-100 μ M). Control and EGF-treated reactions were initiated upon addition of immunoprecipitated EGFR and incubated on ice for 5 min. For H₂O₂-treated re-

actions, immunoprecipitated EGFR was pre-incubated with peroxide for 5 min on ice prior to addition of ATP and an additional incubation on ice for 5 min. To assess the reversibility of H₂O₂-induced EGFR kinase activation, immunoprecipitated EGFR was pre-incubated +/- H₂O₂ as previously stated followed by addition of DTT (1 mM) simultaneous with ATP and EGF (as appropriate) for an additional 5 min on ice. To verify that EGFR autophosphorylation was due to enhanced inherent kinase activity, immunoprecipitated EGFR was pre-incubated with afatinib (0 or 1 μ M) on ice for 5 min prior to additional incubation with ATP and EGF for 5 min on ice. In all cases, reactions were quenched upon addition of 5 μ l LDS sample buffer and bound proteins were eluted by boiling with LDS sample buffer for 10 min, and resolved by SDS-PAGE and analyzed by Western blot.

To assess the role of Cys797 in H₂O₂-induced EGFR autophosphorylation activity, HeLa cells were transfected with EGFR, C797S EGFR, C797A EGFR or empty vector (mock) as previously described. After transfection (24 h), the cells were washed with PBS and serum-starved for 4 h and lysates were generated as described above. WT and C797 mutant EGFR kinase activity was assayed using identical conditions as outlined above with the following modification. Immunoprecipitated WT and mutant EGFR was pre-incubated with EGF (50 or 100 ng/ μ l) or H₂O₂ (0-10 μ M) for 5 min on ice. Kinase assays were initiated upon the addition of ATP (0.5 μ M) and were incubated for an additional 5 min on ice. Reactions were quenched and analyzed as described above.

Sulfenic acid labeling of recombinant EGFR. WT EGFR was stored in 50 mM Tris-HCl pH 7.5, 150 mM NaCl, 2 mM DTT, and 20% glycerol. The protein was reduced with 10 mM DTT for 30 min on ice. DTT was removed by passing the protein through a NAP5 column (GE Healthcare) pre-equilibrated with 50 mM HEPES pH 7.4, 100 mM NaCl. 10 μ M protein was treated with H₂O₂ (5 eq.) for 5 min and labeled with dimedone (5 mM) for 1.5 h at rt with gentle rocking. For

afatinib and PD168393, 10 μ M protein was labeled with inhibitor (1 mM) for 1.5 h at rt with gentle rocking. Following compound treatment, samples were boiled with LDS sample buffer for 10 min, and resolved by SDS-PAGE.

In-gel pepsin digestion of recombinant EGFR. Labeled recombinant EGFR was resolved by SDS-PAGE and stained with Coomassie. After destaining, the gel was washed in H₂O for 30 min. The bands of interest were excised, cut into small cubes, and subjected to in-gel protein digestion. The gel pieces were washed with water (2X), dehydrated with ACN (2X), and reduced with DTT (10 mM) in 25 mM Ambic pH 7.8 for 30 min at 56 °C. Afterwards, DTT was removed and the gel pieces were dehydrated with ACN (1X). The samples were then alkylated with 54 mM NEM in 25 mM Ambic pH 7.8 for 1 h at rt in darkness and agitation. NEM was removed and the gel pieces were dehydrated with ACN (1X), rehydrated with 150 mM K₂HPO₄/150 mM KH₂PO₄ pH 2.5, and dehydrated with ACN (1X). The buffer/ACN solution was removed, and the gel pieces were dried by vacuum centrifugation. Sequencing grade pepsin (Princeton Separations) was resuspended in 75 mM K₂HPO₄/75 mM KH₂PO₄ pH 2.5 at a concentration of 20 ng/ μ l. The pepsin (20 ng/ μ l) was added to the dried gel pieces and incubated on ice for 1 h. Pepsin excess was removed and 75 mM K₂HPO₄/75 mM KH₂PO₄ pH 2.5 was added until the gel pieces were completely covered. The samples were incubated overnight at 37 °C. The following day, the peptides were recovered by collecting the supernatant, desalted using a Zip-Tip (Millipore), and concentrated by vacuum centrifugation. The resulting peptide samples were resuspended in 0.1% formic acid and analyzed by LC-MS/MS.

LC-MS/MS Analysis. Peptides were analyzed on by liquid chromatography-tandem MS (LC-MS/MS) using an EASY-nLC II system coupled to a linear ion trap mass spectrometer (LTQ, Thermo Scientific). Peptides were concentrated and desalted on an RP pre-column (0.1 \times 20 mm EASY column, Thermo Scientific) and eluted onto an analytical RP column (0.075 \times 100 mm EASY column, Thermo Scien-

tific) at a flow rate of 400 nl/min using the following gradient: 5% to 15% B in 5 min, 15% to 55% B in 125 min, and 55% to 95% B in 5 min [solvent A: 0.1% formic acid (v/v); solvent B: 0.1% formic acid (v/v), 80% CH₃CN (v/v)]. For targeted experiments, the LTQ was programmed in the 'selected MS/MS ion monitoring (SMIM) mode (65). A survey scan (m/z 350-1600) was performed to check for the presence of digested peptides, and for peptide separation along the gradient. This survey scan was followed by a dependent MS/MS scan that fragments the most intense ions to make a general identification of the peptides present. Subsequent MS/MS spectra were programmed on +1 charged precursor ions of peptide MPFGCL modified by dimedone (m/z 821.4), or +2 charged precursor ions of peptide MPFGCL modified by afatinib (m/z 584.8) or PD168393 (m/z 526.2). Peptide identification was performed using SEQUEST algorithm (BioWorks 3.2, Thermo Scientific) using the following search parameters: enzyme specificity was pepsin with two missed cleavages permitted, optional modifications (Met oxidation and Cys modification depending on the reagent used), and mass tolerance of 2 and 1.2 amu for precursor and fragment ions, respectively. MS/MS raw files were searched against the human Swiss-Prot database containing porcine pepsin. SEQUEST results were analyzed using the probability ratio method.

Intracellular ROS detection. Intracellular ROS was measured in a 96 well plate format using the fluorescent probe DCF (the intracellular product of H₂-DCF diacetate that fluoresces in the presence of ROS, including H₂O₂). Ramos cells were grown and stimulated with goat anti-human IgM as described in Methods. Following stimulation, the cells were washed with PBS (3X) and seeded into 96-well plates at 1×10^5 cells/well in triplicate. The cells were incubated in the dark for 30 min at rt with 2',7'-dichlorodihydrofluorescein diacetate (H₂DCF-DA; 10 μ M, Sigma) in PBS. H₂-DCF-DA is a cell permeable indicator for ROS that is a non-fluorescent compound that can enter cells, and trapped by intracellular esterase cleavage of the diacetate

group. H₂DCF is then converted into a fluorescent product upon interaction with intracellular ROS. After incubation, the fluorescence intensity was measured at 488/525 nm (excitation/emission) using a SpectraMax M5 microplate reader (Molecular Devices).

4.7 Contributions

T.H.T. performed kinetic experiments. C.E.P. performed immunoprecipitated kinase experiments. T.H.T. performed cell culture experiments. T.H.T. performed mass spectrometry experiments. K.S.C., T.H.T., and C.E.P. designed experimental strategies.

4.8 Supplemental Figures

EGFR	T	Q	L	M	P	F	G	C	L	L	D
HER2	T	Q	L	M	P	Y	G	C	L	L	D
HER4	T	Q	L	M	P	H	G	C	L	L	E
BLK	T	E	Y	M	A	R	G	C	L	L	D
BMX	T	E	Y	I	S	N	G	C	L	L	N
BTK	T	E	Y	M	A	N	G	C	L	L	N
ITK	F	E	F	M	E	H	G	C	L	S	D
JAK3	M	E	Y	L	P	S	G	C	L	R	D
TEC	T	E	F	M	E	R	G	C	L	L	N
TXK	T	E	F	M	E	N	G	C	L	L	N

Figure 4.S1: **Sequence alignment of EGFR and nine additional kinases containing a structurally homologous residue to EGFR Cys797.** This group contains two ErbB2 family members, HER2 and HER4.

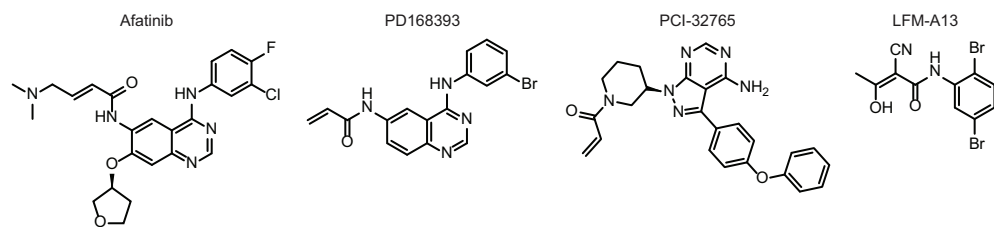


Figure 4.S2: Chemical Structures of compounds used in this study.

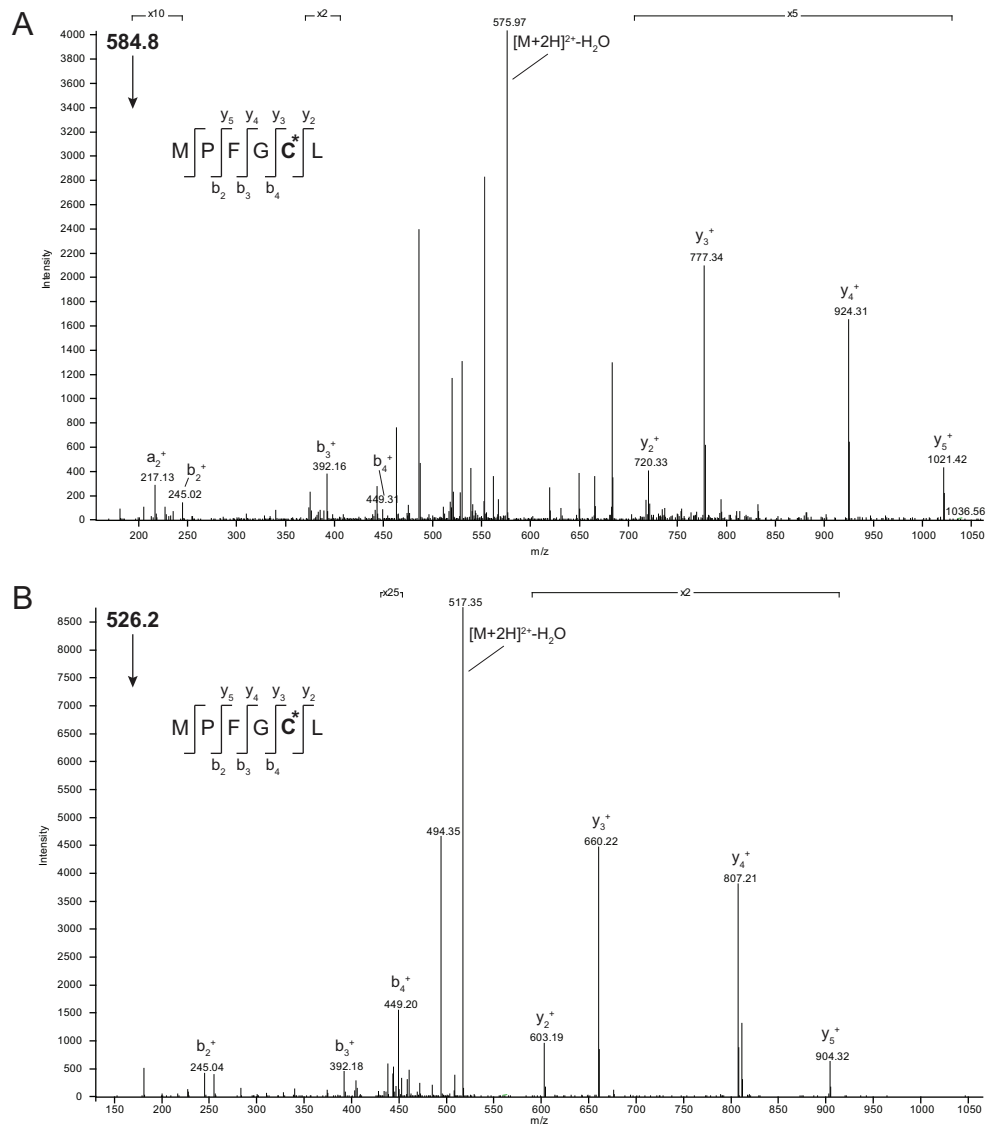


Figure 4.S3: **Identification of the MPFGC*L peptide from EGFR labeled with RSH-targeted inhibitors.** (A) MS/MS spectrum of the precursor ion m/z 584.8 $[M+2H]^{2+}$ corresponding to afatinib labeled peptide (MPFGC*L) from recombinant WT EGFR. (B) MS/MS spectrum of the precursor ion m/z 526.2 corresponding to PD168393 labeled peptide (MPFGC*L) from recombinant WT EGFR.

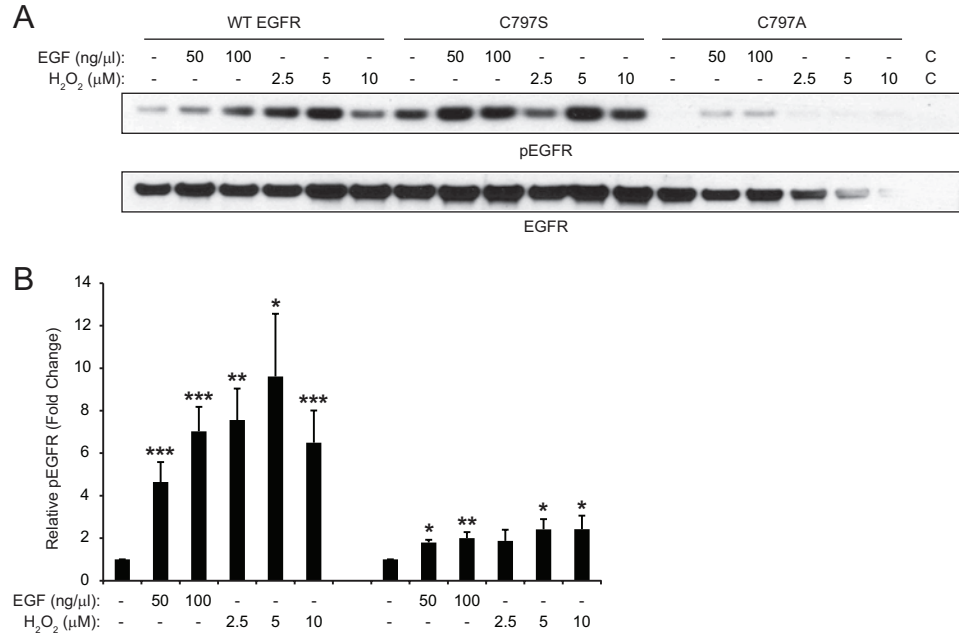


Figure 4.S4: **Cys797 mutants do not exhibit enhanced autophosphorylation levels in response to EGF or H₂O₂ treatment.** (A) Full length WT, C797S, and C797A EGFR was immunoprecipitated from transiently transfected HeLa cells and assayed for tyrosine kinase activity with ATP and stimulated with EGF or H₂O₂ at the indicated concentrations. Western blot shows phosphorylated (p) and total EGFR. (B) Densitometric quantification of A. EGF and H₂O₂ treatment increases autophosphorylation of WT EGFR, but not in C797 mutants. Data are representative of three independent readings and represent the mean \pm s.e.m. * p < 0.05, ** p < 0.01, *** p < 0.001 compared to untreated control.

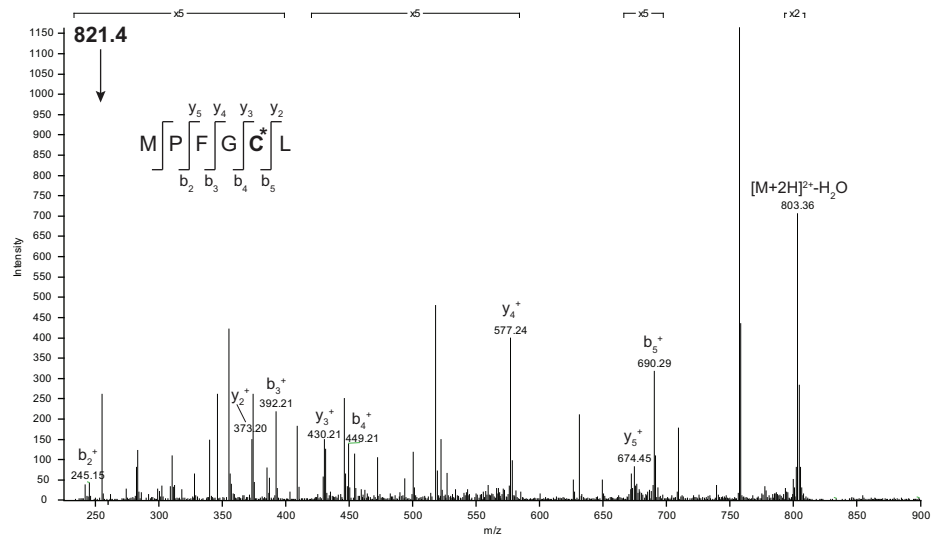


Figure 4.S5: MS/MS spectrum of the precursor ion m/z 821.4 $[M+H]^+$ corresponding to dimedone labeled peptide (MPFGC*L) from recombinant WT EGFR.

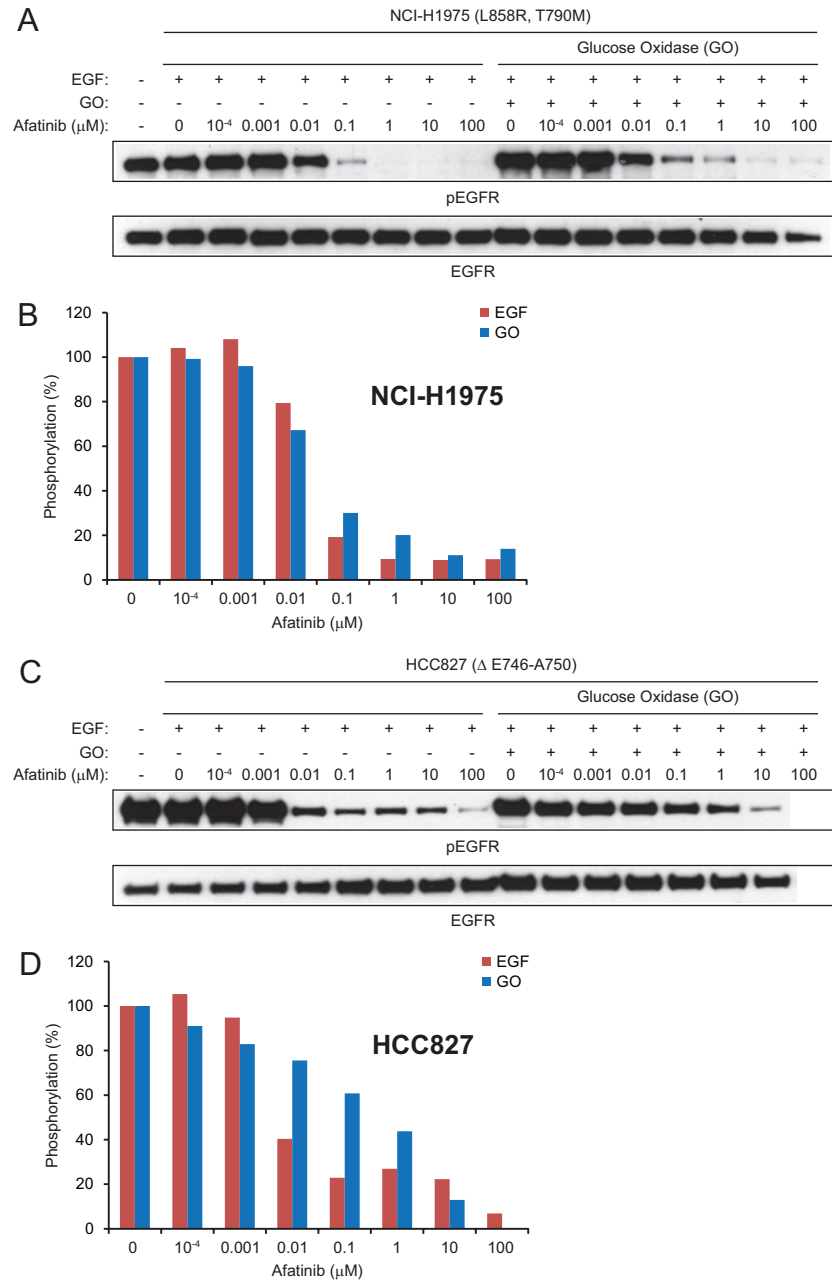


Figure 4.S6: Chronic H₂O₂ treatment reduces potency of PD168393 in common oncogenic mutations. Lung cancer cell lines expressing common EGFR mutations, (A) NCI-H1975 (L858R, T790M) and (C) HCC827 (Δ E746-A750), were incubated with glucose oxidase (2 u/ml) for 2 h to induce chronic H₂O₂ conditions, treated with the indicated concentrations of PD168393 for 1 h, and subsequently stimulated with EGF (100 ng/ml) for 5 min. Western blots show phosphorylated (p) and total EGFR. The potency of PD168393 was reduced in the presence of chronic H₂O₂ in both cases. (B, D) Densitometric quantification of A (NCI-H1975) and C (HCC827), respectively. At higher inhibitor concentrations, phosphorylation levels (%) for chronic H₂O₂-treated samples are higher when compared to their EGF-treated counterpart. Data are representative of two independent readings and represent the mean \pm s.e.m.

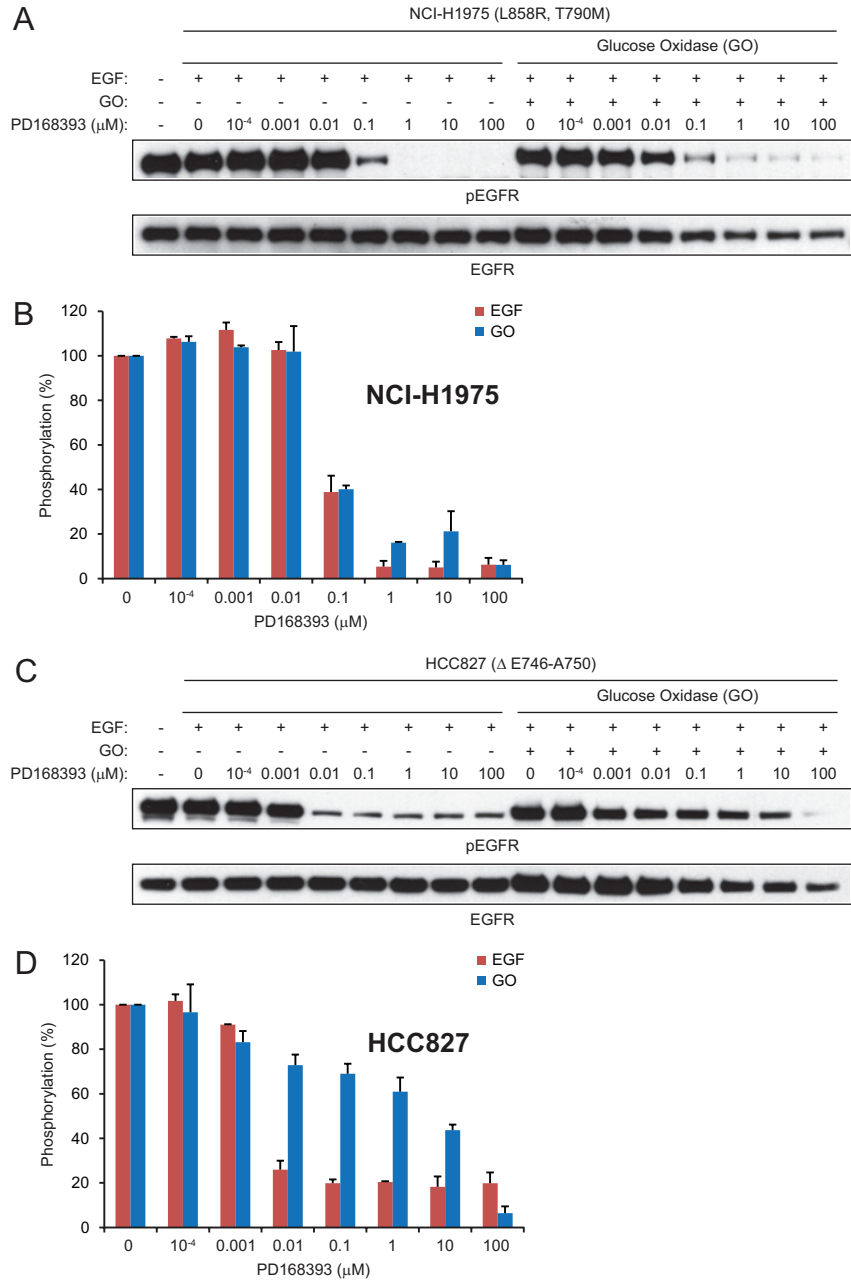


Figure 4.S7: **Chronic H₂O₂ treatment reduces potency of afatinib in common oncogenic mutations.** Lung cancer cell lines expressing common EGFR mutations, (A) NCI-H1975 (L858R, T790M) and (C) HCC827 (Δ E746-A750), were incubated with glucose oxidase (2 u/ml) for 2 h to induce chronic H₂O₂ conditions, treated with the indicated concentrations of afatinib for 1 h, and subsequently stimulated with EGF (100 ng/ml) for 5 min. Western blots show phosphorylated (p) and total EGFR. The potency of afatinib was reduced in the presence of chronic H₂O₂ in both cases. (B, D) Densitometric quantification of A (NCI-H1975) and C (HCC827), respectively. At higher inhibitor concentrations, phosphorylation levels (%) for chronic H₂O₂-treated samples are higher when compared to their EGF-treated counterpart.

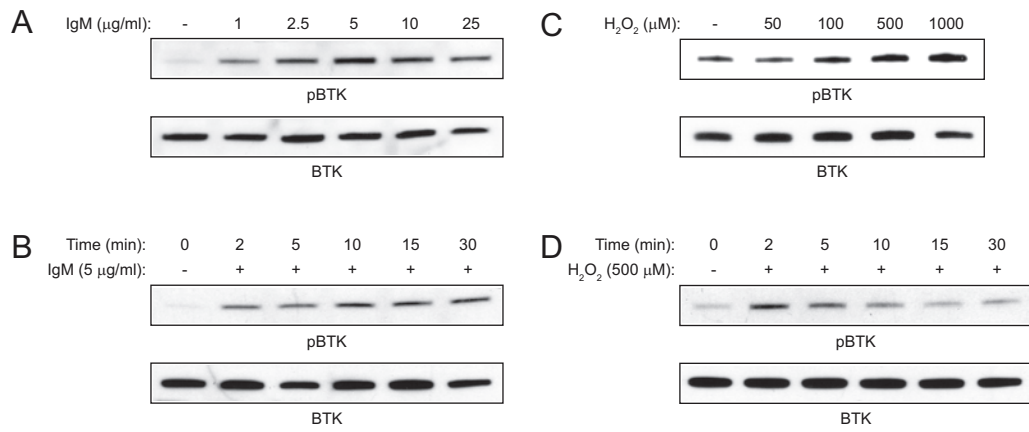


Figure 4.S8: **H_2O_2 treatment mimics IgM-induced activation of BTK.** (A) Dose and (B) time-dependent effect of IgM on BTK activation in Ramos cells. Cells were stimulated with IgM at the indicated concentrations (A) or times (B). (C) Dose and (D) time-dependent effect of H_2O_2 on BTK activation in Ramos cells. Cells were stimulated with H_2O_2 at the indicated concentrations (C) or times (D). Western blot shows phosphorylated (p) and total BTK.

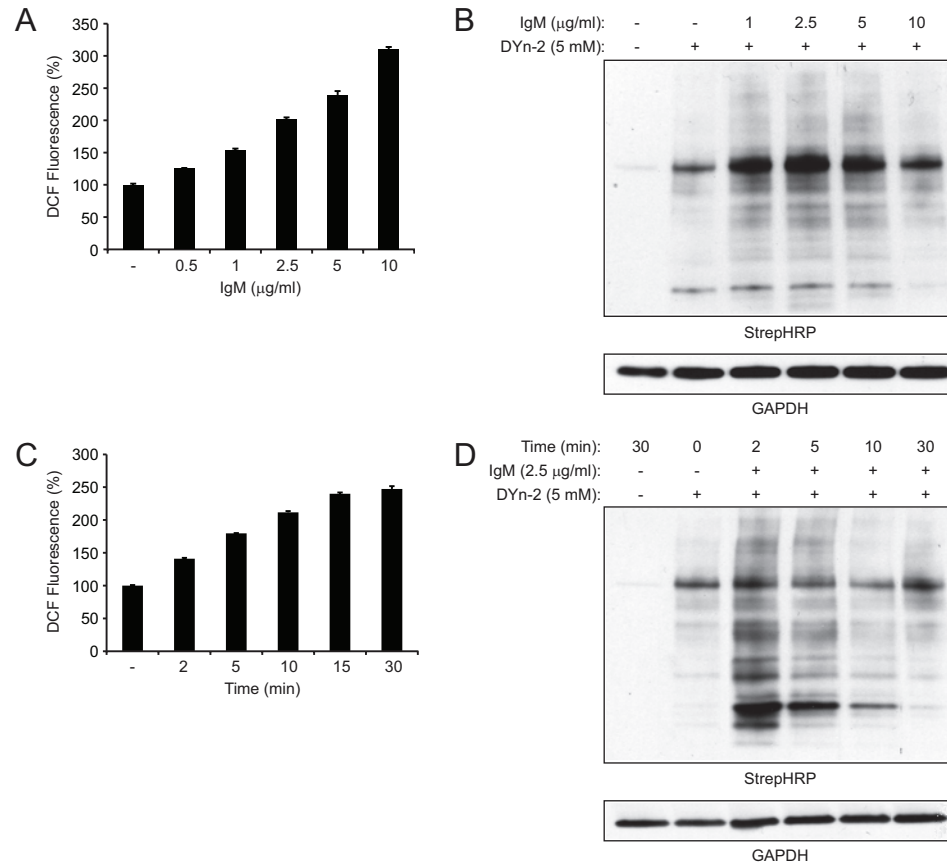


Figure 4.S9: **IgM-mediated ROS production and protein sulfenylation.** (A) Dose and (C) time-dependence of ROS production as indicated by DCF fluorescence in Ramos cells. Cells were stimulated with IgM at the indicated concentrations (A) or times (C). (B) Dose and (D) time-dependence of global protein sulfenylation in Ramos cells. Cells were stimulated with IgM at the indicated concentrations (B) or times (D), and sulfenic acids were detected through western blot with Strep-HRP. GAPDH was used as a loading control.

4.9 Chapter References

1. Schlessinger, J. (2000). Cell signaling by receptor tyrosine kinases. *Cell*, *103*(2), 211–25.
2. Bae, Y. S., Kang, S. W., Seo, M. S., Baines, I. C., Tekle, E., Chock, P. B., & Rhee, S. G. (1997). Epidermal growth factor (egf)-induced generation of hydrogen peroxide. role in egf receptor-mediated tyrosine phosphorylation. *J Biol Chem*, *272*(1), 217–21.
3. Sundaresan, M., Yu, Z. X., Ferrans, V. J., Irani, K., & Finkel, T. (1995). Requirement for generation of h₂o₂ for platelet-derived growth factor signal transduction. *Science*, *270*(5234), 296–9.
4. Rhee, S. G. (2006). Cell signaling. h₂o₂, a necessary evil for cell signaling. *Science*, *312*(5782), 1882–3.
5. Dickinson, B. C. & Chang, C. J. (2011). Chemistry and biology of reactive oxygen species in signaling or stress responses. *Nat Chem Biol*, *7*(8), 504–11.
6. Finkel, T. (2011). Signal transduction by reactive oxygen species. *J Cell Biol*, *194*(1), 7–15.
7. Miller, E. W., Tulyathan, O., Isacoff, E. Y., & Chang, C. J. (2007). Molecular imaging of hydrogen peroxide produced for cell signaling. *Nat Chem Biol*, *3*(5), 263–7.
8. Woo, H. A., Yim, S. H., Shin, D. H., Kang, D., Yu, D. Y., & Rhee, S. G. (2010). Inactivation of peroxiredoxin i by phosphorylation allows localized h(2)o(2) accumulation for cell signaling. *Cell*, *140*(4), 517–28.
9. Paulsen, C. E. & Carroll, K. S. (2010). Orchestrating redox signaling networks through regulatory cysteine switches. *ACS Chem Biol*, *5*(1), 47–62.
10. Paulsen, C. E. & Carroll, K. S. (2013, July). Cysteine-mediated redox signaling: chemistry, biology, and tools for discovery. *Chem Rev*, *113*(7), 4633–4679. doi:10.1021/cr300163e
11. Paulsen, C. E., Truong, T. H., Garcia, F. J., Homann, A., Gupta, V., Leonard, S. E., & Carroll, K. S. (2012). Peroxide-dependent sulfenylation of the egfr catalytic site enhances kinase activity. *Nat Chem Biol*, *8*(1), 57–64.
12. Zhang, X., Gureasko, J., Shen, K., Cole, P. A., & Kuriyan, J. (2006). An allosteric mechanism for activation of the kinase domain of epidermal growth factor receptor. *Cell*, *125*(6), 1137–1149.
13. Penel, S., Hughes, E., & Doig, A. J. (1999). Side-chain structures in the first turn of the alpha-helix. *J Mol Biol*, *287*(1), 127–43.

14. Anderson, T. A. & Sauer, R. T. (2003). Role of an n(cap) residue in determining the stability and operator-binding affinity of arc repressor. *Biophys Chem*, *100*(1-3), 341–50.
15. Miranda, J. J. (2003). Position-dependent interactions between cysteine residues and the helix dipole. *Protein Sci*, *12*(1), 73–81.
16. Blume-Jensen, P. & Hunter, T. (2001). Oncogenic kinase signalling. *Nature*, *411*(6835), 355–65.
17. Hynes, N. E. & Lane, H. A. (2005, May). Erbb receptors and cancer: the complexity of targeted inhibitors. *Nat Rev Cancer*, *5*(5), 341–354. doi:10.1038/nrc1609
18. Wakeling, A. E., Guy, S. P., Woodburn, J. R., Ashton, S. E., Curry, B. J., Barker, A. J., & Gibson, K. H. (2002, October). Zd1839 (iressa): an orally active inhibitor of epidermal growth factor signaling with potential for cancer therapy. *Cancer Res*, *62*(20), 5749–5754.
19. Pollack, V. A., Savage, D. M., Baker, D. A., Tsaparikos, K. E., Sloan, D. E., Moyer, J. D., . . . Morin, M. J. (1999, November). Inhibition of epidermal growth factor receptor-associated tyrosine phosphorylation in human carcinomas with cp-358,774: dynamics of receptor inhibition in situ and antitumor effects in athymic mice. *J Pharmacol Exp Ther*, *291*(2), 739–748.
20. Johnson, B. E. & Janne, P. A. (2005, September). Epidermal growth factor receptor mutations in patients with non-small cell lung cancer. *Cancer Res*, *65*(17), 7525–7529. doi:10.1158/0008-5472.CAN-05-1257
21. Gazdar, A. F., Shigematsu, H., Herz, J., & Minna, J. D. (2004, October). Mutations and addiction to egfr: the achilles 'heel' of lung cancers? *Trends Mol Med*, *10*(10), 481–486. doi:10.1016/j.molmed.2004.08.008
22. Chan, S. K., Gullick, W. J., & Hill, M. E. (2006, January). Mutations of the epidermal growth factor receptor in non-small cell lung cancer – search and destroy. *Eur J Cancer*, *42*(1), 17–23. doi:10.1016/j.ejca.2005.07.031
23. Shigematsu, H. & Gazdar, A. F. (2006, January). Somatic mutations of epidermal growth factor receptor signaling pathway in lung cancers. *Int J Cancer*, *118*(2), 257–262. doi:10.1002/ijc.21496
24. Yun, C.-H., Boggon, T. J., Li, Y., Woo, M. S., Greulich, H., Meyerson, M., & Eck, M. J. (2007). Structures of lung cancer-derived egfr mutants and inhibitor complexes: mechanism of activation and insights into differential inhibitor sensitivity. *Cancer Cell*, *11*(3), 217–227.

25. Carey, K. D., Garton, A. J., Romero, M. S., Kahler, J., Thomson, S., Ross, S., . . . Sliwkowski, M. X. (2006, August). Kinetic analysis of epidermal growth factor receptor somatic mutant proteins shows increased sensitivity to the epidermal growth factor receptor tyrosine kinase inhibitor, erlotinib. *Cancer Res*, *66*(16), 8163–8171. doi:10.1158/0008-5472.CAN-06-0453
26. Paez, J. G., Janne, P. A., Lee, J. C., Tracy, S., Greulich, H., Gabriel, S., . . . Meyerson, M. (2004, June). Egfr mutations in lung cancer: correlation with clinical response to gefitinib therapy. *Science*, *304*(5676), 1497–1500. doi:10.1126/science.1099314
27. Lynch, T. J., Bell, D. W., Sordella, R., Gurubhagavatula, S., Okimoto, R. A., Brannigan, B. W., . . . Haber, D. A. (2004, May). Activating mutations in the epidermal growth factor receptor underlying responsiveness of non-small-cell lung cancer to gefitinib. *N Engl J Med*, *350*(21), 2129–2139. doi:10.1056/NEJMoa040938
28. Rosell, R., Moran, T., Queralt, C., Porta, R., Cardenal, F., Camps, C., . . . Spanish Lung Cancer Group. (2009, September). Screening for epidermal growth factor receptor mutations in lung cancer. *N Engl J Med*, *361*(10), 958–967. doi:10.1056/NEJMoa0904554
29. Kobayashi, S., Boggon, T. J., Dayaram, T., Janne, P. A., Kocher, O., Meyerson, M., . . . Halmos, B. (2005, February). Egfr mutation and resistance of non-small-cell lung cancer to gefitinib. *N Engl J Med*, *352*(8), 786–792. doi:10.1056/NEJMoa044238
30. Yun, C.-H., Mengwasser, K. E., Toms, A. V., Woo, M. S., Greulich, H., Wong, K.-K., . . . Eck, M. J. (2008). The t790m mutation in egfr kinase causes drug resistance by increasing the affinity for atp. *Proc Natl Acad Sci U S A*, *105*(6), 2070–2075.
31. Kwak, E. L., Sordella, R., Bell, D. W., Godin-Heymann, N., Okimoto, R. A., Brannigan, B. W., . . . Haber, D. A. (2005, May). Irreversible inhibitors of the egf receptor may circumvent acquired resistance to gefitinib. *Proc Natl Acad Sci U S A*, *102*(21), 7665–7670. doi:10.1073/pnas.0502860102
32. Li, Q., Zhang, Y., Marden, J. J., Banfi, B., & Engelhardt, J. F. (2008). Endosomal nadph oxidase regulates c-src activation following hypoxia/reoxygenation injury. *Biochem J*, *411*(3), 531–41.
33. Kobayashi, S., Ji, H., Yuza, Y., Meyerson, M., Wong, K.-K., Tenen, D. G., & Halmos, B. (2005, August). An alternative inhibitor overcomes resistance caused by a mutation of the epidermal growth factor receptor. *Cancer Res*, *65*(16), 7096–7101. doi:10.1158/0008-5472.CAN-05-1346
34. Barnham, K. J., Masters, C. L., & Bush, A. I. (2004). Neurodegenerative diseases and oxidative stress. *Nat Rev Drug Discov*, *3*(3), 205–14.

35. Finkel, T., Serrano, M., & Blasco, M. A. (2007). The common biology of cancer and ageing. *Nature*, *448*(7155), 767–74.
36. Seo, Y. H. & Carroll, K. S. (2009). Profiling protein thiol oxidation in tumor cells using sulfenic acid-specific antibodies. *Proc Natl Acad Sci U S A*, *106*(38), 16163–8.
37. Rabindran, S. K., Discafani, C. M., Rosfjord, E. C., Baxter, M., Floyd, M. B., Golas, J., . . . Wissner, A. (2004, June). Antitumor activity of hki-272, an orally active, irreversible inhibitor of the her-2 tyrosine kinase. *Cancer Res*, *64*(11), 3958–3965. doi:10.1158/0008-5472.CAN-03-2868
38. Brignola, P. S., Lackey, K., Kadwell, S. H., Hoffman, C., Horne, E., Carter, H. L., . . . Wood, E. R. (2002, January). Comparison of the biochemical and kinetic properties of the type 1 receptor tyrosine kinase intracellular domains. demonstration of differential sensitivity to kinase inhibitors. *J Biol Chem*, *277*(2), 1576–1585. doi:10.1074/jbc.M105907200
39. Cohen, S., Carpenter, G., & King, J., L. (1980). Epidermal growth factor-receptor-protein kinase interactions. co-purification of receptor and epidermal growth factor-enhanced phosphorylation activity. *J Biol Chem*, *255*(10), 4834–42.
40. Benitez, L. V. & Allison, W. S. (1974). The inactivation of the acyl phosphatase activity catalyzed by the sulfenic acid form of glyceraldehyde 3-phosphate dehydrogenase by dimedone and olefins. *J Biol Chem*, *249*(19), 6234–43.
41. Reddie, K. G., Seo, Y. H., Muse Iii, W. B., Leonard, S. E., & Carroll, K. S. (2008). A chemical approach for detecting sulfenic acid-modified proteins in living cells. *Mol Biosyst*, *4*(6), 521–31.
42. Leonard, S. E., Reddie, K. G., & Carroll, K. S. (2009). Mining the thiol proteome for sulfenic acid modifications reveals new targets for oxidation in cells. *ACS Chem Biol*, *4*(9), 783–99.
43. Depuydt, M., Leonard, S. E., Vertommen, D., Denoncin, K., Morsomme, P., Wahni, K., . . . Collet, J.-F. (2009). A periplasmic reducing system protects single cysteine residues from oxidation. *Science*, *326*(5956), 1109–1111.
44. Godin-Heymann, N., Bryant, I., Rivera, M. N., Ulkus, L., Bell, D. W., Riese, D. J., 2nd, . . . Haber, D. A. (2007, August). Oncogenic activity of epidermal growth factor receptor kinase mutant alleles is enhanced by the t790m drug resistance mutation. *Cancer Res*, *67*(15), 7319–7326. doi:10.1158/0008-5472.CAN-06-4625
45. Fry, D. W., Bridges, A. J., Denny, W. A., Doherty, A., Greis, K. D., Hicks, J. L., . . . Dobrusin, E. M. (1998, September). Specific, irreversible inactivation of the epidermal growth factor receptor and erbb2, by a new class of tyrosine kinase inhibitor. *Proc Natl Acad Sci U S A*, *95*(20), 12022–12027.

46. Singh, J., Petter, R. C., & Kluge, A. F. (2010). Targeted covalent drugs of the kinase family. *Curr Opin Chem Biol*, *14*(4), 475–80.
47. Singh, J., Dobrusin, E. M., Fry, D. W., Haske, T., Whitty, A., & McNamara, D. J. (1997). Structure-based design of a potent, selective, and irreversible inhibitor of the catalytic domain of the erbB receptor subfamily of protein tyrosine kinases. *J Med Chem*, *40*(7), 1130–5.
48. Raba, J. & Mottola, H. A. (1995). Glucose-oxidase as an analytical reagent. *Critical Reviews in Analytical Chemistry*, *25*, 1–42.
49. Fluckiger, A. C., Li, Z., Kato, R. M., Wahl, M. I., Ochs, H. D., Longnecker, R., ... Rawlings, D. J. (1998, April). Btk/tec kinases regulate sustained increases in intracellular ca²⁺ following b-cell receptor activation. *EMBO J*, *17*(7), 1973–1985. doi:10.1093/emboj/17.7.1973
50. Pan, Z., Scheerens, H., Li, S.-J., Schultz, B. E., Sprengeler, P. A., Burrill, L. C., ... Palmer, J. T. (2007, January). Discovery of selective irreversible inhibitors for bruton's tyrosine kinase. *ChemMedChem*, *2*(1), 58–61. doi:10.1002/cmde.200600221
51. Honigberg, L. A., Smith, A. M., Sirisawad, M., Verner, E., Loury, D., Chang, B., ... Buggy, J. J. (2010, July). The bruton tyrosine kinase inhibitor pci-32765 blocks b-cell activation and is efficacious in models of autoimmune disease and b-cell malignancy. *Proc Natl Acad Sci U S A*, *107*(29), 13075–13080. doi:10.1073/pnas.1004594107
52. Truong, T. H. [T. H.] & Carroll, K. S. (2012). Redox regulation of epidermal growth factor receptor signaling through cysteine oxidation. *Biochemistry*, *51*(50), 9954–65.
53. Truong, T. H. [Thu H.] & Carroll, K. S. (2013). Redox regulation of protein kinases. *Crit Rev Biochem Mol Biol*, *48*(4), 332–356. doi:10.3109/10409238.2013.790873
54. Singh, J., Petter, R. C., Baillie, T. A., & Whitty, A. (2011). The resurgence of covalent drugs. *Nat Rev Drug Discov*, *10*(4), 307–17.
55. Zhang, J., Yang, P. L., & Gray, N. S. (2009). Targeting cancer with small molecule kinase inhibitors. *Nature Reviews. Cancer*, *9*(1), 28–39.
56. Liu, Q., Sabnis, Y., Zhao, Z., Zhang, T., Buhrlage, S. J., Jones, L. H., & Gray, N. S. (2013). Developing irreversible inhibitors of the protein kinase cysteinome. *Chem Biol*, *20*(2), 146–59.
57. Leonard, S. E., Garcia, F. J., Goodsell, D. S., & Carroll, K. S. (2011). Redox-based probes (rbps) for protein tyrosine phosphatases. *Angew Chem Int Ed Engl*, *in press*.

58. Haber, D. A., Gray, N. S., & Baselga, J. (2011, April). The evolving war on cancer. *Cell*, *145*(1), 19–24. doi:10.1016/j.cell.2011.03.026
59. Capasso, M., Bhamrah, M. K., Henley, T., Boyd, R. S., Langlais, C., Cain, K., . . . Dyer, M. J. S. (2010, March). Hvcn1 modulates bcr signal strength via regulation of bcr-dependent generation of reactive oxygen species. *Nat Immunol*, *11*(3), 265–272. doi:10.1038/ni.1843
60. Crump, K. E., Juneau, D. G., Poole, L. B., Haas, K. M., & Grayson, J. M. (2012, August). The reversible formation of cysteine sulfenic acid promotes b-cell activation and proliferation. *Eur J Immunol*, *42*(8), 2152–2164. doi:10.1002/eji.201142289
61. Honda, F., Kano, H., Kanegane, H., Nonoyama, S., Kim, E.-S., Lee, S.-K., . . . Morio, T. (2012, April). The kinase btk negatively regulates the production of reactive oxygen species and stimulation-induced apoptosis in human neutrophils. *Nat Immunol*, *13*(4), 369–378. doi:10.1038/ni.2234
62. Kemble, D. J. & Sun, G. (2009). Direct and specific inactivation of protein tyrosine kinases in the src and fgfr families by reversible cysteine oxidation. *Proc Natl Acad Sci U S A*, *106*(13), 5070–5.
63. Barker, S. C., Kassel, D. B., Weigl, D., Huang, X., Luther, M. A., & Knight, W. B. (1995, November). Characterization of pp60c-src tyrosine kinase activities using a continuous assay: autoactivation of the enzyme is an intermolecular autophosphorylation process. *Biochemistry*, *34*(45), 14843–14851.
64. Wood, E. R., Truesdale, A. T., McDonald, O. B., Yuan, D., Hassell, A., Dickerson, S. H., . . . Shewchuk, L. (2004, September). A unique structure for epidermal growth factor receptor bound to gw572016 (lapatinib): relationships among protein conformation, inhibitor off-rate, and receptor activity in tumor cells. *Cancer Res*, *64*(18), 6652–6659. doi:10.1158/0008-5472.CAN-04-1168
65. Jorge, I., Casas, E. M., Villar, M., Ortega-Prez, I., Lopez-Ferrer, D., Martinez-Ruiz, A., . . . Vazquez, J. (2007, November). High-sensitivity analysis of specific peptides in complex samples by selected ms/ms ion monitoring and linear ion trap mass spectrometry: application to biological studies. *J Mass Spectrom*, *42*(11), 1391–1403. doi:10.1002/jms.1314

CHAPTER V

Development and Characterization of Nucleophilic RSOH-Targeted Inhibitors Towards EGFR Cys797

5.1 Abstract

Epidermal growth factor receptor (EGFR) plays a significant role in physiologic signaling, and deregulation of its activity can lead to development of cancers. EGFR has recently been identified as a direct target of signal-derived H_2O_2 through cysteine oxidation. This modification occurs at EGFR Cys797, which is also targeted by irreversible inhibitors via an electrophilic acrylamide moiety. Oxidation of EGFR Cys797 can alter the potency of current EGFR inhibitors that cannot recognize the kinase in its oxidized form. Therefore, we propose an alternate method whereby nucleophilic warheads capable of recognizing sulfenic acid are employed to target oxidized EGFR. Herein, we report the development of a panel of first-generation RSOH-targeted inhibitors and evaluate compound selectivity towards EGFR Cys797 in response to concomitant kinase oxidation. Collectively, we demonstrate our compounds are capable of inducing potent inhibition towards EGFR under oxidizing conditions and have broad implications for the continued development of irreversible inhibitors that target H_2O_2 -sensitive cysteines in therapeutically important proteins.

5.2 Introduction

Epidermal growth factor receptor (EGFR) exemplifies the family of receptor tyrosine kinases (RTKs), which have been demonstrated to play pivotal roles in cellular physiology and pathology (1). Upon ligand-dependent activation and concomitant tyrosine phosphorylation, stimulation of RTKs such as EGFR results in localized generation of hydrogen peroxide (H_2O_2) by NADPH-dependent oxidases (Nox) (2–4). Although chronic exposure of H_2O_2 can result in cellular damage, tightly controlled levels of H_2O_2 can act as secondary messengers to regulate signal transduction networks. H_2O_2 modulates biological processes largely through modification of specific cysteine residues in redox-sensitive protein targets. The direct product of the reaction between H_2O_2 and a protein thiolate (RS^-) is sulfenic acid (RSOH), also known as sulfenylation. This modification is reversible, and serves as a central mechanism to detect changes in redox homeostasis (5, 6). In a recent study, we utilized chemical probes selective for sulfenic acid (DYn-2) to demonstrate epidermal growth factor (EGF)-mediated signaling induces global and dynamic changes in protein sulfenylation (7). A central finding of this study provides evidence that EGFR is a directly modified by signal-derived H_2O_2 and becomes sulfenylated at its active site cysteine (Cys797). This modification enhances its intrinsic tyrosine kinase activity, and subsequent work has demonstrated mutation of this residue abrogates kinase activation and sulfenylation, further highlighting the importance of Cys797 with respect to EGFR function (Chapter 4).

Deregulation of physiologic kinase signaling due to mutations and other genetic alterations is a hallmark of many pathologic conditions and can result in aberrant kinase activity and malignant transformation (8, 9). EGFR is mutated or amplified in a number of human carcinomas (i.e. breast and lung), which has motivated the development of reversible ATP-competitive kinase inhibitors (10). These inhibitors, including the 4-anilinoquinazolines gefitinib (11) and erlotinib (12), achieve target

selectivity by recognizing unique features of the kinase ATP-binding pocket and have proven successful in clinical trials. In particular, somatic mutations in the EGFR kinase domain have been identified as a cause of non-small cell lung cancer (NSCLC) (13, 14). The two most frequent mutations are the exon 19 point mutation (L858R) and exon 19 deletion (Δ 746-750) (15, 16). L858R is the single most common mutation (approximately 40%), and lies within the kinase activation loop. This point mutation is 50-fold more active than wild-type EGFR and results in constitutive activation of the kinase through destabilizing its auto-inhibitory conformation, which is normally maintained in the absence of ligand stimulation (17, 18). Interestingly, these mutations exhibit decreased affinity for ATP and confer increased sensitivity to gefitinib and erlotinib through tighter binding compared to wild-type EGFR (19–22).

Unfortunately, lung cancer patients expressing these oncogenic mutations (L858R and Δ 746-750) eventually relapse after 12-18 months of treatment (23). Drug resistance to ATP-competitive reversible inhibitors is due to a second site mutation (T790M) of the gatekeeper residue. This residue is located at the entrance to the hydrophobic pocket in the back of the ATP binding pocket, making it an important determinant of inhibitor specificity. T790M was originally believed to induce resistance to gefitinib and erlotinib as a result of steric hindrance by the bulky methionine group (24). However, this view conflicted with observations that reported T790M mutants remained sensitive to structurally similar irreversible 4-anilinoquinazoline inhibitors such as EKB-569 (25). A later study provided evidence that the T790M mutation confers drug resistance by restoring ATP affinity to the same level as observed for wild-type EGFR, therefore increasing the concentration of ATP-competitive reversible inhibitor required to maintain efficacy (26). For this reason, covalent irreversible inhibitors remain effective and can be utilized to overcome clinical resistance of the L858R/T790M mutation (27, 28).

The development of covalent irreversible inhibitors against EGFR represents an at-

tractive area of research and has garnered great interest over the years (29–31). There has been much controversy regarding covalent inhibitors since these compounds can form reactive drug metabolites that can induce direct tissue damage or elicit immune responses through haptization of proteins (32). When used in conjunction, covalent inhibitors provide an alternate approach to overcome the potency, selectivity, and efficacy challenges faced by ATP-competitive reversible inhibitors (33). Development of covalent EGFR inhibitors have been guided by structure-based design and primarily target the nucleophilic thiol group of a cysteine (Cys797) located in the ATP-binding site (34). These compounds utilize the 4-anilinoquinazoline scaffold and contain an electrophilic acrylamide moiety installed at the 6-position that reacts with the EGFR Cys797 thiolate through Michael addition to achieve irreversible binding. PD168393 was one of the first reported covalent inhibitors utilizing this approach, and is regarded as the prototype 4-anilinoquinazoline-based inhibitor (35). This compound proved to be an effective inhibitor, but exhibited poor bioavailability due to low solubility under physiologic conditions and did not make it to clinical trials. Further development of this scaffold (i.e. fine-tuned electrophilic warhead and orientation, increased bioavailability) resulted in a number of new compounds that have advanced to and shown promise in clinical trials: EKB-569 (pelitinib), HKI-272 (neratinib), and BIBW 2992 (Tovok) (20, 27, 36). In addition, pre-treatment of cells with these covalent inhibitors prevents formation of sulfenyl EGFR Cys797 and highlights the dual importance of this residue regarding its role in kinase signaling and as a direct drug target (7).

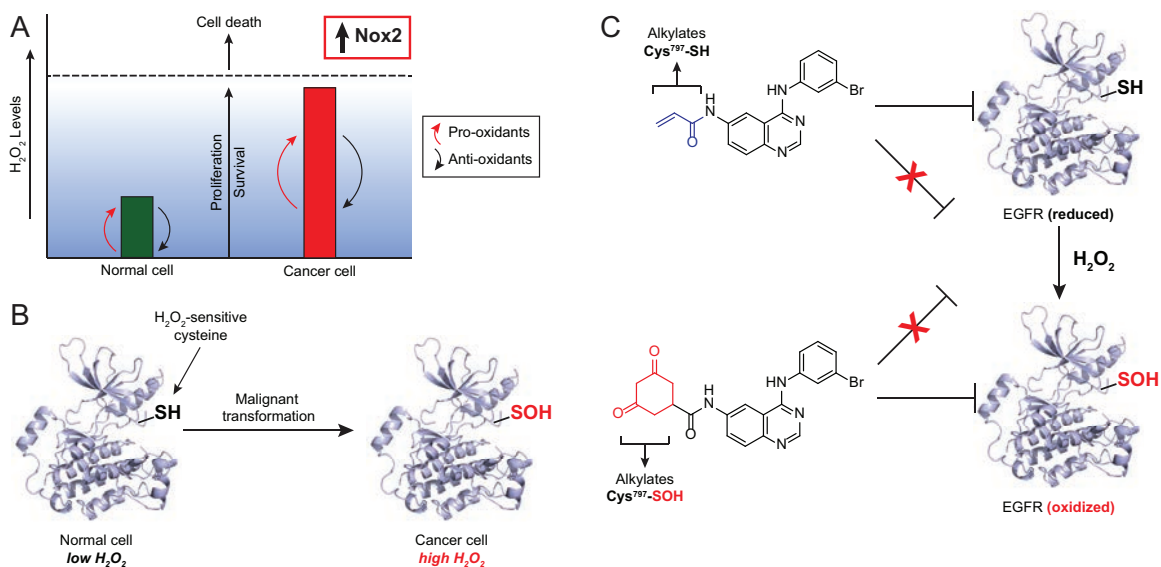


Figure 5.1: **Development of targeted covalent inhibitors for sulfenyl EGFR.** (A) H_2O_2 levels in normal cells are maintained through pro- and anti-oxidants to promote cellular proliferation and survival. Chronically elevated levels of H_2O_2 are often associated with cancers and can ultimately lead to cell death. (B) Oxidation of H_2O_2 -sensitive cysteine residues form transiently in specific proteins during H_2O_2 -mediated signal transduction in normal cells, but form constitutively in diseases (i.e. cancer) with high levels of oxidative stress. (C) Targeted approach to develop covalent inhibitors for sulfenyl EGFR. Current irreversible EGFR inhibitors utilize an acrylamide moiety that undergoes Michael addition with Cys797 in its thiol form, but these compounds do not react with the sulfenic acid form. Oxidation of Cys797 can affect the potency of these inhibitors, particularly under conditions of high oxidative stress often correlated with disease states. In an alternate approach, replacement of the acrylamide group with a nucleophilic warhead (i.e. 1,3-cyclohexanedione) enables the sulfenyl form of the kinase to be targeted.

H_2O_2 levels in normal cells are maintained through pro- and anti-oxidants to promote cellular proliferation and survival (Figure 5.1A). On the contrary, chronically elevated levels of H_2O_2 can ultimately lead to cell death and are prevalent in aging and disease states (37, 38). Oxidation of H_2O_2 -sensitive cysteine residues form transiently in specific proteins during H_2O_2 -mediated signaling under physiologic conditions, but can undergo malignant transformation in disease states (i.e. cancer) associated with high levels of oxidative stress (Figure 5.1B). In particular, overexpression of EGFR and HER2 (member of EGFR subfamily) has been correlated to elevated H_2O_2 levels and global protein sulfenylation in breast cancer cell lines (39). Coupled to the discovery that EGFR Cys797 undergoes sulfenic acid modification, these findings raise several fundamental questions with respect to cysteine oxidation and thiol-targeted

irreversible inhibitors. The acrylamide moiety of covalent EGFR inhibitors undergoes Michael addition with EGFR Cys797 in its reduced thiol form (Figure 5.1C), but would not recognize this residue in its oxidized sulfenic acid form. Consequently, chronically high levels of H_2O_2 affiliated with cancers can lead to aberrant levels of oxidized EGFR Cys797 and alter the potency of these irreversible inhibitors. Alternate mechanisms to target sulfenylated EGFR must be developed to overcome the potential shortcomings of thiol-targeted irreversible inhibitors introduced upon kinase oxidation and may afford further means of achieving selectivity.

Fortunately, sulfenic acid modification represents a new opportunity in covalent inhibitor design whereby nucleophilic warheads (i.e. dimedone-based derivatives) can be utilized to target the electrophilic sulfur in sulfenylated proteins. In this approach, the propensity for H_2O_2 -sensitive cysteines in kinases and other therapeutically relevant proteins (i.e. phosphatases) to undergo sulfenylation can be exploited for the development of inhibitors that target this unique chemical moiety (40). To develop covalent inhibitors towards sulfenyl EGFR, we took a targeted approach wherein we replaced the electrophilic acrylamide group on a common EGFR scaffold (4-anilinoquinazoline) with a nucleophilic warhead (i.e. 1,3-cyclohexanedione) that specifically reacts with sulfenic acids (Figure 5.1C). In particular, we chose PD168393 (Figure 5.2A) as the parent compound for the first generation of nucleophilic RSOH-targeted EGFR inhibitors. Although other covalent EGFR inhibitors such as afatinib or pelitinib have been identified that display more desirable clinical properties, we elected to use PD168393 as a starting point due to synthetic simplicity purposes. We rationalized that if our nucleophilic concept worked with the PD168393 scaffold, it would warrant the development of future generations of RSOH-targeted EGFR inhibitors and justify the increase in synthetic complexity. Additionally, the PD168393 core is simpler and smaller than other EGFR inhibitor scaffolds and can potentially mitigate issues with nucleophilic warhead orientation relative to Cys797 in the EGFR

ATP-binding pocket.

We selected a panel of nucleophilic warheads (Figure 5.2B, **1a-5a**) to derivatize the 4-anilinoquinazoline core structure. Compound **1a** is functionalized with the prototypical sulfenic acid warhead 1,3-cyclohexanedione (dimedone-derivative) (Figure 5.2B, **1a**), which has been shown extensively to specifically react with sulfenyl groups *in vitro* and *in situ* (7, 41, 42). In addition, four other nucleophilic warheads (Figure 5.2B, **2a-5a**) were chosen based on their increased reactivity towards sulfenic acid in comparison to dimedone (V. Gupta and K. Carroll, unpublished results). Blunted control compounds (Figure 5.2B, **1b-5b**) were also synthesized to compare inherent differences in the binding affinities of compounds **1a-5a** relative to PD168393, and to differentiate between reversible and irreversible binding.

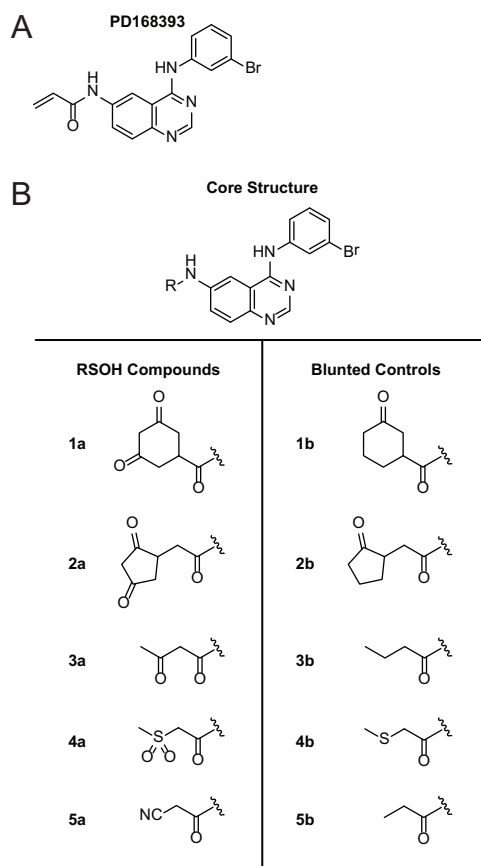


Figure 5.2: **Structures of RSOH-targeted EGFR compounds and blunted controls.** (A) Structure of parent compound PD168393. (B) Structures of RSOH-targeted compounds (**1a-5a**) and blunted controls (**1b-5b**). The 4-anilinoquinazoline core structure is shown at the top.

With these tools in hand, we sought to determine if our nucleophilic RSOH-targeted inhibitors were capable of effectively targeting the sulfenyl form of EGFR. We compared the potency of RSH- and RSOH-targeted compounds under oxidizing conditions (acute and chronic H_2O_2) to determine if our compounds covalently modified EGFR through redox-based inhibition. Next, we evaluated the effect of reducing conditions (i.e. glutathione and antioxidants) on inhibitor potency. Washout experiments were performed to determine whether these compounds inhibited EGFR through reversible or irreversible mechanisms. Additionally, we screened the compounds in lung cancer cell lines harboring common EGFR mutations (L858R/T790M and $\Delta 746-750$) to evaluate their behavior in comparison to wild-type EGFR. Reactivity towards HER2 was also evaluated in breast cancer cells. Finally, the most promising inhibitors were tested in A431 xenograft nude mice models to explore their anti-tumor properties *in vivo*. We observed that increased H_2O_2 levels in addition to concomitant EGFR Cys797 oxidation enhance the extent of RSOH-targeted inhibition *in situ* and *in vivo*. Notably, these studies demonstrate proof of principle of our nucleophilic approach and form the basis for the development of new therapeutic strategies to target H_2O_2 -modulated pathways in disease states.

5.3 Results

Acute and chronic H_2O_2 affects potency of RSH- and RSOH-targeted EGFR inhibitors

To investigate the potency of our nucleophilic inhibitors *in situ*, we used the human epidermoid carcinoma A431 cell line, which naturally expresses high concentrations of EGFR (43). We explored the dose-dependent effect of acute H_2O_2 treatment in A431 cells to identify cellular conditions that would maximize the sulfenyl form of EGFR for covalent modification by our nucleophilic inhibitors, while simultaneously

decreasing the thiol form available for modification by RSH-targeted inhibitors (Supplementary Figure 5.S1A-E). All compounds induced a dose-dependence decrease in EGFR phosphorylation when treated with acute H_2O_2 . IC_{50} values were calculated for each compound from dose-response curves and, on average, determined to be 200 μM with respect to H_2O_2 (Supplementary Table 5.S1). For subsequent experiments, cells were treated with 200 μM H_2O_2 to induce acute oxidizing conditions. As a technical issue, we point out that treating cells in culture with H_2O_2 or other biological oxidants to increase the fraction of sulfenyl EGFR and augment the irreversible potency of our nucleophilic inhibitors also activates EGFR kinase and inhibits tyrosine protein phosphatases (PTPs). Therefore, we included an EGF-stimulation step as a control to reflect the net increase mediated by EGF and H_2O_2 in EGFR autophosphorylation assays.

With these considerations in mind, we examined the potency of our nucleophilic inhibitors under the acute H_2O_2 conditions previously identified. Cells were treated with nucleophilic inhibitors (**1a-5a**) in a dose-dependent manner, and the extent of inhibition was determined by EGFR autophosphorylation (Figure 5.3A, Supplementary Figure 5.S2 A-D). In all cases, the potency of RSOH-targeted inhibitors (**1a-5a**) was increased under acute H_2O_2 and is reflected in their calculated IC_{50} values compared to the respective EGF-stimulation control (Table 5.1). In particular, the IC_{50} value for compound 1a exhibited a 2-fold decrease in response to acute oxidation (Figure 5.3D). To further demonstrate the importance of these results, we subjected cells to chronic H_2O_2 conditions using glucose oxidase (GO). GO is an oxidoreductase that catalyzes the oxidation of glucose to generate H_2O_2 (44). Using this enzyme, we were able to mimic chronic H_2O_2 levels typically associated with disease states through steady production of H_2O_2 over a prolonged period of treatment. Similar to acute H_2O_2 , chronic conditions induced by GO greatly increased the potency of compound 1a (Figure 5.3B) and decreased the IC_{50} value by 20-fold (Figure 5.3D).

Collectively, these results underscore the significant impact that these nucleophilic inhibitors exhibit with respect to inhibition of EGFR phosphorylation and activation under oxidizing conditions.

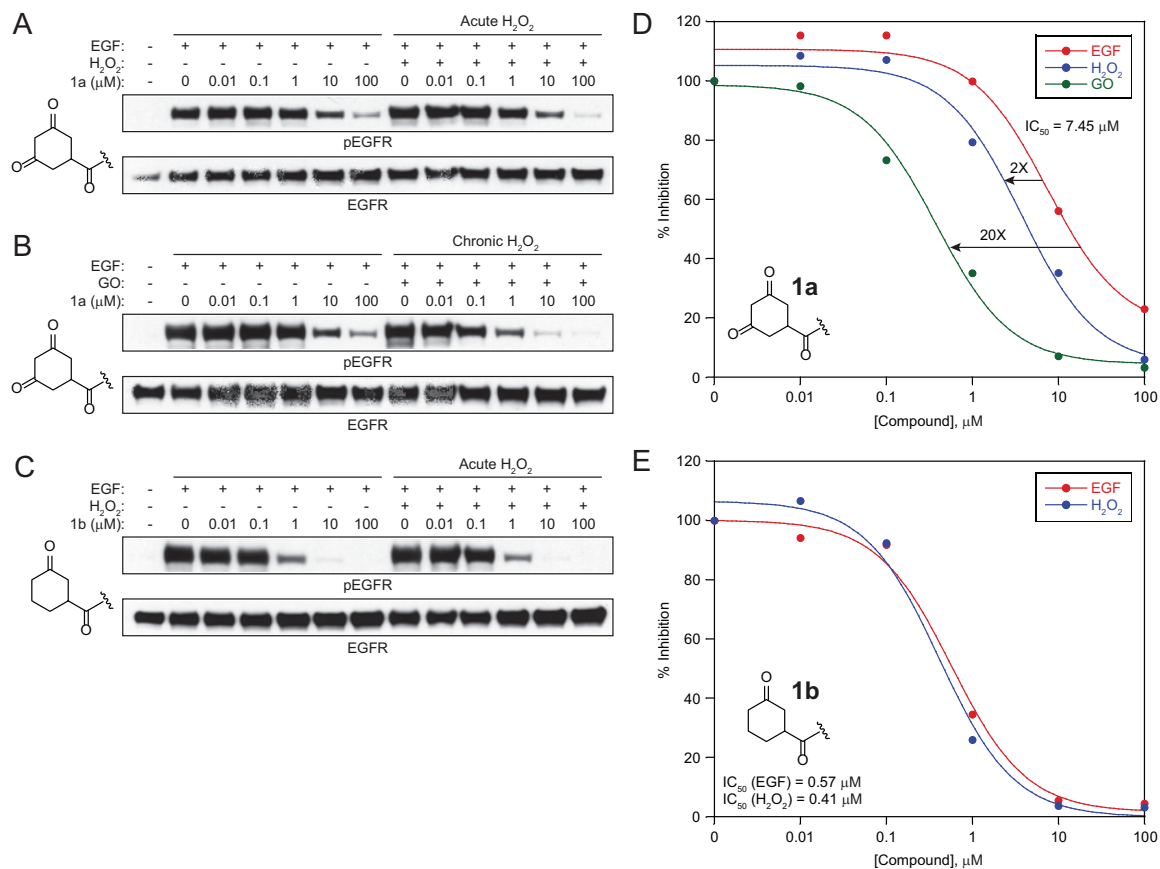


Figure 5.3: **Acute and chronic H_2O_2 treatment increases potency of RSOH-targeted compound 1a.** Western blots show phosphorylated (p) and total EGFR. (A) Acute H_2O_2 treatment increases potency of 1a. A431 cells were stimulated with H_2O_2 (200 μM) for 5 min to induce sulfenic acid formation, treated with the indicated concentrations of 1a for 1 h, and subsequently stimulated with EGF (100 ng/ml) for 5 min. (B) Chronic H_2O_2 treatment increases potency of 1a. A431 cells were incubated glucose oxidase (2 u/ml) for 3 h to induce chronic H_2O_2 conditions, treated with the indicated concentrations of 1a for 1 h, and subsequently stimulated with EGF (100 ng/ml) for 5 min. (C) Blunted control 1b yields negligible change in potency. (D) Comparison of percent inhibition of EGFR autophosphorylation from A (acute H_2O_2) and B (chronic H_2O_2). IC_{50} values exhibit a 2-fold change under acute H_2O_2 , and 20-fold change under chronic H_2O_2 . (E) Percent inhibition of EGFR autophosphorylation from C. Blunted control 1b exhibits little change in IC_{50} values.

Table 5.1: IC₅₀ Values of RSOH-Targeted Compounds and Controls in A431 Cells Treated with Acute H₂O₂

Compound ^a	Structure	IC ₅₀ (μM), EGF ^b	IC ₅₀ (μM), H ₂ O ₂ ^c	Compound	Structure	IC ₅₀ (μM), EGF ^b	IC ₅₀ (μM), H ₂ O ₂ ^c
1a		6.15 ± 1.31	3.30 ± 0.45	1b		0.57	0.41
2a		3.00 ± 0.90	0.48 ± 0.06	2b		1.30	0.16
3a		1.23 ± 0.07	0.31 ± 0.08	3b		0.24 ± 0.03	0.39 ± 0.07
4a		1.24	0.19	4b		0.65	0.047
5a		1.25	0.19	5b		0.41 ± 0.06	0.65 ± 0.43
PD168393		0.022 ± 0.001	0.010 ± 0.01				

^a Cells were pre-treated with H₂O₂ (200 μM, 5 min), incubated with compound (1 h), and stimulated with EGF (100 ng/ml).

^b IC₅₀ values of EGF were determined by Western blot analysis of EGFR autophosphorylation.

^c IC₅₀ values of H₂O₂ were determined by Western blot analysis of EGFR autophosphorylation.

To confirm that the potency of RSOH-targeted inhibitors (1a-5a) was correlated to irreversible redox-modulated inhibition and not due to compound affinity to the kinase ATP-binding pocket, we explored the potency of blunted controls 1b-5b under the same acute H_2O_2 conditions. Although, compound 1b induced inhibition of EGFR phosphorylation (Figure 5.3C), it yielded negligible change in potency (Figure 5.3C, E) when compared to its EGF-stimulated control. Other blunted controls showed similar results (Supplementary Figure 5.S2E-H), and the calculated IC_{50} values did not exhibit significant fold changes as some of their nucleophilic RSOH counterparts (Table 5.1). Some blunted controls (2b, 4b) were found to be slightly more potent, but this may be due to differences in binding affinity in the ATP-binding site. These results indicated that our compounds inhibit EGFR reversibly due to its 4-anilinoquinazoline core, and irreversibly when the compound is functionalized with a nucleophilic warhead.

We also explored the effect of acute and chronic H_2O_2 treatment on potency of our parent compound PD168393. Under acute H_2O_2 , PD168393 inhibited EGFR phosphorylation to a similar extent in the EGF-stimulated control and oxidizing conditions (Figure 5.4A, B). EGFR phosphorylation levels were increased under chronic H_2O_2 conditions, demonstrating that the potency of PD168393 was reduced at higher concentrations of inhibitor (Figure 5.4C, D). These data show that oxidizing conditions (acute and chronic H_2O_2) affect the potency of RSH- and RSOH-targeted EGFR inhibitors, setting the stage for the development of nucleophilic compounds that target the sulfenyl form of EGFR.

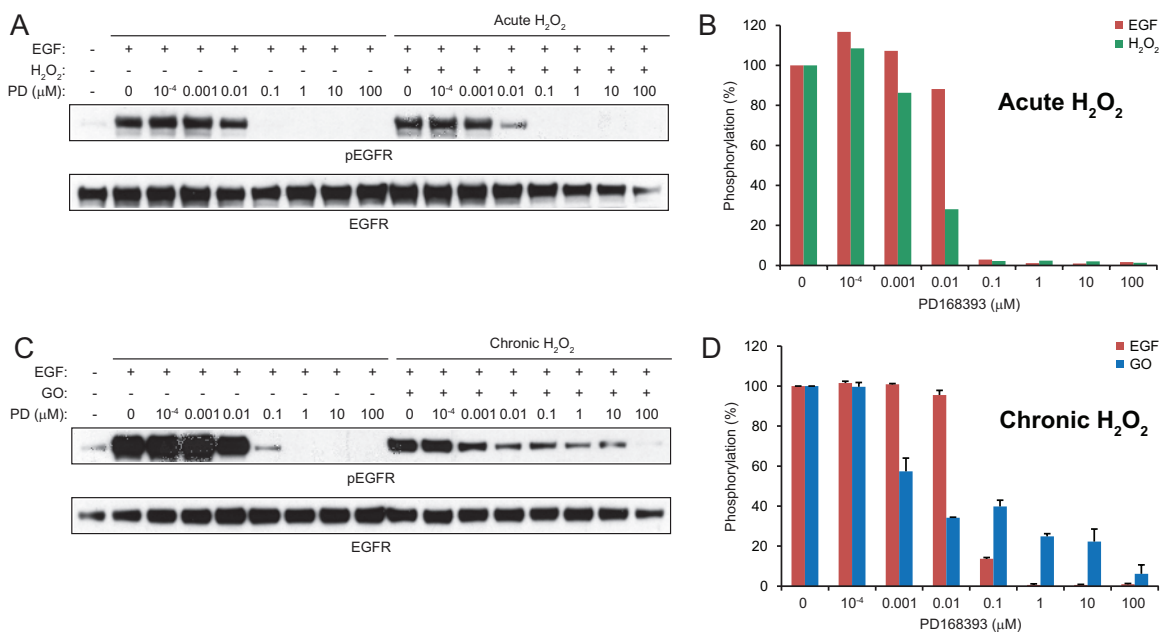


Figure 5.4: Chronic H₂O₂ treatment reduces potency of RSH-targeted irreversible EGFR inhibitors. A431 cells were incubated with (A) H₂O₂ (200 μM) for 5 min to induce acute conditions or (C) glucose oxidase (2 u/ml) for 3 h to induce chronic H₂O₂ conditions, treated with the indicated concentrations of PD168393 for 1 h, and subsequently stimulated with EGF (100 ng/ml) for 5 min. Western blots show phosphorylated (p) and total EGFR. The potency of PD168393 was reduced only in the presence of chronic H₂O₂, and not acute conditions. (B, D) Densitometric quantification of A (acute H₂O₂) and C (chronic H₂O₂), respectively. At higher inhibitor concentrations, phosphorylation levels (%) of chronic H₂O₂-treated samples are higher when compared to their EGF-treated counterpart. Data are representative of two independent readings and represent the mean ± s.e.m.

Reductive stress conditions affect potency of RSOH-targeted EGFR inhibitors

To further examine the mechanism by which our nucleophilic inhibitors induced inhibition of EGFR, we subjected A431 cells to reductive stress conditions to determine the effect of biologically relevant thiols and anti-oxidants. Glutathione (GSH), a tri-peptide containing thiol, is present at millimolar concentrations in the cell and a component of the glutaredoxin/glutathione (Grx/GSH) and glutathione/glutathione reductase (GSH/GSR) buffering systems which function to regulate and maintain intracellular H₂O₂ levels. In cells treated with reduced GSH, compound 2a exhibited decreased inhibition of EGFR phosphorylation (Figure 5.5C). When compared to the potency observed in cells treated with acute H₂O₂ (Figure 5.5A), the IC₅₀ value for

compound **2a** increased 3.5-fold (Figure 5.5D). In addition, the effect of N-acetyl-L-cysteine (NAC), a widely used anti-oxidant, was also explored. Similar to reduced GSH, NAC reduced the potency of compound **2a** (Figure 5.5B) and resulted in a 12-fold increase in its IC₅₀ value compared to acute H₂O₂ conditions (Figure 5.5D). Therefore, reductive stress conditions reverse the potency of our nucleophilic RSOH inhibitors by reducing the amount of sulfenyl EGFR available for covalent modification.

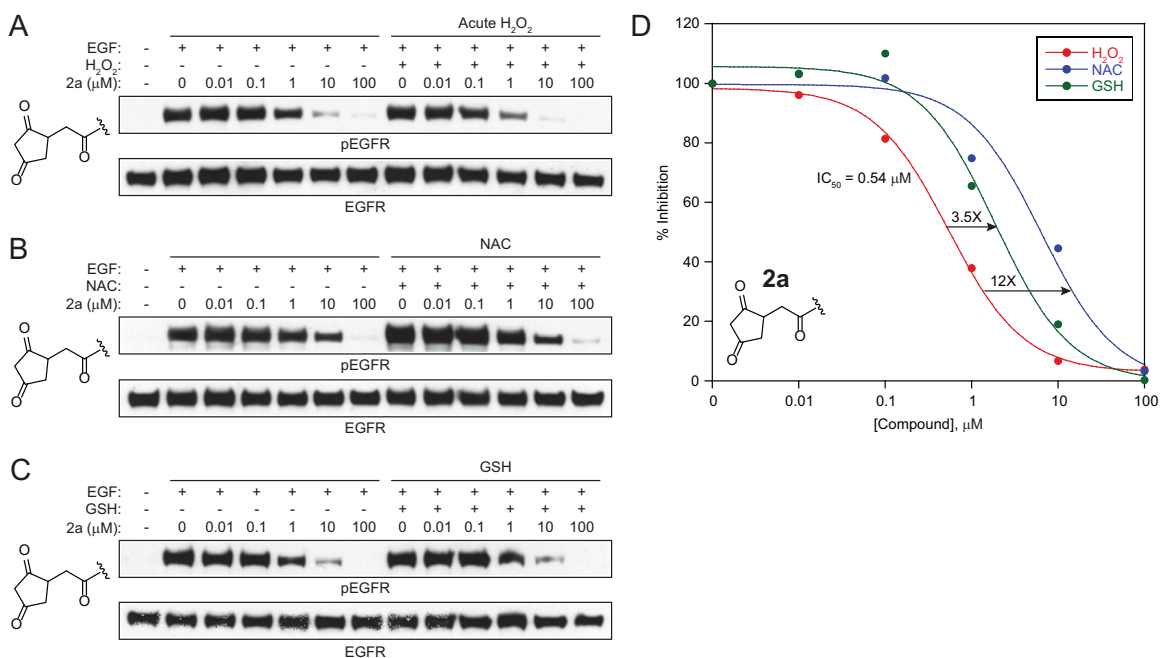


Figure 5.5: Reductive stress conditions decrease potency of RSOH-targeted EGFR compounds. Western blots show phosphorylated (p) and total EGFR. (A) Acute H₂O₂ treatment increases potency of **2a**. A431 cells were stimulated with H₂O₂ (200 μM) for 5 min to induce sulfenic acid formation, treated with the indicated concentrations of **2a** for 1 h, and subsequently stimulated with EGF (100 ng/ml) for 5 min. (B) N-acetyl cysteine (NAC) decreases potency of **2a**. A431 cells were incubated with NAC (20 mM) for 1 h to induce reductive stress. (C) Reduced glutathione (GSH) decreases potency of **2a**. A431 cells were incubated with GSH (10 mM) for 1 h to induce reductive stress. (D) Comparison of percent inhibition of EGFR autophosphorylation from A (acute H₂O₂), B (NAC), and C (GSH). IC₅₀ values exhibit 3.5-fold increase under GSH, and 12-fold increase under NAC.

Abundant protein thiols can interfere with potency of RSH- and RSOH-targeted EGFR inhibitors

In order to evaluate the effectiveness of our compounds as a potential therapeutic, it is important to consider potential interference from abundant protein thiols. Human serum albumin (HSA) is the most abundant protein found in human plasma and contains a redox-sensitive cysteine residue (Cys34) (45). This cysteine is prone to oxidative modification because extracellular fluids contain very small amounts of antioxidant defense enzymes. Although our nucleophilic compounds are expected to target the EGFR kinase domain, non-specific inhibition of other proteins containing H_2O_2 cysteines can potentially occur. To test this, we incubated A431 cells with compound 1a in the presence of HSA (3% w/v). The potency of 1a is completely reversed as indicated by the significant increase in EGFR autophosphorylation compared to its EGF-stimulated control (Supplementary Figure 5.S3A, D). A similar effect is observed with blunted control 1b (Supplementary Figure 5.S3B), demonstrating that HSA interferes with the binding ability of our compounds to the ATP-binding pocket. Most importantly, HSA reverses the potency of the parent compound PD168393 (Supplementary Figure 5.S3C) and significantly increases its calculated IC_{50} value (Supplementary Figure 5.S3E). The effect of HSA on inhibitor potency is much more drastic for PD168393 than that observed for 2a with respect to fold change under non-oxidizing conditions. Therefore, we would expect a similar effect under oxidizing conditions with HSA with our compounds. Based on these results, it appears that abundant proteins containing H_2O_2 -sensitive residues (i.e. HSA) can interfere with the effectiveness of both RSH- and RSOH-targeted EGFR inhibitors.

Nucleophilic RSOH-targeted compounds demonstrate irreversible EGFR adduct formation

The results from Figure 5.3 indicated that our compounds inhibit EGFR reversibly due to its 4-anilinoquinazoline core (Figure 5.3C, E), and to some extent, irreversibly under oxidizing conditions (acute and H_2O_2) when the compound contains a nucleophilic warhead (Figure 5.3A, B, D). In order to determine the extent to which irreversible inhibition occurs, we performed a washout experiment with compounds 2a and 3a. A431 cells were pre-incubated with fixed concentrations of inhibitor and stimulated with H_2O_2 in a dose-dependent manner to induce sulfenic acid formation. Following treatment, cells were subjected to a washout period and subsequently analyzed for EGFR phosphorylation. Washout experiments revealed a dose-dependent decrease in EGFR autophosphorylation with respect to increasing H_2O_2 concentration (Figure 5.6A, B). Although our compounds did not exhibit complete irreversible inhibition after washout, these results indicate that covalent adduct formation does occur with the kinase and confirm our findings from Figure 5.3. In addition, we also explored the anti-proliferative activity of our nucleophilic RSOH-targeted inhibitors (1a-5a) and their respective blunted controls (1b-5b) on A431 cells by standard MTT assay. With the exception of 3a, our nucleophilic compounds exhibited a higher anti-proliferative effect in A431 cells when compared to their blunted control counterpart (Table 5.2). The IC_{50} value of 3a was comparable to its control 3b; however, this observation may be due to the binding affinity of the nucleophilic warhead in the ATP-binding pocket.

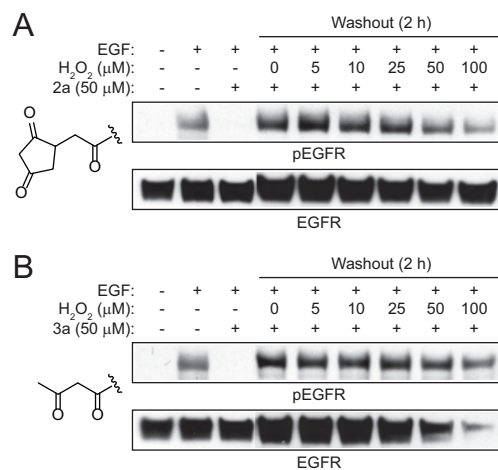


Figure 5.6: **Washout effect of RSOH-targeted compounds.** A431 cells were incubated with (A) **2a** or (B) **3a** for 1 h, treated with H₂O₂ at the indicated concentrations for 1 h, and stimulated with EGF (100 ng/ml) for 5 min preceding a 2 h washout step. Western blots show phosphorylated (p) and total EGFR. Dose-dependent H₂O₂ treatment reveals a correlation to increased inhibition of EGFR autophosphorylation. The compounds tested do not exhibit complete irreversible inhibition after washout, but do demonstrate some irreversible adduct formation with the kinase.

Table 5.2: Anti-Proliferative Effects of RSOH-Targeted Compounds and Controls in A431 Cells^a

Compound ^b	Structure	IC ₅₀ (μM) ^c	Compound	Structure	IC ₅₀ (μM)
1a		10.12 ± 1.15	1b		37.78 ± 1.01
2a		4.17 ± 0.24	2b		36.11 ± 3.29
3a		16.01 ± 2.06	3b		14.09 ± 2.44
4a		0.96 ± 0.11	4b		9.98 ± 0.27
5a		0.91 ± 0.21	5b		3.22 ± 0.46

^a Cellular proliferation was determined by standard MTT assay conditions.

^b Cells were treated with compounds for 72 h prior to assay (0-1000 μM) and replenished every 24 h.

^c IC₅₀ values are representative of three independent trials and represent the mean ± s.e.m.

RSOH-targeted EGFR inhibitors are effective against common oncogenic EGFR mutations

As discussed earlier in the introduction, somatic mutations in the EGFR kinase domain have been identified as a cause of NSCLC. Interestingly, the two most frequently occurring mutations (L858R and Δ746-750) have been shown to confer increased sensitivity to ATP-competitive kinase inhibitors such as gefitinib and erlotinib by decreasing the affinity for ATP (19–21). A second site mutation (T790M) accounts for half of the cases wherein lung cancer patients undergoing treatment eventually relapse (23, 24). Given the proximity of EGFR Cys797 to the inhibitor binding pocket,

we speculate oxidation of Cys797 may be affected to some extent in these oncogenic mutants. To investigate this, we used lung cancer cell lines harboring these somatic mutations: NCI-H1975 (L858R, T790M) and HCC827 (Δ 746-750) (46). Incubation of NCI-H1975 (Figure 5.7A) and HCC827 (Figure 5.7B) with compound 1a induced increased inhibition of EGFR phosphorylation under acute H₂O₂ treatment. Interestingly, compound 1a had nearly no effect on EGFR autophosphorylation in NCI-H1975 cells as shown by the EGF-stimulated control and an IC₅₀ value could not be calculated due to negligible change in phosphorylation levels as the concentration of inhibitor was increased (Figure 5.7C). IC₅₀ dose-response curves for HCC827 demonstrated increased potency of compound 1a (Figure 5.7D). The effect of our other nucleophilic inhibitors was also tested in both cell lines. IC₅₀ values were easily calculated for 1a-5a in NCI-H1975 cells with respect to acute H₂O₂ conditions, but could not be determined for the EGF-stimulated control due to insufficient data sets for the dose-response curves (Supplementary Table 5.S2). For HCC827, IC₅₀ dose-response curves demonstrated increased potency of compound 1a (Figure 5.7D). In addition, compounds 2a-5a were also tested in HCC827 cells to evaluate potency (Supplementary Table 5.S3). Trends in inhibitor potency were not as clear-cut in these oncogenic mutants as they were with wild-type EGFR in A431 cells, and may reflect differences in binding affinity of these compounds. Collectively, these results indicate that our nucleophilic compounds are capable of inhibiting EGFR phosphorylation and activation under acute oxidizing condition in oncogenic EGFR lung cancer mutants.

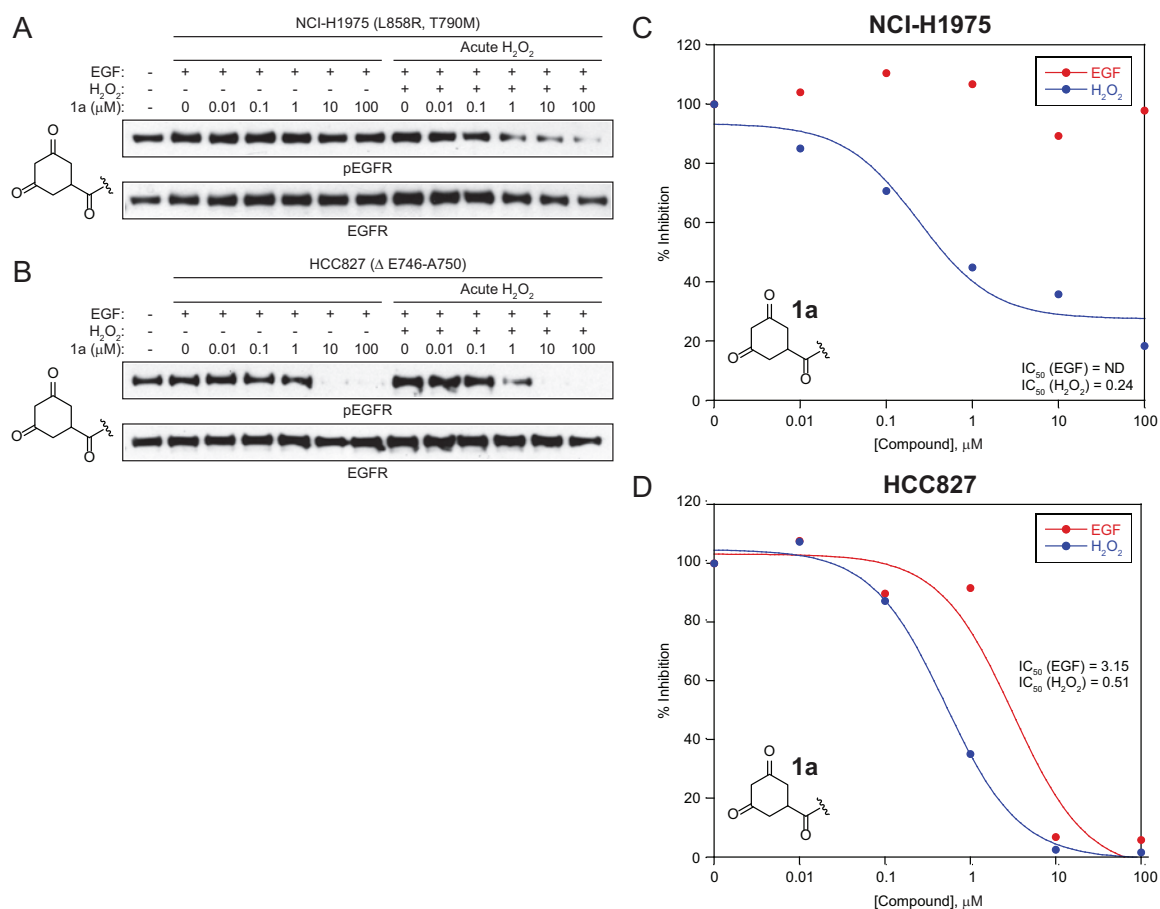


Figure 5.7: **Acute H₂O₂ treatment increases potency of RSOH-targeted EGFR compounds in lung cancer cells.** (A, B) Western blots show phosphorylated (p) and total EGFR. Lung cancer cell lines expressing common EGFR mutations, (A) NCI-H1975 (L858R, T790M) and (B) HCC827 (Δ E746-A750), were stimulated with H₂O₂ (200 μM) for 5 min to induce sulfenic acid formation, treated with the indicated concentrations of **1a** for 1 h, and subsequently stimulated with EGF (100 ng/ml) for 5 min. (C, D) IC₅₀ values in NCI-H1975 and HCC827 cells were determined by Western blot analysis of EGFR autophosphorylation from A and B, respectively.

ErbB2 (HER2) phosphorylation is affected by RSOH-targeted EGFR inhibitors

EGFR is grouped into a subfamily that consists of three additional closely related receptors: HER2 (erbB2), HER3 (erbB3), and HER4 (erbB4). In particular, HER2 overexpression has been shown to play an important role in development and progression in breast cancer. Many reversible and irreversible EGFR inhibitors also target HER2. Therefore, we sought to determine the effect of our RSOH-targeted EGFR inhibitors against HER2. We used the metastatic breast carcinoma MDA-

MB-453, which expresses high levels of HER2, and induced acute H₂O₂ conditions prior to treatment with our nucleophilic inhibitors. Inhibition of EGFR autophosphorylation levels was observed in cells treated with compound 3a (Figure 5.8A) and IC₅₀ dose-response curves reflected a significant increase under acute H₂O₂ treatment (Figure 5.8). Other nucleophilic inhibitors were also screened against HER2 (Supplementary Table 5.S4), but do not give clear trends with respect to inhibitor potency as seen with EGFR in A431 cells. Although it appears that some of our compounds are effective against HER2, we acknowledge that additional data would be needed to support this claim.

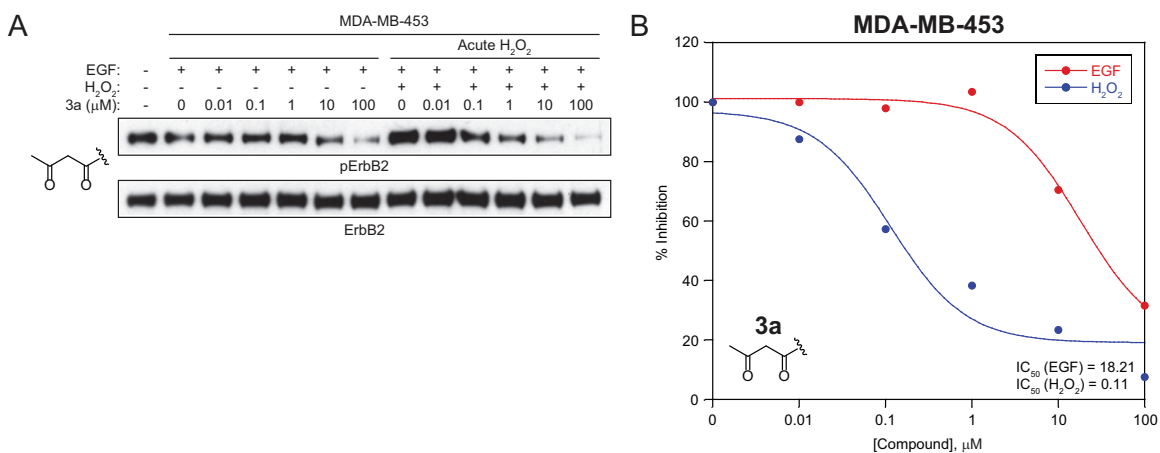


Figure 5.8: **Acute H₂O₂ treatment slightly increases potency of RSOH-targeted EGFR compounds towards ErbB2.** (A) Western blots show phosphorylated (p) and total EGFR. Breast cancer cells (MDA-MB-453) overexpressing ErbB2 were stimulated with H₂O₂ (200 μM) for 5 min to induce sulfenic acid formation, treated with the indicated concentrations of **1a** for 1 h, and subsequently stimulated with EGF (100 ng/ml) for 5 min. (B) IC₅₀ values in MDA-MB-453 cells were determined by Western blot analysis of ErbB2 autophosphorylation from A.

RSOH-targeted EGFR compounds decrease EGFR autophosphorylation and sulfenylation *in vivo*

Collectively, our experimental efforts demonstrated that nucleophilic RSOH-targeted EGFR inhibitors exhibit redox-modulated inhibition that is irreversible to an extent in cell-based assays with wild-type and mutant EGFR. We wanted to explore the anti-tumor properties of our compounds *in vivo*. For this, compounds were selected based on their performance in DMPK studies (Scripps Florida) and subsequently tested in an A431 xenograft nude mouse model (compounds 1a, 3a, 5a). Additionally, 5b and PD168393 were included as controls in these studies. Mice were dosed with 20 or 50 mg/kg of the appropriate compound and the tumors were harvested and analyzed for changes in EGFR phosphorylation and sulfenylation levels. Analysis of EGFR phosphorylation levels revealed that higher dosage of compounds decreased kinase autophosphorylation levels (Figure 5.9A). In particular, 3a seemed to exhibit the most significant effect on inhibiting kinase activation regardless of compound dosage. Blunted control 5b had comparable levels to its nucleophilic counterpart, which may be due to binding affinity of these compounds to the ATP-binding pocket. PD168393 demonstrated nearly complete inhibition of EGFR phosphorylation levels compared to the vehicle control and nucleophilic RSOH inhibitors.

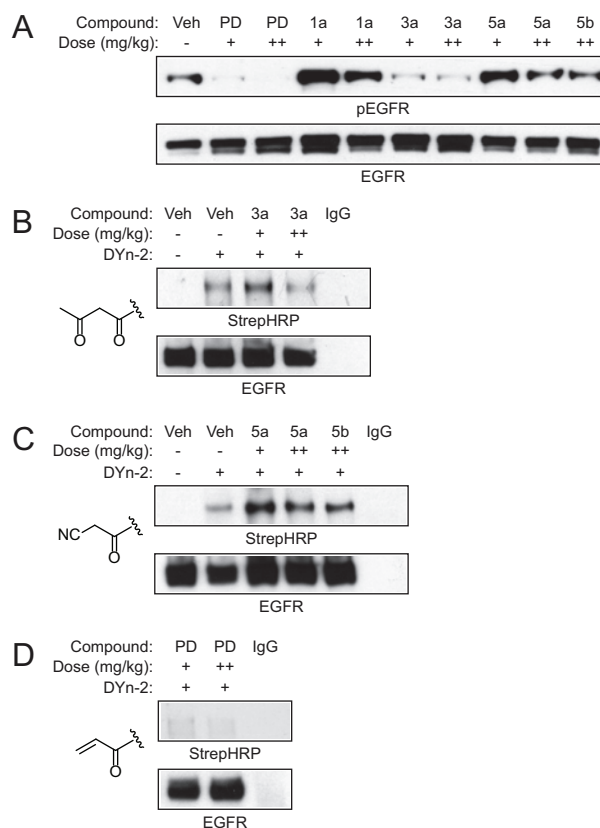


Figure 5.9: RSOH-targeted EGFR compounds decrease EGFR autophosphorylation and sulfenylation levels in xenograft mice models. Mice were dosed with 20 mg/kg (+) or 50 mg/kg (++) of the indicated compound. (A) Increased compound dosage decreases EGFR phosphorylation levels. Western blot shows phosphorylated (p) and total EGFR. (B, C) Increased compound dosage decreases EGFR sulfenylation levels. Tissue samples were lysed in the presence of DYn-2 (10 mM) and sulfenic acids signal were detected by Strep-HRP western blot. (D) PD168393 completely blocks sulfenyl EGFR signal.

Sulfenylation levels of EGFR were also demonstrated that higher dosage of compounds decreased sulfenyl EGFR with respect to compounds 3a and 5a (Figure 5.9B, C). The result is more pronounced with 3a, and agrees with the observations from Figure 5.9A. Treatment with PD168393 blocked EGFR sulfenylation (Figure 5.9D), demonstrating that RSH-targeted inhibitors are successful with regards to covalent inhibition before the sulfenyl form of EGFR could be generated. Collectively, these data demonstrate that our nucleophilic RSOH-targeted compounds decrease EGFR phosphorylation and sulfenylation levels in xenograft nude mice models and show promise *in vivo*.

5.4 Discussion

Sulfenyl modification of EGFR at Cys797 has proven to have a significant impact on kinase activation during EGF-mediated signaling (Chapter 3, 4). This modification enhances its intrinsic tyrosine kinase activity, and mutation of this residue abrogates EGFR autophosphorylation, sulfenylation, and decreases its affinity for ATP (Chapter 4). Deregulation of EGFR signaling leads to the progression of a number of human carcinomas (i.e. breast and lung cancers) and has motivated the development of reversible and irreversible inhibitors to specifically target the kinase. Coincidentally, EGFR Cys797 serves as a therapeutic target for covalent inhibitors which react with the Cys797 thiolate through electrophilic Michael addition to achieve irreversible adduct formation. These inhibitors recognize EGFR Cys797 in its reduced thiol form, but are not able to recognize the residue upon oxidation.

The propensity for EGFR Cys797 to undergo sulfenylation highlights the importance of developing alternate redox-based therapeutic approaches to target this unique modification. Therefore, we proposed a nucleophilic approach whereby sulfenic acid-specific warheads replaced the electrophilic acrylamide group on a common EGFR scaffold (4-anilinoquinazoline) (Figure 5.1C). We first explored the potency of these compounds (Figure 5.2B) with respect to wild-type EGFR in A431 cells. Overall, we observed that oxidizing conditions (acute and chronic H_2O_2) increase the potency of our compounds with respect to their EGF-stimulated controls (Figure 5.3A, B). Moreover, chronic H_2O_2 induced a more significant impact on nucleophilic inhibitor potency because these conditions increased the sulfenyl form of EGFR for covalent redox-based modification in a steady manner (Figure 5.3D). Although the thiolate form of EGFR will always be targeted more effectively with electrophilic irreversible inhibitors, we demonstrated chronic H_2O_2 affects the potency of this class of inhibitors by reducing the amount of EGFR in the thiolate form. This is relevant because disease states such as cancer are often associated with high levels of H_2O_2 .

Evaluation of blunted control compounds (Figure 5.3C, E) and washout experiments (Figure 5.6A, B) revealed key aspects with respect to the mechanism of inhibition by our nucleophilic compounds. Overall, it is clear that our compounds (1a-5a) bind reversibly to the ATP-binding pocket due to the results observed with our blunted controls (1b-5b). However, oxidizing conditions demonstrate that our compounds undergo irreversible redox-modulated inhibition as shown by fold change in the calculated IC₅₀ values from dose-response curves. Washout experiments further confirmed our observations, but also indicated that our compounds are capable of inducing partial, but not complete irreversible inhibition. This is most likely due to slower reactivity rates of the nucleophilic warheads employed in this study compared to the parent compound PD168393 (V. Gupta and K. Carroll, unpublished results).

Although a number of somatic mutations in the EGFR kinase domain have been identified as a cause of NSCLC, we were particularly interested the most frequently occurring ones: L858R/T790M and Δ 746-750. These mutations have been shown to reverse the effectiveness of ATP-competitive reversible inhibitors and have motivated the development of covalent inhibitors to overcome acquired drug resistance. In addition to irreversibly targeting Cys797, researchers have also developed inhibitors to directly target EGFR mutations (i.e. T790M) (47). We speculated that oxidation of Cys797 may be affected to some extent in these oncogenic mutants due to its location in the inhibitor binding pocket. Two different lung cancer cell lines were employed for these studies: NCI-H1975 (L858R, T790M) and HCC827 (Δ 746-750). For the most part, both cell lines exhibited increased compound potency (1a-5a) under acute H₂O₂ conditions. In particular, compound 1a had nearly no effect on EGFR autophosphorylation in the L858R/T790M cell line with respect to the EGF-stimulated control but exhibited increase potency when subjected to oxidizing conditions. It is possible that EGFR Cys797 is rendered more sensitive to oxidation in the L858R/T790M mutant, and explains why the phosphorylation levels were unaffected by 1a under

non-oxidizing conditions. Molecular modeling and structural studies would be necessary to confirm this observation, and would provide more insight as to how oxidation of EGFR Cys797 may perturb potentially significant changes in the inhibitor binding pocket.

In vivo studies conducted in A431 xenograft nude mouse models revealed our compounds were able to induce observable decreases in EGFR phosphorylation and sulfenylation. Complete inhibition was not observed for nucleophilic RSOH-targeted inhibitors, confirming our cell-based washout experiments.

The first generation of RSOH-targeted EGFR inhibitors were successful, but also revealed a number of issues that must to be addressed. First and foremost, we have generated a panel of nucleophilic inhibitors that are capable of targeting and inhibiting EGFR Cys797. Collectively, our results to date demonstrate that the propensity of EGFR Cys797 to undergo sulfenylation can be exploited to develop a new class of inhibitors based on a nucleophilic approach. The mode of inhibition occurs reversibly due to its 4-anilinoquinolazine core, but also irreversibly in response to concomitant EGFR oxidation. Unfortunately, washout experiments and *in vivo* studies indicate that these compounds only induce partial covalent inhibition. To overcome this, a second generation of RSOH-targeted EGFR inhibitors will incorporate some of the following changes. The core structure will be modeled after afatinib, which has proven successful in clinical trials and demonstrates more desirable properties such as improved solubility and bioavailability in comparison to PD168393. We believe the results of our current study warrant the change to a more clinically successful parent compound. Originally, we chose the nucleophilic warheads used in this study based on their improved reactivity rates in comparison to dimedone. These have since proven to still react too slowly to effectively induce complete irreversible inhibition. We have since identified a number of new nucleophilic warheads that exhibit reactivity rates towards sulfenic acid that are several hundred-fold higher than the ones we selected

for this study. Docking studies should be performed with the proposed compounds for the second-generation panel of RSOH-targeted EGFR inhibitors to identify and validate the success of potential compounds.

5.5 Conclusion

The importance of EGFR in physiologic signaling and as a therapeutic target in cancer is clearly apparent and the continued effort to develop new approaches to target EGFR remains an active area of research. The discovery of EGFR as a direct target of H₂O₂ has fostered the development of a nucleophilic-based strategy to exploit the sulfenyl form of the kinase. Most importantly, our efforts have demonstrated proof of principle of this approach and have huge implications for the development of covalent inhibition of other therapeutically relevant proteins.

5.6 Methods

Reagent source, purity, and stock solutions. All stocks were stored at -20 °C, unless otherwise indicated. EGF (30 µg/ml, BD Biosciences) was prepared in ddH₂O. Serial dilutions of H₂O₂ (Sigma) were prepared in ddH₂O. Compounds 1a-5a and 1b-5b (10 mM, ≥ 98% purity) were synthesized by V. Gupta (Carroll lab) and stocks were prepared in DMSO at the indicated concentrations. PD168393 (10 mM, Santa Cruz Biotechnology, ≥ 95% purity) stocks were prepared in DMSO at the indicated concentrations. DYn-2 (250 mM, ≥ 99% purity) was prepared in DMSO and synthesized as previously described [7]. Catalase (20,000 U/ml, Sigma) included in lysis buffers was prepared in 50 mM Tris-HCl pH 7.4 and stored at -80 °C or made up fresh, respectively. Glucose oxidase (500 U/ml, Sigma), N-acetyl-L-cysteine (NAC, Research Products International), and reduced L-glutathione (GSH, Sigma) were prepared fresh in 50 mM Tris-HCl pH 7.4. Human serum albumin

(HSA, fatty acid free, Sigma) was prepared directly in culture media at the indicated concentrations. Azide biotin (5 mM, Invitrogen) was prepared in DMSO. BTTP (100 mM, Peng Wu) was prepared in DMSO, and lower concentrations were made by dilution of stock solution with ddH₂O. Sodium L-ascorbate (Sigma) and CuSO₄ (Sigma) were prepared fresh in ddH₂O.

Cell culture. Mammalian cell lines (American Type Culture Collection) were maintained at 37 °C in a 5% CO₂ humidified atmosphere. A431 and MDA-MB-453 cells were cultured in high glucose DMEM media (Invitrogen) containing 10% FBS (Invitrogen), 1% GlutaMax (Invitrogen), 1% MEM nonessential amino acids (Invitrogen), and 1% penicillin-streptomycin (Invitrogen). NCI-H1975 and HCC827 cells were cultured in RPMI 1640 media with glutamine (Invitrogen) containing 10% FBS (Invitrogen), 1% MEM nonessential amino acids (Invitrogen), and 1% penicillin-streptomycin (Invitrogen).

Cell lysate preparation. For analysis of protein phosphorylation, cells were harvested in phosphorylation lysis buffer [50 mM HEPES pH 7.4, 150 mM NaCl, 1% NP-40, 0.1% SDS, 5 mM sodium pyrophosphate, 50 mM sodium fluoride, 10 μM β-glycerophosphate, 1 mM sodium orthovanadate, 0.5 mM DTT, and 1x complete mini protease inhibitors (Roche)]. After 15 min incubation on ice with frequent mixing, cell debris was removed by centrifugation at 14,000 rpm for 15 min at 4 °C. Protein concentration was determined by BCA assay (Pierce). For analysis of protein phosphorylation in tissue lysate, samples were harvested in HEPES lysis buffer [50 mM HEPES pH 7.4, 150 mM NaCl, 1% NP-40, 10% glycerol, 5 mM sodium pyrophosphate, 50 mM sodium fluoride, 10 μM β-glycerophosphate, 1 mM sodium orthovanadate, 0.5 mM DTT, and 1x complete mini protease inhibitors (Roche)]. For analysis of protein sulfenylation in tissue lysate, samples were harvested in HEPES lysis buffer [50 mM HEPES pH 7.4, 150 mM NaCl, 1% NP-40, 10% glycerol, 1x EDTA-free complete mini protease inhibitors (Roche), and 200 U/ml catalase (Sigma)].

EGFR autophosphorylation assays and data analysis. For autophosphorylation assays, cells were cultured until 80-85% confluency, washed with PBS, and placed in culture media without serum (serum-starved) for 16 h. After serum deprivation, cells were treated with the appropriate reagent (H_2O_2 , glucose oxidase, NAC, reduced GSH, or HSA) at the indicated concentration and time period. Cells were then incubated with the indicated concentration of inhibitor for the indicated time period, washed with PBS, and treated with the indicated concentration of EGF for the indicated time period. Treatment was stopped by removing the media and washing with PBS. Cell lysates were generated as described in Methods. Inhibition of EGFR autophosphorylation was determined by densitometric quantification of Western blots. Percent inhibition was plotted against inhibitor concentration, and IC_{50} values were calculated with a four parameter fit function using KaleidaGraph software.

Washout effect of compounds. For washout assays, cells were cultured until 80-85% confluency, washed with PBS, and serum-starved for 16 h. After serum deprivation, cells were incubated with compound at the indicated concentration for the indicated time period. Cells were washed with PBS to remove excess compound, and treated with H_2O_2 at the indicated concentration and time period to induce sulfenic acid formation. Following H_2O_2 treatment, cells were washed with PBS, and placed in serum-free media for the indicated washout time. After washout, cells were treated with the indicated concentration of EGF for the indicated time period. Treatment was stopped by removing the media and washing with PBS. Cell lysates were generated as described in Methods.

Cell growth inhibition. A431 cells were seeded into 96-well format (2.0×10^4 cells/well) and cultured until 80-85% confluency. Cells were washed with PBS and placed in complete culture media (phenol-free). Cells were incubated with compound for 72 h (0-1000 μM) in triplicate, and media and compound was replenished every

24 h. Cell viability was assessed by tetrazolium dye MTT [3-(4,5-dimethylthiazol-2-yl)-2,5-diphenyltetrazolium bromide] (Life Technologies) according to manufacturer guidelines. IC₅₀ values were calculated using KaleidaGraph software and are representative of three independent trials and represent the mean \pm s.e.m.

Sulfenic acid labeling in tissue lysate. Tissue slices from xenograft mice models were lysed and homogenized in HEPES lysis buffer in the presence of DYN-2 (10 mM). Tissue lysates were cleared of debris by centrifugation at 14,000 rpm for 15 min at 4 °C. The lysates were then passed through a p30 column (BioRad) to remove excess probe and subjected to immunoprecipitation to analyze EGFR sulfenylation levels.

Immunoprecipitation. EGFR was immunoprecipitated from 500 μ g lysate (1 mg/ml) with goat anti-EGFR conjugated agarose (Santa Cruz Biotechnology) or isotype control (normal goat IgG) overnight at 4 °C with gentle rocking. The resin was collected by centrifugation at 100g for 2 min at rt, and washed with cold RIPA buffer (1X) and cold PBS buffer (2X). The resin was subjected to click chemistry as described in Methods, and the bound proteins were eluted by boiling with LDS sample buffer for 10 min, and resolved by SDS-PAGE and analyzed by Western blot.

Click chemistry. For immunoprecipitated protein analyses, the resin was treated with 20 μ l click chemistry mix [azide biotin (100 μ M), CuSO₄ (250 μ M), BTTP (500 μ M), and sodium L-ascorbate (2.5 mM) in PBS] for 1 h at rt with gentle rocking. The reaction was quenched with 1 mM EDTA, and the samples were boiled with LDS sample buffer.

5.7 Contributions

T.H.T. performed cell culture experiments. V.G. performed synthetic experiments. K.S.C., T.H.T., and V.G. designed experimental strategies.

5.8 Supplementary Figures

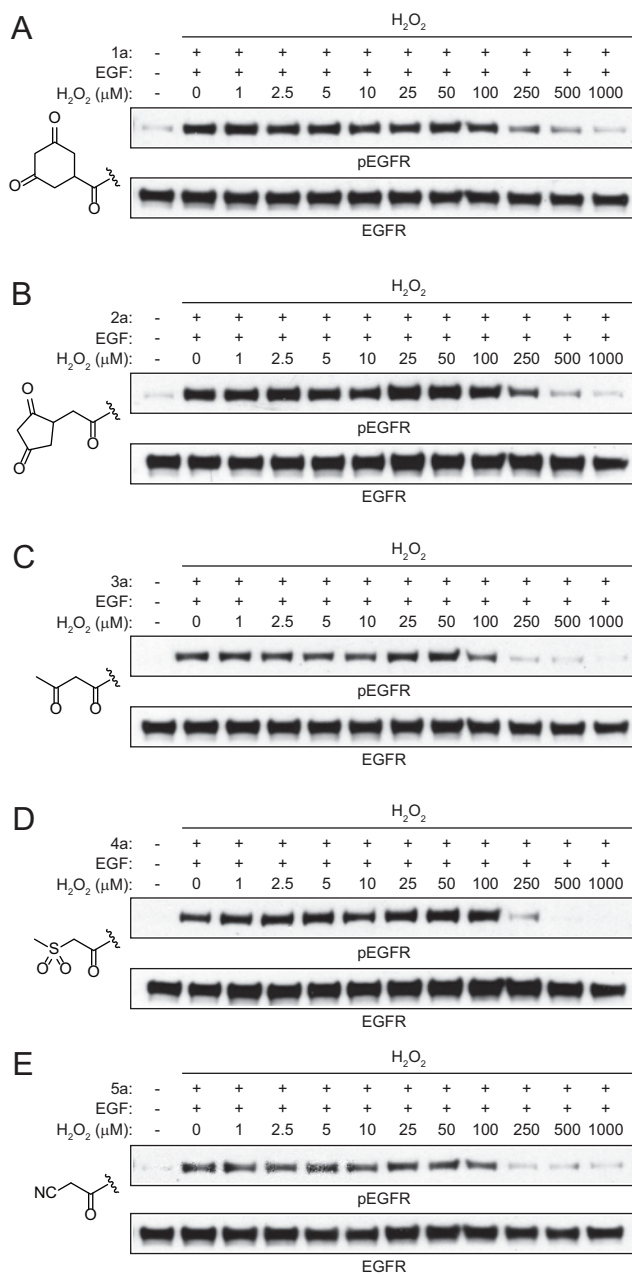


Figure 5.S1: **Dose-dependence of acute H₂O₂ on EGFR phosphorylation levels.** (A-E) Western blots show phosphorylated (p) and total EGFR. A431 cells were stimulated with H₂O₂ at the indicated concentrations for 5 min to induce sulfenic acid formation, treated with the indicated concentrations of **1a-5a**, and subsequently stimulated with EGF (100 ng/ml) for 5 min.

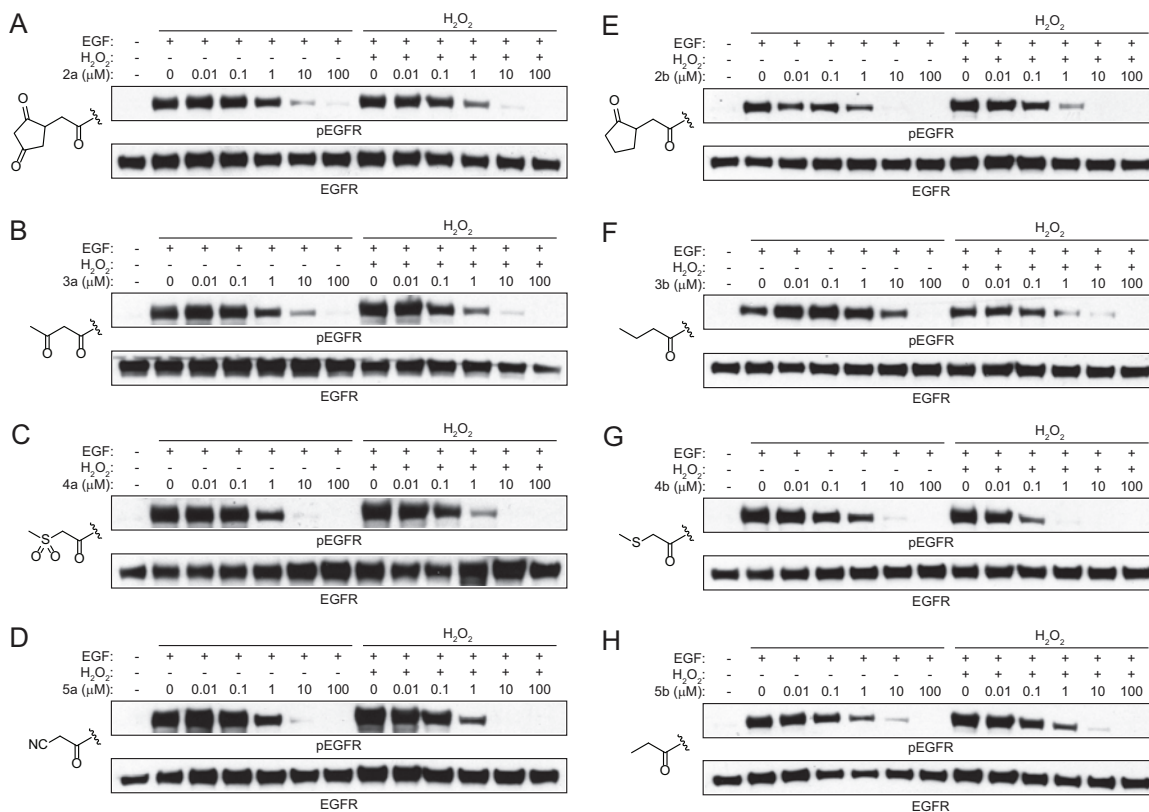


Figure 5.S2: **Acute H₂O₂ treatment increases potency of RSOH-targeted compounds.** Western blots show phosphorylated (p) and total EGFR. (A-D) Acute H₂O₂ treatment increases potency of **2a-5a**, respectively. (E-H) Acute H₂O₂ treatment of **2b-5b**, respectively. A431 cells were stimulated with H₂O₂ (200 μM) for 5 min to induce sulfenic acid formation, treated with the indicated concentrations of **2a-5a** or **2b-5b** for 1 h, and subsequently stimulated with EGF (100 ng/ml) for 5 min.

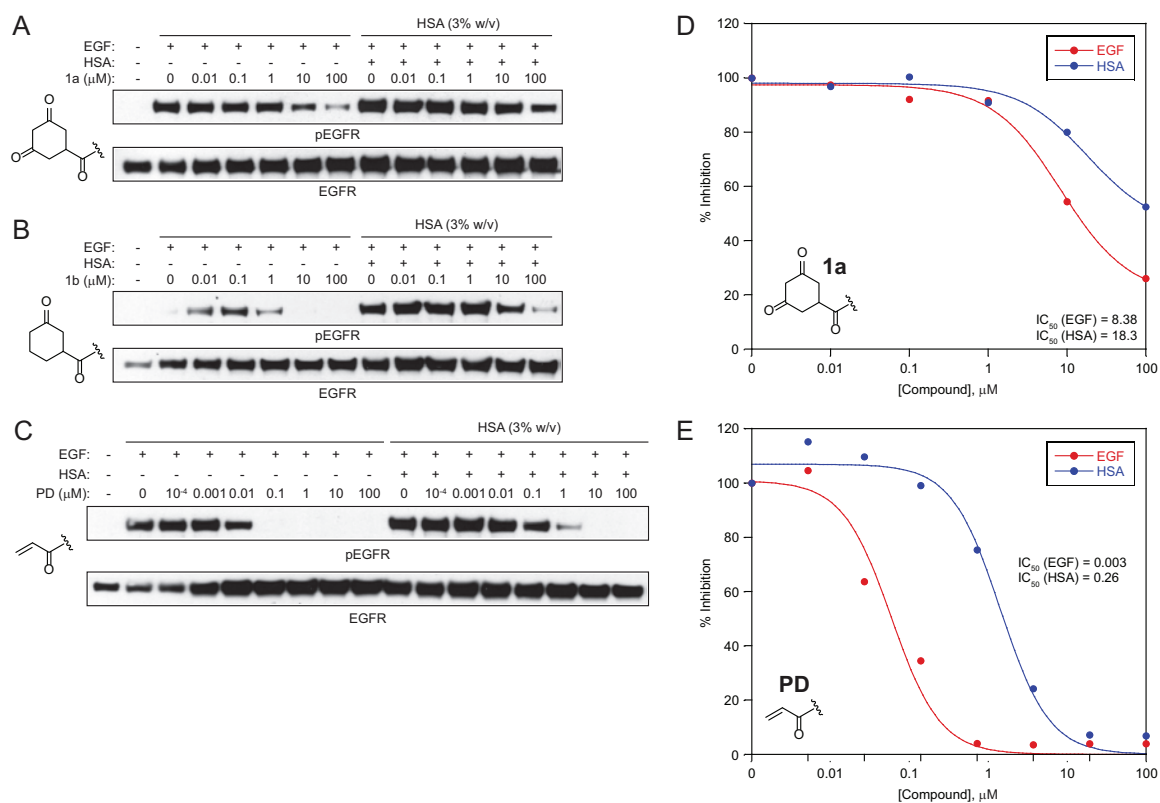


Figure 5.S3: **Human serum albumin (HSA) decreases potency of RSH- and RSOH-targeted compounds.** A431 cells were incubated with (A) 1a, (B) 1b, and (C) PD168393 in the presence of HSA (3% w/v) for 1 h, and subsequently stimulated with EGF (100 ng/ml) for 5 min. All three compounds exhibited decreased potency in the presence of HSA. (D) IC_{50} values for **1a** were determined by Western blot analysis of EGFR autophosphorylation from A. (E) IC_{50} values for **PD168393** were determined by Western blot analysis of EGFR autophosphorylation from C.

5.9 Supplementary Tables

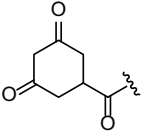
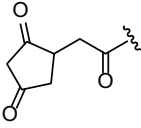
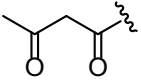
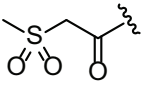
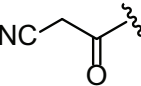
Table 5.S1: IC₅₀ Values of H₂O₂ (Acute) in A431 Cells Treated with 1a-5a

Compound	[Conc] (μ M) ^a	IC ₅₀ (μ M), H ₂ O ₂
1a	10	266.9
2a	5	236.8
3a	1	129.2
4a	1	224.0
5a	1	177.4

^a Compound was maintained at the listed concentration.

^b IC₅₀ values of H₂O₂ were determined by Western blot analysis of EGFR autophosphorylation

Table 5.S2: IC₅₀ Values of RSOH-Targeted Compounds in NCI-H1975 Cells Treated with Acute H₂O₂

Compound	Structure	IC ₅₀ (μM), EGF ^b	IC ₅₀ (μM), H ₂ O ₂ ^c
1a		ND ^d	0.59 ± 0.35
2a		ND	5.65
3a		ND	4.49
4a		ND	1.65
5a		ND	14.08

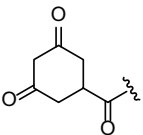
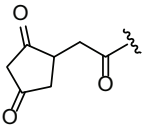
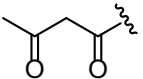
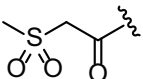
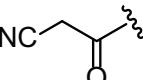
^a Cells were pre-treated with H₂O₂ (200 μM, 5 min), incubated with compound (1 h), and stimulated with EGF (100 ng/ml).

^b IC₅₀ values of EGF were determined by Western blot analysis of EGFR autophosphorylation.

^c IC₅₀ values of H₂O₂ were determined by Western blot analysis of EGFR autophosphorylation.

^d ND, not determined. In some cases, the IC₅₀ value could not be calculated because no change in phosphorylation levels was observed.

Table 5.S3: IC₅₀ Values of RSOH-Targeted Compounds in HCC827 Cells Treated with Acute H₂O₂

Compound	Structure	IC ₅₀ (μM), EGF ^b	IC ₅₀ (μM), H ₂ O ₂ ^c
1a		3.51	0.51
2a		0.45	0.40
3a		0.041	0.46
4a		ND ^d	0.15
5a		0.69	0.26

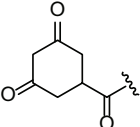
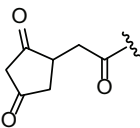
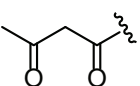
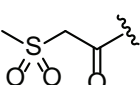
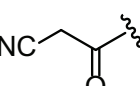
^a Cells were pre-treated with H₂O₂ (200 μM, 5 min), incubated with compound (1 h), and stimulated with EGF (100 ng/ml).

^b IC₅₀ values of EGF were determined by Western blot analysis of EGFR autophosphorylation.

^c IC₅₀ values of H₂O₂ were determined by Western blot analysis of EGFR autophosphorylation.

^d ND, not determined. In some cases, the IC₅₀ value could not be calculated because no change in phosphorylation levels was observed.

Table 5.S4: IC₅₀ Values of RSOH-Targeted Compounds in MDA-MB-453 Cells Treated with Acute H₂O₂

Compound	Structure	IC ₅₀ (μM), EGF ^b	IC ₅₀ (μM), H ₂ O ₂ ^c
1a		ND ^d	0.90
2a		53.70	50.48
3a		18.21	0.22
4a		3.42	8.69
5a		22.62	0.17

^a Cells were pre-treated with H₂O₂ (200 μM, 5 min), incubated with compound (1 h), and stimulated with EGF (100 ng/ml).

^b IC₅₀ values of EGF were determined by Western blot analysis of EGFR autophosphorylation.

^c IC₅₀ values of H₂O₂ were determined by Western blot analysis of EGFR autophosphorylation.

^d ND, not determined. In some cases, the IC₅₀ value could not be calculated because no change in phosphorylation levels was observed.

5.10 Chapter References

1. Schlessinger, J. (2000). Cell signaling by receptor tyrosine kinases. *Cell*, *103*(2), 211–25.
2. Bae, Y. S., Kang, S. W., Seo, M. S., Baines, I. C., Tekle, E., Chock, P. B., & Rhee, S. G. (1997). Epidermal growth factor (egf)-induced generation of hydrogen peroxide. role in egf receptor-mediated tyrosine phosphorylation. *J Biol Chem*, *272*(1), 217–21.
3. Miller, E. W., Tulyathan, O., Isacoff, E. Y., & Chang, C. J. (2007). Molecular imaging of hydrogen peroxide produced for cell signaling. *Nat Chem Biol*, *3*(5), 263–7.
4. Woo, H. A., Yim, S. H., Shin, D. H., Kang, D., Yu, D. Y., & Rhee, S. G. (2010). Inactivation of peroxiredoxin i by phosphorylation allows localized h₂o₂ accumulation for cell signaling. *Cell*, *140*(4), 517–28.
5. Paulsen, C. E. & Carroll, K. S. (2010). Orchestrating redox signaling networks through regulatory cysteine switches. *ACS Chem Biol*, *5*(1), 47–62.
6. Paulsen, C. E. & Carroll, K. S. (2013, July). Cysteine-mediated redox signaling: chemistry, biology, and tools for discovery. *Chem Rev*, *113*(7), 4633–4679. doi:10.1021/cr300163e
7. Paulsen, C. E., Truong, T. H., Garcia, F. J., Homann, A., Gupta, V., Leonard, S. E., & Carroll, K. S. (2012). Peroxide-dependent sulfenylation of the egfr catalytic site enhances kinase activity. *Nat Chem Biol*, *8*(1), 57–64.
8. Blume-Jensen, P. & Hunter, T. (2001). Oncogenic kinase signalling. *Nature*, *411*(6835), 355–65.
9. Haber, D. A., Gray, N. S., & Baselga, J. (2011, April). The evolving war on cancer. *Cell*, *145*(1), 19–24. doi:10.1016/j.cell.2011.03.026
10. Hynes, N. E. & Lane, H. A. (2005, May). ErbB receptors and cancer: the complexity of targeted inhibitors. *Nat Rev Cancer*, *5*(5), 341–354. doi:10.1038/nrc1609
11. Wakeling, A. E., Guy, S. P., Woodburn, J. R., Ashton, S. E., Curry, B. J., Barker, A. J., & Gibson, K. H. (2002, October). ZD1839 (Iressa): an orally active inhibitor of epidermal growth factor signaling with potential for cancer therapy. *Cancer Res*, *62*(20), 5749–5754.
12. Pollack, V. A., Savage, D. M., Baker, D. A., Tsaparikos, K. E., Sloan, D. E., Moyer, J. D., . . . Morin, M. J. (1999, November). Inhibition of epidermal growth factor receptor-associated tyrosine phosphorylation in human carcinomas with CP-358,774: dynamics of receptor inhibition in situ and antitumor effects in athymic mice. *J Pharmacol Exp Ther*, *291*(2), 739–748.

13. Johnson, B. E. & Janne, P. A. (2005, September). Epidermal growth factor receptor mutations in patients with non-small cell lung cancer. *Cancer Res*, *65*(17), 7525–7529. doi:10.1158/0008-5472.CAN-05-1257
14. Gazdar, A. F., Shigematsu, H., Herz, J., & Minna, J. D. (2004, October). Mutations and addiction to egfr: the achilles 'heal' of lung cancers? *Trends Mol Med*, *10*(10), 481–486. doi:10.1016/j.molmed.2004.08.008
15. Chan, S. K., Gullick, W. J., & Hill, M. E. (2006, January). Mutations of the epidermal growth factor receptor in non-small cell lung cancer – search and destroy. *Eur J Cancer*, *42*(1), 17–23. doi:10.1016/j.ejca.2005.07.031
16. Shigematsu, H. & Gazdar, A. F. (2006, January). Somatic mutations of epidermal growth factor receptor signaling pathway in lung cancers. *Int J Cancer*, *118*(2), 257–262. doi:10.1002/ijc.21496
17. Yun, C.-H., Boggon, T. J., Li, Y., Woo, M. S., Greulich, H., Meyerson, M., & Eck, M. J. (2007). Structures of lung cancer-derived egfr mutants and inhibitor complexes: mechanism of activation and insights into differential inhibitor sensitivity. *Cancer Cell*, *11*(3), 217–227.
18. Zhang, X., Gureasko, J., Shen, K., Cole, P. A., & Kuriyan, J. (2006). An allosteric mechanism for activation of the kinase domain of epidermal growth factor receptor. *Cell*, *125*(6), 1137–1149.
19. Carey, K. D., Garton, A. J., Romero, M. S., Kahler, J., Thomson, S., Ross, S., . . . Sliwkowski, M. X. (2006, August). Kinetic analysis of epidermal growth factor receptor somatic mutant proteins shows increased sensitivity to the epidermal growth factor receptor tyrosine kinase inhibitor, erlotinib. *Cancer Res*, *66*(16), 8163–8171. doi:10.1158/0008-5472.CAN-06-0453
20. Paez, J. G., Janne, P. A., Lee, J. C., Tracy, S., Greulich, H., Gabriel, S., . . . Meyerson, M. (2004, June). Egfr mutations in lung cancer: correlation with clinical response to gefitinib therapy. *Science*, *304*(5676), 1497–1500. doi:10.1126/science.1099314
21. Lynch, T. J., Bell, D. W., Sordella, R., Gurubhagavatula, S., Okimoto, R. A., Brannigan, B. W., . . . Haber, D. A. (2004, May). Activating mutations in the epidermal growth factor receptor underlying responsiveness of non-small-cell lung cancer to gefitinib. *N Engl J Med*, *350*(21), 2129–2139. doi:10.1056/NEJMoa040938
22. Pao, W., Miller, V., Zakowski, M., Doherty, J., Politi, K., Sarkaria, I., . . . Varmus, H. (2004, September). Egf receptor gene mutations are common in lung cancers from "never smokers" and are associated with sensitivity of tumors to gefitinib and erlotinib. *Proc Natl Acad Sci U S A*, *101*(36), 13306–13311. doi:10.1073/pnas.0405220101

23. Rosell, R., Moran, T., Queralt, C., Porta, R., Cardenal, F., Camps, C., . . . Spanish Lung Cancer Group. (2009, September). Screening for epidermal growth factor receptor mutations in lung cancer. *N Engl J Med*, *361*(10), 958–967. doi:10.1056/NEJMoa0904554
24. Kobayashi, S., Boggon, T. J., Dayaram, T., Janne, P. A., Kocher, O., Meyerson, M., . . . Halmos, B. (2005, February). Egfr mutation and resistance of non-small-cell lung cancer to gefitinib. *N Engl J Med*, *352*(8), 786–792. doi:10.1056/NEJMoa044238
25. Kwak, E. L., Sordella, R., Bell, D. W., Godin-Heymann, N., Okimoto, R. A., Brannigan, B. W., . . . Haber, D. A. (2005, May). Irreversible inhibitors of the egf receptor may circumvent acquired resistance to gefitinib. *Proc Natl Acad Sci U S A*, *102*(21), 7665–7670. doi:10.1073/pnas.0502860102
26. Yun, C.-H., Mengwasser, K. E., Toms, A. V., Woo, M. S., Greulich, H., Wong, K.-K., . . . Eck, M. J. (2008). The t790m mutation in egfr kinase causes drug resistance by increasing the affinity for atp. *Proc Natl Acad Sci U S A*, *105*(6), 2070–2075.
27. Li, Q., Zhang, Y., Marden, J. J., Banfi, B., & Engelhardt, J. F. (2008). Endosomal nadph oxidase regulates c-src activation following hypoxia/reoxygenation injury. *Biochem J*, *411*(3), 531–41.
28. Kobayashi, S., Ji, H., Yuza, Y., Meyerson, M., Wong, K.-K., Tenen, D. G., & Halmos, B. (2005, August). An alternative inhibitor overcomes resistance caused by a mutation of the epidermal growth factor receptor. *Cancer Res*, *65*(16), 7096–7101. doi:10.1158/0008-5472.CAN-05-1346
29. Zhang, J., Yang, P. L., & Gray, N. S. (2009). Targeting cancer with small molecule kinase inhibitors. *Nature Reviews. Cancer*, *9*(1), 28–39.
30. Singh, J., Petter, R. C., & Kluge, A. F. (2010). Targeted covalent drugs of the kinase family. *Curr Opin Chem Biol*, *14*(4), 475–80.
31. Liu, Q., Sabnis, Y., Zhao, Z., Zhang, T., Buhrlage, S. J., Jones, L. H., & Gray, N. S. (2013). Developing irreversible inhibitors of the protein kinase cysteinome. *Chem Biol*, *20*(2), 146–59.
32. Singh, J., Petter, R. C., Baillie, T. A., & Whitty, A. (2011). The resurgence of covalent drugs. *Nat Rev Drug Discov*, *10*(4), 307–17.
33. Barf, T. & Kaptein, A. (2012, July). Irreversible protein kinase inhibitors: balancing the benefits and risks. *J Med Chem*, *55*(14), 6243–6262. doi:10.1021/jm3003203

34. Singh, J., Dobrusin, E. M., Fry, D. W., Haske, T., Whitty, A., & McNamara, D. J. (1997). Structure-based design of a potent, selective, and irreversible inhibitor of the catalytic domain of the erbb receptor subfamily of protein tyrosine kinases. *J Med Chem*, *40*(7), 1130–5.
35. Fry, D. W., Bridges, A. J., Denny, W. A., Doherty, A., Greis, K. D., Hicks, J. L., . . . Dobrusin, E. M. (1998, September). Specific, irreversible inactivation of the epidermal growth factor receptor and erbb2, by a new class of tyrosine kinase inhibitor. *Proc Natl Acad Sci U S A*, *95*(20), 12022–12027.
36. Rabindran, S. K., Discafani, C. M., Rosfjord, E. C., Baxter, M., Floyd, M. B., Golas, J., . . . Wissner, A. (2004, June). Antitumor activity of hki-272, an orally active, irreversible inhibitor of the her-2 tyrosine kinase. *Cancer Res*, *64*(11), 3958–3965. doi:10.1158/0008-5472.CAN-03-2868
37. Barnham, K. J., Masters, C. L., & Bush, A. I. (2004). Neurodegenerative diseases and oxidative stress. *Nat Rev Drug Discov*, *3*(3), 205–14.
38. Finkel, T., Serrano, M., & Blasco, M. A. (2007). The common biology of cancer and ageing. *Nature*, *448*(7155), 767–74.
39. Seo, Y. H. & Carroll, K. S. (2009). Facile synthesis and biological evaluation of a cell-permeable probe to detect redox-regulated proteins. *Bioorg Med Chem Lett*, *19*(2), 356–9.
40. Leonard, S. E., Garcia, F. J., Goodsell, D. S., & Carroll, K. S. (2011). Redox-based probes (rbps) for protein tyrosine phosphatases. *Angew Chem Int Ed Engl*, *in press*.
41. Reddie, K. G., Seo, Y. H., Muse Iii, W. B., Leonard, S. E., & Carroll, K. S. (2008). A chemical approach for detecting sulfenic acid-modified proteins in living cells. *Mol Biosyst*, *4*(6), 521–31.
42. Leonard, S. E., Reddie, K. G., & Carroll, K. S. (2009). Mining the thiol proteome for sulfenic acid modifications reveals new targets for oxidation in cells. *ACS Chem Biol*, *4*(9), 783–99.
43. Cohen, S., Carpenter, G., & King, J., L. (1980). Epidermal growth factor-receptor-protein kinase interactions. co-purification of receptor and epidermal growth factor-enhanced phosphorylation activity. *J Biol Chem*, *255*(10), 4834–42.
44. Raba, J. & Mottola, H. A. (1995). Glucose-oxidase as an analytical reagent. *Critical Reviews in Analytical Chemistry*, *25*, 1–42.
45. Oettl, K. & Marsche, G. (2010). Redox state of human serum albumin in terms of cysteine-34 in health and disease. *Methods Enzymol*, *474*, 181–195. doi:10.1016/S0076-6879(10)74011-8

46. Godin-Heymann, N., Bryant, I., Rivera, M. N., Ulkus, L., Bell, D. W., Riese, D. J., 2nd, ... Haber, D. A. (2007, August). Oncogenic activity of epidermal growth factor receptor kinase mutant alleles is enhanced by the t790m drug resistance mutation. *Cancer Res*, *67*(15), 7319–7326. doi:10.1158/0008-5472.CAN-06-4625
47. Zhou, W., Ercan, D., Chen, L., Yun, C.-H., Li, D., Capelletti, M., ... Janne, P. A. (2009, December). Novel mutant-selective egfr kinase inhibitors against egfr t790m. *Nature*, *462*(7276), 1070–1074. doi:10.1038/nature08622

CHAPTER VI

Conclusions

6.1 Abstract

The data presented in the previous chapters provides evidence that protein sulfenylation directly modulates kinase activity during cellular signaling events and can be exploited for the development of new therapeutics in disease states associated with high levels of oxidative stress. In the present chapter, we summarize these findings and the significance of this work. Moreover, we discuss future directions aimed at the continued investigation of general mechanisms underlying redox regulation of protein kinases and the development of novel irreversible RSOH-targeted inhibitors for epidermal growth factor receptor (EGFR).

6.2 Summary

Hydrogen peroxide (H_2O_2) acts as a second messenger to modulate signal transduction networks through chemoselective oxidation of cysteine residues in protein targets (1). Although the development of chemical probes to detect sulfenic acids have greatly facilitated the detection of sulfenylated proteins (2), a large majority of H_2O_2 -modulated targets and the extent to which reversible oxidation influences protein activity remains largely unknown. The overall goal of this thesis was to use

sulfenic acid probes developed in our lab to elucidate the regulatory role of protein sulfenylation within the context of kinase signaling, specifically EGFR. In Chapter 1, we presented an overview of the molecular mechanisms involved in redox-based regulation of EGFR and its downstream signaling pathways (3).

In Chapter 2, we presented the development and application of a modified approach that allows relative quantification of sulfenic acids based on a pair of light and heavy isotope labeled probes (DAz-2 and d6-DAz-2) in conjunction with a complementary acid-cleavable linker (Yn-ACL) (4). This method can be used to directly map sites of cysteine oxidation and compare sulfenic acid levels in normal and disease states. One advantage of this method is that it utilizes an avidin enrichment step to maximize identification of probe-labeled proteins.

In Chapter 3, we reported the development and application of a new alkyne-based probe (DYn-2) for detection of sulfenic acids (5). These studies demonstrated epidermal growth factor (EGF) signaling mediates endogenous H_2O_2 production and induces dynamic changes in global protein sulfenylation in A431 cells. Three protein tyrosine phosphatases (PTPs) were identified as direct targets of ligand-dependent oxidation and exhibited a unique sulfenylation profile based on their subcellular locations. In addition, EGFR was identified as a direct target of signal-derived H_2O_2 at its active site cysteine (Cys797), which enhances its tyrosine kinase activity. The results of this study revealed sulfenylation acts as a global signaling mechanism that is akin to phosphorylation and has regulatory implications for other protein kinases and have broad therapeutic implications for redox-sensitive cysteine residues.

In Chapter 4, we performed molecular characterization to delineate the role of EGFR Cys797 sulfenylation and determine its effect on kinase activity. *In vitro* and cell-based assays demonstrate that mutation of this residue abrogates EGFR autophosphorylation, sulfenylation, and decreases its affinity for ATP. Moreover, oxidation affects the propensity of Cys797 to undergo sulfenylation in common oncogenic

EGFR mutants and the potency of inhibitors that target this residue in its reduced thiolate form. Additionally, we demonstrate HER2 and BTK undergo sulfenylation, providing evidence that kinases harboring a structurally homologous cysteine to Cys797 may be redox-regulated.

In Chapter 5, we reported the development of a panel of first generation nucleophilic ROSH-targeted inhibitors and evaluated compound potency and selectivity towards EGFR Cys797 in response to concomitant EGFR oxidation. We demonstrated our nucleophilic compounds were capable of inhibiting EGFR autophosphorylation under oxidizing conditions and occurred through partial irreversible mechanisms. Our work provided proof of principle and indicates that the propensity of EGFR Cys797 to form sulfenic acid can be exploited to develop new classes of inhibitors.

6.3 Future Directions

Continued investigation of general mechanisms involved in redox regulation of receptor and non-receptor kinases

Of the ~95 receptor and non-receptor protein tyrosine kinases (PTKs) in the human genome, nine additional members contain a structurally homologous cysteine residue to EGFR Cys797 (Figure 6.1) (6). This group contains two EGFR subfamily members, HER2 and HER4. In Chapter 4, we demonstrated that HER2 undergoes EGF-mediated sulfenylation. HER2 can form a heterodimer with EGFR upon stimulation, and oxidation of HER2 may be facilitated by receptor dimerization. Overexpression of HER2 has been shown to play a role in the development and progression of breast cancer. Additionally, increased protein oxidation and sulfenylation have been observed in breast cancer cells with elevated EGFR and HER2 expression levels (7). Coupled to previous literature work, our findings highlight the importance of understanding the full extent of HER2 oxidation because of its close relationship as

an EGFR subfamily member and its potential therapeutic implications (8).

We also explored the ability of Bruton's tyrosine kinase (BTK) to undergo sulfenic acid formation. Unlike receptor kinases EGFR and HER2, BTK is a non-receptor kinase that plays an essential role in regulating calcium signaling during B-cell receptor (BCR) activation. We chose BTK because it is the only other kinase in this group (Figure 6.1) besides EGFR and HER2 that currently has inhibitors undergoing clinical trials (8). Using sulfenic acid specific probes, we were able to demonstrate BTK undergoes sulfenic acid modification at Cys481 upon IgM stimulation. Moreover, pre-treatment with irreversible BTK inhibitor PCI-32765 decreased IgM-mediated sulfenylation, albeit not completely. Therefore, we speculated that additional mechanisms may be involved in modulating the oxidation status of BTK Cys481. It is possible that Cys481 undergoes redox-mediated disulfide bond formation with a second cysteine residue (Cys527) located in the BTK kinase active site. Continued efforts to delineate the effect and extent of oxidation on BTK activity will help determine if this conserved residue (EGFR Cys797) acts as a general mechanism to regulate kinase signaling. BTK is a member of the TEC family of kinases and include TEC, ITK TXK, and BMX, all of whom are also structural homologues of EGFR (Figure 6.1). Findings demonstrating redox regulation of BTK may be applicable to the TEC kinase family, as previously observed with the EGFR subfamily (i.e. EGFR and HER2). Another subfamily of protein tyrosine kinases, which includes cytoplasmic Src and FGFR1, contains a conserved cysteine residue located within its glycine rich loop in the kinase active site. Oxidation of this residue has been shown to inhibit kinase activity of c-Src and FGFR1 in vitro (9), but neither of these kinases has been confirmed as an intracellular target of H_2O_2 to date. More than 150 kinases contain a cysteine residue in or around the nucleotide-binding site and may have similar regulatory roles, but a broader examination will be required to define the scope and underlying details of the redox-regulated kinome.

EGFR	T	Q	L	M	P	F	G	C	L	L	D
HER2	T	Q	L	M	P	Y	G	C	L	L	D
HER4	T	Q	L	M	P	H	G	C	L	L	E
BLK	T	E	Y	M	A	R	G	C	L	L	D
BMX	T	E	Y	I	S	N	G	C	L	L	N
BTK	T	E	Y	M	A	N	G	C	L	L	N
ITK	F	E	F	M	E	H	G	C	L	S	D
JAK3	M	E	Y	L	P	S	G	C	L	R	D
TEC	T	E	F	M	E	R	G	C	L	L	N
TXK	T	E	F	M	E	N	G	C	L	L	N

Figure 6.1: Sequence alignment of EGFR and nine additional kinases containing a structurally homologous residue to EGFR Cys797.

Continued development of irreversible RSOH-targeted inhibitors of EGFR

EGFR is mutated or amplified in a number of human cancers (i.e. breast and lung), which has motivated the development of reversible ATP-competitive and irreversible inhibitors (8, 10). Many covalent EGFR inhibitors contain an electrophilic acrylamide moiety that reacts with the EGFR Cys797 thiolate through Michael addition to achieve irreversible binding. Our findings demonstrate oxidation of EGFR Cys797 reduces potency of these RSH-targeted inhibitors and suggest alternate mechanisms to target the sulfenyl form of EGFR must be developed to overcome the potential shortcomings of current inhibitors. To address this, we generated a panel of nucleophilic RSOH-targeted inhibitors and evaluated their potency towards EGFR Cys797. Our studies demonstrate that oxidizing conditions (acute and chronic H₂O₂) increased the potency of our compounds. Subsequent washout experiments indicated that our compounds were capable of inducing partial, but not complete irreversible inhibition. We speculate that this is most likely due to the slower reactivity rates of the nucleophilic warheads employed in our study with sulfenic acid (V. Gupta and K. Carroll, unpublished results).

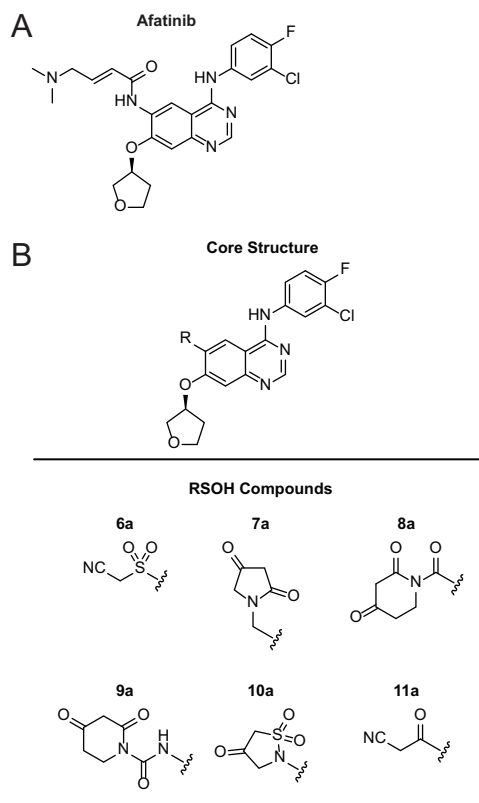


Figure 6.2: **Structures of 2nd generation RSOH-targeted EGFR compounds.** (A) Structure of parent compound afatinib. (B) Structures of 2nd generation RSOH-targeted compounds (**6a-11a**). The core structure is shown at the top.

Although our first generation of RSOH-targeted EGFR inhibitors were successful in demonstrating proof of principle of the nucleophilic warhead approach, our studies revealed a number of issues that must be addressed. First and foremost, alternate nucleophilic warheads must be identified in order to facilitate faster reactivity rates with sulfenic acid. Additionally, solubility and bioavailability issues must be explored as well. The parent compound, PD168393, was considered an effective inhibitor, but did not make it to clinical trials due to poor bioavailability. We observed similar solubility issues with our first generation compounds, indicating that an alternate core structure must be considered for future inhibitor development. To address these concerns, the synthesis of a second generation of RSOH-targeted EGFR inhibitors is currently in progress and will incorporate some of the following changes. The core structure will be modeled after afatinib (Figure 6.2A), which has proven successful

in clinical trials. The afatinib core contains a water-solubilizing group (dialkylamine) attached at the end of its Michael acceptor (acrylamide). This additional group enhances the rate of the Michael addition reaction and increases solubility of the compound. Second, we have since identified a number of new nucleophilic warheads that exhibit reactivity rates towards sulfenic acid that are much faster than the ones we selected for our original study (V. Gupta and K. Carroll, unpublished results). These new nucleophiles will be used in place of our current ones, in order to enhance reactivity rates with EGFR Cys797 (Figure 6.2B).

6.4 Concluding Remarks

This thesis presents key findings that demonstrate the important role of protein sulfenylation during kinase-mediated signaling events. Continued work to understand the scope of sulfenylation indicates that general mechanisms may have evolved to regulate protein kinase function. Additionally, this modification can be exploited for the development of new therapeutic approaches to treat pathologic conditions characterized with high oxidative stress levels and presage an exciting future for elucidating the role of sulfenic acids in normal and disease states.

6.5 Chapter References

1. Paulsen, C. E. & Carroll, K. S. (2010). Orchestrating redox signaling networks through regulatory cysteine switches. *ACS Chem Biol*, *5*(1), 47–62.
2. Paulsen, C. E. & Carroll, K. S. (2013, July). Cysteine-mediated redox signaling: chemistry, biology, and tools for discovery. *Chem Rev*, *113*(7), 4633–4679. doi:10.1021/cr300163e
3. Truong, T. H. & Carroll, K. S. (2012). Redox regulation of epidermal growth factor receptor signaling through cysteine oxidation. *Biochemistry*, *51*(50), 9954–65.
4. Truong, T. H., Garcia, F. J., Seo, Y. H., & Carroll, K. S. (2011). Isotope-coded chemical reporter and acid-cleavable affinity reagents for monitoring protein sulfenic acids. *Bioorg Med Chem Lett*, *21*(17), 5015–20.
5. Paulsen, C. E., Truong, T. H., Garcia, F. J., Homann, A., Gupta, V., Leonard, S. E., & Carroll, K. S. (2012). Peroxide-dependent sulfenylation of the egfr catalytic site enhances kinase activity. *Nat Chem Biol*, *8*(1), 57–64.
6. Singh, J., Petter, R. C., & Kluge, A. F. (2010). Targeted covalent drugs of the kinase family. *Curr Opin Chem Biol*, *14*(4), 475–80.
7. Seo, Y. H. & Carroll, K. S. (2009). Profiling protein thiol oxidation in tumor cells using sulfenic acid-specific antibodies. *Proc Natl Acad Sci U S A*, *106*(38), 16163–8.
8. Liu, Q., Sabnis, Y., Zhao, Z., Zhang, T., Buhrlage, S. J., Jones, L. H., & Gray, N. S. (2013). Developing irreversible inhibitors of the protein kinase cysteinome. *Chem Biol*, *20*(2), 146–59.

9. Kemble, D. J. & Sun, G. (2009). Direct and specific inactivation of protein tyrosine kinases in the src and fgfr families by reversible cysteine oxidation. *Proc Natl Acad Sci U S A*, 106(13), 5070–5.
10. Zhang, J., Yang, P. L., & Gray, N. S. (2009). Targeting cancer with small molecule kinase inhibitors. *Nature Reviews. Cancer*, 9(1), 28–39.

APPENDICES

APPENDIX A

Bioorthogonal Chemical Reporters for Analyzing Protein Sulfenylation in Cells

Abstract

Protein sulfenylation (RSOH), the redox-based modification of cysteine thiol side chains by hydrogen peroxide (H_2O_2) is an important mechanism in signal transduction. Likewise, dysregulated protein sulfenylation contributes to a range of human pathologies, including cancer. Efforts to elucidate the diverse roles of protein sulfenylation in physiology and disease have been hampered by the lack of techniques to probe these modifications in native environments. To address this problem, we have recently introduced selective chemical reporters for the detection and identification of sulfenylated proteins directly in cells. In this approach, a cyclic β -diketone warhead is functionalized with an azide or alkyne chemical handle. An orthogonally functionalized biotin or fluorescent reporter is then appended to the probe post-homogenization *via* click chemistry for downstream analysis. These bi-functional probes are exquisitely selective for protein sulfenyl modifications, non-toxic, and do not perturb intracellular redox balance. Our laboratory has utilized these reagents to investigate sulfenylation

in vitro and identify intracellular protein targets of H₂O₂ during cell signaling. These methods are presented in this unit, and provide a facile way to detect protein sulfenic acids. With the information gained from on-going studies, researchers can continue to uncover the biological role of cysteine oxidation with regards to physiological and pathological events.

Introduction

Although historically viewed as purely harmful, recent studies demonstrate that hydrogen peroxide (H₂O₂) functions as an important physiological regulator of intracellular signaling pathways, including cell growth and proliferation (1, 2). In this context, H₂O₂ is produced by a family of membrane-bound NADPH-dependent oxidases whose expression is tightly regulated, compartmentalized, and tissue-specific (3). The downstream effects of H₂O₂ are mediated by covalent modification of cysteine residues found within redox-sensitive target proteins (4, 5). Oxidation of these specific and reactive cysteine residues in turn can lead to modulation of protein activity, much like *O*-phosphorylation (6).

Sulfenic acid (RSOH), also known as sulfenylation, is the direct product of cysteine modification by H₂O₂. The reactivity of a cysteine thiol toward H₂O₂ is profoundly influenced by the protein environment. Important factors include accessibility and proximity to side chains that may interact with the thiol, peroxide, or the oxidized product. Most reactive are cysteine residues with low pK_a values that exist as the nucleophilic thiolate anion at physiological pH. However, other factors are undoubtedly involved as the documented reactivity of protein thiolate anions with H₂O₂ ranges across seven orders of magnitude (1-10⁷ M⁻¹s⁻¹) (7). Some of these factors are coming to light, but consensus motifs have not yet emerged and our understanding of the molecular basis of sensitivity toward H₂O₂ for a given cysteine residue remains largely ill-defined.

Once formed, sulfenyl modifications can be stabilized by the microenvironment or, in some cases, react with nearby protein or exogenous thiols to form disulfides (Figure A.1a). Indirect evidence for the formation and stabilization of sulfenic acid in proteins was first reported for the glycolytic enzyme GAPDH in the 1970's (8), but was not fully appreciated until detailed biochemical and structural analysis of NADH peroxidase in the late 1990's (9, 10). These landmark studies led to the discovery that sulfenyl groups function as catalytic redox centers (11), alter enzyme chemistry (12), and act as reversible sensors of H₂O₂ levels in microbial transcription factors (13). Under conditions of oxidative stress, sulfenyl groups can also oxidize further to the sulfinic (SO₂H) or sulfonic acid (SO₃H). On the other hand, mounting evidence also points to the existence of specialized enzymes that mediate the direct reduction of the sulfenyl modification back to the thiol state (14).

Historically, methods to detect reactive cysteines and H₂O₂-mediated oxidation of protein thiols required the homogenization of cells, which disrupts the native environment (15). Under these crude conditions, cellular redox balance and protein structure are compromised, leading to artifactual oxidation during sample processing. The severity of this issue cannot be disregarded and greatly increases the challenges associated with identifying sites of modification in low-abundance proteins, as well as for interpreting the biological significance of the data.

To overcome this problem, we have developed small-molecule probes that enable sulfenylated proteins to be trapped and tagged directly in cells (16–18). In this approach, a cyclic β -diketone warhead (**2**; Figure A.1c) that is chemically selective for sulfenic acids known as dimedone (8) (**1**; Figure A.1b) is functionalized with an azide (**3-5**; Figure A.1c) or alkyne (**6-8**; Figure B.1c) reporter group. An orthogonally functionalized biotin or fluorescent tag is then appended post-homogenization for detection via the Staudinger ligation (19) or Huisgen [3+2] cycloaddition (*i.e.* click chemistry) (20). In addition, we have developed two complementary isotope-coded

probe pairs to quantify changes in protein sulfenylation (**9, 10**; Figure A.1c) (21, 22). Most recently, we have reported tri-functional probes to monitor reversible oxidation of protein tyrosine phosphatases (PTPs) comprised of a warhead bearing the cyclic β -diketone group, a binding module that targets the probe to the PTP active site, and an azide chemical reporter (**11, 12**; Figure A.1c) (15).

This collection of Basic Protocols presents a series of methods utilizing our probes for *in vitro* detection of sulfenyl modifications within recombinant purified proteins (Basic Protocol 1) and *in situ* detection in cultured mammalian cells (Basic Protocols 2 and 3). Labeled sulfenylated proteins can then be visualized by either Western blot analysis (Basic Protocol 4) or in-gel fluorescence (Basic Protocol 5) after being coupled to a biotin or fluorescent tag. Overall, our general approach provides a facile method for profiling sulfenyl modifications in proteins.

On-going development of chemical tools for selective detection of protein sulfenylation and other cysteine "oxoforms" are crucial for the progression of this rapidly growing area of research. While it is known that cysteines residues are the primary target of H_2O_2 (4), and that sulfenylation can lead to dramatic changes in protein function, our knowledge regarding the individual sites, extent or dynamics of these modifications in cells is still at an early phase. Acquiring such information is a key step in delineating the molecular mechanisms that underlie redox-dependent control of intracellular signaling networks in physiology and disease. Furthermore, the exploitation of redox-modulating strategies for cancer therapy requires a detailed understanding of the structure-activity relationships of sulfenyl modifications and their roles in complex biological processes.

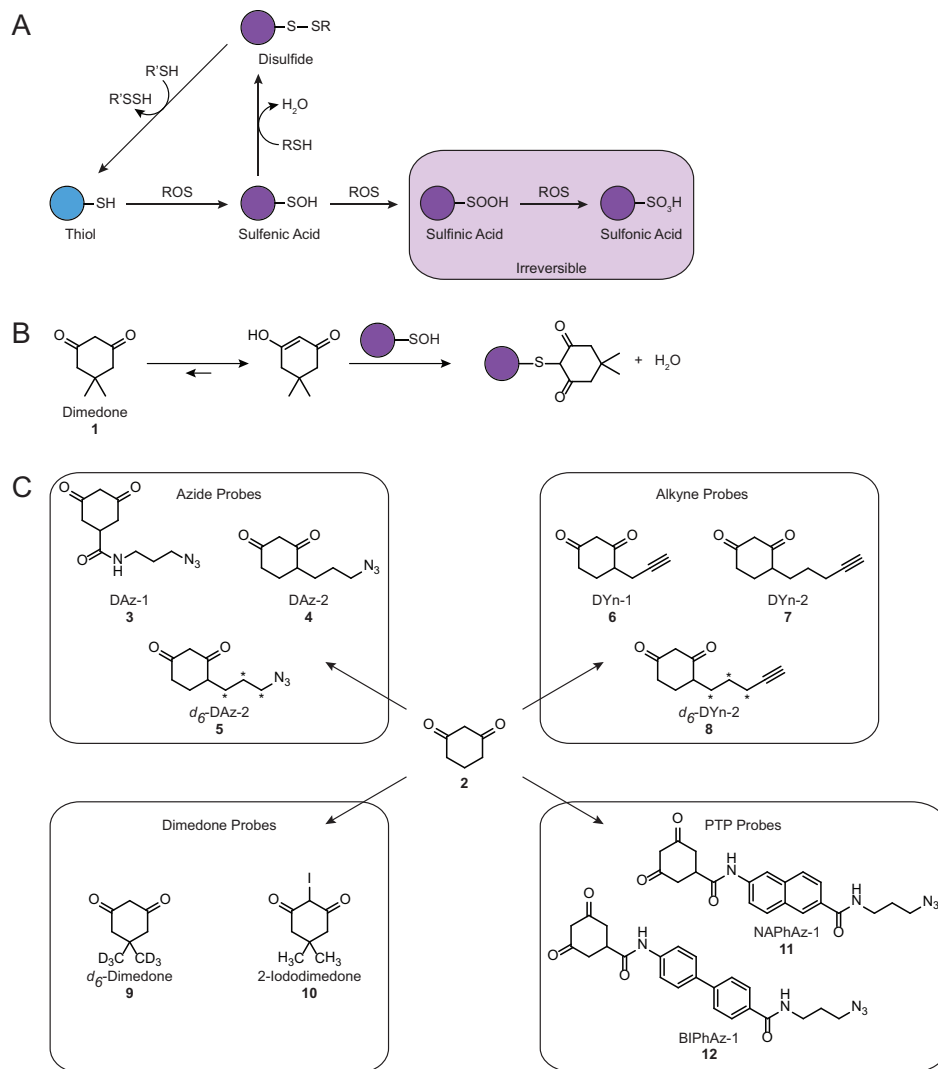


Figure A.1: **Bioorthogonal detection of protein cysteine oxidation.** (A) Oxidative modifications of protein cysteines. Low pKa thiols susceptible to oxidation can react with H_2O_2 to form a sulfenic acid, also known as sulfenylation. This modification may be stabilized by the protein microenvironment or condense with a second thiol to form an intra- or inter-molecular disulfide. Alternatively, the sulfenic acid can undergo further oxidation to the sulfinic or sulfonic acid under conditions of high oxidative stress, typically associated with disease states. (B) Chemoselective reaction between sulfenic acid and 5,5-dimethyl-1,3-cyclohexanedione (dimedone, 1). (C) Selective probes for detecting protein sulfenic acids based on the 1,3-cyclohexanedione scaffold (2). These probes are functionalized with azide (3-5) or alkyne (6-8) chemical reporter groups, allow for relative quantification of sulfenic acids (9-10), and can target specific classes of redox-regulated proteins, such as protein tyrosine phosphatases (PTPs) (11-12).

Strategic Planning

Labeling Sulfenylated Proteins In Vitro.

In Basic Protocol 1, we demonstrate the application of our method *in vitro* for a purified protein using the commercially available enzyme, glyceraldehyde 3-phosphate dehydrogenase (GAPDH). Upon exposure to H₂O₂, GAPDH becomes sulfenylated at the active-site cysteine (C149) (8) and the modification is readily detected by our probes (16, 23). Naturally, this method can be applied to investigate oxidation in other proteins that harbor H₂O₂-sensitive cysteine residues. The experimental parameters for oxidation and protein labeling described in Basic Protocol 1 have been optimized for GAPDH. Nevertheless, depending on the properties of the protein under study, it may be necessary to adjust some of the conditions if the reported procedure does not yield satisfactory results. For example, the H₂O₂ dose and exposure time can be adjusted to modulate the extent of cysteine oxidation. Similarly, probe concentration or labeling time can be changed in order to optimize the signal: noise ratio. For reference, the reaction rate of dimedone-based probes with protein sulfenic acids is on the order of 10³ M⁻¹ min⁻¹ (24). It is recommended that the user first attempt the conditions outlined in Basic Protocol 1 with their protein of interest prior to adjusting any experimental conditions. If the candidate protein demonstrates H₂O₂-sensitivity, downstream experiments may involve site-directed mutagenesis of the target cysteine and/or mass spectrometry (MS) analysis of intact and digested protein after probe labeling to map the site(s) of modification. In particular, our lab has demonstrated this with respect to wild-type and C36S Gpx3 with DAz-1 (25) and with isotope-coded probe pairs (21, 22).

Labeling Sulfenylated Proteins in Living Cells.

We present an approach for detecting protein sulfenyl modifications *in situ* for two human cell lines, A431 and HepG2 (Figure A.2a). A431 epithelial cells are a rich model for studying the biology of epidermal growth factor receptor (EGFR) signaling and for preclinical evaluation of EGFR therapeutics. The HepG2 epithelial cell line is also a suitable model system for the study of receptor-mediated H₂O₂ production and concomitant protein sulfenylation. In Basic Protocol 2, we demonstrate that EGF stimulation of A431 cells leads to dynamic global changes in protein sulfenylation, which may be important for growth factor signaling. Naturally, it is also possible to adapt Basic Protocol 2 to monitor changes in sulfenylation with other cell lines and stimulants. The dose- and time-dependent effects of a particular stimulant on protein sulfenylation should be evaluated for each new cell line. Likewise, probe concentration and labeling time may require some optimization. In addition, serum starvation of cells may be required to reduce high basal levels of sulfenylation. The procedure outlined in Basic Protocol 2 is somewhat involved and may prove difficult for investigators new to mammalian cell culture. Consequently, in Basic Protocol 3, we present a scaled-down method for detecting protein sulfenylation in HepG2 cells exposed to exogenous H₂O₂. HeLa cells may also be used in Basic Protocol 3, as they are another robust cell line that is easily propagated in the lab. We also note that Basic Protocol 2 and 3 call for the preparation of a single cell suspension from adherent culture for probe labeling. Therefore, it is prudent to work efficiently and avoid significant time delay after stimulation. As labeling in suspension may not prove ideal for some cell lines or stimulants, we also provide an alternative method for labeling cells that remain attached to the plate in Alternate Protocol 1 and 2.

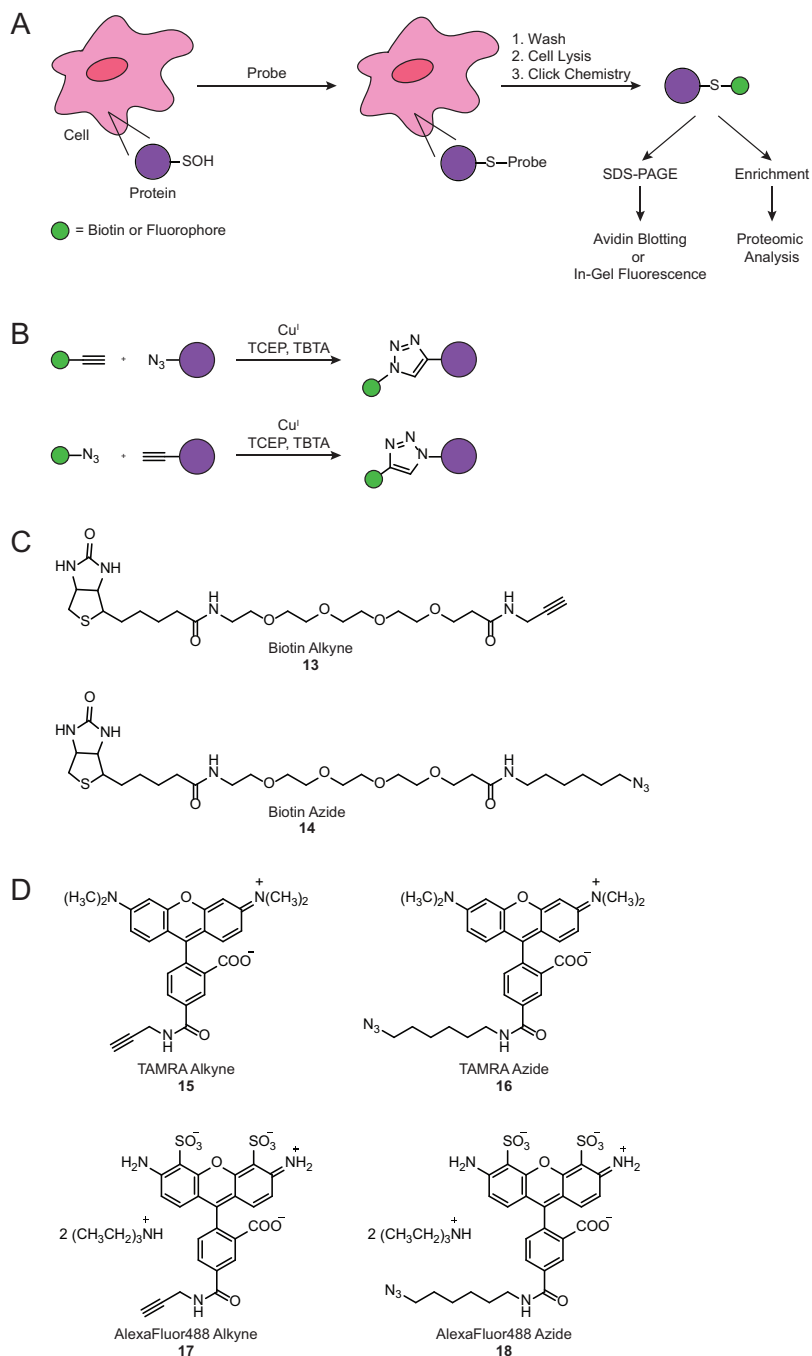


Figure A.2: Cell-based detection of protein sulfenylation. (A) Strategy to detect protein sulfenylation in living cells. Sulfenic acids are labeled in situ using selective, cell-permeable chemical probes. Cells are then washed, homogenized, and probe-labeled proteins are conjugated to a biotin or fluorescent tag via the bioorthogonal click chemistry reaction. This approach enables downstream detection by immunoblot or in-gel fluorescence. Alternatively, biotinylated proteins may be enriched for proteomic analysis. (B) Generic scheme for click chemistry bioconjugation. (C) Biotin tags utilized in this study. (D) Fluorescent tags utilized in this study.

Choice of Chemical Reporter for Analyzing Protein Sulfenylation.

DAz-2 and DYn-2 (**4** and **7**; Figure A.1c) can both be used to detect protein sulfenylation directly in cells. The major difference between these two probes is the identity of the chemical reporter group (azide or alkyne), which dictates the orientation of the triazole when "clicked" to the appropriate reporter tag (Figure A.2b). The choice of probe depends on downstream analysis methods. If Western blot detection is desired, either probe can be utilized with the corresponding biotin reporter tag (**13** or **14**; Figure A.2). However, for in-gel fluorescent detection we recommend the exclusive use of DYn-2 probe and azide-functionalized fluorescent tags (**16** or **18**; Figure A.2d) owing to the lower background signal reported for this orientation (26).

Bioorthogonal Ligation of Reporter-Labeled Proteins.

Once proteins are labeled with DAz-2 or DYn-2, they can be detected via bioorthogonal ligation with a biotin or fluorescent tag (Figure A.2b). In our protocol, we describe click chemistry as the main method of bioorthogonal ligation. We and other researchers have demonstrated the utility of click chemistry *in vitro* and in cells (17, 22, 27, 28). It is also possible to detect azide-tagged proteins through Staudinger ligation with various phosphine-based reactive partners (16, 18). Although this approach is not included in this particular collection of protocols, the user is welcome to explore this alternative bioorthogonal ligation method if they are interested.

Other Considerations.

For labeling sulfenylated proteins *in vitro* or in live cells, it is important to consider factors that can influence basal levels of cysteine oxidation. For example, reactive cysteines in recombinant proteins can undergo oxidation in the presence of oxygen and trace amounts of transition metal ions in phosphate or Tris-based buffer solutions. If this presents an issue for the user, buffer solutions can be made anaerobic by purging

with nitrogen. In addition, cells should be cultured carefully (*i.e.*, regular schedule for splitting, appropriate plating density, no more than 20 passages, mycoplasma testing) in high quality medium. Poor culturing conditions can lead to cell stress and higher basal levels of cysteine oxidation. It is also recommended that the user occasionally monitor cellular ROS levels by using carboxy-H₂DCFDA (Invitrogen) and/or a general protein marker for oxidative stress, such as an antibody against the hyper-oxidized form of peroxiredoxin (Prx-SO₃, Abcam). Furthermore, analogous to phosphorylation studies, serum starvation may be required to reduce high basal levels of protein sulfenylation. Lastly, control reactions should always be performed in the absence of chemical probe, as indicated in each section below.

Basic Protocols

Basic Protocol 1

LABELING SULFENYLATED PROTEINS IN VITRO.

The following is a standard protocol for *in vitro* labeling of sulfenyl modifications in purified proteins. We chose GAPDH as the model system here because it is well known to undergo sulfenylation at its active-site cysteine (C149). This protocol can be applied to investigate sulfenylation in any other protein of interest. Proteins can be labeled with a number of biotin or fluorescent chemical reporters, allowing for Western blot or in-gel fluorescent detection of labeled proteins.

Materials

- GAPDH, lyophilized powder (Sigma-Aldrich) or other purified protein of interest
- Bio-Spin 6 Columns, pre-packed in Tris buffer (BioRad)
- Tris labeling buffer (see recipe)

- Click labeling buffer (see recipe)
 - PBS, 1X (Boston BioProducts)
 - DMSO (vehicle; Sigma-Aldrich)
 - 25 mM DAz-2 (Cayman Chemicals) or DYn-2 (Cayman Chemicals), prepared in DMSO
 - 1 mM H₂O₂ stock (Sigma-Aldrich), prepared fresh in H₂O and maintained on ice
 - 5 mM biotin tag (biotin alkyne or azide; Invitrogen) in DMSO *or* 5 mM fluorescent tag (TAMRA or AlexaFluor488 azide; Invitrogen) in DMSO
 - 50 mM tris(2-carboxyethyl) phosphine hydrochloride (TCEP; Sigma-Aldrich), prepared fresh in H₂O
 - 2 mM tris[(1-benzyl-1*H*-1,2,3-triazol-4-yl)methyl] amine (TBTA; Sigma Aldrich), prepared in 4: 1 DMSO: *t*-butanol. TBTA can also be synthesized by published methods (29).
 - 50 mM CuSO₄, prepared fresh in H₂O
 - Laemmli sample buffer, 2X with 10% β-mercaptoethanol (BioRad)
 - Mini-Protean TGX 4-15% Tris-Glycine protein gels (BioRad)
1. Resuspend GAPDH in Tris labeling buffer (4 mg/ml).

We recommend using GAPDH at 4 mg/ml in order to obtain a starting concentration of ~110 μM. If using a different protein, the protein of interest should have a starting concentration of ~100-110 μM. The relatively high protein concentration facilitates downstream gel-based MS analysis. However, if this is not desired, lower initial protein concentrations can be used.

2. Reduce GAPDH with 1 mM TCEP for 30 min at rt.

A freshly made stock solution of 50 mM TCEP should be used to obtain a final concentration of 1 mM TCEP for reduction of protein thiols.

3. After protein reduction, remove excess TCEP with Bio-Spin 6 columns (pre-equilibrated with Tris labeling buffer). Load 100 μ l GAPDH protein per column. To collect the reduced GAPDH protein, centrifuge the columns for 4 min at 1000 \times g, rt.

The Bio-Spin 6 columns must be pre-equilibrated with the appropriate buffer prior to use. To achieve this, centrifuge the columns for 2 min at 1000 \times g to remove packing buffer. Apply the new Tris labeling buffer in 500 μ l aliquots. After each application of new buffer, centrifuge the column for 1 min at 1000 \times g. Repeat as required. We use four washes which results in >99.9% of buffer exchanged.

4. Determine GAPDH protein concentration.

We determine the concentration of GAPDH using a NanoDrop2000c Spectrophotometer (Thermo Scientific) and a molar extinction coefficient of $\epsilon_{280} = 32890 \text{ M}^{-1} \text{ cm}^{-1}$.

5. Label 25 μ M GAPDH with 1 mM DAz-2 or DYn-2 (from 25 mM probe stock). Incubate GAPDH with 1.5 eq. H_2O_2 (37.5 μ M from 1 mM H_2O_2 stock) or H_2O (mock treatment). Total volume of the labeling reactions should be 100 μ l. In addition, a no-probe control sample should always be prepared for comparison to the experimental sample. Reaction components should be added in the following order:

- a. GAPDH

- b. Tris labeling buffer (to make up remaining reaction volume)
 - c. 3.75 μl of 1 mM H_2O_2 (final concentration of 37.5 μM)
 - d. 4 μl of 25 mM DAz-2 or DYn-2 (final concentration of 1 mM)
6. Rock the labeling reactions for 1 h at 37 °C.
 7. After protein labeling, remove excess probe with Bio-Spin 6 columns (pre-equilibrated with click labeling buffer). Load 95 μl labeling reaction per column. To collect the labeled GAPDH protein, centrifuge the columns for 4 min at 1000 \times g, rt.
 8. Detect probe-labeled proteins by orthogonal click chemistry. Total volume of the click chemistry reaction should be 100 μl . Add the reaction components in the following order to each sample and mix well:
 - a. 2 μl of 5 mM biotin or fluorescent reporter tag (final concentration of 100 μM)
 - b. 2 μl of 50 mM TCEP (final concentration of 1 mM)
 - c. 5 μl of 2 mM TBTA (final concentration of 100 μM)
 - d. 2 μl of 50 mM CuSO_4 (final concentration of 1 mM)
 9. Rock the click chemistry reactions for 1 h at rt.

If a fluorescent reporter tag is being used (i.e. TAMRA or AlexaFluor488 azide), perform the reactions in the dark. In addition, take all necessary precautions to carry out remaining steps in the dark if a fluorescent tag is used.
 10. After click chemistry, remove excess reagents with Bio-Spin 6 columns (pre-equilibrated with PBS). Load 95 μl labeling reaction per column. To collect the labeled GAPDH protein, centrifuge the columns for 4 min at 1000 \times g, rt.
 11. Add 100 μl 2X Laemmli sample buffer (10% β -ME) to each column eluate.

Note that the expected recovery of GAPDH applied to a Bio-Spin 6 column is $\sim 80\%$. This parameter must be empirically determined if a protein other than GAPDH is used.

12. Boil the protein samples for 10 min at 95 °C, using a heating block.
13. Resolve samples by SDS-PAGE using Mini-Protean TGX 4-15% Tris-Glycine gels.

For GAPDH, we typically load 200 ng protein per lane.

14. Analyze the results of the experiment with the detection method of choice.
 - a. Basic Protocol 4 Western blot
 - i. Figure A.3a DAz-2/Biotin Alkyne
 - ii. Figure A.3b DYn-2/Biotin Azide
 - b. Basic Protocol 5 In-gel fluorescence
 - i. Figure A.3c DYn-2/TAMRA Azide
 - ii. Figure A.3d DYn-2/AlexaFluor488 Azide

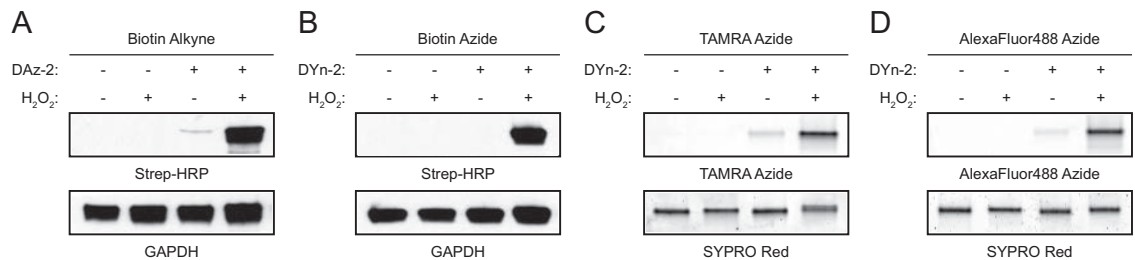


Figure A.3: Detection of sulfenyl modifications with purified protein in vitro. GAPDH was stimulated with H_2O_2 and labeled with DAz-2 or DYn-2 for 1 hr. Probe-labeled GAPDH can be detected by streptavidin-HRP immunoblot (A-B) or in-gel fluorescence (C-D). Equal protein loading is demonstrated by reprobing the immunoblot with antibodies to GAPDH (immunoblot) or by SYPRO red dye staining of the SDS-PAGE gel (fluorescence).

Basic Protocol 2

LABELING ENDOGENOUS SULFENYLATED PROTEINS IN CELL SUSPENSION.

The following is the standard protocol for labeling of intact A431 cells in suspension. We have recently demonstrated that A431 cells produce H_2O_2 upon stimulation with EGF, which leads to dynamic global changes in protein sulfenylation (17). In these experiments, the EGFR kinase is activated in A431 cells by stimulation with EGF ligand. We encourage the user to examine other cell lines and stimulants as appropriate in their experiments. Additionally, we recommend that the user consider starting with Basic Protocol 3 in order to gain basic proficiency in these techniques prior to attempting the more involved system described in Basic Protocol 2. Labeled proteins can be detected by Western blot or in-gel fluorescence.

Materials

- A431 cells (ATCC)
- DMEM complete culture medium (high glucose DMEM supplemented with 10% FBS, 1% GlutaMax, 1% MEM nonessential amino acids, and 1% penicillin-streptomycin; Invitrogen)
- DMEM only (serum-free high glucose DMEM; Invitrogen)
- 0.25% trypsin (Invitrogen)
- 30 μ g/ml EGF stock (BD Biosciences), prepared in H_2O and kept on ice
- DMSO (vehicle; Sigma-Aldrich)
- 250 mM DAz-2 (Cayman Chemicals) or DYn-2 (Cayman Chemicals), prepared in DMSO

- Modified RIPA lysis buffer supplemented with EDTA-free protease inhibitors and 200 U/ml catalase (see recipe)
 - PBS, 1X (Boston BioProducts)
 - BCA protein assay (Pierce)
 - 5 mM biotin tag (biotin alkyne or azide; Invitrogen) in DMSO *or* 5 mM fluorescent tag (TAMRA or AlexaFluor488 azide; Invitrogen) in DMSO
 - 50 mM TCEP (Sigma-Aldrich), prepared fresh in H₂O
 - 2 mM TBTA (Sigma Aldrich), prepared in 4:1 DMSO: *t*-butanol. TBTA can also be synthesized by published methods (29).
 - 50 mM CuSO₄, prepared fresh in H₂O
 - 0.5 M EDTA (Boston BioProducts)
 - 10% SDS, prepared in H₂O
 - Laemmli sample buffer, 2X with 10% β -mercaptoethanol (BioRad)
 - Mini-Protean TGX 4-15% Tris-Glycine protein gels (BioRad)
1. Grow A431 cells to 75-80% confluency in DMEM complete culture medium.

Our cells are grown in 100 mm tissue culture dishes. All volumes used in the remainder of this protocol are reported with respect to 100 mm dishes.

2. Remove the DMEM complete culture medium, wash plates 3X with PBS, and incubate cells in 10 ml serum-free DMEM for 16 h at 37 °C.

Culture medium and other cell culture reagents (e.g. 0.25% trypsin) should always be pre-warmed to 37 °C prior to use in an experiment. Cells are very

sensitive to changes in temperature and all precautions should be taken in order to avoid sudden alterations in culture environment.

3. After serum-starvation, remove the serum-free DMEM and wash plates 3X with PBS.
4. Add 5 ml of serum-free DMEM containing 100 ng/ml EGF to each plate of cells and stimulate for 5 min at 37 °C.

A control should be performed in parallel using unstimulated cells in order to assess EGF-dependent changes in protein sulfenylation.

5. At the end of the incubation period, remove the stimulation medium and wash plates 3X with PBS.
6. Lift cells with 0.25% trypsin. Add 5 ml of serum-free DMEM to quench trypsin, and collect cells by centrifugation for 2 min at $1500 \times g$ at rt.
7. Remove medium and resuspend cells in serum-free DMEM at a density of $3-4 \times 10^6$ cells/ml.

One 100 mm plate of A431 cells will typically yield $\sim 3 \times 10^6$ cells. Accordingly, we resuspend each plate in 800 μ l serum-free DMEM and transfer 400 μ l aliquots of cell suspension to 1.5 ml microcentrifuge tubes for labeling experiments.

8. Label cells with 5 mM DAz-2 or DYn-2 (from 250 mM probe stock).

To 400 μ l of cell suspension add 8.2 μ l DAz-2 or DYn-2 to each sample and gently mix. DMSO should be used as concurrent vehicle control for all probe-labeling experiments.

9. Incubate cell labeling reactions for 1 h at 37 °C.

After 30 min, gently mix cells. Labeling times may range from 15 min to 2 h. This variable is cell- and stimulant-type dependent.

10. After cell labeling, remove excess probe by washing cells 3X with PBS (500 μ l, 2 min at 1500 \times g) at rt.

At this point, washed cell pellets can be frozen in liquid N₂ and stored at -80 °C. Otherwise, we recommend continuing the experiment up to the precipitation step.

11. Lyse cells in modified RIPA lysis buffer for 20 min on ice.

Cell lysis can be aided by vortexing or pipetting up and down.

12. Clear lysate of cell debris by centrifuging for 20 min at 16,000 \times g, 4 °C.

13. Quantify protein content of cleared cell lysate using a standard BCA assay.

Protein concentrations typically range from 2-8 mg/ml, depending on the cell type.

14. If a biotin tag is used to detect labeled proteins by Western blot, a pre-clear step is recommend to remove endogenous biotinylated proteins prior to click chemistry. If a fluorescent tag is used to detect labeled proteins by in-gel fluorescence, the pre-clear step can be omitted and the user may continue to the next step of this protocol.

Please refer to Support Protocol 1 for the pre-clear step.

15. Transfer 100 μ g cell lysate to 1.5 microcentrifuge tubes for each sample.
16. Detect probe-labeled proteins via click chemistry. The total volume of the click chemistry reaction should be 100 μ l. Add the reaction components in the following order to each sample and mix well:

- a. 89 μl cell lysate (100 μg)

Make up any remaining volume with the modified RIPA lysis buffer.

- b. 2 μl of 5 mM biotin or fluorescent reporter tag (final concentration of 100 μM)
- c. 2 μl of 50 mM TCEP (final concentration of 1 mM)
- d. 5 μl of 2 mM TBTA (final concentration of 100 μM)
- e. 2 μl of 50 mM CuSO_4 (final concentration of 1 mM)

17. Rock click chemistry reactions for 1 h at rt.

If a fluorescent tag is used (i.e. TAMRA or AlexaFluor488 azide) perform reactions in the dark. In addition, take all necessary precautions to carry out the remaining steps of the experiment in the dark if a fluorescent reagent is used.

18. Quench the click chemistry reactions with 40 mM EDTA (from 0.5 M stock). Rock the reactions for 5 min at rt.

EDTA chelates any remaining copper, thereby quenching the click chemistry reaction.

19. Perform a methanol or methanol/chloroform precipitation of the protein.

- a. Support Protocol 2 Methanol precipitation
- b. Support Protocol 3 Methanol/chloroform precipitation

Either precipitation method works well with our protocol and the choice is dictated by user preference.

20. Add 20 μl 10% SDS to dissolve protein pellets.

A bath sonicator may be used at this step to help re-solubilize the protein pellets.

21. Add 20 μ l Laemmli sample buffer, 2X (10% β -ME) to each sample and mix well.
22. Boil the protein samples for 10 min at 95 °C using a heating block.
23. Vortex the samples and centrifuge for 1 min at 16,000 \times g, rt.
24. Resolve samples by SDS-PAGE using Mini-Protean TGX 4-15% Tris-Glycine gels.

Typically, 25 μ g protein/lane is adequate to detect protein sulfenylation.

25. Analyze experimental results with the detection method of choice.
 - a. Basic Protocol 4 Western blot
 - i. Figure A.4a DAZ-2/Biotin Alkyne
 - ii. Figure A.4b DYn-2/Biotin Azide
 - b. Basic Protocol 5 In-gel fluorescence
 - i. Figure A.4c DYn-2/TAMRA Azide
 - ii. Figure A.4d DYn-2/AlexaFluor488 Azide

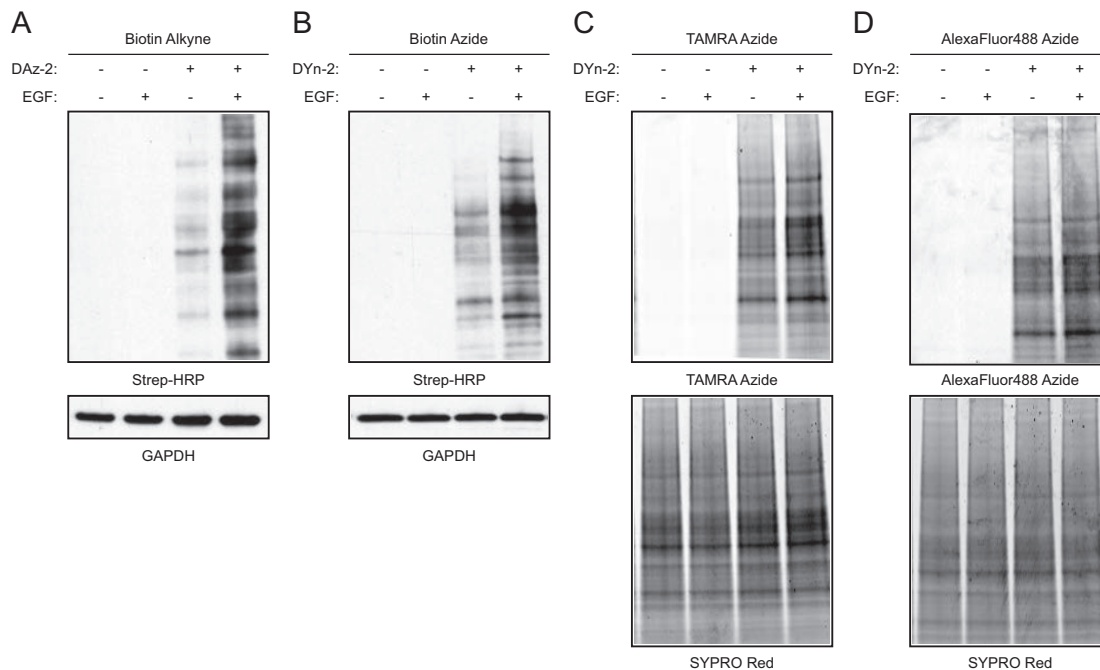


Figure A.4: **Detection of EGF-mediated protein sulfenylation in A431 cells.** A431 cells were stimulated with 100 ng/ml EGF for 5 min. EGFR activation leads to the production of endogenous H_2O_2 and concomitant changes in protein sulfenylation. Cells were labeled with DAz-2 or DYn-2 for 1 hr. Sulfenylated proteins can be detected by streptavidin-HRP immunoblot (A-B) or in-gel fluorescence (C-D). Equal protein loading is demonstrated by reprobing the immunoblot with antibodies to GAPDH (immunoblot) or by SYPRO red dye staining of the SDS-PAGE gel (fluorescence).

Basic Protocol 3

LABELING EXOGENOUS SULFENYLATED PROTEINS IN CELL SUSPENSION.

The following is a standard protocol for live cell labeling of sulfenyl modifications in HepG2 cells, which are easy to subculture and manipulate. In this protocol, exogenous H₂O₂ is applied directly to cells as opposed to ligand stimulation of endogenous H₂O₂ production. The user is also welcome to substitute HeLa cells for HepG2 cells in these experiments (16).

Materials

- HepG2 cells (ATCC)
- MEM complete culture medium (MEM supplemented with 10% FBS, 1% GlutaMax, 1% MEM nonessential amino acids, and 1% penicillin-streptomycin; Invitrogen)
- MEM with 0.5% FBS (MEM supplemented with 0.5% FBS; Invitrogen)
- 0.25% trypsin (Invitrogen)
- 100 mM H₂O₂ stock (Sigma-Aldrich), prepared fresh in H₂O and maintained on ice
- DMSO (vehicle; Sigma-Aldrich)
- 250 mM DAz-2 (Cayman Chemicals) or DYn-2 (Cayman Chemicals), prepared in DMSO
- Modified RIPA lysis buffer supplemented with EDTA-free protease inhibitors and 200 U/ml catalase (see recipe)
- PBS, 1X (Boston BioProducts)

- BCA protein assay (Pierce)
 - 5 mM biotin tag (biotin alkyne or azide; Invitrogen) in DMSO or 5 mM fluorescent tag (TAMRA or AlexaFluor488 azide; Invitrogen) in DMSO
 - 50 mM TCEP (Sigma-Aldrich), prepared fresh in H₂O
 - 2 mM TBTA (Sigma Aldrich), prepared in 4:1 DMSO: *t*-butanol
 - 50 mM CuSO₄, prepared fresh in H₂O
 - 0.5 M EDTA (Boston BioProducts)
 - 10% SDS, prepared in H₂O
 - Laemmli sample buffer, 2X with 10% β-mercaptoethanol (BioRad)
 - Mini-Protean TGX 4-15% Tris-Glycine protein gels (BioRad)
1. Grow HepG2 cells to 75-80% confluency in MEM complete culture medium.

Our cells are grown in 100 mm tissue culture dishes. All volumes used in the remainder of this protocol are reported with respect to 100 mm dishes. Culture medium and other cell culture reagents (e.g. 0.25% trypsin) should always be pre-warmed to 37 °C prior to use in an experiment.

2. Remove MEM complete culture medium, and wash plates 3X with PBS. 3. Add 5 ml MEM (0.5% FBS) containing 500 μM H₂O₂ to each plate. Incubate cells with H₂O₂ for 5 min at 37 °C.

A control should be performed in parallel using untreated cells in order to assess H₂O₂ -dependent changes in protein sulfenylation.

3. Remove MEM (0.5% FBS) containing 500 μM H₂O₂. Wash plates 3X with PBS.

4. Continue the rest of the experiment as in Basic Protocol 2, steps 6 to 25.

For HepG2 cells, take care to use MEM (0.5% FBS) medium throughout the rest of the experiment.

5. Expected results for HepG2 cells can be found in:

a. Figure A.5a DAz-2/Biotin Alkyne

b. Figure A.5b DYn-2/Biotin Azide

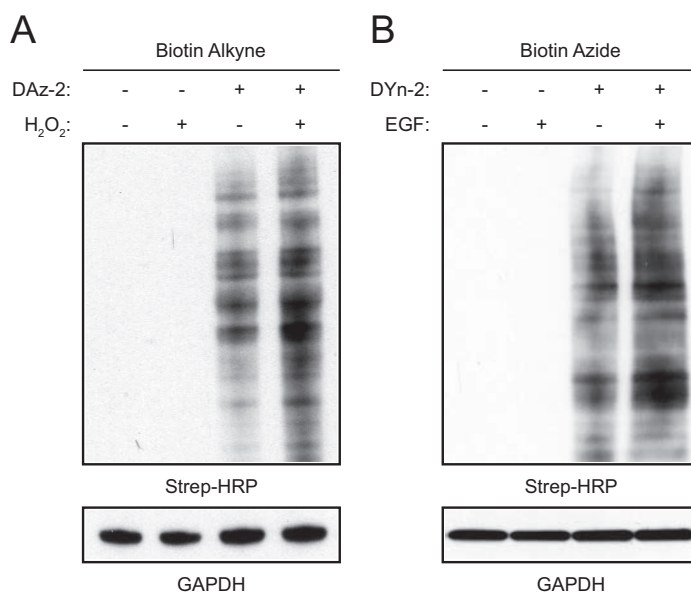


Figure A.5: **Global changes of protein sulfenylation in HepG2 cells exposed to exogenous H₂O₂.** HepG2 cells were treated with 500 μ M H₂O₂ for 5 min. Cells were labeled with DAz-2 or DYn-2 for 1 hr. Sulfenylated proteins can be detected by streptavidin-HRP immunoblot (A-B) or in-gel fluorescence (not shown). Equal protein loading is demonstrated by reprobing the immunoblot with antibodies to GAPDH (immunoblot).

Basic Protocol 4

WESTERN BLOT DETECTION OF BIOTINYLATED PROTEINS

The following is a standard protocol for Western blot detection of biotinylated proteins. After completing Basic Protocol 1, 2, or 3, the user should refer to this section if a biotin tag (*i.e.* biotin alkyne or azide) was employed during the click chemistry step.

Materials

- SDS-PAGE gel with resolved samples
 - PVDF membrane, 0.2 μm (BioRad)
 - TBST (Boston BioProducts)
 - 3% BSA (Fisher), prepared in TBST
 - Streptavidin-HRP antibody (GE-Healthcare)
 - GAPDH antibody (Santa Cruz Biotechnology)
 - Rabbit anti-mouse IgG-HRP (Invitrogen)
 - ECL Plus Western Blot Detection System (GE Healthcare)
1. Transfer SDS-PAGE gel with samples of interest onto a PVDF membrane using standard Western blot transfer techniques (30).
 2. After transfer, block the PVDF membrane with 3% BSA for 1 h at rt.
 3. Wash the membrane 2X with TBST for 10 min.
 4. Incubate the membrane with streptavidin-HRP (1: 80,000) for 1 h at rt.

All antibodies in this protocol should be diluted in TBST.

5. After antibody incubation, wash the membrane 2X with TBST for 10 min.
6. Develop the membrane with chemiluminescence using the ECL plus Western blot detection system, as indicated by the manufacturer's (GE Healthcare) instructions.
7. Image the results by film.
8. After imaging, re-block the membrane with 3% BSA for 1 h at rt.
9. Wash the membrane 2X with TBST for 10 min.
10. Incubate the membrane with GAPDH primary antibody (1: 200) for 1 h at rt.

GAPDH serves as a loading control. Other protein standards may be used, as necessary.

11. After primary antibody incubation, wash the membrane 2X with TBST for 10 min.
12. Incubate the membrane with rabbit anti-mouse HRP (1: 50,000) for 1 h at rt.
13. After secondary antibody incubation, wash the membrane 2X with TBST for 10 min.
14. Develop the membrane with chemiluminescence using the ECL plus Western blot detection system, as indicated by the manufacturer's instructions.
15. Image the results by film.

Basic Protocol 5

IN-GEL DETECTION OF FLUOROPHORE-TAGGED PROTEINS

The following is a standard protocol for in-gel detection of fluorophore-tagged proteins. After completing Basic Protocol 1, 2, or 3, the user should refer to this

section if a fluorescent tag (i.e. TAMRA or AlexaFluor488 azide) was used during the click chemistry step.

Materials

- SDS-PAGE gel with resolved samples
 - Destain solution (see recipe)
 - Wash solution (see recipe)
 - SYPRO Ruby Protein Stain (BioRad)
 - Fluorescence gel scanner (e.g. Amersham Biosciences Typhoon 9400 variable mode imager)
1. Destain SDS-PAGE gel with the samples of interest 2X with destain solution for 10 min.

The gel should be rocked during the destaining process. This step is necessary to remove any background fluorescence from excess reagents. Gels should be handled carefully during all destain and wash steps to avoid background smudging.

2. Wash the gel with H₂O for 10 min, while rocking.
3. Scan the gel using a fluorescence gel scanner.

We use a Typhoon 9400 variable mode imager (Amersham Biosciences) for in-gel fluorescence analysis. The fluorescent reagents used in this protocol have the following excitation and emission wavelengths:

- a. TAMRA Azide 555/580 nm (ex/em)
- b. AlexaFluor488 Azide 495/519 nm (ex/em)

4. After visualizing results from the fluorescent reagent of choice, soak gel in destain solution for 30 min.
5. Stain gel with SYPRO ruby protein stain to demonstrate equal protein loading, as indicated by the manufacturers instructions.

The SYPRO ruby signal can typically be seen after 3 h incubation. After staining, the gel can be washed 2X with wash solution for 10 min, and 1X with H₂O for 10 min prior to imaging. SYPRO ruby has the following excitation and emission wavelengths: 280 or 450/610 nm (ex/em).

Support Protocols

Support Protocol 1

PRE-CLEARING CELL LYSATES OF ENDOGENOUS BIOTINYLATED PROTEINS

The following is a standard protocol to pre-clear cell lysates of endogenous biotinylated proteins prior to the click chemistry step.

Materials

- Cell lysates
 - Modified RIPA buffer (see recipe)
 - NeutrAvidin agarose resin (Pierce)
1. Aliquot NeutrAvidin resin into 1.5 ml microcentrifuge tubes for each sample.

To pre-clear 100 µg cell lysate, use 50 µl of NeutrAvidin resin.

2. Pre-equilibrate NeutrAvidin resin with modified RIPA buffer (3 × 500 µl) for 2 min at 2300 × g.

After the last wash, take care to completely remove modified RIPA buffer to maintain consistent protein concentration between each sample.

3. Load 100 μg cell lysate onto pre-equilibrated NeutrAvidin resin. Make up any remaining volume with the modified RIPA lysis buffer.

The click chemistry reaction is the next step of the protocol, and these reactions should have a total volume of 100 μl for 100 μg cell lysate (i.e. final protein concentration = 1mg/ml). It is important to maintain this volume during the pre-clear step and to consider the subsequent volume of added click chemistry reagents. For example, the volume of the cell lysate loaded onto the NeutrAvidin resin for the pre-clear step should not exceed 89 μl for 100 μg cell lysate as the remaining volume (11 μl) will be the click chemistry reagents.

4. Rock pre-cleared samples for 30 min at 4 $^{\circ}\text{C}$.
5. To collect pre-cleared cell lysate, centrifuge sample for 2 min at 2,300 \times g, rt. Transfer cell lysate to a clean 1.5 ml microcentrifuge tube. Discard NeutrAvidin resin used for the pre-clear step.

The cell lysates are now free of endogenous biotinylated proteins. Continue with the rest of the Basic Protocol 2 for A431 cells or Basic Protocol 3 for HepG2 cells.

Support Protocol 2

METHANOL PRECIPITATION OF PROTEINS.

The following is a standard protocol for methanol precipitation of proteins after click chemistry. Alternatively, the user may choose to perform a methanol/chloroform (Support Protocol 3) precipitation.

Materials

- Click chemistry reaction of cell lysate
 - Methanol, ice-cold
1. Add 1 ml ice-cold methanol to each sample and vortex to mix.
 2. Allow proteins to precipitate overnight at $-80\text{ }^{\circ}\text{C}$.
 3. Collect protein pellet by centrifuging the samples for 10 min at $16,000 \times g$, $4\text{ }^{\circ}\text{C}$.
 4. Carefully remove methanol, being careful not to disturb the protein pellet. Wash the protein pellet with 1 ml ice-cold methanol.

The second methanol wash is necessary to remove any residual click chemistry reagents.

5. Centrifuge samples for 10 min at $16,000 \times g$, $4\text{ }^{\circ}\text{C}$.
6. Carefully remove the methanol, leaving the protein pellet behind. Continue with the rest of the protocol.

Make sure to remove all traces of excess methanol prior to continuing to the next step of the experiment.

Support Protocol 3

METHANOL/CHLOROFORM PRECIPITATION OF PROTEINS

The following is a standard protocol for methanol/chloroform precipitation of proteins after click chemistry.

Materials

- Click chemistry reaction of cell lysate
 - Methanol, ice-cold
 - Chloroform, ice-cold
 - H₂O, ice-cold
1. To perform a methanol/chloroform precipitation, add the precipitation components in the following order to each sample. Vortex the sample after the addition of each component to mix.
 - a. 600 μ l of methanol
 - b. 150 μ l of chloroform
 - c. 400 μ l of H₂O
 2. Centrifuge the samples for 10 min at 16,000 \times g, 4 °C.
 3. Carefully remove and discard as much of the upper aqueous layer as possible, without disturbing the interface layer containing the protein precipitate.
 - *A thin interface layer containing the precipitated protein should form between the upper aqueous layer and the lower organic layer.*
 4. Add 1 ml ice-cold methanol to each sample and vortex to mix.
 5. Centrifuge the samples for 10 min at 16,000 \times g, 4 °C.

6. Carefully remove methanol, being careful not to disturb the protein pellet. Wash the protein pellet with 1 ml ice-cold methanol.
 - *The second methanol wash is necessary to remove any residual click chemistry reagents.*
7. Centrifuge samples for 10 min at $16,000 \times g$, 4°C .
8. Carefully remove methanol, leaving the protein pellet behind. Allow any remaining methanol or chloroform to evaporate by leaving the sample tubes open on the bench. Allow protein pellet to air-dry for 30 min to 1 h at rt. Continue with the rest of the protocol.
 - *The dried protein pellet will be thin and have a translucent white color. It is crucial to allow the protein pellet to completely dry prior to proceeding with the rest of the experiment. If it is not dry, the protein pellet will be extremely difficult to resuspend.*

Alternate Protocols

Alternate Protocol 1

ON-PLATE LABELING OF ENDOGENOUS PROTEIN SULFENYLATION IN CELLS.

The following is a standard protocol for labeling cells that remain attached to the plate. Although we observe comparable results for suspension versus plate detection of sulfenyl modifications (Figure A.4 a and Figure A.6 a), labeling cells in suspension may not provide ideal for some cell lines or stimulants. The user should determine which labeling method is best for their purposes.

Materials

1. Follow steps 1-5 in Basic Protocol 2.
 - *For on-plate labeling, cells can be grown in 60 mm tissue culture dishes to reduce probe consumption. Media volumes should be adjusted accordingly for smaller culture plates. For example, EGF stimulation should be performed with 2 ml for 60 mm plates, instead of 5 ml for 100 mm plates.*
2. Add 2 ml serum-free DMEM containing 5 mM DAz-2 or DYn-2 (from 250 mM probe stock) to each plate of cells.
 - *For 2 ml medium, 40.8 μ l of 250 mM DAz-2 or DYn-2 is needed to achieve a final concentration of 5 mM. In addition, a DMSO vehicle control should always be included for unstimulated and EGF-stimulated cells.*
3. Label cells for 1 h at 37 °C.
4. Remove serum-free DMEM containing 5 mM DAz-2 or DYn-2. Wash the plates 3X with PBS.
5. Lyse cells in modified RIPA lysis buffer using a rubber policeman. Transfer cell lysates to a clean 1.5 ml microcentrifuge tube.
6. Follow steps 11-25 in Basic Protocol 2.
7. Expected results for on-plate labeling of protein sulfenyl modifications in A431 cells can be found in:
 - a. Figure A.6a DAz-2/Biotin Alkyne

Time-dependent labeling of A431 cells that remain attached to the plate indicates that 1 h yields the best results.

Alternatie Protocol 2

ON-PLATE LABELING OF EXOGENOUS PROTEIN SULFENYLATION IN CELLS

The following is a standard protocol for on-plate labeling of sulfenylated proteins in HepG2 cells.

Materials

See materials list for Basic Protocol 3

1. Follow steps 1-4 in Basic Protocol 3.

For on-plate labeling, cells can be grown in 60 mm tissue culture dishes to reduce probe consumption. Media volumes should be adjusted accordingly for smaller culture plates. For example, the H₂O₂ stimulation should be performed with 2 ml for 60 mm plates, instead of 5 ml for 100 mm plates.

2. Add 2 ml MEM (0.5% FBS) containing 5 mM DAz-2 or DYn-2 (from 250 mM probe stock) to each plate of cells.

For 2 ml medium, 40.8 μ l of 250 mM DAz-2 or DYn-2 is needed to achieve a final concentration of 5 mM. In addition, a DMSO control should always be included for untreated and H₂O₂-exposed cells.

3. Label cells for 1 h at 37 °C.
4. Remove MEM (0.5% FBS) containing 5 mM DAz-2 or DYn-2. Wash the plates 3 \times with PBS.
5. Lyse cells in modified RIPA lysis buffer using a rubber policeman. Transfer cell lysate to a clean 1.5 ml microcentrifuge tube.
6. Follow steps 11-25 in Basic Protocol 2.

7. Expected results for on-plate labeling of HepG2 cells can be found in:

a. Figure A.6b DAz-2/Biotin Alkyne

Time-dependent labeling of HepG2 cells that remain attached to the plate indicates that 1 h yields the best results.

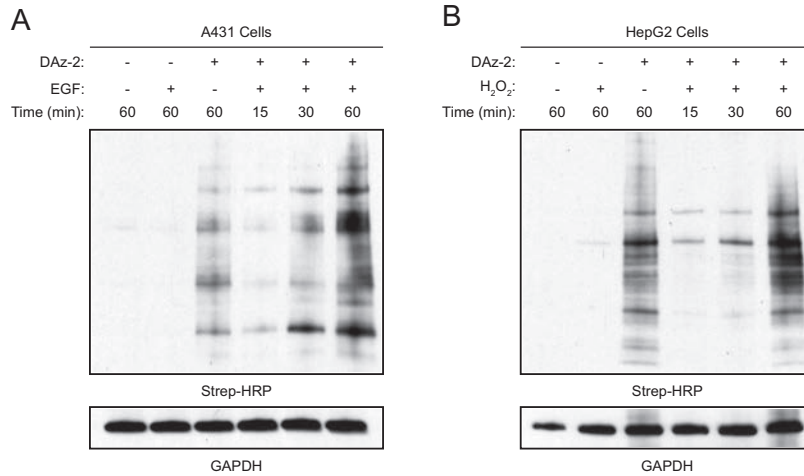


Figure A.6: **Labeling and detection of protein sulfenylation in adherent A431 and HepG2 cells.** Cells were exposed to 100 ng/ml EGF (A431) or 500 μ M H₂O₂ (HepG2) for 5 min. After treatment, cells remained attached to the tissue culture plate and were labeled with DAz-2 for the indicated times. Sulfenylated proteins were visualized by streptavidin-HRP immunoblot for (A) A431 cells and (B) HepG2 cells. Equal protein loading is demonstrated by reprobing the immunoblot with antibodies to GAPDH (immunoblot).

Reagents And Solutions

Use Milli-Q purified water in all recipes and protocol steps.

Tris labeling buffer, pH 7.4

50 mM Tris-HCl, pH 7.4

150 mM NaCl

Sterilize by passing through a 0.2- μ m filter and store for up to 6 months at rt.

Click labeling buffer, pH 7.4

50 mM triethanolamine, pH 7.4

1% SDS

Sterilize by passing through a 0.2- μ m filter and store for up to 6 months at rt.

Modified RIPA lysis buffer, pH 7.4

50 mM triethanolamine, pH 7.4

150 mM NaCl

1% NP-40

1% sodium deoxycholate

0.1% SDS

Sterilize by passing through a 0.2- μ m filter and store for up to 1 month at rt.

Shortly before use, add EDTA-free complete mini protease inhibitors (Roche) according to the manufacturer's instructions and 200 U/ml catalase (Sigma-Aldrich).

Destain solution

40% methanol

50% H₂O

10% acetic acid

Mix 400 ml methanol, 500 ml H₂O, and 100 ml acetic acid to make 1 L destain solution. Store for up to 1 year at rt.

Wash solution

10% methanol

70% H₂O

10% acetic acid

Mix 100 ml methanol, 700 ml H₂O, and 100 ml acetic acid to make 1 L wash solution. Store for up to 1 year at rt.

Commentary

Background Information

Historically, methods to detect reactive cysteines and H₂O₂-mediated oxidation of protein thiols require the homogenization of cells, which disrupts the native environment. Under these conditions, cellular redox balance and protein structure are compromised, leading to artifactual oxidation during sample processing. This core issue is typically ignored in redox proteomic studies, but casts a pall on the biological significance of such data. To address this problem, we have developed small-molecule probes that enable sulfenylated proteins to be trapped and tagged directly in cells. Using this new approach, we have dissected the molecular mechanism of H₂O₂-sensing in

yeast (25), reported the first *in situ* proteomic study of protein sulfenylation in mammalian cells (16), uncovered striking differences in sulfenylation profiles among breast cancer subtypes (31), discovered a bacterial protein that functions in desulfenylation (14), and demonstrated that sulfenylation functions a global signaling mechanism akin to phosphorylation during EGFR signaling (17). Clearly, selective chemical reporters have opened the door to a better understanding of the important biological role of protein cysteine sulfenylation.

Our first global analysis of sulfenylated proteins in HeLa cells revealed that potentially modulatory cysteine residues exist in almost 200 individual proteins, including kinases, phosphatases, transporters, GTPases, and transcription factors, thereby extending this form of redox regulation to a wide range of biological activities (16). Nonetheless, the vast majority of H₂O₂-sensitive protein cysteine residues await identification. This is a vigorous area of research in our lab and, towards this end we have developed two complementary isotope-coded probe pairs to quantify changes in protein sulfenylation (**9-10** and **4-5**; Figure A.1 c) (21, 22). Most recently, we have reported reagents to selectively monitor reversible oxidation of PTPs by adding an active site-targeting module to the sulfenyl probes (**10, 11**; Figure A.1 c) (15).

Critical Parameters and Trouble Shooting

The order in which reagents are added during experiments to purified protein *in vitro* or cells is an important consideration. In general, we add the ligand stimulant (or H₂O₂) before the probe-labeling step. However, this parameter should be investigated on a case-by-case basis, in addition to dose and time-dependent changes in labeling.

For cell labeling experiments, cells should be cultured carefully without sudden changes in the culture environment. For example, culture reagents such as media and trypsin should be pre-warmed to 37 °C prior to use. Depending on the cell line, culture media should be replenished every 2-3 days. As with many biological

processes studied in a cell culture model, the confluency at the time of stimulation and labeling can impact the final results. If stimulant- or H₂O₂-dependent changes in protein sulfenylation are difficult to discern, a number of factors should be checked. All stocks (ligand stimulant and probes) should always be kept on ice during the experiment and otherwise stored at -30 °C when not in use. In addition, lysis buffer and cell lysates should be kept on ice at all times. Once cells have been stimulated, downstream wash and lifting steps should be carried out in a timely manner. Any unnecessary delays in sample handling prior to cell lysis should be avoided, as this may also affect final results. Additionally, for maximum probe potency, culture media used during cell labeling should not exceed 0.5% FBS.

Click chemistry reactions should always be performed with fresh TCEP and CuSO₄ stocks. We typically make these stocks up fresh directly before setting up the reactions. TCEP can oxidize over time, which would reduce the efficiency of the reaction since it is required for reduction of CuSO₄ to Cu(I). In addition, the second methanol wash in both precipitation procedures is crucial in order to completely remove excess click chemistry reagents. Failure to do so may result in higher background signals during the visualization process. If equal loading is not observed, it is also important to ensure that the protein pellets are completely re-solubilized. In some cases, this can be a challenge, particularly for samples that have been methanol/chloroform precipitated. Protein pellets must be completely free of chloroform prior to re-solubilization, otherwise they will not fully return to solution.

For in-gel fluorescence experiments, special precautions should be taken once the fluorescent tag is added to the sample. Steps such as the click chemistry reaction, SDS-PAGE analysis, and destaining should be done in the dark to avoid sample bleaching. During SDS-PAGE analysis, the dye front should be run completely off the gel during electrophoresis to remove any unincorporated fluorescent tag and minimize background fluorescence. Gels should also be thoroughly destained and washed prior

to imaging. In addition, only clean gloves and containers should be used to handle the gels. Because in-gel fluorescence is an extremely sensitive technique, faulty gel handling can lead to fingerprints and smudges during the visualization process. Gels should only be handled on the edges as carefully as possible, to avoid undesirable blemishes on the scanned image.

Anticipated Results

Anticipated results for labeling of sulfenic acids in a purified protein (GAPDH) can be found in Figure A.3 for both Western blot (Figure A.3 a and b) and in-gel fluorescence detection (Figure A.3 c and d). It is expected that the active site cysteine should exhibit a robust H_2O_2 -dependent increase in probe labeling. If a peroxide dependent effect is not observed in the protein of interest, it is possible that the cysteine(s) are not H_2O_2 -sensitive or that the basal level of oxidation is high. Similarly, anticipated results for labeling of protein sulfenylation in cells (A431) with a stimulant (EGF) that leads to endogenous production of H_2O_2 can be found in Figure A.4 and Figure A.6 for Western blot (Figure A.4 a, b, and Figure A.6 a) and in-gel fluorescence detection (Figure A.4 c and d). If a stimulant induces endogenous H_2O_2 production, an increase in sulfenylated proteins should be observed. Finally, we provide a protocol for cells (HepG2) stimulated with H_2O_2 so that the user may develop and hone their skills as necessary (Figure A.5 a, b, and Figure A.6 b). DMSO vehicle control lanes should have negligible background signal. In cell lysate samples that have been pre-cleared with NeutrAvidin agarose resin, signal may still be evident at ~ 66 and 97 kDa. In fact, these bands may be observed for unlabeled and probe-labeled samples. This is not cause for major concern and indicates that biotinylated proteins could not be completely depleted from samples. Results can be considered successful if the signal from probe-labeled samples is higher than the control lanes, and if a stimulant-dependent increase of signal is observed. If the user

finds it difficult to observe the desired stimulant-dependent response, a number of solutions can be explored. Simple adjustments such as changing the concentration of the probe, stimulant, labeling times, and protein loading should be considered (see Strategic Planning or Critical Parameters and Troubleshooting for more detailed explanations). The sensitivity of the detection method can also be a factor and thus, Western blot and in-gel fluorescence should both be explored.

Time Considerations

The experiments outlined in this protocol can typically be completed between 2-3 days from labeling to detection of sulfenylated proteins. Experiments with purified protein *in vitro* (Basic Protocol 1) can be paused after sample buffer has been added to click chemistry reactions (6-8 h). Western blot or in-gel fluorescence detection can be carried out on the same or following day, depending on the user. Live cell experiments (Basic Protocol 2 and 3) can be paused at the methanol or methanol/chloroform precipitation step (6-8 h). For live cell experiments, detection of sulfenylated proteins should be performed the next day after samples have been resuspended. Additionally, the user may pause the experiment directly after the cells are labeled with DAz-2 or DYn-2. After washing cells to remove labeling media, cell pellets can be harvested and stored at -80 °C (see Basic Protocol 2, step 10). However, after cell lysis we recommend that the experiment be continued to the precipitation step to avoid compromising the click chemistry reaction. We highly encourage the user to explore Basic Protocol 2 with other cell types and stimulants relevant to their own research programs, but to be aware that optimizing their system may take some time.

Acknowledgements

The authors acknowledge funding from the Camille Henry Dreyfus Teacher Scholar Award (to K.S.C.) and the American Heart Association Scientist Development Award (0835419N to K.S.C.) for support of this work. The authors also gratefully acknowledge Crystal L. Yan for her assistance with experiments.

Chapter References

1. Dickinson, B. C. & Chang, C. J. (2011). Chemistry and biology of reactive oxygen species in signaling or stress responses. *Nat Chem Biol*, 7(8), 504–11.
2. Rhee, S. G. (2006). Cell signaling. h_2O_2 , a necessary evil for cell signaling. *Science*, 312(5782), 1882–3.
3. Lambeth, J. D. (2004). Nox enzymes and the biology of reactive oxygen. *Nat Rev Immunol*, 4(3), 181–9.
4. Paulsen, C. E. & Carroll, K. S. (2010). Orchestrating redox signaling networks through regulatory cysteine switches. *ACS Chem Biol*, 5(1), 47–62.
5. Reddie, K. G. & Carroll, K. S. (2008). Expanding the functional diversity of proteins through cysteine oxidation. *Curr Opin Chem Biol*, 12(6), 746–54.
6. Rhee, S. G., Bae, Y. S., Lee, S. R., & Kwon, J. (2000, October). Hydrogen peroxide: a key messenger that modulates protein phosphorylation through cysteine oxidation. *Sci STKE*, 2000(53), pe1. doi:10.1126/stke.2000.53.pe1
7. Winterbourn, C. C. (2008). Reconciling the chemistry and biology of reactive oxygen species. *Nat Chem Biol*, 4(5), 278–86.
8. Benitez, L. V. & Allison, W. S. (1974). The inactivation of the acyl phosphatase activity catalyzed by the sulfenic acid form of glyceraldehyde 3-phosphate dehydrogenase by dimedone and olefins. *J Biol Chem*, 249(19), 6234–43.
9. Crane, E., 3rd, Vervoort, J., & Claiborne, A. (1997, July). ^{13}C nmr analysis of the cysteine-sulfenic acid redox center of enterococcal nadh peroxidase. *Biochemistry*, 36(28), 8611–8618. doi:10.1021/bi9707990
10. Yeh, J. I., Claiborne, A., & Hol, W. G. (1996, August). Structure of the native cysteine-sulfenic acid redox center of enterococcal nadh peroxidase refined at 2.8 Å resolution. *Biochemistry*, 35(31), 9951–9957. doi:10.1021/bi961037s
11. Wood, Z. A., Schroder, E., Robin Harris, J., & Poole, L. B. (2003). Structure, mechanism and regulation of peroxiredoxins. *Trends Biochem Sci*, 28(1), 32–40.
12. Salmeen, A., Andersen, J. N., Myers, M. P., Meng, T. C., Hinks, J. A., Tonks, N. K., & Barford, D. (2003). Redox regulation of protein tyrosine phosphatase 1b involves a sulphenyl-amide intermediate. *Nature*, 423(6941), 769–73.
13. Zheng, M., Aslund, F., & Storz, G. (1998). Activation of the oxyR transcription factor by reversible disulfide bond formation. *Science*, 279(5357), 1718–21.
14. Depuydt, M., Leonard, S. E., Vertommen, D., Denoncin, K., Morsomme, P., Wahni, K., ... Collet, J.-F. (2009). A periplasmic reducing system protects single cysteine residues from oxidation. *Science*, 326(5956), 1109–1111.

15. Leonard, S. E., Garcia, F. J., Goodsell, D. S., & Carroll, K. S. (2011). Redox-based probes (rbps) for protein tyrosine phosphatases. *Angew Chem Int Ed Engl*, *in press*.
16. Leonard, S. E., Reddie, K. G., & Carroll, K. S. (2009). Mining the thiol proteome for sulfenic acid modifications reveals new targets for oxidation in cells. *ACS Chem Biol*, *4*(9), 783–99.
17. Paulsen, C. E., Truong, T. H., Garcia, F. J., Homann, A., Gupta, V., Leonard, S. E., & Carroll, K. S. (2012). Peroxide-dependent sulfenylation of the egfr catalytic site enhances kinase activity. *Nat Chem Biol*, *8*(1), 57–64.
18. Reddie, K. G., Seo, Y. H., Muse Iii, W. B., Leonard, S. E., & Carroll, K. S. (2008). A chemical approach for detecting sulfenic acid-modified proteins in living cells. *Mol Biosyst*, *4*(6), 521–31.
19. Saxon, E. & Bertozzi, C. R. (2000). Cell surface engineering by a modified staudinger reaction. *Science*, *287*(5460), 2007–10.
20. Rostovtsev, V. V., Green, L. G., Fokin, V. V., & Sharpless, K. B. (2002). A step-wise huisgen cycloaddition process: copper(i)-catalyzed regioselective "ligation" of azides and terminal alkynes. *Angew Chem Int Ed Engl*, *41*(14), 2596–9.
21. Seo, Y. H. & Carroll, K. S. (2011). Quantification of protein sulfenic acid modifications using isotope-coded dimedone and iododimedone. *Angew Chem Int Ed Engl*, *50*(6), 1342–5.
22. Truong, T. H., Garcia, F. J., Seo, Y. H., & Carroll, K. S. (2011). Isotope-coded chemical reporter and acid-cleavable affinity reagents for monitoring protein sulfenic acids. *Bioorg Med Chem Lett*, *21*(17), 5015–20.
23. Seo, Y. H. & Carroll, K. S. (2009a). Facile synthesis and biological evaluation of a cell-permeable probe to detect redox-regulated proteins. *Bioorg Med Chem Lett*, *19*(2), 356–9.
24. Poole, L. B., Klomsiri, C., Knaggs, S. A., Furdui, C. M., Nelson, K. J., Thomas, M. J., ... King, S. B. (2007). Fluorescent and affinity-based tools to detect cysteine sulfenic acid formation in proteins. *Bioconjug Chem*, *18*(6), 2004–17.
25. Paulsen, C. E. & Carroll, K. S. (2009). Chemical dissection of an essential redox switch in yeast. *Chem Biol*, *16*(2), 217–25.
26. Charron, G., Zhang, M. M., Yount, J. S., Wilson, J., Raghavan, A. S., Shamir, E., & Hang, H. C. (2009). Robust fluorescent detection of protein fatty-acylation with chemical reporters. *J Am Chem Soc*, *131*(13), 4967–4975.
27. Speers, A. E., Adam, G. C., & Cravatt, B. F. (2003, April). Activity-based protein profiling in vivo using a copper(i)-catalyzed azide-alkyne [3 + 2] cycloaddition. *J Am Chem Soc*, *125*(16), 4686–4687. doi:10.1021/ja034490h

28. Wilson, J. P., Raghavan, A. S., Yang, Y.-Y., Charron, G., & Hang, H. C. (2011, March). Proteomic analysis of fatty-acylated proteins in mammalian cells with chemical reporters reveals s-acylation of histone h3 variants. *Mol Cell Proteomics*, *10*(3), M110.001198. doi:10.1074/mcp.M110.001198
29. Chan, T. R., Hilgraf, R., Sharpless, K. B., & Fokin, V. V. (2004, August). Polytriazoles as copper(i)-stabilizing ligands in catalysis. *Org Lett*, *6*(17), 2853–2855. doi:10.1021/ol0493094
30. Gallagher, S., Winston, S. E., Fuller, S. A., & Hurrell, J. G. R. (2008, July). Immunoblotting and immunodetection. *Curr Protoc Mol Biol*, *Chapter 10*, Unit 10.8. doi:10.1002/0471142727.mb1008s83
31. Seo, Y. H. & Carroll, K. S. (2009b). Profiling protein thiol oxidation in tumor cells using sulfenic acid-specific antibodies. *Proc Natl Acad Sci U S A*, *106*(38), 16163–8.

APPENDIX B

Redox Regulation of Protein Kinases

Abstract

Protein kinases represent one of the largest families of genes found in eukaryotes. Kinases mediate distinct cellular processes ranging from proliferation, differentiation, survival, and apoptosis. Ligand-mediated activation of receptor kinases can lead to the production of endogenous H_2O_2 by membrane-bound NADPH oxidases. In turn, H_2O_2 can be utilized as a secondary messenger in signal transduction pathways. This review presents an overview of the molecular mechanisms involved in redox regulation of protein kinases and its effects on signaling cascades. In the first half, we will focus primarily on receptor tyrosine kinases (RTKs), whereas the latter will concentrate on downstream non-receptor kinases involved in relaying stimulant response. Select examples from the literature are used to highlight the functional role of H_2O_2 regarding kinase activity, as well as the components involved in H_2O_2 production and regulation during cellular signaling. In addition, studies demonstrating direct modulation of protein kinases by H_2O_2 through cysteine oxidation will be emphasized. Identification of these redox-sensitive residues may help uncover signaling mechanisms conserved

within kinase subfamilies. In some cases, these residues can even be exploited as targets for the development of new therapeutics. Continued efforts in this field will further basic understanding of kinase redox regulation, and delineate the mechanisms involved in physiologic and pathological H_2O_2 responses.

Introduction

The response to extracellular stimuli relies on an integrated network of signal transduction pathways that function in a highly coordinated manner. Crosstalk between these networks is modulated in part by phosphorylation of target proteins by protein kinases and the complementary actions of protein phosphatases (1). Initiation of signaling cascades occurs through the activation of receptor tyrosine kinases (RTKs) upon stimulation with growth factors and other ligands. RTKs relay signals downstream through activation of effector proteins, such as non-receptor kinases. Protein kinases (receptor and non-receptor) are among one of the largest families of genes found within eukaryotes. For example, the human genome contains ~ 518 kinase genes, constituting about 1.7% of all human genes (2). Kinases are critical enzymes involved in mediating a number of fundamental processes including the cell cycle, proliferation, differentiation, metabolism, migration, and survival (3, 4). Perturbation of physiologic kinase signaling due to mutations and other genetic alterations can result in aberrant kinase activity and malignant transformation, as characterized in a number of human disease states (5).

During cellular signaling, kinase activity can also be modulated by additional mechanisms in conjunction with phosphorylation. A wealth of evidence now implicates the regulatory role of reactive oxygen species (ROS) in signal transduction networks (6–8). Controlled production of endogenous hydrogen peroxide (H_2O_2) can be induced when stimulants bind to their respective receptors (i.e. RTKs) (9). In turn, H_2O_2 modulates downstream pathways by reacting with specific protein targets

through oxidative modification of key cysteine residues. Protein kinases represent a large number of candidates that are regulated by and utilize H_2O_2 as secondary messengers (10, 11). For more detailed discussion of general concepts underlying redox signaling, the interested reader is referred to the following extensive reviews for additional information on these topics (7, 8, 12–17). Abnormal H_2O_2 production can result in promiscuous damage of biomolecules, and is prevalent in aging and disease states such as human cancers, neurodegenerative disorders, and diabetes (18–20).

In this review, we provide an overview of the molecular mechanisms involved in redox regulation of protein kinases and its effects on downstream signaling cascades. We begin by highlighting key examples of receptor kinases characterized by stimulant-induced H_2O_2 production as well as non-receptor kinases. Components involved in the production and modulation of H_2O_2 levels during kinase signaling will be addressed. In addition, we discuss the functional role of H_2O_2 -mediated signaling with regards to kinase activity. Finally, we shift our focus to examples from the literature that demonstrates direct modulation of protein kinases by H_2O_2 occurs through cysteine oxidation of key residues. Depending on the kinase, direct oxidation can result in activation or deactivation. Continued efforts geared towards identifying protein targets of signal-derived H_2O_2 will further our mechanistic understanding of redox-based kinase signaling, and may lead to the development of new therapeutic strategies.

Evidence for Redox Regulation of Receptor Tyrosine Kinases

RTKs play an important role in recognition and response to stimulant binding. These enzymes are composed of an extracellular ligand binding domain, a transmembrane domain, and an intracellular domain containing a conserved tyrosine kinase core and additional regulatory sequences. The RTKs covered in this review, with the exception of the insulin receptor kinase (IRK), exist as monomers in the cellular membrane. In a simplified model (Figure B.1a), the receptor-ligand interaction

induces receptor dimerization (homo- or hetero-), followed by autophosphorylation of key residues located within the tyrosine kinase core to provide docking sites for binding proteins. Once activated, the RTK relays the signal downstream through non-receptor kinases to mediate a number of biological processes.

Beginning in the 1990s, several groups observed that growth factor stimulation resulted in rapid bursts of intracellular H_2O_2 . Contrary to the preconceived notion that once considered ROS as toxic byproducts of aerobic respiration, ensuing efforts have established that these species can act as secondary messengers. In a landmark study by Finkel and colleagues, platelet-derived growth factor (PDGF)-induced H_2O_2 production was shown to have downstream effects on global Tyr phosphorylation levels, activation of MAPK pathways, DNA synthesis, and chemotaxis (21). Thereafter, epidermal growth factor (EGF) was reported to induce increased endogenous ROS levels upon receptor binding (22). Inhibition of ROS production by peroxide-detoxifying enzymes and chemical inhibitors blocked normal Tyr signaling triggered by growth factor stimulation. These observations, along with additional growth factors (Table B.1), suggest that RTK stimulation may utilize redox-based mechanisms during signal transduction in parallel to protein phosphorylation.

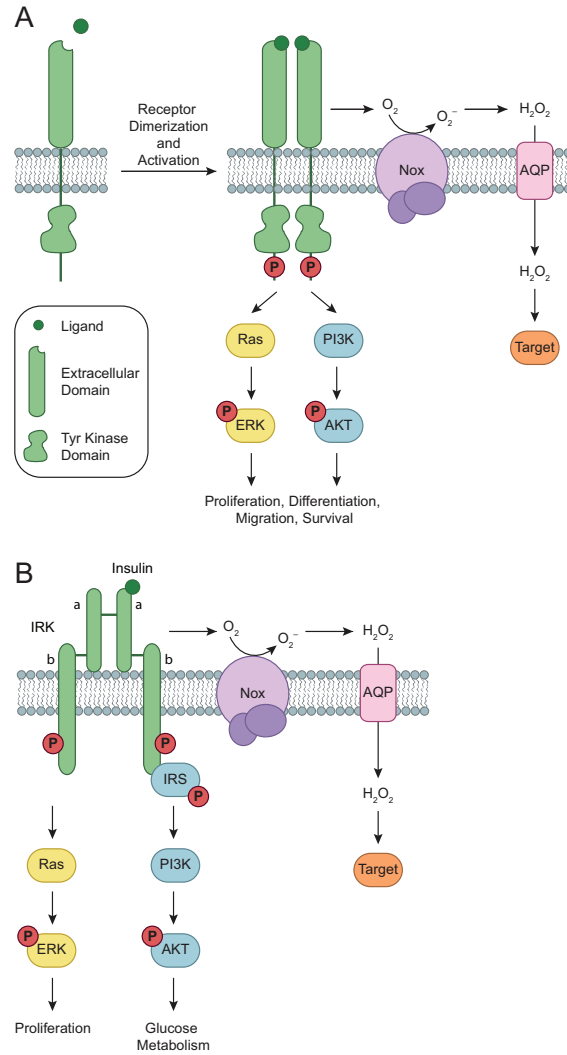


Figure B.1: **Activation of RTKs and downstream signaling cascades.** (a) Growth factors bind to RTKs to induce receptor dimerization, followed by autophosphorylation of key Tyr residues (red circles) located within its cytoplasmic domain. In turn, these phosphorylated Tyr residues serve as docking sites for associating proteins to activate a number of downstream signaling cascades. Two such pathways, Ras/ ERK and PI3K/AKT, are shown here for simplicity. Ligand-receptor interactions also trigger the assembly and activation of Nox complexes, followed by subsequent production of H_2O_2 through spontaneous dismutation or action of SOD. Once formed, endogenous H_2O_2 may pass through specific aquaporin (AQP) channels and/or diffuse across the membrane to reach the intracellular cytosol. Transient increases in H_2O_2 lead to the oxidation of localized redox targets. (b) Unlike other RTKs, IRK exists as a heterotetrameric receptor composed of two extracellular α -subunits and two transmembrane β -subunits. Binding of insulin to IRK α subunits induces a conformational change in its quaternary structure to enable ATP binding, receptor autophosphorylation, and production of Nox-derived H_2O_2 . Once activated, IRK recruits members of the IRS protein family to initiate glucose metabolism through the PI3K/AKT pathway. Insulin signaling also has mitogenic effects that are mediated through Ras/ERK.

Downstream Signaling Pathways Mediated by RTKs

Ligand stimulation of RTKs activates a number of signaling routes that include, but are not limited to the following: 1) Ras/mitogen activated protein kinase (MAPK) pathway, 2) phosphatidylinositol 3' kinase (PI3K)/Akt pathway, or 3) phospholipase C- γ (PLC- γ). RTKs essentially share similar transduction machinery to elicit, in many cases, different cellular responses. In the Ras/MAPK pathway, signaling is triggered in a sequential order (Ras-Raf-MEK-Erk1/2). This pathway is initiated by receptor recruitment of adaptor protein SHC, growth factor receptor-bound protein 2 (Grb2), and a guanine nucleotide exchange protein (SOS) to form a tertiary complex. SOS facilitates GDP exchange to activate the small GTPase Ras. Ras completes the relay by stimulating a kinase cascade through activation of Raf (MAP3K), MEK, and Erk1/2 (MAPK). Upon activation, Erk1/2 (extracellular regulated kinase 1/2) translocates to the nucleus whereby it phosphorylates substrates (\sim 200 known targets to date) ranging from transcription factors, other kinases and phosphatases, and cytoskeletal elements (23, 24). Small fractions of Erk1/2 may localize to other sub-cellular compartments such as the mitochondria, Golgi apparatus, or cell membrane to dictate signal specificity. Erk1/2 regulates cellular proliferation, differentiation, and survival, whereas other MAPKs such as JNK (Jun N-terminal kinase) and p38 function mainly as stress-activated kinases involved in inflammatory response and apoptosis (25, 26). MAPK pathways are known to be subject to redox regulation, albeit mainly through indirect mechanisms occurring upstream (27).

The PI3K/Akt pathway represents a common route activated by RTKs susceptible to redox-based modulation (28). Upon stimulation, PI3K increases the intracellular levels of phosphatidylinositol (3,4,5) triphosphate (PIP₃). PI3K phosphorylates phosphatidylinositol (4,5) bisphosphate (PIP₂) at its 3-hydroxyl position to generate PIP₃. PIP₃ acts as a lipid secondary messenger to activate Akt (also known as PKB, protein kinase B) by binding to its pleckstrin homology (PH) domain (29, 30). This results

in translocation of Akt to the membrane, wherein it undergoes phosphorylation by PDK1 (phosphoinositide dependent kinase 1) and the mTOR (mammalian target of rapamycin)-riCTOR kinase complex to enable full activation. Akt phosphorylates a number of targets (~ 100 known to date) to mediate a vast range of biological processes involved in pro-survival events (31). PI3K/Akt activity is negatively regulated by a dual protein and lipid phosphatase, PTEN (phosphatase and tensin homologue) (32). PTEN modulates PI3K activity by hydrolyzing the 3-phosphate group from PIP₃, and thereby functions as a crucial tumor suppressor in this pathway (33, 34).

Table B.1: Growth factors that induce ROS production

Growth factor	Organism*	ROS source[†]	Effect of stimulant	Reference
PDGF	M, R	Nox	Proliferation, migration	Sundaresan <i>et al.</i> , 1995 Sundaresan <i>et al.</i> , 1996
EGF	H	Nox	Proliferation	Bae <i>et al.</i> , 1997 Miller <i>et al.</i> , 2002
VEGF	H, P	L, Nox	Proliferation, migration, angiogenesis	Colavitti <i>et al.</i> , 2002 Ushio-Fukai <i>et al.</i> , 2002
PGF	B	Nox	Proliferation	Lo & Cruz, 1995
Insulin	M, R	Nox	Glucose, metabolism, glucose uptake/ transport	May & de Haen, 1979b Mahadev <i>et al.</i> , 2001b

* B, bovine; H, human; M, mouse; P, pig; R, rat. † L, lipoxygenase; ND, not determined.

Sources of Reactive Oxygen Species

Biologically relevant ROS include superoxide (O_2^-), hydrogen peroxide (H_2O_2), and the hydroxyl radical (OH). The half-lives of superoxide ($t_{1/2} = 10^{-6}$ s) and hydroxyl radicals ($t_{1/2} = 10^{-9}$ s) are considerably shorter when compared to hydrogen peroxide ($t_{1/2} = 10^{-5}$ s) (12). Superoxide can spontaneously dismutate to H_2O_2 ($\sim 10^5 M^{-1} s^{-1}$), a process greatly enhanced by superoxide dismutases (SODs) (35, 36). SODs catalyze the conversion of superoxide into H_2O_2 and O_2 ($\sim 7 \times 10^9 M^{-1} s^{-1}$) to maintain steady-state levels of superoxide ($\sim 10^{-10}$ M) (37, 38). Reaction of H_2O_2 with trace metal ions (Fe^{2+} or Cu^{2+}) through Fenton or Haber-Weiss chemistry generates OH (*in vivo* concentration of 10^{-15} M) (39). H_2O_2 is the most abundant form of ROS (*in vivo* concentration of 10^{-7} M), and considered to be the most stable species generated in response to biological stimuli. Its rapid production is selectively perceived by downstream targets, and subsequently undergoes controlled degradation by antioxidant defense systems. The uncharged nature and relative stability of H_2O_2 permits it to freely diffuse across membranes to participate as a messenger in signal transduction. More recently, evidence has demonstrated that aquaporin channels can facilitate translocation of H_2O_2 across membranes (40–42).

Spatial and temporal production of H_2O_2 allows specificity during cellular signaling. The NADPH oxidase (Nox) family of enzymes represents a major source of endogenous ROS generated during redox-mediated kinase signaling. Nox enzymes produce ROS by translocating an electron from reduced nicotinamide adenine dinucleotide phosphate (NADPH) across the cell membrane (13). The prototypical Nox enzyme, Nox2 (also known as gp91^{phox}), was initially thought to be confined to phagocytes to protect against microbial invasion by generating millimolar quantities of H_2O_2 . Other Nox homologues (Nox1-5 and Duox1-2) have since been identified in nonphagocytes and exhibit differential subcellular localization and cell- and tissue-specific expression patterns (43–45). Activation of Nox complexes requires binding

of flavin adenine dinucleotide (FAD) cofactors, association of cytoplasmic coactivator proteins (Nox1-4, Duox1-2), and/or calcium to its intracellular domain (Nox5, Duox1-2).

Mitochondrial-derived oxidants represent another major source of intracellular ROS. Formation of ROS occurs when electrons leak prematurely from the electron transport chain (ETC) and result in the incomplete reduction of O_2 and generation of superoxide (46, 47). This process was believed to be an inevitable repercussion of aerobic existence, but cellular stimuli have been shown to initiate controlled mitochondrial ROS production (*i.e.* redox enzyme p66^{Shc}) (48, 49). It is important to note that other enzymes such as xanthine oxidase, cytochrome P-450, cyclooxygenases, and lipoxygenases can also serve as critical sources of ROS within the cellular context (9).

Reactive nitrogen species (RNS) may also act as biologically relevant signaling molecules. Reaction of cysteine thiols with RNS, such as nitric oxide (NO), generates nitrosothiols (SNO). This process, known as S-nitrosylation, is reversible and participates in cellular signaling (50). Evidence supporting S-nitrosylation during kinase signaling will be referenced appropriately within their respective sections.

Regulation of ROS Levels During Signal Transduction

The concentration of H_2O_2 must increase rapidly above a certain threshold, ranging from low nanomolar to low micromolar levels, and remain elevated long enough for it to oxidize its effectors in order to serve as an efficient signaling molecule (14). Signal duration can be mediated through the collective efforts of antioxidant defense systems. Enzymes such as catalase, peroxiredoxins (Prxs), and glutathione peroxidases (Gpxs) contribute by catalyzing the dismutation (catalase) or reduction (Prxs, Gpxs) of H_2O_2 (51, 52). Peroxiredoxins, namely 2-Cys Prxs, exist as homodimers and contain a peroxidatic cysteine. This residue becomes oxidized upon reaction

with H_2O_2 to a sulfenic acid, and condenses with a resolving cysteine in an adjoining subunit to form an intermolecular disulfide. Glutathione peroxidases (i.e. in higher eukaryotes) contain a selenocysteine that is oxidized by H_2O_2 to SeOH , and forms a disulfide with glutathione. Disulfide bonds are reduced by buffering systems such as thioredoxin/thioredoxin reductase (Trx/TrxR) (for Prxs) or glutathione/glutaredoxin (GSH/Grx) (for Gpxs) with the aid of reducing equivalents provided by NADPH. Completion of the catalytic cycle enables these enzymes to maintain intracellular H_2O_2 levels as deemed necessary.

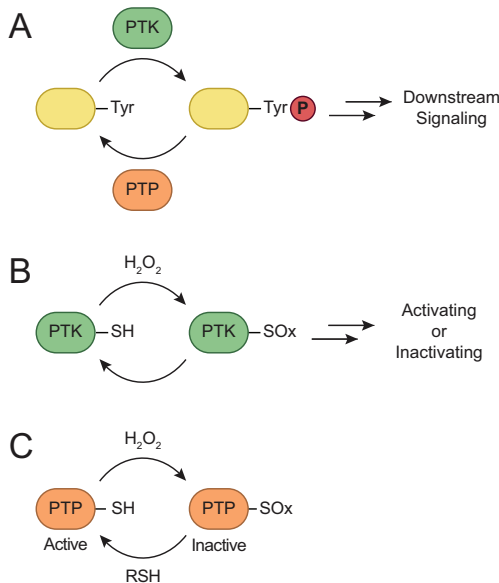


Figure B.2: **Model for redox-dependent signal transduction.** (a) PTKs catalyze the transfer of γ -phosphoryl groups from ATP to tyrosine hydroxyls of proteins, whereas PTPs remove phosphate groups from phosphorylated Tyr residues. (b) Regulatory cysteines in protein kinases can undergo oxidation/reduction to modulate their function. Depending on the kinase, redox modifications can stimulate or inhibit enzymatic function. (c) PTPs function in a coordinated manner with PTKs to control signaling pathways to regulate a diverse array of cellular processes. Oxidation of the conserved active site cysteine residue in PTPs inactivates these enzymes, and can be restored by reducing the oxidized residue back to its thiol form. SOx: oxidized cysteine.

Coordination of Reversible Tyrosine Phosphorylation through Redox-Dependent Signaling

The distinct but complementary function of kinases and phosphatases represents a finely tuned process wherein crosstalk occurs between separate but interrelated networks (Figure B.2a). Redox-based mechanisms coordinate enzymatic activity between the two groups (Figure B.2b, c). Localized changes in redox homeostasis can be sensed through oxidative modification of cysteine residues within specific protein targets. The initial product of the reaction between H_2O_2 and a thiolate (SH) is sulfenic acid (SOH) (Figure B.3). This reversible modification, also known as sulfenylation, can be directly reduced back to the thiol or indirectly by disulfide bonds. Alternatively, sulfenic acids can be stabilized by the protein microenvironment or undergo additional modifications. Other relevant oxoforms include disulfides, sulfenamides, nitrosothiols (SNO), sulfinic (SO_2H), and sulfonic (SO_3H) acids. The reversibility of sulfenic acid represents a mechanism whereby redox-based signaling can be regulated, akin to phosphorylation. In addition, disulfide exchange and bond formation can also play an important role in maintaining specificity during redox signaling (15–17). The utility and functional role of reversible cysteine oxidation has been evidenced by an increasing number of studies (53–55). In particular, protein tyrosine phosphatases (PTPs) were originally implicated as targets of signal-induced H_2O_2 production due to early studies by Denu and Tanner (56). The PTP superfamily contains a signature motif, (I/V)-H-C-X-X-G-X-X-R-(S/T), which includes a conserved cysteine that functions as a nucleophile during catalysis. The susceptibility of certain residues to oxidation is inherently dependent on its nucleophilicity, and provides a basis for specificity during redox-mediated signaling. Thiolate anions are intrinsically more reactive than their protonated counterparts (57), exhibiting enhanced reactivity towards H_2O_2 ranging across seven orders of magnitude ($1\text{-}10^7 \text{ M}^{-1} \text{ s}^{-1}$) (58). Free cysteines are typically protonated at physiological pH, and have a pK_a of ~ 8.5 . Pro-

tein microenvironments can profoundly influence the pKa of cysteine thiols and in some cases, decrease the pKa to as low as 3.5 (59, 60). These factors include metal coordination, residue accessibility, proximity to the oxidant source, and stabilization of the thiolate anion by electrostatic interactions from neighboring residues. The catalytic cysteine of PTPs is characterized by a low pKa value ranging from 4.6 to 5.5 owing to the unique chemical environment of its active site, which renders it susceptible to oxidative inactivation (61, 62). Although PTPs were initially suggested to be the sole targets of ligand-induced ROS production, attention has also shifted towards protein kinases. In the following sections, biochemical studies and evidence for redox regulation will be presented for select kinase examples.

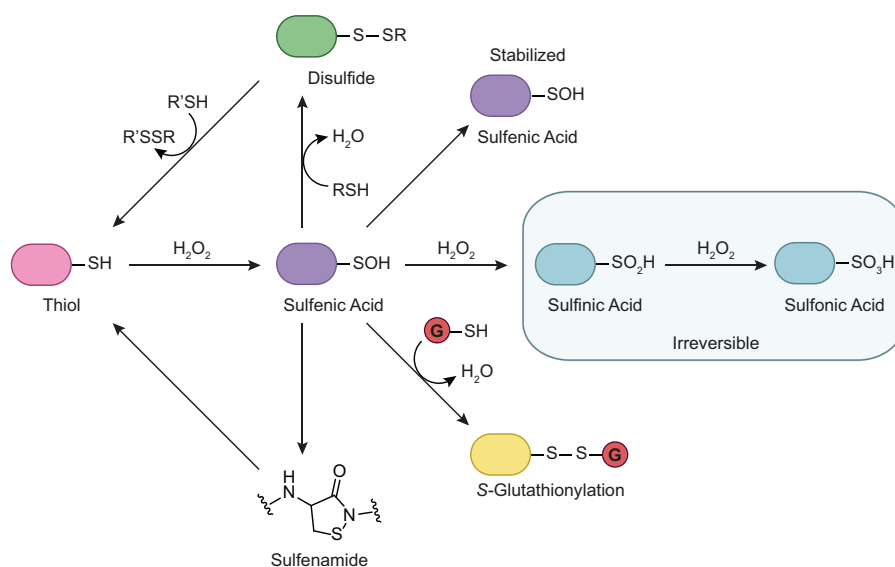


Figure B.3: **Oxidative modification of cysteine residues by H_2O_2 .** The initial reaction product of a thiolate with H_2O_2 yields sulfenic acid (RSOH). This modification, also known as sulfenylation, is reversible and can be directly reduced back to the thiol form or indirectly through disulfide bond formation. Sulfenic acids can be stabilized by the protein microenvironment and/or undergo subsequent modification. For example, sulfenic acids can condense with a second cysteine in the same or different protein to generate disulfide bonds. Alternatively, reaction with the low molecular weight thiol glutathione (GSH, red circle) affords a mixed disulfide through a process known as *S*-glutathionylation. In some proteins, such as PTP1B, nucleophilic attack of a backbone amide on RSOH results in sulfenamide formation. Sulfenyl groups can also oxidize further to the sulfinic (RSO₂H) and/or sulfonic (RSO₃H) acid forms under conditions of high oxidative stress.

Receptor Tyrosine Kinases

Platelet-Derived Growth Factor Receptor (PDGFR)

PDGF exists as a homo- or heterodimer connected by disulfide bonds, and is composed from a combination of four isoforms (PDGF-A, PDGF-B, PDGF-C, and PDGF-D). PDGF initiates signal transduction by binding to its receptor, PDGFR ($-\alpha$ or $-\beta$ forms). Activation of PDGFR engages signaling routes such as Ras/MAPK, PI3K/Akt, or binding of PLC- γ to elicit mitogenic and anti-apoptotic effects. For example, PDGF plays crucial roles in embryonic development, blood vessel formation, and wound response (63). PDGF-mediated signaling specificity in various cell types (i.e. fibroblasts, smooth muscle cells) is achieved by different ligand-receptor combinations (64). Therefore, discrepancies in the literature may actually reflect the diverse signaling nature of these isoforms. For the purpose of this section, ligand and receptor isoforms will be referenced when deemed necessary. In particular, the majority of work discussed regarding PDGFR redox regulation is comprised of observations obtained from PDGF-BB/ PDGFR- β interactions.

The biological relevance of growth factor-induced H_2O_2 production was first highlighted in vascular smooth muscle cells (VSMCs) (21). Endogenous ROS levels peaked rapidly upon PDGF stimulation, and were inhibited by enzymatic and chemical H_2O_2 scavengers. Transient H_2O_2 increases were also accompanied by elevated Tyr phosphorylation levels and activation of the MAPK pathway. PDGF stimulation of adipocytes has been shown to induce intracellular H_2O_2 , originating from a membrane-bound Nox complex (65). Signal-derived H_2O_2 subsequently participates in facilitation and enhancement of adipose differentiation, albeit this observation is isoform-specific (PDGF-AA) (66).

Many research efforts have been devoted to elucidating the molecular mechanisms that produce and regulate endogenous H_2O_2 during cellular signaling. Activation

of PI3K, a downstream effector of PDGFR, is required for growth factor-mediated production of H_2O_2 (67). Mutation of PI3K binding sites (Tyr740 and Tyr751) or exposure to PI3K inhibitors (LY294002 and wortmannin) failed to induce H_2O_2 production upon ligand stimulation. These results and others (68) suggest that PIP_3 , the product of activated PI3K, is essential for redox-based PDGF signaling. Additionally, expression of a dominant negative (DN) mutant of the small GTPase Rac1 (Rac1N17) blocks increases in H_2O_2 and corroborates earlier observations in fibroblasts (69). Rac1 is one of several subunits comprising the Nox enzyme complex, and contains an effector region (residues 124-135) required for Nox activation. Deletion of this region does not interfere with its functional abilities, but abrogates Rac1-mediated superoxide production through Nox (70). PIP_3 stimulates Rac1 activation through guanine nucleotide exchange factors (GEFs). Therefore, it appears that Rac1 activation of Nox is inherently dependent on PI3K production of PIP_3 , which has also been demonstrated with regards to EGF-mediated signaling (71). Nox complexes serve as the main oxidant source during PDGF signaling, as established by chemical inhibition and enzyme overexpression studies (72, 73).

PDGFR activation can also occur through an alternate mechanism known as trans-activation, and is specific to the β -receptor isoform (74, 75). In this scenario, angiotensin II (AngII) binds to GPCRs (G protein-coupled receptors) to trigger H_2O_2 production and mobilization of Ca^{2+} from intracellular stores. In turn, H_2O_2 activates additional kinases such as c-Src and PKC (protein kinase C) to promote RTK phosphorylation (76). The underlying mechanisms regarding H_2O_2 production during these events remains unclear, although some evidence indicates that mitochondrial function may play a role (77). Trans-activation represents an additional level whereby alternate stimulants can initiate signaling of ligand-inaccessible RTKs in lieu of traditional ligand-receptor interactions (Figure B.4).

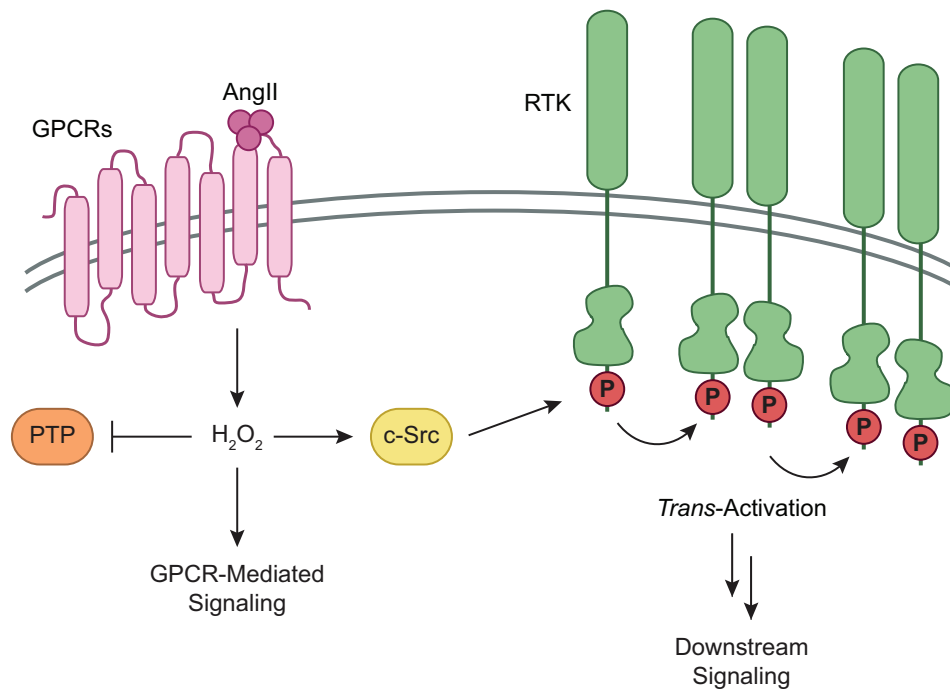


Figure B.4: *Trans*-activation of PDGFR and EGFR. Alternative stimulants such as AngII can initiate activation of ligand-inaccessible RTKs in lieu of traditional ligandreceptor interactions. In this scenario, AngII binds to GPCRs to promote endogenous H₂O₂ production and activation of redox regulated PTKs such as c-Src. Src promotes phosphorylation of PDGFR or EGFR, and neighboring receptors can be activated in a lateral-based mechanism. Additionally, concurrent PTP inactivation has also been suggested to promote RTK *trans*-activation.

PDGFR activity is modulated by a number of PTPs, such as low molecular weight PTP (LMW-PTP) (78) and SHP-2 (79). LMW-PTP is characterized by a unique feature among the PTP family whereby it contains two cysteine residues, Cys12 and Cys17, located in its catalytic pocket (80). Upon PDGF stimulation, endogenous H_2O_2 inactivates LMW-PTP through disulfide bond formation to enable increased receptor activity (73). GSH depletion by treatment with buthionine sulfoxide (BSO), an inhibitor of γ -glutamylcysteine synthetase, severely impairs rescue of oxidized LMW-PTP, and suggests phosphatase reactivation proceeds through a GSH-dependent process. Glutaredoxin (Grx) was later identified as a component of GSH-dependent modulation of LMW-PTP (81). LMW-PTP mutant C17A is unable to recover from oxidative inactivation, and suggests Cys17 forms a disulfide bond with Cys12 to protect the catalytic cysteine from hyperoxidation (*i.e.* sulfinic or sulfonic acids). Follow-up studies imply PTPs may regulate the duration of PDGFR signal by preferentially targeting membrane-exposed receptors, whereas the endosomal receptor pool has been shown to remain phosphorylated for up to 2 h (82).

The extent of growth factor signaling can also be controlled by antioxidant defense systems. In particular, PrxII functions as a negative regulator of PDGF signaling (83). PrxII deficient mouse embryonic fibroblast (MEF) cells exhibit 2-fold increases in H_2O_2 production and enhanced activation of PDGFR and PLC- γ 1. Co-immunoprecipitation demonstrates that active PrxII is recruited to the receptor upon ligand stimulation. Translocated PrxII relieves oxidative inactivation of membrane-associated PTPs by eliminating localized H_2O_2 production within the PDGFR microenvironment. These results demonstrate PrxII regulates site-selective amplification of PDGFR phosphorylation through endogenous H_2O_2 (Figure B.5a). Alternatively, mechanisms have evolved to allow localized H_2O_2 accumulation during signaling. Prxs are extremely efficient at H_2O_2 elimination, and react with H_2O_2 at second-order rate constants ranging from $10^5 - 10^8 \text{ M}^{-1} \text{ s}^{-1}$ (84, 85). Therefore, it is

intriguing how H_2O_2 can accumulate within the cytosol long enough to modulate its effectors. Recent studies have discovered phosphorylation of Tyr194 inactivates PrxI (86). PrxI phosphorylation is induced in several cell types (NIH 3T3, A431, Ramos B cells, Jurkat T cells) upon activation of various receptors (PDGFR, EGFR, BCR, and TCR), and found to be localized to membrane microdomains. Nox1 deficient mice exhibit a 60% reduction in PrxI phosphorylation, and suggests Nox1-derived H_2O_2 induces inactivation of PrxI and PTPs to promote localized H_2O_2 accumulation. Knockdown c-Src siRNA experiments decrease PrxI inactivation by 25-50%, thereby identifying c-Src as the partially responsible kinase. This study provides a key contribution that demonstrates localized PrxI inactivation enables transient H_2O_2 accumulation near the membrane, while simultaneously preventing toxic ROS increases elsewhere during signaling (Figure B.5b). Additionally, the two aforementioned studies highlight isoform-specific Prx responses involved in maintaining growth factor-induced H_2O_2 production.

Until now, we have only discussed indirect mechanisms related to redox-based modulation of PDGFR. Currently, there is little evidence to support direct modification of PDGFR through cysteine oxidation. In an early study, PDGF stimulation was reported to induce covalent receptor dimerization through disulfide bonds within the extracellular domain (87). Unfortunately, the identification of residues responsible for PDGFR dimerization has not been reported. A separate study examined the functional role of conserved cysteine residues located in the cytoplasmic domain of PDGFR. Treatment with the sulfhydryl-specific alkylating agent, *N*-ethylmaleimide (NEM), inhibits kinase activity and suggests the receptor contains critical cysteine residues located within its kinase domain (88). MS analysis identified two residues, Cys822 and Cys940, deemed necessary for receptor activity by *in vitro* assays using Ser mutants. Cys822 is located in the catalytic loop at the enzyme active site, whereas Cys940 is located in the C-lobe of the kinase domain. These residues do not

participate in disulfide bond formation, as determined by non-reducing gel analysis. Additionally, they do not interfere with ATP substrate binding as is observed in other RTKs (*i.e.* EGFR). Proteolytic cleavage assays demonstrate Cys940 affects receptor activity by inducing a conformational change, but the mechanism by which this proceeds remains unclear. Although the preceding studies indicate PDGFR may require specific cysteines for functional activity, it remains unknown whether the receptor contains cysteine residues that are directly modulated by H_2O_2 .

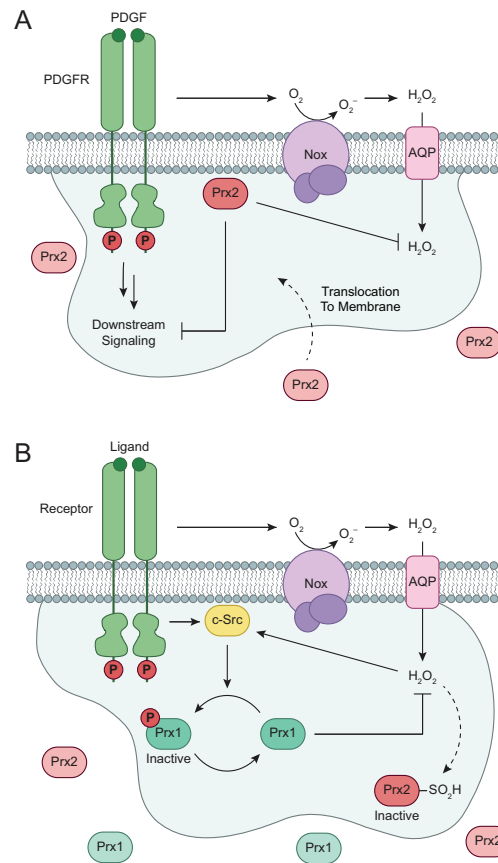


Figure B.5: **Isoform-specific roles of Prx during redox-based PDGFR signaling.** (a) PrxII functions as a negative regulator of PDGF signaling. Upon growth factor stimulation, active PrxII is recruited to the membrane and serves to relieve oxidative inactivation of membrane-associated PTPs by eliminating localized H_2O_2 production within the PDGFR microenvironment. (b) Receptor activation can also induce localized phosphorylation and inactivation of PrxI by PTKs, such as the redox-regulated c-Src. Deactivation of PrxI reduces the redox-buffering capacity adjacent to the cellular membrane, allowing for transient and localized increases in H_2O_2 for signal transduction. Additionally, increased H_2O_2 concentrations can also inactivate Prx2 by oxidation of its catalytic cysteine to sulfinic acid

Epidermal Growth Factor Receptor (EGFR)

Epidermal growth factor receptor (EGFR) was the first RTK to be identified, and has since been widely characterized in physiologic and pathological settings (89–91). EGFR, also known as erbB1 (or HER1), is grouped into a subfamily that consists of three other closely related receptors: erbB2 (HER2), erbB3 (HER3), and erbB4 (HER4). EGFR forms a homo- or heterodimer followed by autophosphorylation of key residues upon stimulation (92). Once activated, EGFR relays the signal through one of its two major pro-survival signaling routes, Ras/MAPK or PI3K/Akt. The erbB family of receptors is activated by various ligand-receptor combinations to achieve signaling specificity in different cell types and signaling cascades (93). Therefore, we will mainly focus on effects resulting from the EGF-EGFR interaction for the purpose of this review. EGFR and other erbB family members have been found to be mutated or amplified in human cancers such as breast and lung, making them attractive targets for the development of therapeutic strategies (94, 95).

Culminating evidence has established that EGFR is modulated by and utilizes H_2O_2 as a secondary messenger during cellular signaling (96, 97). Early reports demonstrate exogenous H_2O_2 increases [^{32}P] phosphate incorporation, albeit the signal is half of what is observed in EGF-stimulated cells (98). Tryptic phosphopeptide mapping attributes this difference to preferential enhancement of EGFR Tyr phosphorylation by H_2O_2 , whereas EGF triggers a combination of Ser/Thr and Tyr receptor phosphorylation. In a landmark study, EGF was reported to increase endogenous H_2O_2 levels upon receptor stimulation in cells overexpressing EGFR (A431) (22). Catalase incorporation abolishes EGF-induced H_2O_2 production and blunts increased Tyr phosphorylation of EGFR and PLC- γ 1, a well-characterized target of EGFR. Additionally, assays with mutated EGFR receptors demonstrate EGF-dependent H_2O_2 formation requires intrinsic kinase activity, but not necessarily its autophosphorylation sites. Subsequent reports have shown H_2O_2 activates EGFR kinase and markedly

enhances receptor half-life in conjunction with the native ligand (99). From these results, it is apparent that H_2O_2 modulates EGFR activation and influences downstream signaling. Other studies suggest *S*-nitrosylation may regulate EGFR activity, albeit with contradictory results (100–102). Additionally, EGFR is the only other RTK besides PDGFR known to undergo *trans*-activation by AngII, and proceeds through H_2O_2 -dependent c-Src activation (103–105). Neighboring EGFR kinases may be activated in a lateral-based mechanism, and concurrent PTP inactivation has been suggested to promote EGFR *trans*-activation (106). (Figure B.4)

PTPs were one of the first redox-based targets identified in EGF signaling. EGFR was originally identified as an *in vivo* substrate of PTP1B using a substrate-trapping mutant technique (107). These mutants retain their ability to bind substrates in a cellular context, but lack catalytic functionality to enable stabilization of enzyme-substrate complexes for isolation purposes. PTP1B is localized exclusively on the cytoplasmic face of the endoplasmic reticulum (ER), and serves to dephosphorylate activated EGFR that has been internalized and transported for endocytosis (108, 109). Signal-derived H_2O_2 inactivates PTP1B to enable equilibrium between EGFR and PTP1B activity (110). PTP1B exhibits decreased time-dependent incorporation of radiolabeled iodoacetic acid (IAA) in A431 cells when stimulated with EGF. IAA is a sulfhydryl-modifying reagent known to react with the catalytic cysteine of PTP1B (Cys215). PTEN is another PTP known to maintain a close relationship with EGFR, and functions as a negative regulator of the PI3K/Akt pathway. Recent evidence implicates PTEN regulates EGFR by targeting the receptor for degradation through ubiquitylation (111). EGFR ubiquitylation is mediated by the Cbl family of E3 ubiquitin ligases, which bind to the activated receptor to form a complex stabilized by the phosphatase. PTEN contains five cysteine residues within its catalytic domain and undergoes reversible inactivation by H_2O_2 . Mutation of these residues reveals Cys124 is oxidized upon exposure to exogenous H_2O_2 , and forms an intramolecular

disulfide with Cys71 that can be rescued by Trx (112). Subsequent work has shown that EGF-induced H₂O₂ inactivates PTEN similarly to PTP1B (68). Collectively, these studies provide evidence that growth factor activation of RTKs may not be sufficient to increase the steady-state level of protein phosphorylation during signaling, and that concomitant inactivation of PTPs is also required. Interestingly, Nox1 overexpression induces increased PIP3 levels (68) and is a component involved in EGFR activation of PI3K (71). PTEN inactivation represents a positive feedback loop that promotes continued accumulation of intracellular PIP3 during EGF signaling.

EGF-induced H₂O₂ is produced and regulated by distinct components. Multiple Nox isoforms mediate H₂O₂ production within EGF signaling cascades. For example, a positive feedback loop due to sequential activation of PI3K- β Pix-Rac1-Nox1 is involved in endogenous H₂O₂ production (71). In this loop, EGF stimulation activates PI3K to elicit increased PIP3 production. These lipid products activate β Pix by interacting with its PH domain, which then catalyzes GDP exchange to activate Rac1. Finally, Rac1 directly binds to Nox1 to promote NADPH electron transfer and H₂O₂ generation. β Pix siRNA-based knockdown experiments block EGF-induced H₂O₂ production and Rac1 activation. A separate study reports Nox1 is negatively modulated during EGF signaling by phosphorylation of Ser282 of Nox activator 1 (NOXA1, a Nox1 subunit) by Erk1/2 and Ser172 by PKC to prevent hyperactivation (113, 114). Nox4 is another isoform that regulates EGFR in a spatially dependent manner through PTP1B inactivation (115). Confocal microscopy and cellular fractionation experiments with the ER marker protein GRP78 confirmed ER localization of Nox4. Upon EGF stimulation, co-localization of Nox4 and PTP1B to the ER is required for phosphatase inactivation in aortic endothelial cells. Nox4 siRNA knockdown increases reduced PTP1B levels, indicating Nox4 serves as the primary oxidant source for PTP1B oxidation within the ER and consequently allows Nox4 to spatially modulate the duration of EGFR signaling. These results were validated by PTP1B

substrate-trapping mutants, which were attenuated in their ability to effectively bind EGFR due to Nox4 overexpression.

As described earlier, SODs catalyze the conversion of superoxide into H_2O_2 to maintain steady-state levels. Treatment with SOD1 inhibitor ATN-224 decreases intracellular H_2O_2 levels and attenuates EGFR activation and downstream targets (116). Furthermore, SOD1 was shown to mediate transient oxidation of PTPs such as PTP1B and PTEN. Separate studies demonstrate H_2O_2 utilized during EGF signaling is generated extracellularly at the receptor-ligand interface, and permeates across the membrane to facilitate kinase activation (117, 118). *In vitro* assays with recombinant protein containing only the extracellular EGFR binding domain provides evidence that this domain is sufficient to induce H_2O_2 production upon ligand binding. Once generated, H_2O_2 can freely diffuse across membranes or be transported through aquaporin channels to elicit signaling events (42). Thereafter, buffering systems and peroxide-detoxifying enzymes such as Prx and Gpx mediate signal duration by maintaining appropriate H_2O_2 levels (119–121).

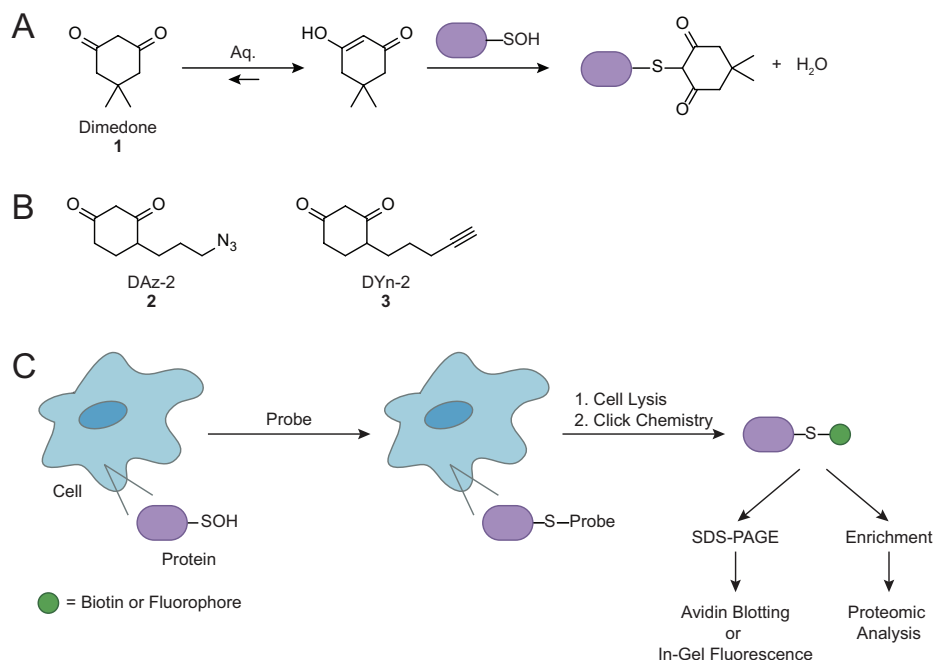


Figure B.6: **General strategy for detecting protein sulfenic acids in cells.** (a) Chemoselective reaction between 5,5-dimethyl-1,3-cyclohexanedione (dimedone, 1) and sulfenic acid. (b) Azide and alkyne-functionalized small-molecule probes for trapping and tagging protein sulfenic acids include DAz-2 (2) and DYn-2 (3). (c) Detection of protein sulfenic acids in living cells. Target cells are incubated with cell-permeable probes to trap and tag protein sulfenic acids *in situ*. After labeling, cell lysates are prepared and tagged proteins are bioorthogonally ligated to biotin or fluorescent reporter tags *via* click chemistry to enable detection by Western blot or in-gel fluorescence. Alternatively, biotinylated proteins can be enriched for proteomic analysis.

Mounting evidence has established redox-based modulation of EGFR activity, albeit mainly through indirect mechanisms. Although EGFR contains ~ 50 cysteine residues, 9 of which are located within its intracellular domain, none of these have been implicated to undergo oxidative modification until recently (122). Early work demonstrates EGFR autophosphorylation is inactivated by NEM alkylation (123, 124). NEM treatment blocks reaction of a nucleotide analog [(*p*-fluorosulfonyl)-benzoyl]-5 adenosine (5-FSBA) with the kinase active site, suggesting alkylation may exert an inhibitory effect by reacting with a cysteine residue located in the ATP binding site (123). These observations were corroborated in separate studies whereby co-incubation of EGFR with AMP-PNP, a hydrolysis-resistant ATP analog, blocks receptor inactivation by NEM (125). Although these studies alluded that a cysteine

residue may play a role in redox-based EGFR signaling, specific modification sites were not identified. Sulfhydryl alkylating agents represent an indirect method to detect cysteine modifications because they readily react with reduced thiols, but are unable to modify other cysteine oxoforms important to signaling such as sulfenic acids. Therefore, the detection of relevant cysteine modifications represents a tremendous need for the development of tools geared towards this goal. Techniques based on chemical probes (53, 126–130) and antibodies (131, 132) have recently been developed to detect sulfenic acid formation. In particular, cell permeable probes enable direct trapping of sulfenylated proteins within their native cellular environment. These probes are functionalized with an azide or alkyne reporter group (53, 122, 128), and utilize a cyclic β -diketone warhead chemically selective for sulfenic acids (133) (Figure B.6 a, b). Bioorthogonal biotin or fluorescent reporter tags can be appended post-lysis for detection via the Staudinger ligation (134) or Huisgen [3+2] cycloaddition (*i.e.* click chemistry) (135). Overall, this general approach provides a facile method to profile protein sulfenylation in a cellular context (Figure B.6 c).

Overexpression of EGFR and HER2 in breast cancer cell lines is correlated to high H_2O_2 levels and increased global protein sulfenylation (131). In more recent work, the functional role of protein sulfenylation during EGFR signaling was explored in detail (Figure B.7a). Sulfenic acid formation was profiled in A431 cells upon ligand stimulation, and captured with cell-permeable probe DYn-2 (122). Ensuing analysis revealed EGF stimulation induces dynamic and global increases in protein sulfenylation. This occurs in a dose- and time-dependent manner relative to EGF, and is accompanied by Nox2-derived H_2O_2 production. DYn-2 was used in a targeted approach to confirm sulfenylation of three phosphatases involved in EGFR signaling: SHP2, PTEN, and PTP1B. Immunoprecipitation demonstrated each PTP was sulfenylated in an EGF-dependent manner in cells. Moreover, individual PTPs displayed distinct oxidation profiles as a function of growth factor concentration. PTP

sensitivity to EGF-mediated oxidation suggests this observation may be related to subcellular protein localization, and is supported by previous work (115). Finally, EGFR itself was shown to be activated and directly modified upon EGF stimulation, peaking at low concentrations (4 ng/ml). The EGFR kinase domain contains six cysteine residues, one of which is a conserved cysteine (Cys797) that resides in the ATP binding site (Fig. 7b). This residue is selectively targeted by irreversible EGFR inhibitors (*i.e.* afatinib) currently undergoing clinical trials for breast and non-small cell lung cancers (136, 137). Treatment with irreversible EGFR inhibitors (afatinib, canertinib, or pelitinib) abrogates the ability of DYn-2 to detect EGFR oxidation, and suggests Cys797 may be susceptible to oxidation as evidenced by signal loss of EGFR sulfenylation. Cys797 was identified as the site of EGFR modification by MS analysis. These results demonstrate EGFR Cys797 is a direct target of growth factor-induced H₂O₂, and that EGF signaling induces dynamic sulfenic acid formation within EGFR signaling pathways (122). Phosphorylation and sulfenylation appear to work in parallel with each other to regulate receptor kinase activity during EGF signaling.

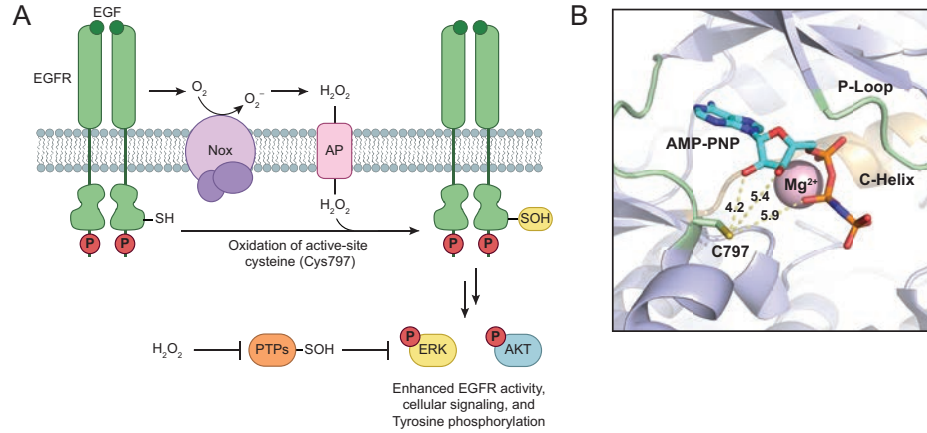


Figure B.7: **Model for H₂O₂-dependent regulation of EGFR activation.** (a) Binding of EGF to the receptor induces production of H₂O₂ through Nox2. Nox-derived H₂O₂ directly modifies EGFR to sulfenic acid at a conserved cysteine residue (Cys797) located in its active site, which enhances the receptor's intrinsic tyrosine kinase activity. Endogenous H₂O₂ can also oxidize and deactivate localized PTPs, leading to a net increase in EGFR phosphorylation and activation of downstream signaling cascades. (b) Crystal structure of the EGFR kinase domain (PDB 3GT8) bound to AMP-PNP, a hydrolysis-resistant ATP analog, and Mg²⁺. The yellow dashed lines and accompanying numbers indicate the distance (Å) between the γ -sulfur atom of Cys797 and key substrate functional groups. It is important to note that Cys797 can adopt different rotamers, and sulfenylation of this residue may enhance its ability to participate in electrostatic and hydrogen bonding interactions with its substrate.

Vascular Endothelial Growth Factor Receptor (VEGFR)

Angiogenesis is the physiological process whereby new blood vessels are formed from pre-existing vasculature. This is a vital process involved in embryonic development, skeletal growth, wound repair, and reproductive functions (138). A wide range of diseases including chronic inflammation, vascular ischemia, and atherosclerosis have been linked to angiogenesis (139). Vascular endothelial growth factor (VEGF) is a key angiogenic growth factor that stimulates cellular proliferation, migration, and tube formation of endothelial cells (ECs). The biological effects of VEGF are mediated by three RTKs, VEGFR-1 (Flt-1), VEGFR-2 (KDR/Flk1), and VEGFR-3, which differ considerably in their signaling properties. VEGFR activation initiates downstream signaling through Ras/MAPK, PI3K/Akt, PLC- γ , and Src family of kinases to induce endothelial growth and mediate pro-survival effects. For the purpose of this section, we will focus primarily on VEGFR-2 due to its involvement in VEGF-mediated redox signaling (140).

Growth factor-induced H₂O₂ production modulates RTK activity, as discussed in preceding sections. Interestingly, H₂O₂ treatment of ECs has been shown to up-regulate gene expression of VEGF (141, 142). Further analysis with inhibitors of protein (cycloheximide) and RNA synthesis (actinomycin D) demonstrate induction of VEGF mRNA levels by H₂O₂ is inhibited by actinomycin D, indicating that de novo RNA synthesis is required for this response. In a later study, H₂O₂ was also found to elicit increased VEGFR-2 mRNA levels (143). The biological relevance of these observations was explored in detail, and suggests upregulation of VEGF and VEGFR-2 functions primarily to protect ECs against oxidative injury. Additionally, VEGF-mediated signaling is also accompanied by bursts of intracellular ROS (144). Akin to its RTK counterparts, VEGF-induced H₂O₂ production increases receptor autophosphorylation and activation of downstream targets such as Erk1/2, Akt, and PLC- γ 1. Phosphatase inhibition with vanadate restores Tyr phosphorylation levels

during VEGF stimulation, and reinforces the idea that oxidative inactivation of PTPs such as PTP1B (145) and DEP-1 (146) promotes kinase activity. Similar to results observed with PDGFR and EGFR, activation of PI3K was shown to be essential for VEGF-derived H₂O₂ production using PI3K inhibitors (wortmannin) and Rac1N17.

Nox enzymes serve as the major source of endothelial H₂O₂, and are required for EC proliferation and migration (147–149). Therefore, efforts quickly focused on elucidating the potential role of Nox-derived H₂O₂ during VEGF-mediated signaling and angiogenesis (150). Treatment of ECs with various Nox inhibitors (DPI, apocynin, and AEBSF) and gp91^{phox} antisense oligonucleotides attenuate receptor autophosphorylation, VEGF-stimulated proliferation and migration, and H₂O₂ production. Rac1N17 overexpression results in similar decreases, indicating Nox2 activation is Rac1-dependent. Evidence suggests that Nox-derived H₂O₂ during VEGF signaling is spatially and temporally controlled by various components within discrete subcellular compartments including caveolae/lipid rafts, focal adhesions/complexes, and at the leading edge (151). Caveolae are flask-shaped membrane microdomains primarily composed of protein caveolae (*i.e.* caveolin-1), and are subsets of lipid rafts that compartmentalize signaling components such as RTKs, GPCRs, and Rac1. Caveolin-1 negatively modulates VEGFR-2 by binding to the receptor (152). VEGF stimulation promotes Tyr phosphorylation of caveolin-1, and triggers its dissociation from VEGFR-2. Once released, activated VEGFR-2 localizes with p-caveolin-1 at focal adhesions/complexes to initiate signaling. Focal adhesions are dynamic protein complexes that mediate cell anchorage and motility with respect to the extracellular matrix (ECM). A later study identified that co-localization of VEGFR-2 with Rac1 and the small GTPase ARF6 (ADP-ribosylation factor 6) occurs in caveolae/lipid rafts (153). Expression of DN ARF6 mutant (T27N) inhibits Rac1 activation, Tyr phosphorylation of caveolin-1, and translocation of VEGFR-2 from caveolae/lipid rafts. Additionally, ARF6 (T27N) attenuates VEGF-induced H₂O₂ production and suggests

ARF6 mediates recruitment of activated VEGFR-2 to focal adhesions/complexes through Rac1-dependent Nox activation (Figure B.8a). Alternatively, Nox1 overexpression has been shown to promote tumor angiogenesis through upregulation of VEGF and VEGFR-2 (154).

VEGF signaling can also be modulated by extracellular SOD (ecSOD). ecSOD is the major SOD found in the vascular extracellular space, and anchors to the EC surface by binding to heparin sulfate proteoglycans (HSPGs) through its heparin-binding domain (HBD). Extracellular H₂O₂ derived from ecSOD enhances VEGFR-2 autophosphorylation, and functions in a HBD-dependent manner (155). As discussed earlier, VEGFR activation initially occurs in caveolin-enriched lipid rafts where Nox complex subunits are localized within ECs. Sucrose gradient fractionation with ecSOD and ecSOD- Δ HBD expressing cells demonstrate that the HBD is required for ecSOD localization within caveolin-enriched lipid rafts. Additionally, PTPs involved in regulating VEGFR-2 activity such as PTP-1B and DEP-1 were oxidatively inactivated by ecSOD-derived H₂O₂. These PTPs were only inactivated in caveolae/lipid rafts, thereby indicating ecSOD promotes VEGF-induced H₂O₂ production and receptor autophosphorylation in a localized manner.

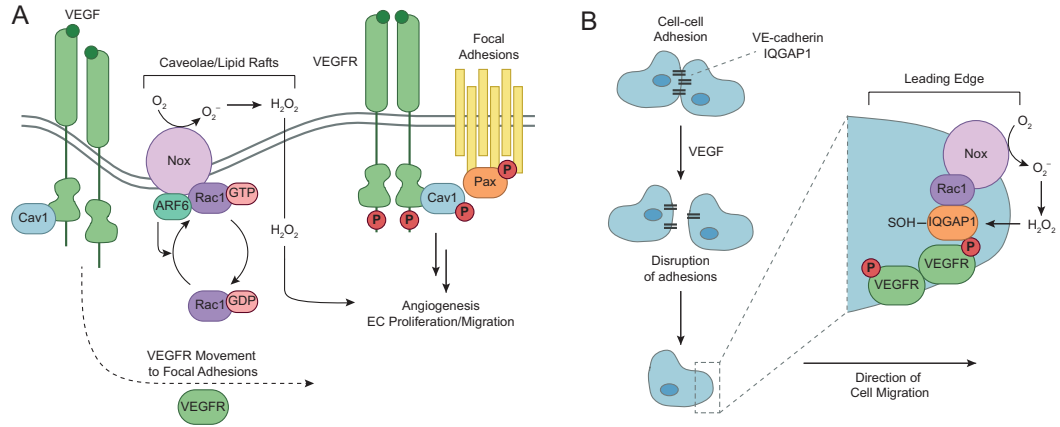


Figure B.8: **Spatial and temporal modulation of VEGFR2 signaling occurs in discrete subcellular compartments.** (a) In the basal state, caveolin-1 (Cav1) negatively modulates VEGFR2 by binding to the receptor in caveolae/lipid rafts. VEGF initiates activation of VEGFR2 by promoting dissociation of Cav1 from the receptor. Once released, activated VEGFR2 localizes with phosphorylated Cav1 and paxillin (Pax) at focal adhesions/complexes to initiate downstream signaling. Growth factor stimulation also recruits small GTPases, ARF6 and Rac1, to activate Nox complexes located in caveolae/ lipid rafts. Localized production of H_2O_2 acts as a secondary messenger during VEGF signaling to promote angiogenesis, proliferation, and migration in ECs. (b) Endothelial migration is a key event that occurs during angiogenesis in ECs. Cell-cell adhesions are mediated by interactions between VE-cadherin and IQGAP1, which are disrupted upon VEGF stimulation to initiate the migration process. During active migration, IQGAP1 functions as a scaffolding protein to recruit signaling components such as activated VEGFR2, Nox, and Rac1 to the leading edge. Additionally, Nox-derived H_2O_2 induces localized sulfenic acid formation in IQGAP1 to promote directional migration events. Adapted from Ushio-Fukai (2007).

Endothelial migration is essential for the formation of new blood vessels. Cell-cell adhesion is mediated primarily by VE-cadherin, and requires co-localization of IQGAP1 in quiescent ECs (156). VEGF initiates endothelial migration by reducing IQGAP1/VE-cadherin interactions to disengage cellular contacts. IQGAP1 is a VEGFR-2 binding protein originally identified in a library screen, and preferentially binds to the activated receptor at the leading edge in actively migrating cells (157). IQGAP1 functions as a scaffolding protein that controls cellular motility and morphogenesis by directly interacting with cytoskeletal and cell adhesion elements, in addition to small GTPases such as Rac1. Co-immunoprecipitation demonstrates VEGF stimulation rapidly promotes recruitment of Rac1 to IQGAP1, and initiates complex formation with VEGFR-2. IQGAP1 siRNA knockdown inhibits VEGF-induced H_2O_2 production and activation of downstream pathways such as PI3K/Akt.

In a wound scratch assay, Nox2 translocates to the leading edge and co-localizes with IQGAP1 upon VEGF stimulation (158). Collectively, these studies highlight the crucial role of IQGAP1 in endothelial migration during redox-mediated VEGFR signaling (Figure B.8b). A recent study using a dimedone-based trapping reagent (DCP-Bio1) demonstrates IQGAP1 undergoes localized sulfenic acid formation at the leading edge induced by VEGF-mediated H₂O₂ generation (159). Sulfenyl modification of IQGAP1 positively impacts its ability to promote directional migration events, and was also observed in hindlimb ischemia models.

VEGFR-2 can also undergo direction modulation through cysteine oxidation. During VEGF signaling, Nox2-derived H₂O₂ selectively exerts its effects on the PI3K/Akt pathway by inducing c-Src activation (160). A cysteinyl labeling strategy highly sensitive to sulfenic acid detection (161) was used to examine potential oxidation of VEGFR-2 and c-Src during VEGF signaling. Both kinases were identified to contain redox-active cysteines, and require Nox-2 derived H₂O₂ to elicit downstream signaling. This study does not identify the specific residues responsible for these observations, although there have been numerous reports of redox-sensitive cysteines present in c-Src (discussed later). Interestingly, a separate study reports VEGFR-2 activity is negatively modulated by an intramolecular disulfide bond between Cys1209 (catalytic) and Cys1199 (resolving) in its C-terminal tail (162). PrxII preserves VEGF signaling in vascular ECs by rescuing VEGFR-2 from oxidative inactivation, as shown by PrxII siRNA knockdown. Incorporation of cytosolic and membrane-targeted catalase effectively abrogates VEGF-induced H₂O₂ production; however, VEGFR-2 phosphorylation is only restored in the presence of membrane-targeted catalase. This suggests that PrxII, a cytosolic enzyme, must translocate to the cellular membrane to positively modulate VEGFR-2 activity. PrxII has been previously identified to be distributed within caveolae structures in vascular ECs, which coincides with known locations of subcellular VEGFR-2 signaling (86). Sucrose gradient fractionation demonstrates

co-localization of VEGFR-2 and PrxII occurs only within caveolae-enriched fractions. Additionally, oxidatively inactivated VEGFR-2 was only found in caveolae fractions in PrxII knockdown cells. These findings reinforce the idea that redox modulation of VEGFR-2 signaling occurs in a highly localized manner in ECs and contrasting effects of H₂O₂ on VEGFR-2 activity may be due to subcellular factors.

Insulin Receptor Kinase (IRK)

Insulin is the major hormone responsible for critical energy functions such as glucose and lipid metabolism. Insulin activates insulin receptor kinase (IRK), which is a heterotetrameric receptor composed of two extracellular α subunits and two transmembrane β subunits. Binding of insulin to the IRK extracellular domain induces a conformational change in its quaternary structure that enables ATP binding and leads to increased receptor autophosphorylation (163). Once activated, IRK elicits Tyr phosphorylation of various cytosolic docking proteins, most notably adaptor protein SHC and members of the insulin receptor substrate (IRS) protein family (164). Insulin signaling has mitogenic effects that are primarily associated with the Ras/MAPK pathway through SHC (165). Unlike other RTKs previously discussed in this review, IRK utilizes IRS docking proteins to initiate signal transduction (Figure B.1b). Activated IRS proteins recruit effectors to relay downstream signaling through the PI3K/Akt pathway and GLUT4, which play major roles in insulin function. For example, Akt activation induces glycogen synthesis through inhibition of GSK-3 (glycogen synthase kinase-3) (166). Additionally, the PI3K/Akt pathway mediates insulin-induced glucose uptake by translocation of GLUT4 vesicles to the cellular membrane (167, 168). Although RTKs mediate long-term events such as cellular differentiation and mitogenesis, the primary function of IRK is the acute regulation of glucose metabolism in muscle and adipose cells. Despite these differences, RTKs and IRK essentially share the same transduction machinery to elicit their respective

responses.

For many years, exogenous H_2O_2 has been recognized to mimic the effects of insulin (i.e. glucose transport) in adipocytes (169). Insulin-induced production of intracellular H_2O_2 was first observed in rat adipocytes (170). These observations were coupled to increased glucose metabolism, and suggest H_2O_2 acts as a secondary messenger to mediate the observed effects of insulin. H_2O_2 can enhance or reduce insulin responsiveness, depending on the concentration and duration of the oxidant. Prolonged exposure to H_2O_2 can impair insulin action and trigger insulin resistance, a characteristic feature of type 2 diabetes (171–173). Under normal conditions, insulin-induced H_2O_2 mediates early signaling events during the insulin action response. Akin to previously discussed RTKs, endogenous H_2O_2 enhances activation of IRK and IRS proteins through Tyr phosphorylation of key residues (174). Concomitant inactivation of PTPs such as PTP1B and PTEN has similarly been shown to propagate kinase activity during insulin signaling in hepatoma and adipose cells (175). Follow-up studies have also demonstrated the role of insulin-dependent H_2O_2 generation with regards to distal insulin response events (176). Signal-derived H_2O_2 blocked with chemical inhibitors attenuated response events associated with the PI3K/Akt pathway, such as glucose uptake and GLUT4 translocation. It is interesting to note that unlike PDGF (67), insulin-induced H_2O_2 production is independent of PI3K activation. Treatment of 3T3-L1 adipocytes with PI3K inhibitors (i.e. wortmannin or LY294002) does not block H_2O_2 production upon insulin stimulation, and most likely proceeds through a different mechanism than those identified in other RTKs.

Insulin-induced H_2O_2 production was originally linked to a membrane-bound complex identified in adipocytes with enzymatic characteristics consistent with Nox activity (65, 177). Northern blot analysis and reverse-transcriptase PCR (RT-PCR) identified Nox4 as the isoform responsible for H_2O_2 production within the insulin action pathway (178). Expression of Nox4 deletion constructs lacking NADPH or

FAD/NADPH cofactor binding domains functioned in a dominant-negative manner in differentiated adipocytes. These constructs attenuate insulin-derived H₂O₂ production, Tyr phosphorylation of IRK and IRS proteins, PI3K/Akt pathway activation, and subsequent insulin response events. Collectively, these results provide crucial evidence linking H₂O₂ production to insulin-mediated signal transduction. Additionally, co-expression of PTP1B and Nox4 reverses phosphatase activity and increases Tyr phosphorylation. PTP1B plays an important role in downregulation of insulin signaling and is an established therapeutic target for type 2 diabetes (179). PTP1B knockout mice are healthy and exhibit heightened insulin sensitivity, enhanced glucose and insulin tolerance, and are resistant to diet-induced obesity (180, 181). In particular, this has stimulated therapeutic-based approaches that target and recognize the inactive form of PTPs (182, 183).

Accumulating evidence has speculated that direct modulation of IRK occurs upon H₂O₂ exposure, but the functional details of this process are not fully characterized (184, 185). Iodoacetamide (IAM) treatment increases the catalytic activity of the IRK cytoplasmic domain, whereas another alkylating agent, NEM, inhibits the receptor (124). Regardless, both sulfhydryl agents strongly indicate that functional activity of IRK can be mediated by oxidative modification of one or more cysteine residues located within the IRK β chains. In a separate study, inhibitors of glutathione synthetase (BSO) or glutathione reductase (BCNU, 1,3-bis-(2-chloroethyl)-1-nitrosourea) were used to modulate intracellular GSH levels in IRK transfected CHO cells (186). Both inhibitors increase the GSSG/GSH ratio to induce a moderate shift to mildly oxidative conditions, and lead to structural and functional changes in the IRK β -chain. Additionally, decreased sulfhydryl groups were observed in IRK β -chains in the absence of detectable Tyr phosphorylation. These results suggest IRK may proceed through a "redox-priming stage", wherein specific cysteine residues undergo oxidative modification prior to full activation through receptor autophos-

phorylation. Later studies with isolated IRK from transfected CHO cells provide a functional role for redox-based receptor modulation (187). IRK autophosphorylation is inhibited by binding of ADP within its catalytic active site, which serves to regulate kinase activity. Exposure to H_2O_2 induces oxidation of two residues (Cys1245 and Cys1308), nucleotide release, and reverses receptor inhibition. It is important to note that direct redox modulation of IRK can promote insulin signaling, but may also contribute to obesity. In muscle cells, cytoplasmic creatine kinase mediates the rapid removal of ADP to promote IRK activation (188). This process does not occur in adipocytes, and represents a potentially advantageous mechanism to modulate IRK activity in muscle cells. This advantage may be decreased if ADP conversion in adipocytes is elevated due to increased H_2O_2 levels.

Fibroblast Growth Factor Receptor (FGFR)

Fibroblast growth factors (FGF) and their receptors (FGFRs) regulate developmental signaling pathways and are expressed in many different cell types (189). The mammalian FGF family is composed of 18 distinct ligands, and exerts its actions through 4 highly conserved transmembrane RTKs (FGFR1, FGFR2, FGFR3, and FGFR4). Upon stimulation, FGFR undergoes receptor dimerization and Tyr autophosphorylation within its intracellular kinase domain. These residues act as docking sites for adaptor proteins and lead the activation of four key downstream pathways: 1) Ras/MAPK pathway, 2) PI3K/Akt pathway, 3) STAT (signal transducer and activator of transcription), and 4) PLC- γ .

The molecular mechanisms underlying redox regulation of FGFR remains the least characterized amongst other RTKs. Initial studies demonstrate that basic FGF (bFGF) induces H_2O_2 production upon stimulation in chondrocytes (190). FGF signaling promotes early response genes such as *c-fos* and *c-jun*, which dimerize to form the AP-1 transcription factor. Exposure to exogenous H_2O_2 recapitulates these ob-

servations in chondrocytes and other cell types (191, 192). Additionally, cells treated with DPI exhibit decreased H_2O_2 levels upon growth factor stimulation. These results suggest that a Nox complex may serve as the oxidant source during FGF signaling, albeit further studies are necessary to confirm these observations. In an isoform-specific study with PDGF and FGF, endogenous H_2O_2 facilitates adipose differentiation in 3T3-L1 adipocytes (66). Alternatively, FGF stimulation may generate H_2O_2 through mechanisms independent of Nox complexes. In lung fibroblasts, Nox activity was measured and remained unchanged during growth factor stimulation. Expression of a dominant-negative Ras mutant (RasN17) diminishes signal-induced H_2O_2 production and suggests it may proceed through a Ras-dependent mechanism (193).

A more recent study identifies direct oxidation of cysteine residues in FGFR. These residues were first characterized in cytoplasmic Src (c-Src) using cysteine mutants to distinguish decreased responses to H_2O_2 exposure (194). Mutation of c-Src Cys277 abolishes its sensitivity to H_2O_2 during *in vitro* assays, and maintains the kinase in a constitutively active form. Gel analysis reveals oxidation of Cys277 inactivates c-Src by forming homodimers connected by a disulfide bond. Cys277 is located within a glycine rich loop (GQGCFG, Gly loop), which participates in catalysis by interacting with the γ -phosphate of ATP. The Gly loop is a universally conserved signature motif present among all protein kinases, but intervening residues can be variable (195). Sequence analysis reveals that only a small subset of protein kinases (~ 8) contains a homologous residue at an equivalent position to c-Src Cys277. These include 3 of 10 Src family kinase members (Src, Yes, Fgr) and all 4 FGFR family members. To confirm its significance, the equivalent residue in FGFR1 (Cys488) was mutated and subjected to similar assays to assess its functional role. C488A attenuates the ability of FGFR1 to respond to H_2O_2 and inactivates the kinase, as observed with c-Src. This mutation does not completely abolish FGFR1 dimerization and suggests that there may be other contributing factors. Although this study identifies a conserved

redox active cysteine found in Src and FGFR family members, the cellular significance of this modification currently remains unknown and presents a potential regulatory mechanism unique to a small subset of kinases.

Non-Receptor Kinases

Akt (also named Protein Kinase B, PKB)

The serine/threonine kinase Akt is a central node downstream of growth factors, cytokines, and other cellular stimuli (31). As described earlier, Akt can be activated by a wide range of stimulants, and is dependent on upstream production of lipid products by PI3K. Negative regulation of Akt is maintained through direct dephosphorylation by protein phosphatase 2A (PP2A) (196), or phosphatase activity of PTEN towards PIP3 (197). Akt has three isoforms (Akt1, Akt2, and Akt3), and achieves signaling specificity through tissue-specific expression (198). Akt1 is the predominantly expressed isoform in a majority of tissues, whereas Akt2 is found to be highly enriched within insulin targeted-tissues (199, 200). In particular, Akt2-deficient mice are insulin resistant and display a diabetic-like phenotype (201). Akt1-null mice have normal glucose tolerance, but exhibit severe growth retardation (202, 203). These mice models demonstrate Akt isoforms are not functionally redundant and are differentially expressed based on substrate preference and subcellular distribution. Aberrant gain or loss of Akt function underlies the pathological states in a variety of diseases, and represents a prominent target for the development of therapeutic strategies (204).

Signal-mediated production of endogenous H₂O₂ has been shown to increase Akt activation in numerous cell types and is modulated by a various signaling components (205). Exposure to PI3K inhibitors (wortmannin and LY294002) strongly attenuates Akt phosphorylation levels and indicates upstream PI3K activation is required for

redox-based modulation of Akt (206). Studies report that H₂O₂ can induce PIP₃ levels in cells overexpressing Nox1 (68), or accumulate PIP₂ under conditions of oxidative stress (207). These lipids bind to Akt to increase its activity and propagate downstream events. H₂O₂ activation of Akt is also mediated in part by Src kinase (208). The detailed mechanism underlying this relationship has not been completely delineated, but may be due to Src-mediated interference of PTEN phosphatase activity (209). Additionally, EGFR-dependent activation of Akt enhances cell survival during H₂O₂-induced apoptosis (210). Overexpression of constitutively active Akt in HeLa and NIH 3T3 fibroblasts results in approximately 40% fewer apoptotic cells when compared to control cells. These results indicate Akt activity may be elevated under conditions of stress to promote cell survival, parallel to observations obtained with Erk1/2 (211). Interestingly, Akt nitrosylation inactivates the kinase and is suggested to contribute to redox-based insulin resistance as well (212, 213).

Redox modulation of multiple cysteine residues have been identified and shown to regulate Akt kinase activity. Treatment with NEM blocks PDGF-induced Akt activation without affecting PI3K function (214). Additionally, NEM inhibits phosphorylation of several Akt downstream effectors, which includes the p70S6K, 4E-BP1, BAD, and FKHR family of transcription factors. These results suggest that sulfhydryl alkylation interferes with the PI3K/Akt pathway at the Akt level. Crystal structures reveal Akt2 forms an intramolecular disulfide bond (Cys297 and Cys311) within its activation loop, which inactivates the kinase (215). These residues are conserved in all three Akt isoforms, but do not significantly alter kinase activity in other isoforms. Inactive Akt2 can be rescued by glutaredoxin (Grx) through reduction of this disulfide to protect cells against apoptosis (216). Grx overexpression suppresses recruitment of PP2A to Akt to sustain phosphatase activity and promote cell survival. A more recent study identifies a third cysteine residue responsible for isoform-specific redox regulation of Akt (217). Using DCP-Bio1, the authors observed that Akt2 forms

a sulfenic acid in response to PDGF stimulation that inactivates the kinase. MS analysis coupled with dimedone labeling and H₂O₂-treated Akt2 identified a sulfenyl modification at Akt2 Cys124. This residue is located in the Akt2 linker region, is not conserved in other isoforms, and is partially responsible for oxidative inactivation of Akt2. Parallel H₂O₂ treatment of NIH 3T3 cells induces indiscriminate Tyr phosphorylation of Akt1 and Akt2, but eventually leads to oxidative inactivation of only Akt2. Additionally, glucose uptake was decreased in WT Akt2, and was unperturbed in an Akt2 C124S mutant. Although H₂O₂ induces Akt activation in many scenarios, it appears that oxidative modification of these three cysteine residues may serve to control the amplitude of Akt2 during signaling.

MAPK (Erk1/2, JNK, p38)

MAPKs are serine/threonine specific kinases that are modulated by a number of receptor-ligand interactions (218–221). Although MAP kinases are composed of five subfamilies, we will focus mainly on evidence implicating redox modulation of Erk1/2, JNK, and p38. Activation of MAPKs proceeds through a three-tiered cascade that begins with a MAP kinase kinase kinase (MEKK or MAP3K), MAP kinase kinase (MEK or MAP2K), and ends with MAPK to elicit its respective effectors. MAPKs have distinct functional roles; Erk1/2 mediates pro-survival events, whereas JNK and p38 are mainly involved in stress-related responses (222, 223). The components involved in redox regulation of MAPKs have been covered extensively in other reviews (27). Therefore, specific examples emphasizing the functional role of cysteine modifications in MAPK pathways will be highlighted for the purpose of the following section.

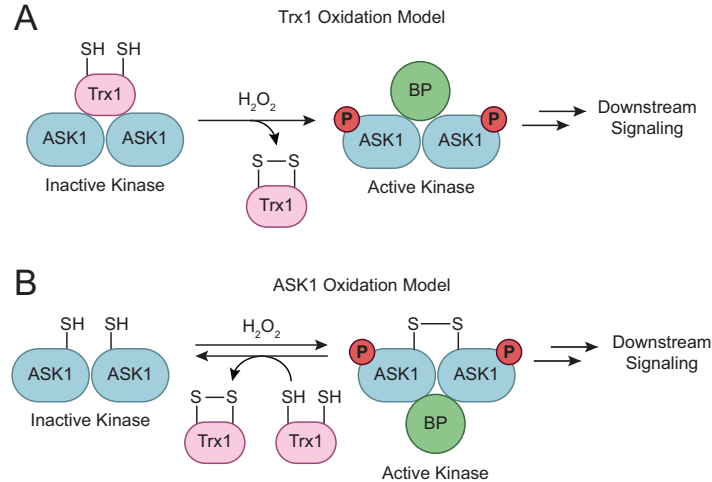


Figure B.9: **Two proposed models for redoxbased activation of ASK1.** (a) Trx1 oxidation model. In the cell, ASK1 assembles into multimers that interact with Trx1. Association of Trx1 with ASK1 sequesters the kinase in an inactive conformation that is released upon oxidation of Trx1 by H_2O_2 . Once released, activated ASK1 interacts with additional binding proteins (BPs) to initiate downstream signaling. (b) ASK1 oxidation model. In this second model, H_2O_2 induces intermolecular disulfide bond formation between ASK1 monomers to promote kinase activation and multimerization. Trx1 is suggested to negatively regulate ASK1 signaling by maintaining the kinase in its reduced state.

Early studies demonstrate that Erk1/2 is activated in response to H_2O_2 and enhances cell survival following oxidant injury (211, 224). H_2O_2 treatment increases Erk1/2 phosphorylation levels 10-20 fold, and moderately for JNK and p38 (~ 3-5 fold). RasN17 expression diminishes H_2O_2 -induced Erk1/2 activation, and renders cells more sensitive to apoptosis when compared to WT controls. Ras can undergo *S*-nitrosylation at Cys118, and represents one mechanism by which redox regulation of Erk1/2 can occur upstream (225). Additionally, overexpression of constitutively active MEK promotes increased cellular resistance to H_2O_2 toxicity. These results demonstrate stimulant-induced H_2O_2 production appears to affect protein targets upstream of Erk1/2 to initiate kinase activity.

Distinct mechanisms have evolved to regulate redox-based responses of MAPK family members. For example, c-Src mediates JNK activation by promoting Cas-Crk complex formation in response to H_2O_2 (226). Cas is a c-Src substrate known to trigger JNK signaling (227). Furthermore, JNK is inhibited in Src-deficient mice or

when treated with Src inhibitors (PP2). This mechanism is unique to JNK, and is not observed with respect to Erk1/2 or p38. Alternatively, Prxs represent another regulatory component involved in JNK signaling. Although the major role of Prxs is to catalyze H_2O_2 decomposition, one study provides mechanistic evidence demonstrating direct JNK activation by Prx (228). Sty1, a JNK homologue found in fission yeast, forms a H_2O_2 -induced intermolecular disulfide bond with Tpx1 (2-Cys Prx). This bond activates Sty1, and forms between the catalytic cysteine of Tpx1 (Cys48) and Sty1 (Cys35). Both residues are conserved in their mammalian counterparts, and suggest similar mechanisms may exist in other eukaryotes. In macrophages, JNK is negatively modulated by S-nitrosylation at Cys116 (229).

Additionally, upstream elements of MAPKs are also subject to direct redox regulation. The apoptosis signal-regulating kinase (ASK1)/Trx1 system is a well-known complex explored by many researchers. ASK1 is a MAP3K responsible for activating JNK and p38 pathways, and is required for tumor necrosis factor- α (TNF- α) mediated apoptosis (230). Two models have been proposed to describe H_2O_2 -induced ASK1 activation. In the first model (Figure B.9a), Trx1 sequesters ASK1 in an inactive complex and undergoes intramolecular disulfide formation upon TNF- α or H_2O_2 stimulation. This releases ASK1, permits oligomerization, and leads to formation of the active complex (231, 232). However, a later study (Figure B.9b) demonstrates stable ASK1 oligomerization and activation is mediated by disulfide bond formation between ASK1 monomers (233). This alternate model suggests Trx1 negatively regulates ASK1 by maintaining its reduced state. Oxidation of ASK1 Cys250 is essential for H_2O_2 -dependent activation of JNK, albeit the exact details underlying this modification are unknown (234). ASK1 C250A mutants attenuate Trx1 association, but do not activate JNK. These results suggest simple dissociation of Trx1 is not sufficient to promote downstream signaling and that oxidative modification of C250 may induce conformational changes in ASK1 to prompt pathway activation. Contrastingly,

S-nitrosylation of ASK1 (Cys869) inactivates the kinase by interfering with MAP2K binding (235).

MEKK1 is another MAP3K responsible for JNK activation, and forms a glutathione adduct at Cys1238 upon H₂O₂ treatment (236). This residue is located in the ATP binding domain, and represents one of many mechanisms utilized to obtain signaling specificity in MAPK pathways. Interestingly, MKK6 (MAP2K activator of p38) was recently identified to form an intramolecular disulfide bond (Cys109 and Cys196) (237). Bond formation negatively regulates p38 by interfering with its ATP binding ability. Sequence alignment of MKK6 reveals that these two residues are conserved in all 7 human MAP2Ks. Similar experiments demonstrate that other MAP2Ks (MKK1 and MKK4) undergo oxidative inactivation analogous to MKK6. Another study demonstrates p38 may also contain redox-sensitive cysteines (Cys119 and Cys162) that reversibly inactivate the kinase upon oxidation (238). Non-reducing gel analysis suggests these residues do not form an intramolecular disulfide, but the exact identity of this modification remains unclear and further studies are necessary to probe its functional relevance. Although many studies have reported H₂O₂-induced activation of MAPK pathways, redox-based inactivation of upstream components also serves to modulate MAPK signal duration.

c-Src

Cytoplasmic Src (c-Src) is a tyrosine kinase and a key regulator of proliferation, survival, cytoskeletal organization, and integrin-dependent signaling responses (239, 240). Abnormal expression or hyperactivation of c-Src is present in several human malignancies and has been linked to the development of human cancers (241). As mentioned previously, c-Src interacts with many ligand-activated RTKs and affects a number of substrates that include adaptor proteins, focal-adhesion proteins, and transcription factors. The Src family of kinases (SFKs) is composed of nine mem-

bers and can be mostly grouped into two subfamilies, namely the Src-related (Src, Yes, Fyn, Fgr) and the Lyn-related (Lyn, Hck, Lck, Blk) kinases. c-Src and other SFK members share a conserved domain architecture composed of an N-terminal region with high variability among family members to enable distinct functionality, followed by SH3, SH2, and tyrosine kinase (SH1) domains flanked by a C-terminal tail (Figure B.10). c-Src contains two residues (Tyr416 and Tyr527) endowed with opposing regulatory mechanisms. Phosphorylation of C-terminal Tyr527 locks Src in an inactive conformation by binding to its SH2 domain, and is further clinched by interactions between the SH2 and SH3 domains (242). In this conformation, the activation loop (A-loop) adopts a compacted structure that precludes ATP access and kinase activation through Tyr416. Concurrent dephosphorylation of Tyr527 and disruption of SH2/SH3 interactions induces an open conformation to enable Tyr416 phosphorylation, leading to full activation of c-Src.

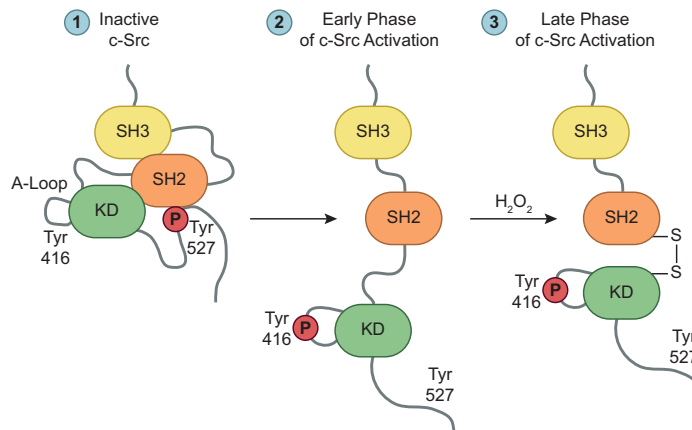


Figure B.10: **Regulation of c-Src.** Inactive c-Src exhibits a "closed" conformation, characterized by binding of phosphorylated Tyr527 to its SH2 domain and interactions between its SH2/SH3 domains. Growth factors and cytokines initiate c-Src activation by promoting concurrent dephosphorylation of Tyr527 and disruption of SH2/SH3 interactions to induce an "open" conformation for Tyr416 autophosphorylation. In the late phase of activation, signal-derived H₂O₂ mediates the formation of an intramolecular disulfide bond between c-Src Cys245 and Cys487. Bond formation promotes kinase activation, Src-mediated cell adhesion, and cytoskeletal reorganization events. Adapted from (243).

Studies reporting H₂O₂-induced Src activation are typically accompanied by increased Tyr416 phosphorylation (244, 245), whereas inactivation is invariably accompanied by increased Tyr527 phosphorylation (246, 247). These complications make it difficult to ascertain whether these effects are due to direct or indirect regulatory mechanisms (243, 248). c-Src is involved in mediating redox-based responses of many signaling components within the Ras/MAPK or PI3K/Akt pathways, and Nox complexes. Suppression of c-Src activity with chemical inhibitors, antisense oligonucleotides, or Src knockout mice interferes with the ability of these pathways to effectively respond to oxidants during signaling and conditions of oxidative stress (249–251). Negative regulation of Src is due to phosphorylation of Tyr527 by Csk (C-terminal Src kinase). Csk is unique among other tyrosine kinases because it only phosphorylates one class of substrate, the conserved Tyr residue located within the C-terminal tail of SFKs (252). Interestingly, evidence suggests the relationship between Src and Csk may be subject to redox regulation. The SH2 domain of Csk contains two cysteine residues (Cys122 and Cys164) that form a unique intramolecular disulfide bond, and is not present in other known SH2 domains (253). Bond formation induces a conformational change and is correlated to decreased Csk catalytic activity. Therefore, this disulfide may serve as a regulatory mechanism to suppress Src inhibition through Csk-mediated phosphorylation. Crystal structures of the Csk-Src complex reveal that disulfide formation occurs between Src Cys277 and Csk Cys290 (254). This does not form within the same kinase-substrate complex, but rather, is composed from Src and Csk in two separate heterodimers. Structural analysis demonstrates this disulfide is crucial in positioning the C-terminal tail of c-Src near the Csk active site to promote Tyr527 phosphorylation. Many Tyr kinases contain a canonical substrate binding site allowing for phosphorylation of several effectors that is destabilized in Csk. Consequently, Csk solely phosphorylates SFK members due to this. The two aforementioned studies demonstrate different functional roles that

disulfide bond formation plays in modulating Src activation.

Cellular studies provide evidence that cysteine oxidation can directly affect c-Src activity, albeit with contradictory conclusions. Evidence for both cases will be presented, but it is important to note contrasting results may be due to the cell types used or sample manipulation. An initial study reports treatment of NIH 3T3 fibroblasts or immunoprecipitated c-Src with exogenous NO donors (*i.e.* SNAP) promotes kinase activation through S-nitrosylation (255). The sulfhydryl residues responsible for this were not identified, but seemingly enhanced Tyr416 autophosphorylation. More recent work identifies c-Src Cys498, a conserved residue in SFK members, as the target of NO-mediated kinase activation (256). H₂O₂ activation of c-Src has also been reported to occur during cell adhesion events. Integrin ligation elicits production of H₂O₂ by lipoxygenases (5-LipOX) to induce c-Src activation through an intramolecular disulfide bond (Cys245 and Cys487) (257). These residues are respectively located within the SH2 and kinase domains of c-Src. During cell adhesion, evidence suggests c-Src proceeds through a biphasic activation process that begins with an early phase characterized by formation of focal adhesions and Tyr527 dephosphorylation. A late phase quickly ensues and is distinguished by lipoxygenase-derived H₂O₂ and phosphorylation of Tyr416. c-Src cysteine mutants demonstrate that disulfide bond formation is required to induce Tyr416 hyperactivation. These combined events demonstrate H₂O₂ promotes kinase activation and Src-mediated cell adhesion and cytoskeletal reorganization (Figure B.10). Lyn, another SFK member, contains a single cysteine residue (Cys466) that functions as a redox sensor to mediate leukocyte wound attraction in zebrafish (258). Alternatively, H₂O₂ has also been shown to suppress Src activation in other studies. As discussed in detail in the FGFR section, a conserved cysteine residue (Cys277) originally identified in c-Src promotes kinase inactivation upon oxidative modification. The significance of this residue, homologous in SFK and FGFR members, was similarly demonstrated with FGFR1. Therefore, it is reason-

able to conclude that opposing regulatory redox mechanisms exist to modulate c-Src activity akin to its phosphorylation sites.

IKK (Inhibitory κ B kinase)

Inhibitory κ B kinase (IKK) is a serine/threonine kinase primarily responsible for activation of transcription factor nuclear factor- κ B (NF- κ B). IKK is composed of two catalytic subunits, IKK α and IKK β , and regulatory subunit IKK γ . Stimulation with cytokines such as TNF α (tumor necrosis factor α) or interleukins induces Ser phosphorylation of IKK α and IKK β subunits by upstream kinases (i.e. MEKK1, Akt). The activated IKK complex phosphorylates inhibitory κ B (I κ B) proteins, which maintain and sequester NF- κ B in its latent form in the cytoplasm. Phosphorylation fosters inducible degradation of I κ B proteins and unmasks the nuclear localization signal (NLS) of NF- κ B to promote nuclear translocation (Figure B.11). NF- κ B binds to recognition motifs and activates gene transcription of over \sim 100 target genes that mediate inflammatory response, proliferation, and survival. NF- κ B can be directly activated by ROS during TNF α signaling and has been extensively analyzed in a number of studies (259).

ROS can also modulate activity of upstream components within the NF- κ B pathway. For example, IKK becomes inactivated upon stimulation with NO or H₂O₂. Exposure of epithelial cells with exogenous NO donor SNAP inhibits IKK kinase activity, but does not interfere with enzyme activation (260). These results suggest NO directly modifies IKK rather than acting upon upstream components. MS analysis identified IKK β Cys179 as the major target for *S*-nitrosylation leading to kinase inactivation. Repression of endogenous NO using NO synthase (NOS) inhibitors relieved SNO-based IKK complex inactivation in Jurkat T cells. Cys179 is strategically located between the two Ser residues (Ser177 and Ser181) required for IKK β activation by TNF α . Therefore, it is probable that IKK phosphorylation at its Ser residues

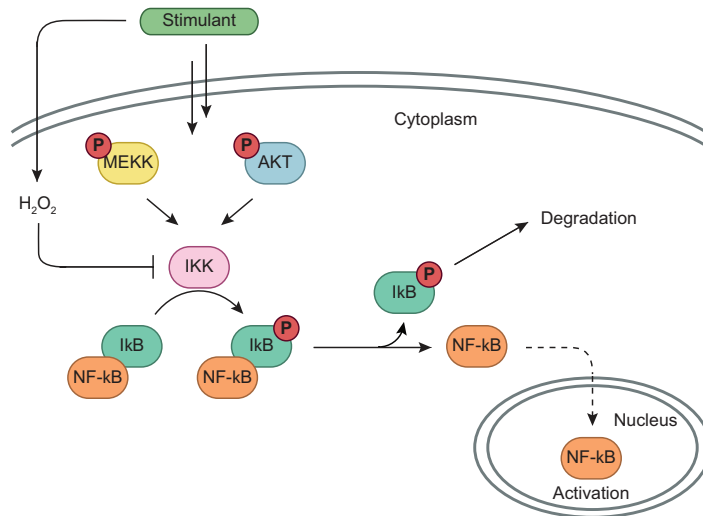


Figure B.11: **IKK activation of NF- κ B**. Stimulation with cytokines (i.e. TNF α or interleukins) triggers Ser phosphorylation of the IKK complex by upstream kinases such as MEKK1 or Akt. Once activated, IKK phosphorylates I κ B proteins, which negatively regulate NF- κ B and maintain the latent transcription factor in the cytoplasm. Phosphorylation of I κ B unmasks the nuclear localization signal of NF- κ B, and promotes nuclear translocation. Once NF- κ B is released, I κ B proteins are subsequently degraded by proteasomes. In addition, IKK can be inactivated by endogenously produced H₂O₂ or NO through direct modulation of Cys179.

may induce a negatively charged environment surrounding Cys179 to promote its susceptibility to *S*-nitrosylation. Interestingly, IKK β Cys179 undergoes inactivation upon exposure to environmental toxins (261). IKK inhibition due to H₂O₂-induced oxidation is also observed in TNF α stimulated epithelial cells (262). MS analysis and dimedone-based experiments reveal that IKK β Cys179 proceeds through a sulfenic acid intermediate to form a glutathione adduct (263). *S*-glutathionylation of IKK β Cys179 is reversed by Grx to restore intrinsic kinase activity. Collectively, these results demonstrate *S*-glutathionylation is a physiologically relevant mechanism that controls the magnitude of NF- κ B activation. Multiple studies have identified a number of Cys179 modification states due to different oxidant sources, indicating redox regulation of the IKK complex functions in a complex manner. In contrast, studies have also reported H₂O₂-mediated activation of IKK; however, it is important to note this may be due to different cell types or oxidant concentration utilized in the studies (264, 265).

Table B.2: Example of redox-regulated protein kinases.

Kinase	Oxidant/source*	Residue/location	Oxoform [†]	Effect of modification	Reference
PDGFR	NA	Cys822 (catalytic loop)	NA	Activation, initiates kinase activity	Lee <i>et al.</i> , 2004
EGFR	H ₂ O ₂ (Nox)	Cys940 Cys797 (ATP-binding site)	Sulfenic acid	Activation, facilitates EGF signaling	Paulsen <i>et al.</i> , 2012
VEGFR	H ₂ O ₂ (Nox)	Cys1209 (C-terminal tail) Cys1199 (C-terminal tail)	Disulfide (intra)	Inactivation	Kang <i>et al.</i> , 2011
IRK	H ₂ O ₂ (exo)	Cys1245 (kinase domain)	Disulfide bond (intra) or <i>S</i> -glutathionylation	Activation, promotes release of ADP from kinase domain	Schmitt <i>et al.</i> , 2005
FGFR	H ₂ O ₂ (exo)	Cys488 (Gly loop in catalytic domain)	Disulfide (inter)	Inactivation	Kemble & Sun, 2009
Akt	H ₂ O ₂ (exo)	Cys297 (activation loop) Cys311 (activation loop)	Disulfide (intra)	Inactivation	Huan <i>et al.</i> , 2003 Murata <i>et al.</i> , 2003
Sty1 (JNK yeast homolog)	H ₂ O ₂ (exo)	Cys35	Disulfide (inter) with Tpx1 (2 Cys-Prx yeast homolog)	Activation	Veal <i>et al.</i> , 2004
JNK	NO (NOS)	Cys116	<i>S</i> -nitrosylation	Inactivation, anti-apoptotic	Park <i>et al.</i> , 2000

* exo, exogenous; L, lipoygenase; NA, not applicable. †intra, intramolecular; inter, intermolecular; ND, not determined.

(Continued on next page.)

Table B.2: Example of redox-regulated protein kinases (Continued.).

Kinase	Oxidant/source*	Residue/location	Oxoform†	Effect of modification	Reference
ASK1	NO (exo), NO (NOS)	Cys869 (kinase domain)	S-nitrosylation	Inactivation, inhibits binding to MKK3/MMK6	Park <i>et al.</i> , 2004b
		Cys22 and/or Cys30, Cys250, Cys835, Cys1052, Cys1361	Disulfide (inter), multimerization	Activation, induction of apoptosis and JNK signaling	Nadeau <i>et al.</i> , 2007
MEKK1	H ₂ O ₂ (exo)	Cys1238 (catalytic domain)	S-glutathionylation	Inactivation	Cross & Templeton, 2004
MKK6	H ₂ O ₂ (exo)	Cys109	Disulfide (intra)	Inactivation, inhibits ATP binding	Diao <i>et al.</i> , 2010
p38	H ₂ O ₂ (exo)	Cys196, Cys199, Cys162	ND	Inactivation	Templeton <i>et al.</i> , 2010
c-Src	NO (NOS), H ₂ O ₂ (L)	Cys498 (C-terminal), Cys245	S-nitrosylation, Disulfide (intra)	Activation, Activation, promotes proliferation and cell adhesion	Rahman <i>et al.</i> , 2010 Giannoni <i>et al.</i> , 2005
		Cys487			
	H ₂ O ₂ (Nox)	Cys277 (Gly loop in catalytic domain)	Disulfide (inter)	Inactivation	Kemble & Sun, 2009
Lyn	H ₂ O ₂ (Nox)	Cys466 (C-terminal kinase domain)	ND	Activation, leukocyte wound attraction	Yoo <i>et al.</i> , 2009

* exo, exogenous; L, lipoxigenase; NA, not applicable. †intra, intramolecular; inter, intermolecular; ND, not determined.

(Continued on next page.)

Table B.2: Example of redox-regulated protein kinases (*Continued.*).

Kinase	Oxidant/source*	Residue/location	Oxoform†	Effect of modification	Reference
IKK	NO (NOS)	Cys179 (IKK β subunit)	S-nitrosylation	Inactivation, represses NF- κ B	Reynaert <i>et al.</i> , 2004
	H ₂ O ₂ (TNF α -induced)	Cys179 (IKK β subunit)	S-glutthionylation	Inactivation, represses NF- κ B	Reynaert <i>et al.</i> , 2006
ATM	H ₂ O ₂ (exo)	Cys2991 (FATC domain)	Disulfide (inter)	Activation, redox sensor	Guo <i>et al.</i> , 2010
PKM2	H ₂ O ₂	Cys358	Disulfide (intra)	Inactivation, generates reducing potential for ROS detoxification	Anastasiou <i>et al.</i> , 2011

* exo, exogenous; L, lipoxygenase; NA, not applicable. †intra, intramolecular; inter, intermolecular; ND, not determined.

Future Perspectives

Although PTPs were originally identified as the main targets of signal-derived H_2O_2 , direct modulation of protein kinases by reversible cysteine oxidation has been identified in a continuously growing number of examples (Table B.2). For instance, *S*-glutathionylation of c-Abl, a non-receptor Tyr kinase, serves to regulate kinase activity under conditions of oxidation stress (266). Specific cysteine residues in two other kinases, ataxia-telangiectasia mutated (ATM) kinase and pyruvate kinase M2 (PKM2), have recently been identified and exhibit distinct functional responses to oxidation. ATM is activated by DNA double-strand breaks (DSBs) and orchestrates signaling pathways that initiate DNA damage response. Upon exposure to H_2O_2 , ATM is activated through an intermolecular disulfide at Cys2991 (267, 268). Redox-based ATM activation occurs separately from DNA damage-based kinase activation, and represents a branch point wherein ATM can also act to modulate global cellular responses to oxidative stress. Moreover, oxidation of PKM2 at Cys358 was shown to inactivate the kinase in A549 lung cancer cells (269). PKM2 inactivation diverts glucose flux into the pentose phosphate pathway and results in increased generation of reducing equivalents (NADPH) for the detoxification of ROS through Prx, GSH, and Trx systems. These recent discoveries demonstrate the likelihood that other kinases may rely on redox-based mechanisms that remain to be unraveled.

The catalytic cysteine of PTPs serves as a well-established regulatory switch during H_2O_2 -mediated signaling to promote kinase activation and downstream signaling in a controlled manner. Therefore, it is intriguing that similar mechanisms may regulate PTKs containing conserved cysteine residues. Eight protein kinases, which include SFK and FGFR members, share a cysteine residue located within a conserved glycine-rich loop (194). This residue causes kinase inactivation *in vitro*, albeit the cellular function of this modification remains unknown. Of the ~ 95 receptor and non-receptor PTKs in the human genome, nine additional members harbor a cys-

EGFR	T	Q	L	M	P	F	G	C	L	L	D
HER2	T	Q	L	M	P	Y	G	C	L	L	D
HER4	T	Q	L	M	P	H	G	C	L	L	E
BLK	T	E	Y	M	A	R	G	C	L	L	D
BMX	T	E	Y	I	S	N	G	C	L	L	N
BTK	T	E	Y	M	A	N	G	C	L	L	N
ITK	F	E	F	M	E	H	G	C	L	S	D
JAK3	M	E	Y	L	P	S	G	C	L	R	D
TEC	T	E	F	M	E	R	G	C	L	L	N
TXK	T	E	F	M	E	N	G	C	L	L	N

Figure B.12: **Abbreviated sequence alignment of EGFR and nine additional kinases that harbor a cysteine residue structurally homologous to EGFR Cys797.** This group includes two erbB family members, HER2 and HER4.

teine residue that corresponds to EGFR Cys797, including two erbB family members (HER2 and HER4) (Figure B.12). Cys797 and its structural homologues serve as the N-terminal end of an alpha helix known as the N_{cap} position. Interestingly, cysteine is the most sparsely occurring N_{cap} residue in proteins and comprises less than 1% of these positions (270). Interaction of a cysteine residue with the helical dipole within an N_{cap} context reduces the pKa of the residue, which inherently increases its reactivity (271). Efforts focused on delineating the molecular mechanisms by which protein kinases are directly modulated by H_2O_2 could uncover general signaling mechanisms that regulate kinases and their structural homologues.

Aberrant kinase activation has been identified in a number of human pathologies, as referenced for each kinase within its respective section. This has stimulated efforts to develop therapeutic strategies such as antibodies and reversible inhibitors to target specific kinase classes. Many reversible inhibitors attenuate kinase activation by interfering with the ATP binding site. Additionally, irreversible inhibitors have also been developed for certain kinases (272, 273). For example, EGFR is mutated or amplified in a number of human carcinomas such as breast and lung cancers. This has motivated the development of a class of selective kinase inhibitors that covalently modify EGFR Cys797 (274, 275). Several of these irreversible EGFR inhibitors are currently under-

going preclinical or clinical trials (136, 137). Overexpression of EGFR and HER2 is correlated to increased H_2O_2 levels and global protein oxidation in breast cancer cell lines (276). When coupled to recent evidence that identifies sulfenic acid modification of EGFR Cys797, these findings raise several fundamental questions regarding cysteine modifications versus thiol-targeted covalent inhibitors. The aforementioned irreversible EGFR inhibitors contain an acrylamide moiety that undergoes Michael addition with Cys797 in its thiol form, but are not capable of reacting with sulfenic acid or disulfide states. Oxidative modification of Cys797 could impact the potency of these inhibitors, particularly in cancers characterized by high levels of stress and aberrant H_2O_2 levels. Therefore, the sulfenyl form of EGFR Cys797 could be exploited to develop new classes of irreversible inhibitors that incorporate nucleophilic warheads akin to chemical probes recently developed for PTPs (277). If successful, redox-based EGFR inhibitors would exhibit enhanced selectivity for cancerous cells exhibiting high levels of oxidative stress, and may reduce the toxicity caused by acrylamide-based compounds. Analogous approaches could be employed to generate nucleophilic warheads for other classes of redox-modulated protein families as well.

Conclusions

The role of protein kinases in physiologic and pathological settings represents an active and exciting area of research. The collective efforts of several individuals have contributed tremendously towards uncovering the underlying mechanisms involved in redox-regulation of protein kinases. These studies have expanded our knowledge and demonstrate that kinases may be modulated both directly and indirectly upon stimulant-induced H_2O_2 production. The continued efforts to dissect kinase function will further our basic understanding of kinase redox-regulation, uncover new protein targets, and could lead to the development of new redox-based strategies for therapeutics.

Chapter References

1. Chiarugi, P. & Buricchi, F. (2007). Protein tyrosine phosphorylation and reversible oxidation: two cross-talking posttranslation modifications. *Antioxid Redox Signal*, *9*(1), 1–24.
2. Manning, G., Whyte, D. B., Martinez, R., Hunter, T., & Sudarsanam, S. (2002). The protein kinase complement of the human genome. *Science*, *298*(5600), 1912–34.
3. Schlessinger, J. (2000). Cell signaling by receptor tyrosine kinases. *Cell*, *103*(2), 211–25.
4. Hubbard, S. R. & Till, J. H. (2000). Protein tyrosine kinase structure and function. *Annu Rev Biochem*, *69*, 373–98.
5. Blume-Jensen, P. & Hunter, T. (2001). Oncogenic kinase signalling. *Nature*, *411*(6835), 355–65.
6. Rhee, S. G. (2006). Cell signaling. H_2O_2 , a necessary evil for cell signaling. *Science*, *312*(5782), 1882–3.
7. D’Autreaux, B. & Toledano, M. B. (2007). Ros as signalling molecules: mechanisms that generate specificity in ros homeostasis. *Nat Rev Mol Cell Biol*, *8*(10), 813–24.
8. Dickinson, B. C. & Chang, C. J. (2011). Chemistry and biology of reactive oxygen species in signaling or stress responses. *Nat Chem Biol*, *7*(8), 504–11.
9. Finkel, T. (2011). Signal transduction by reactive oxygen species. *J Cell Biol*, *194*(1), 7–15.
10. Nakashima, I., Kato, M., Akhand, A. A., Suzuki, H., Takeda, K., Hossain, K., & Kawamoto, Y. (2002). Redox-linked signal transduction pathways for protein tyrosine kinase activation. *Antioxid Redox Signal*, *4*(3), 517–31.
11. Aslan, M. & Ozben, T. (2003). Oxidants in receptor tyrosine kinase signal transduction pathways. *Antioxid Redox Signal*, *5*(6), 781–8.
12. Giorgio, M., Trinei, M., Migliaccio, E., & Pelicci, P. G. (2007). Hydrogen peroxide: a metabolic by-product or a common mediator of ageing signals? *Nat Rev Mol Cell Biol*, *8*(9), 722–8.
13. Lambeth, J. D. (2004). Nox enzymes and the biology of reactive oxygen. *Nat Rev Immunol*, *4*(3), 181–9.
14. Stone, J. R. & Yang, S. (2006). Hydrogen peroxide: a signaling messenger. *Antioxid Redox Signal*, *8*(3-4), 243–70.

15. Mamathambika, B. S. & Bardwell, J. C. (2008). Disulfide-linked protein folding pathways. *Annu Rev Cell Dev Biol*, *24*, 211–35.
16. Go, Y. M. & Jones, D. P. (2013). Thiol/disulfide redox states in signaling and sensing. *Crit Rev Biochem Mol Biol*.
17. Depuydt, M., Messens, J., & Collet, J. F. (2011). How proteins form disulfide bonds. *Antioxid Redox Signal*, *15*(1), 49–66.
18. Finkel, T., Serrano, M., & Blasco, M. A. (2007). The common biology of cancer and ageing. *Nature*, *448*(7155), 767–74.
19. Barnham, K. J., Masters, C. L., & Bush, A. I. (2004). Neurodegenerative diseases and oxidative stress. *Nat Rev Drug Discov*, *3*(3), 205–14.
20. Lowell, B. B. & Shulman, G. I. (2005). Mitochondrial dysfunction and type 2 diabetes. *Science*, *307*(5708), 384–7.
21. Sundaresan, M., Yu, Z. X., Ferrans, V. J., Irani, K., & Finkel, T. (1995). Requirement for generation of h₂o₂ for platelet-derived growth factor signal transduction. *Science*, *270*(5234), 296–9.
22. Bae, Y. S., Kang, S. W., Seo, M. S., Baines, I. C., Tekle, E., Chock, P. B., & Rhee, S. G. (1997). Epidermal growth factor (egf)-induced generation of hydrogen peroxide. role in egf receptor-mediated tyrosine phosphorylation. *J Biol Chem*, *272*(1), 217–21.
23. Lu, Z. & Xu, S. (2006). Erk1/2 map kinases in cell survival and apoptosis. *IUBMB Life*, *58*(11), 621–31.
24. Wortzel, I. & Seger, R. (2011). The erk cascade: distinct functions within various subcellular organelles. *Genes Cancer*, *2*(3), 195–209.
25. Mebratu, Y. & Tesfaiqzi, Y. (2009). How erk1/2 activation controls cell proliferation and cell death: is subcellular localization the answer? *Cell Cycle*, *8*(8), 1168–75.
26. Matsuzawa, A. & Ichijo, H. (2005). Stress-responsive protein kinases in redox-regulated apoptosis signaling. *Antioxid Redox Signal*, *7*(3-4), 472–81.
27. McCubrey, J. A., Lahair, M. M., & Franklin, R. A. (2006). Reactive oxygen species-induced activation of the map kinase signaling pathways. *Antioxid Redox Signal*, *8*(9-10), 1775–89.
28. Leslie, N. R. (2006). The redox regulation of pi 3-kinase-dependent signaling. *Antioxid Redox Signal*, *8*(9-10), 1765–74.
29. Stokoe, D., Stephens, L. R., Copeland, T., Gaffney, P. R., Reese, C. B., Painter, G. F., . . . Hawkins, P. T. (1997). Dual role of phosphatidylinositol-3,4,5-trisphosphate in the activation of protein kinase b. *Science*, *277*(5325), 567–70.

30. Franke, T. F., Kaplan, D. R., Cantley, L. C., & Toker, A. (1997). Direct regulation of the akt proto-oncogene product by phosphatidylinositol-3,4-bisphosphate. *Science*, *275*(5300), 665–8.
31. Manning, B. D. & Cantley, L. C. (2007). Akt/pkb signaling: navigating downstream. *Cell*, *129*(7), 1261–74.
32. Leslie, N. R., Bennett, D., Lindsay, Y. E., Stewart, H., Gray, A., & Downes, C. P. (2003). Redox regulation of pi 3-kinase signalling via inactivation of pten. *EMBO J*, *22*(20), 5501–10.
33. Stambolic, V., Suzuki, A., de la Pompa, J. L., Brothers, G. M., Mirtsos, C., Sasaki, T., . . . Mak, T. W. (1998). Negative regulation of pkb/akt-dependent cell survival by the tumor suppressor pten. *Cell*, *95*(1), 29–39.
34. Cantley, L. C. & Neel, B. G. (1999). New insights into tumor suppression: pten suppresses tumor formation by restraining the phosphoinositide 3-kinase/akt pathway. *Proc Natl Acad Sci U S A*, *96*(8), 4240–5.
35. McCord, J. M. & Fridovich, I. (1969). Superoxide dismutase. an enzymic function for erythrocuprein (hemocuprein). *J Biol Chem*, *244*(22), 6049–55.
36. Hsu, J. L., Hsieh, Y., Tu, C., O'Connor, D., Nick, H. S., & Silverman, D. N. (1996). Catalytic properties of human manganese superoxide dismutase. *J Biol Chem*, *271*(30), 17687–91.
37. Fridovich, I. (1995). Superoxide radical and superoxide dismutases. *Annu Rev Biochem*, *64*, 97–112.
38. Gardner, P. R., Raineri, I., Epstein, L. B., & White, C. W. (1995). Superoxide radical and iron modulate aconitase activity in mammalian cells. *J Biol Chem*, *270*(22), 13399–405.
39. Jacob, C. & Winyard, P. (2009). *Redox signaling and regulation in biology and medicine*. Weinheim: Wiley-VCH.
40. Bienert, G. P., Schjoerring, J. K., & Jahn, T. P. (2006). Membrane transport of hydrogen peroxide. *Biochim Biophys Acta*, *1758*(8), 994–1003.
41. Bienert, G. P., Moller, A. L., Kristiansen, K. A., Schulz, A., Moller, I. M., Schjoerring, J. K., & Jahn, T. P. (2007). Specific aquaporins facilitate the diffusion of hydrogen peroxide across membranes. *J Biol Chem*, *282*(2), 1183–92.
42. Miller, E. W., Dickinson, B. C., & Chang, C. J. (2010). Aquaporin-3 mediates hydrogen peroxide uptake to regulate downstream intracellular signaling. *Proc Natl Acad Sci U S A*, *107*(36), 15681–6.
43. Suh, Y. A., Arnold, R. S., Lassegue, B., Shi, J., Xu, X., Sorescu, D., . . . Lambeth, J. D. (1999). Cell transformation by the superoxide-generating oxidase mox1. *Nature*, *401*(6748), 79–82.

44. Cheng, G., Cao, Z., Xu, X., van Meir, E. G., & Lambeth, J. D. (2001). Homologs of gp91phox: cloning and tissue expression of nox3, nox4, and nox5. *Gene*, *269*(1-2), 131–40.
45. De Deken, X., Wang, D., Many, M. C., Costagliola, S., Libert, F., Vassart, G., ... Miot, F. (2000). Cloning of two human thyroid cdnas encoding new members of the nadph oxidase family. *J Biol Chem*, *275*(30), 23227–33.
46. Raha, S. & Robinson, B. H. (2000). Mitochondria, oxygen free radicals, disease and ageing. *Trends Biochem Sci*, *25*(10), 502–8.
47. St-Pierre, J., Buckingham, J. A., Roebuck, S. J., & Brand, M. D. (2002). Topology of superoxide production from different sites in the mitochondrial electron transport chain. *J Biol Chem*, *277*(47), 44784–90.
48. Migliaccio, E., Giorgio, M., Mele, S., Pelicci, G., Reboldi, P., Pandolfi, P. P., ... Pelicci, P. G. (1999). The p66shc adaptor protein controls oxidative stress response and life span in mammals. *Nature*, *402*(6759), 309–13.
49. Giorgio, M., Migliaccio, E., Orsini, F., Paolucci, D., Moroni, M., Contursi, C., ... Pelicci, P. G. (2005). Electron transfer between cytochrome c and p66shc generates reactive oxygen species that trigger mitochondrial apoptosis. *Cell*, *122*(2), 221–33.
50. Hess, D. T. & Stamler, J. S. (2012). Regulation by s-nitrosylation of protein post-translational modification. *J Biol Chem*, *287*(7), 4411–8.
51. Hall, A., Karplus, P. A., & Poole, L. B. (2009). Typical 2-cys peroxiredoxins—structures, mechanisms and functions. *FEBS J*, *276*(9), 2469–77.
52. Klomsiri, C., Karplus, P. A., & Poole, L. B. (2011). Cysteine-based redox switches in enzymes. *Antioxid Redox Signal*, *14*(6), 1065–77.
53. Reddie, K. G., Seo, Y. H., Muse Iii, W. B., Leonard, S. E., & Carroll, K. S. (2008). A chemical approach for detecting sulfenic acid-modified proteins in living cells. *Mol Biosyst*, *4*(6), 521–31.
54. Paulsen, C. E. & Carroll, K. S. (2010). Orchestrating redox signaling networks through regulatory cysteine switches. *ACS Chem Biol*, *5*(1), 47–62.
55. Jacob, C., Battaglia, E., Burkholz, T., Peng, D., Bagrel, D., & Montenarh, M. (2012). Control of oxidative posttranslational cysteine modifications: from intricate chemistry to widespread biological and medical applications. *Chem Res Toxicol*, *25*(3), 588–604.
56. Denu, J. M. & Tanner, K. G. (1998). Specific and reversible inactivation of protein tyrosine phosphatases by hydrogen peroxide: evidence for a sulfenic acid intermediate and implications for redox regulation. *Biochemistry*, *37*(16), 5633–42.

57. Winterbourn, C. C. & Metodiewa, D. (1999). Reactivity of biologically important thiol compounds with superoxide and hydrogen peroxide. *Free Radic Biol Med*, 27(3-4), 322–8.
58. Winterbourn, C. C. (2008). Reconciling the chemistry and biology of reactive oxygen species. *Nat Chem Biol*, 4(5), 278–86.
59. Salsbury, J., F. R., Knutson, S. T., Poole, L. B., & Fetrow, J. S. (2008). Functional site profiling and electrostatic analysis of cysteines modifiable to cysteine sulfenic acid. *Protein Sci*, 17(2), 299–312.
60. Banerjee, R. (2008). *Redox biochemistry*. Hoboken, NJ: John Wiley & Sons.
61. Zhang, Z. Y. & Dixon, J. E. (1993). Active site labeling of the yersinia protein tyrosine phosphatase: the determination of the pka of the active site cysteine and the function of the conserved histidine 402. *Biochemistry*, 32(36), 9340–5.
62. Lohse, D. L., Denu, J. M., Santoro, N., & Dixon, J. E. (1997). Roles of aspartic acid-181 and serine-222 in intermediate formation and hydrolysis of the mammalian protein-tyrosine-phosphatase ptp1. *Biochemistry*, 36(15), 4568–75.
63. Heldin, C. H. & Westermark, B. (1999). Mechanism of action and in vivo role of platelet-derived growth factor. *Physiol Rev*, 79(4), 1283–316.
64. Andrae, J., Gallini, R., & Betsholtz, C. (2008). Role of platelet-derived growth factors in physiology and medicine. *Genes Dev*, 22(10), 1276–312.
65. Krieger-Brauer, H. I. & Kather, H. (1992). Human fat cells possess a plasma membrane-bound h₂o₂-generating system that is activated by insulin via a mechanism bypassing the receptor kinase. *J Clin Invest*, 89(3), 1006–13.
66. Krieger-Brauer, H. I. & Kather, H. (1995). Antagonistic effects of different members of the fibroblast and platelet-derived growth factor families on adipose conversion and nadph-dependent h₂o₂ generation in 3t3 l1-cells. *Biochem J*, 307 (Pt 2), 549–56.
67. Bae, Y. S., Sung, J. Y., Kim, O. S., Kim, Y. J., Hur, K. C., Kazlauskas, A., & Rhee, S. G. (2000). Platelet-derived growth factor-induced h₂o₂ production requires the activation of phosphatidylinositol 3-kinase. *J Biol Chem*, 275(14), 10527–31.
68. Kwon, J., Lee, S. R., Yang, K. S., Ahn, Y., Kim, Y. J., Stadtman, E. R., & Rhee, S. G. (2004). Reversible oxidation and inactivation of the tumor suppressor pten in cells stimulated with peptide growth factors. *Proc Natl Acad Sci U S A*, 101(47), 16419–24.
69. Sundaresan, M., Yu, Z. X., Ferrans, V. J., Sulciner, D. J., Gutkind, J. S., Irani, K., ... Finkel, T. (1996). Regulation of reactive-oxygen-species generation in fibroblasts by rac1. *Biochem J*, 318 (Pt 2), 379–82.

70. Joneson, T. & Bar-Sagi, D. (1998). A rac1 effector site controlling mitogenesis through superoxide production. *J Biol Chem*, *273*(29), 17991–4.
71. Park, H. S., Lee, S. H., Park, D., Lee, J. S., Ryu, S. H., Lee, W. J., . . . Bae, Y. S. (2004). Sequential activation of phosphatidylinositol 3-kinase, beta pix, rac1, and nox1 in growth factor-induced production of h2o2. *Mol Cell Biol*, *24*(10), 4384–94.
72. Lassegue, B., Sorescu, D., Szocs, K., Yin, Q., Akers, M., Zhang, Y., . . . Griendling, K. K. (2001). Novel gp91(phox) homologues in vascular smooth muscle cells : nox1 mediates angiotensin ii-induced superoxide formation and redox-sensitive signaling pathways. *Circ Res*, *88*(9), 888–94.
73. Chiarugi, P., Fiaschi, T., Taddei, M. L., Talini, D., Giannoni, E., Raugei, G., & Ramponi, G. (2001). Two vicinal cysteines confer a peculiar redox regulation to low molecular weight protein tyrosine phosphatase in response to platelet-derived growth factor receptor stimulation. *J Biol Chem*, *276*(36), 33478–87.
74. Saito, Y. & Berk, B. C. (2001). Transactivation: a novel signaling pathway from angiotensin ii to tyrosine kinase receptors. *J Mol Cell Cardiol*, *33*(1), 3–7.
75. Heeneman, S., Haendeler, J., Saito, Y., Ishida, M., & Berk, B. C. (2000). Angiotensin ii induces transactivation of two different populations of the platelet-derived growth factor beta receptor. key role for the p66 adaptor protein shc. *J Biol Chem*, *275*(21), 15926–32.
76. Saito, S., Frank, G. D., Mifune, M., Ohba, M., Utsunomiya, H., Motley, E. D., . . . Eguchi, S. (2002). Ligand-independent trans-activation of the platelet-derived growth factor receptor by reactive oxygen species requires protein kinase c-delta and c-src. *J Biol Chem*, *277*(47), 44695–700.
77. Chen, K., Thomas, S. R., Albano, A., Murphy, M. P., & Keaney, J., J. F. (2004). Mitochondrial function is required for hydrogen peroxide-induced growth factor receptor transactivation and downstream signaling. *J Biol Chem*, *279*(33), 35079–86.
78. Chiarugi, P., Cirri, P., Raugei, G., Camici, G., Dolfi, F., Berti, A., & Ramponi, G. (1995). Pdgf receptor as a specific in vivo target for low m(r) phosphotyrosine protein phosphatase. *FEBS Lett*, *372*(1), 49–53.
79. Meng, T.-C., Fukada, T., & Tonks, N. K. (2002). Reversible oxidation and inactivation of protein tyrosine phosphatases in vivo. *Mol Cell*, *9*(2), 387–399.
80. Caselli, A., Marzocchini, R., Camici, G., Manao, G., Moneti, G., Pieraccini, G., & Ramponi, G. (1998). The inactivation mechanism of low molecular weight phosphotyrosine-protein phosphatase by h2o2. *J Biol Chem*, *273*(49), 32554–60.

81. Kanda, M., Ihara, Y., Murata, H., Urata, Y., Kono, T., Yodoi, J., ... Kondo, T. (2006). Glutaredoxin modulates platelet-derived growth factor-dependent cell signaling by regulating the redox status of low molecular weight protein-tyrosine phosphatase. *J Biol Chem*, *281*(39), 28518–28.
82. Chiarugi, P., Cirri, P., Taddei, M. L., Talini, D., Doria, L., Fiaschi, T., ... Ramponi, G. (2002). New perspectives in pdgf receptor downregulation: the main role of phosphotyrosine phosphatases. *J Cell Sci*, *115*(Pt 10), 2219–32.
83. Choi, M. H., Lee, I. K., Kim, G. W., Kim, B. U., Han, Y. H., Yu, D. Y., ... Kang, S. W. (2005). Regulation of pdgf signalling and vascular remodelling by peroxiredoxin ii. *Nature*, *435*(7040), 347–53.
84. Parsonage, D., Karplus, P. A., & Poole, L. B. (2008). Substrate specificity and redox potential of ahpc, a bacterial peroxiredoxin. *Proc Natl Acad Sci U S A*, *105*(24), 8209–14.
85. Peskin, A. V., Low, F. M., Paton, L. N., Maghzal, G. J., Hampton, M. B., & Winterbourn, C. C. (2007). The high reactivity of peroxiredoxin 2 with h(2)o(2) is not reflected in its reaction with other oxidants and thiol reagents. *J Biol Chem*, *282*(16), 11885–92.
86. Woo, H. A., Yim, S. H., Shin, D. H., Kang, D., Yu, D. Y., & Rhee, S. G. (2010). Inactivation of peroxiredoxin i by phosphorylation allows localized h(2)o(2) accumulation for cell signaling. *Cell*, *140*(4), 517–28.
87. Li, W. & Schlessinger, J. (1991). Platelet-derived growth factor (pdgf)-induced disulfide-linked dimerization of pdgf receptor in living cells. *Mol Cell Biol*, *11*(7), 3756–61.
88. Lee, C., Lee, S. M., Mukhopadhyay, P., Kim, S. J., Lee, S. C., Ahn, W.-S., ... Ryu, S. E. (2004). Redox regulation of oxyr requires specific disulfide bond formation involving a rapid kinetic reaction path. *Nat Struct Mol Biol*, *11*(12), 1179–1185.
89. Cohen, S., Carpenter, G., & King, J., L. (1980). Epidermal growth factor-receptor-protein kinase interactions. co-purification of receptor and epidermal growth factor-enhanced phosphorylation activity. *J Biol Chem*, *255*(10), 4834–42.
90. Carpenter, G., King, J., L., & Cohen, S. (1978). Epidermal growth factor stimulates phosphorylation in membrane preparations in vitro. *Nature*, *276*(5686), 409–10.
91. Cohen, S. (2008). Origins of growth factors: ngf and egf. *J Biol Chem*, *283*(49), 33793–7.
92. Schlessinger, J. (2002). Ligand-induced, receptor-mediated dimerization and activation of egf receptor. *Cell*, *110*(6), 669–72.

93. Yarden, Y. & Sliwkowski, M. X. (2001). Untangling the erbb signalling network. *Nat Rev Mol Cell Biol*, 2(2), 127–37.
94. Macias, A., Azavedo, E., Hagerstrom, T., Klintenberg, C., Perez, R., & Skoog, L. (1987). Prognostic significance of the receptor for epidermal growth factor in human mammary carcinomas. *Anticancer Res*, 7(3 Pt B), 459–64.
95. Herbst, R. S. (2004). Review of epidermal growth factor receptor biology. *Int J Radiat Oncol Biol Phys*, 59(2 Suppl), 21–6.
96. Finkel, T. (2012). From sulfenylation to sulfhydration: what a thiolate needs to tolerate. *Sci Signal*, 5(215), pe10.
97. Truong, T. H. & Carroll, K. S. (2012). Redox regulation of epidermal growth factor receptor signaling through cysteine oxidation. *Biochemistry*, 51(50), 9954–65.
98. Gamou, S. & Shimizu, N. (1995). Hydrogen peroxide preferentially enhances the tyrosine phosphorylation of epidermal growth factor receptor. *FEBS Lett*, 357(2), 161–4.
99. Goldkorn, T., Balaban, N., Matsukuma, K., Chea, V., Gould, R., Last, J., . . . Chavez, C. (1998). Egf-receptor phosphorylation and signaling are targeted by h2o2 redox stress. *Am J Respir Cell Mol Biol*, 19(5), 786–98.
100. Murillo-Carretero, M., Torroglosa, A., Castro, C., Villalobo, A., & Estrada, C. (2009). S-nitrosylation of the epidermal growth factor receptor: a regulatory mechanism of receptor tyrosine kinase activity. *Free Radic Biol Med*, 46(4), 471–9.
101. Lam, Y. W., Yuan, Y., Isaac, J., Babu, C. V., Meller, J., & Ho, S. M. (2010). Comprehensive identification and modified-site mapping of s-nitrosylated targets in prostate epithelial cells. *PLoS One*, 5(2), e9075.
102. Switzer, C. H., Glynn, S. A., Cheng, R. Y., Ridnour, L. A., Green, J. E., Ambs, S., & Wink, D. A. (2012). S-nitrosylation of egfr and src activates an oncogenic signaling network in human basal-like breast cancer. *Mol Cancer Res*, 10(9), 1203–15.
103. Ushio-Fukai, M., Griending, K. K., Becker, P. L., Hilenski, L., Halleran, S., & Alexander, R. W. (2001). Epidermal growth factor receptor transactivation by angiotensin ii requires reactive oxygen species in vascular smooth muscle cells. *Arterioscler Thromb Vasc Biol*, 21(4), 489–95.
104. Chen, K., Vita, J. A., Berk, B. C., & Keaney, J., J. F. (2001a). C-jun n-terminal kinase activation by hydrogen peroxide in endothelial cells involves src-dependent epidermal growth factor receptor transactivation. *J Biol Chem*, 276(19), 16045–50.

105. Giannoni, E. [E.], Buricchi, F., Grimaldi, G., Parri, M., Cialdai, F., Taddei, M. L., ... Chiarugi, P. (2008). Redox regulation of anoikis: reactive oxygen species as essential mediators of cell survival. *Cell Death Differ*, *15*(5), 867–78.
106. Reynolds, A. R., Tischer, C., Verveer, P. J., Rocks, O., & Bastiaens, P. I. (2003). Egfr activation coupled to inhibition of tyrosine phosphatases causes lateral signal propagation. *Nat Cell Biol*, *5*(5), 447–53.
107. Flint, A. J., Tiganis, T., Barford, D., & Tonks, N. K. (1997). Development of "substrate-trapping" mutants to identify physiological substrates of protein tyrosine phosphatases. *Proc Natl Acad Sci U S A*, *94*(5), 1680–5.
108. Haj, F. G., Markova, B., Klaman, L. D., Bohmer, F. D., & Neel, B. G. (2003). Regulation of receptor tyrosine kinase signaling by protein tyrosine phosphatase-1b. *J Biol Chem*, *278*(2), 739–44.
109. Haj, F. G., Verveer, P. J., Squire, A., Neel, B. G., & Bastiaens, P. I. (2002). Imaging sites of receptor dephosphorylation by ptp1b on the surface of the endoplasmic reticulum. *Science*, *295*(5560), 1708–11.
110. Lee, S. R., Kwon, K. S., Kim, S. R., & Rhee, S. G. (1998). Reversible inactivation of protein-tyrosine phosphatase 1b in a431 cells stimulated with epidermal growth factor. *J Biol Chem*, *273*(25), 15366–72.
111. Vivanco, I., Rohle, D., Versele, M., Iwanami, A., Kuga, D., Oldrini, B., ... Mellinghoff, I. K. (2010). The phosphatase and tensin homolog regulates epidermal growth factor receptor (egfr) inhibitor response by targeting egfr for degradation. *Proc Natl Acad Sci U S A*, *107*(14), 6459–64.
112. Lee, S. R., Yang, K. S., Kwon, J., Lee, C., Jeong, W., & Rhee, S. G. (2002). Reversible inactivation of the tumor suppressor pten by h2o2. *J Biol Chem*, *277*(23), 20336–42.
113. Oh, H., Jung, H. Y., Kim, J., & Bae, Y. S. (2010). Phosphorylation of serine282 in nadph oxidase activator 1 by erk desensitizes egf-induced ros generation. *Biochem Biophys Res Commun*, *394*(3), 691–6.
114. Kroviarski, Y., Debbabi, M., Bachoual, R., Perianin, A., Gougerot-Pocidallo, M. A., El-Benna, J., & Dang, P. M. (2010). Phosphorylation of nadph oxidase activator 1 (nox1) on serine 282 by map kinases and on serine 172 by protein kinase c and protein kinase a prevents nox1 hyperactivation. *FASEB Journal*, *24*(6), 2077–92.
115. Chen, K., Kirber, M. T., Xiao, H., Yang, Y., & Keaney, J., J. F. (2008). Regulation of ros signal transduction by nadph oxidase 4 localization. *J Cell Biol*, *181*(7), 1129–39.

116. Juarez, J. C., Manuia, M., Burnett, M. E., Betancourt, O., Boivin, B., Shaw, D. E., . . . Donate, F. (2008). Superoxide dismutase 1 (sod1) is essential for h2o2-mediated oxidation and inactivation of phosphatases in growth factor signaling. *Proc Natl Acad Sci U S A*, *105*(20), 7147–52.
117. DeYulia, J., G. J., Carcamo, J. M., Borquez-Ojeda, O., Shelton, C. C., & Golde, D. W. (2005). Hydrogen peroxide generated extracellularly by receptor-ligand interaction facilitates cell signaling. *Proc Natl Acad Sci U S A*, *102*(14), 5044–9.
118. DeYulia, J., G. J. & Carcamo, J. M. (2005). Egf receptor-ligand interaction generates extracellular hydrogen peroxide that inhibits egfr-associated protein tyrosine phosphatases. *Biochem Biophys Res Commun*, *334*(1), 38–42.
119. Halvey, P. J., Watson, W. H., Hansen, J. M., Go, Y. M., Samali, A., & Jones, D. P. (2005). Compartmental oxidation of thiol-disulphide redox couples during epidermal growth factor signalling. *Biochem J*, *386*(Pt 2), 215–9.
120. Kang, S. W., Chae, H. Z., Seo, M. S., Kim, K., Baines, I. C., & Rhee, S. G. (1998). Mammalian peroxiredoxin isoforms can reduce hydrogen peroxide generated in response to growth factors and tumor necrosis factor-alpha. *J Biol Chem*, *273*(11), 6297–302.
121. Handy, D. E., Lubos, E., Yang, Y., Galbraith, J. D., Kelly, N., Zhang, Y. Y., . . . Loscalzo, J. (2009). Glutathione peroxidase-1 regulates mitochondrial function to modulate redox-dependent cellular responses. *J Biol Chem*, *284*(18), 11913–21.
122. Paulsen, C. E., Truong, T. H., Garcia, F. J., Homann, A., Gupta, V., Leonard, S. E., & Carroll, K. S. (2012). Peroxide-dependent sulfenylation of the egfr catalytic site enhances kinase activity. *Nat Chem Biol*, *8*(1), 57–64.
123. Buhrow, S. A., Cohen, S., & Staros, J. V. (1982). Affinity labeling of the protein kinase associated with the epidermal growth factor receptor in membrane vesicles from a431 cells. *J Biol Chem*, *257*(8), 4019–22.
124. Clark, S. & Konstantopoulos, N. (1993). Sulphydryl agents modulate insulin- and epidermal growth factor (egf)-receptor kinase via reaction with intracellular receptor domains: differential effects on basal versus activated receptors. *Biochem J*, *292* (Pt 1), 217–23.
125. Woltjer, R. L. & Staros, J. V. (1997). Effects of sulfhydryl modification reagents on the kinase activity of the epidermal growth factor receptor. *Biochemistry*, *36*(32), 9911–6.
126. Poole, L. B., Zeng, B. B., Knaggs, S. A., Yakubu, M., & King, S. B. (2005). Synthesis of chemical probes to map sulfenic acid modifications on proteins. *Bioconjug Chem*, *16*(6), 1624–8.

127. Poole, L. B., Klomsiri, C., Knaggs, S. A., Furdai, C. M., Nelson, K. J., Thomas, M. J., . . . King, S. B. (2007). Fluorescent and affinity-based tools to detect cysteine sulfenic acid formation in proteins. *Bioconjug Chem*, *18*(6), 2004–17.
128. Leonard, S. E., Reddie, K. G., & Carroll, K. S. (2009). Mining the thiol proteome for sulfenic acid modifications reveals new targets for oxidation in cells. *ACS Chem Biol*, *4*(9), 783–99.
129. Seo, Y. H. & Carroll, K. S. (2011). Quantification of protein sulfenic acid modifications using isotope-coded dimedone and iododimedone. *Angew Chem Int Ed Engl*, *50*(6), 1342–5.
130. Truong, T. H., Garcia, F. J., Seo, Y. H., & Carroll, K. S. (2011). Isotope-coded chemical reporter and acid-cleavable affinity reagents for monitoring protein sulfenic acids. *Bioorg Med Chem Lett*, *21*(17), 5015–20.
131. Seo, Y. H. & Carroll, K. S. (2009a). Profiling protein thiol oxidation in tumor cells using sulfenic acid-specific antibodies. *Proc Natl Acad Sci U S A*, *106*(38), 16163–8.
132. Maller, C., Schroder, E., & Eaton, P. (2011). Glyceraldehyde 3-phosphate dehydrogenase is unlikely to mediate hydrogen peroxide signaling: studies with a novel anti-dimedone sulfenic acid antibody. *Antioxid Redox Signal*, *14*(1), 49–60.
133. Benitez, L. V. & Allison, W. S. (1974). The inactivation of the acyl phosphatase activity catalyzed by the sulfenic acid form of glyceraldehyde 3-phosphate dehydrogenase by dimedone and olefins. *J Biol Chem*, *249*(19), 6234–43.
134. Saxon, E. & Bertozzi, C. R. (2000). Cell surface engineering by a modified Staudinger reaction. *Science*, *287*(5460), 2007–10.
135. Rostovtsev, V. V., Green, L. G., Fokin, V. V., & Sharpless, K. B. (2002). A step-wise Huisgen cycloaddition process: copper(i)-catalyzed regioselective "ligation" of azides and terminal alkynes. *Angew Chem Int Ed Engl*, *41*(14), 2596–9.
136. Singh, J., Petter, R. C., & Kluge, A. F. (2010). Targeted covalent drugs of the kinase family. *Curr Opin Chem Biol*, *14*(4), 475–80.
137. Singh, J., Petter, R. C., Baillie, T. A., & Whitty, A. (2011). The resurgence of covalent drugs. *Nat Rev Drug Discov*, *10*(4), 307–17.
138. Ferrara, N., Gerber, H. P., & LeCouter, J. (2003). The biology of vegf and its receptors. *Nat Med*, *9*(6), 669–76.
139. Olsson, A. K., Dimberg, A., Kreuger, J., & Claesson-Welsh, L. (2006). Vegf receptor signalling - in control of vascular function. *Nat Rev Mol Cell Biol*, *7*(5), 359–71.

140. Ushio-Fukai, M. (2007). Vegf signaling through nadph oxidase-derived ros. *Antioxid Redox Signal*, *9*(6), 731–9.
141. Chua, C. C., Hamdy, R. C., & Chua, B. H. (1998). Upregulation of vascular endothelial growth factor by h₂O₂ in rat heart endothelial cells. *Free Radic Biol Med*, *25*(8), 891–7.
142. Kuroki, M., Voest, E. E., Amano, S., Beerepoot, L. V., Takashima, S., Tolentino, M., . . . Adamis, A. P. (1996). Reactive oxygen intermediates increase vascular endothelial growth factor expression in vitro and in vivo. *J Clin Invest*, *98*(7), 1667–75.
143. Gonzalez-Pacheco, F. R., Deudero, J. J., Castellanos, M. C., Castilla, M. A., Alvarez-Arroyo, M. V., Yague, S., & Caramelo, C. (2006). Mechanisms of endothelial response to oxidative aggression: protective role of autologous vegf and induction of vegfr2 by h₂O₂. *Am J Physiol Heart Circ Physiol*, *291*(3), H1395–401.
144. Colavitti, R., Pani, G., Bedogni, B., Anzevino, R., Borrello, S., Waltenberger, J., & Galeotti, T. (2002). Reactive oxygen species as downstream mediators of angiogenic signaling by vascular endothelial growth factor receptor-2/kdr. *J Biol Chem*, *277*(5), 3101–8.
145. Nakamura, Y., Patrushev, N., Inomata, H., Mehta, D., Urao, N., Kim, H. W., . . . Ushio-Fukai, M. (2008). Role of protein tyrosine phosphatase 1b in vascular endothelial growth factor signaling and cell-cell adhesions in endothelial cells. *Circ Res*, *102*(10), 1182–91.
146. Grazia Lampugnani, M., Zanetti, A., Corada, M., Takahashi, T., Balconi, G., Breviario, F., . . . Dejana, E. (2003). Contact inhibition of vegf-induced proliferation requires vascular endothelial cadherin, beta-catenin, and the phosphatase dep-1/cd148. *J Cell Biol*, *161*(4), 793–804.
147. Babior, B. M. (2000). The nadph oxidase of endothelial cells. *IUBMB Life*, *50*(4-5), 267–9.
148. Gorlach, A., Brandes, R. P., Nguyen, K., Amidi, M., Dehghani, F., & Busse, R. (2000). A gp91phox containing nadph oxidase selectively expressed in endothelial cells is a major source of oxygen radical generation in the arterial wall. *Circ Res*, *87*(1), 26–32.
149. Abid, M. R., Kachra, Z., Spokes, K. C., & Aird, W. C. (2000). Nadph oxidase activity is required for endothelial cell proliferation and migration. *FEBS Lett*, *486*(3), 252–6.
150. Ushio-Fukai, M., Tang, Y., Fukai, T., Dikalov, S. I., Ma, Y., Fujimoto, M., . . . Alexander, R. W. (2002). Novel role of gp91(phox)-containing nad(p)h oxidase in vascular endothelial growth factor-induced signaling and angiogenesis. *Circ Res*, *91*(12), 1160–7.

151. Ushio-Fukai, M. (2006). Localizing nadph oxidase-derived ros. *Sci STKE*, 2006(349), re8.
152. Labrecque, L., Royal, I., Surprenant, D. S., Patterson, C., Gingras, D., & Bellevue, R. (2003). Regulation of vascular endothelial growth factor receptor-2 activity by caveolin-1 and plasma membrane cholesterol. *Mol Biol Cell*, 14(1), 334–47.
153. Ikeda, S., Ushio-Fukai, M., Zuo, L., Tojo, T., Dikalov, S., Patrushev, N. A., & Alexander, R. W. (2005). Novel role of arf6 in vascular endothelial growth factor-induced signaling and angiogenesis. *Circ Res*, 96(4), 467–75.
154. Arbiser, J. L., Petros, J., Klafter, R., Govindajaran, B., McLaughlin, E. R., Brown, L. F., ... Lambeth, J. D. (2002). Reactive oxygen generated by nox1 triggers the angiogenic switch. *Proc Natl Acad Sci U S A*, 99(2), 715–20.
155. Oshikawa, J., Urao, N., Kim, H. W., Kaplan, N., Razvi, M., McKinney, R., ... Ushio-Fukai, M. (2010). Extracellular sod-derived h2o2 promotes vegf signaling in caveolae/lipid rafts and post-ischemic angiogenesis in mice. *PLoS One*, 5(4), e10189.
156. Yamaoka-Tojo, M., Tojo, T., Kim, H. W., Hilenski, L., Patrushev, N. A., Zhang, L., ... Ushio-Fukai, M. (2006). Iqgap1 mediates ve-cadherin-based cell-cell contacts and vegf signaling at adherence junctions linked to angiogenesis. *Arterioscler Thromb Vasc Biol*, 26(9), 1991–7.
157. Yamaoka-Tojo, M., Ushio-Fukai, M., Hilenski, L., Dikalov, S. I., Chen, Y. E., Tojo, T., ... Alexander, R. W. (2004). Iqgap1, a novel vascular endothelial growth factor receptor binding protein, is involved in reactive oxygen species-dependent endothelial migration and proliferation. *Circ Res*, 95(3), 276–83.
158. Ikeda, S., Yamaoka-Tojo, M., Hilenski, L., Patrushev, N. A., Anwar, G. M., Quinn, M. T., & Ushio-Fukai, M. (2005). Iqgap1 regulates reactive oxygen species-dependent endothelial cell migration through interacting with nox2. *Arterioscler Thromb Vasc Biol*, 25(11), 2295–300.
159. Kaplan, N., Urao, N., Furuta, E., Kim, S. J., Razvi, M., Nakamura, Y., ... Ushio-Fukai, M. (2011). Localized cysteine sulfenic acid formation by vascular endothelial growth factor: role in endothelial cell migration and angiogenesis. *Free Radic Res*, 45(10), 1124–35.
160. Abid, M. R., Spokes, K. C., Shih, S. C., & Aird, W. C. (2007). Nadph oxidase activity selectively modulates vascular endothelial growth factor signaling pathways. *J Biol Chem*, 282(48), 35373–85.
161. Boivin, B., Zhang, S., Arbiser, J. L., Zhang, Z. Y., & Tonks, N. K. (2008). A modified cysteinyl-labeling assay reveals reversible oxidation of protein tyrosine phosphatases in angiomyolipoma cells. *Proc Natl Acad Sci U S A*, 105(29), 9959–64.

162. Kang, D. H., Lee, D. J., Lee, K. W., Park, Y. S., Lee, J. Y., Lee, S. H., . . . Kang, S. W. (2011). Peroxiredoxin ii is an essential antioxidant enzyme that prevents the oxidative inactivation of vegf receptor-2 in vascular endothelial cells. *Mol Cell*, *44*(4), 545–58.
163. Youngren, J. F. (2007). Regulation of insulin receptor function. *Cell Mol Life Sci*, *64*(7-8), 873–91.
164. Kido, Y., Nakae, J., & Accili, D. (2001). Clinical review 125: the insulin receptor and its cellular targets. *J Clin Endocrinol Metab*, *86*(3), 972–9.
165. Avruch, J. (1998). Insulin signal transduction through protein kinase cascades. *Mol Cell Biochem*, *182*(1-2), 31–48.
166. Cross, D. A., Alessi, D. R., Cohen, P., Andjelkovich, M., & Hemmings, B. A. (1995). Inhibition of glycogen synthase kinase-3 by insulin mediated by protein kinase b. *Nature*, *378*(6559), 785–9.
167. Kohn, A. D., Summers, S. A., Birnbaum, M. J., & Roth, R. A. (1996). Expression of a constitutively active akt ser/thr kinase in 3t3-l1 adipocytes stimulates glucose uptake and glucose transporter 4 translocation. *J Biol Chem*, *271*(49), 31372–8.
168. Ueki, K., Yamamoto-Honda, R., Kaburagi, Y., Yamauchi, T., Tobe, K., Burgering, B. M., . . . Kadowaki, T. (1998). Potential role of protein kinase b in insulin-induced glucose transport, glycogen synthesis, and protein synthesis. *J Biol Chem*, *273*(9), 5315–22.
169. May, J. M. & de Haen, C. (1979a). The insulin-like effect of hydrogen peroxide on pathways of lipid synthesis in rat adipocytes. *J Biol Chem*, *254*(18), 9017–21.
170. May, J. M. & de Haen, C. (1979b). Insulin-stimulated intracellular hydrogen peroxide production in rat epididymal fat cells. *J Biol Chem*, *254*(7), 2214–20.
171. Rudich, A., Tirosh, A., Potashnik, R., Hemi, R., Kanety, H., & Bashan, N. (1998). Prolonged oxidative stress impairs insulin-induced glut4 translocation in 3t3-l1 adipocytes. *Diabetes*, *47*(10), 1562–9.
172. Lin, Y., Berg, A. H., Iyengar, P., Lam, T. K., Giacca, A., Combs, T. P., . . . Scherer, P. E. (2005). The hyperglycemia-induced inflammatory response in adipocytes: the role of reactive oxygen species. *J Biol Chem*, *280*(6), 4617–26.
173. Houstis, N., Rosen, E. D., & Lander, E. S. (2006). Reactive oxygen species have a causal role in multiple forms of insulin resistance. *Nature*, *440*(7086), 944–8.
174. Mahadev, K., Zilbering, A., Zhu, L., & Goldstein, B. J. (2001). Insulin-stimulated hydrogen peroxide reversibly inhibits protein-tyrosine phosphatase 1b in vivo and enhances the early insulin action cascade. *J Biol Chem*, *276*(24), 21938–42.

175. Nakashima, N., Sharma, P. M., Imamura, T., Bookstein, R., & Olefsky, J. M. (2000). The tumor suppressor pten negatively regulates insulin signaling in 3t3-l1 adipocytes. *J Biol Chem*, *275*(17), 12889–95.
176. Mahadev, K., Wu, X., Zilbering, A., Zhu, L., Lawrence, J. T., & Goldstein, B. J. (2001). Hydrogen peroxide generated during cellular insulin stimulation is integral to activation of the distal insulin signaling cascade in 3t3-l1 adipocytes. *J Biol Chem*, *276*(52), 48662–9.
177. Krieger-Brauer, H. I., Medda, P. K., & Kather, H. (1997). Insulin-induced activation of nadph-dependent h2o2 generation in human adipocyte plasma membranes is mediated by galphai2. *J Biol Chem*, *272*(15), 10135–43.
178. Mahadev, K., Motoshima, H., Wu, X., Ruddy, J. M., Arnold, R. S., Cheng, G., . . . Goldstein, B. J. (2004). The nad(p)h oxidase homolog nox4 modulates insulin-stimulated generation of h2o2 and plays an integral role in insulin signal transduction. *Mol Cell Biol*, *24*(5), 1844–54.
179. Saltiel, A. R. & Kahn, C. R. (2001). Insulin signalling and the regulation of glucose and lipid metabolism. *Nature*, *414*(6865), 799–806.
180. Elchebly, M., Payette, P., Michaliszyn, E., Cromlish, W., Collins, S., Loy, A. L., . . . Kennedy, B. P. (1999). Increased insulin sensitivity and obesity resistance in mice lacking the protein tyrosine phosphatase-1b gene. *Science*, *283*(5407), 1544–8.
181. Klamman, L. D., Boss, O., Peroni, O. D., Kim, J. K., Martino, J. L., Zabolotny, J. M., . . . Kahn, B. B. (2000). Increased energy expenditure, decreased adiposity, and tissue-specific insulin sensitivity in protein-tyrosine phosphatase 1b-deficient mice. *Mol Cell Biol*, *20*(15), 5479–89.
182. Haque, A., Andersen, J. N., Salmeen, A., Barford, D., & Tonks, N. K. (2011). Conformation-sensing antibodies stabilize the oxidized form of ptp1b and inhibit its phosphatase activity. *Cell*, *147*(1), 185–98.
183. Leonard, S. E., Garcia, F. J., Goodsell, D. S., & Carroll, K. S. (2011a). Redox-based probes for protein tyrosine phosphatases. *Angew Chem Int Ed Engl*, *50*(19), 4423–7.
184. Mukherjee, S. P., Lane, R. H., & Lynn, W. S. (1978). Endogenous hydrogen peroxide and peroxidative metabolism in adipocytes in response to insulin and sulfhydryl reagents. *Biochem Pharmacol*, *27*(22), 2589–94.
185. Wilden, P. A. & Pessin, J. E. (1987). Differential sensitivity of the insulin-receptor kinase to thiol and oxidizing agents in the absence and presence of insulin. *Biochem J*, *245*(2), 325–31.

186. Schmid, E., El Benna, J., Galter, D., Klein, G., & Droge, W. (1998). Redox priming of the insulin receptor beta-chain associated with altered tyrosine kinase activity and insulin responsiveness in the absence of tyrosine autophosphorylation. *FASEB J*, *12*(10), 863–70.
187. Schmitt, T. L., Hotz-Wagenblatt, A., Klein, H., & Droge, W. (2005). Interdependent regulation of insulin receptor kinase activity by adp and hydrogen peroxide. *J Biol Chem*, *280*(5), 3795–801.
188. Stockler-Ipsiroglu, S. (1997). Creatine deficiency syndromes: a new perspective on metabolic disorders and a diagnostic challenge. *J Pediatr*, *131*(4), 510–1.
189. Turner, N. & Grose, R. (2010). Fibroblast growth factor signalling: from development to cancer. *Nat Rev Cancer*, *10*(2), 116–29.
190. Lo, Y. Y. & Cruz, T. F. (1995). Involvement of reactive oxygen species in cytokine and growth factor induction of c-fos expression in chondrocytes. *J Biol Chem*, *270*(20), 11727–30.
191. Devary, Y., Gottlieb, R. A., Lau, L. F., & Karin, M. (1991). Rapid and preferential activation of the c-jun gene during the mammalian uv response. *Mol Cell Biol*, *11*(5), 2804–11.
192. Nose, K., Shibamura, M., Kikuchi, K., Kageyama, H., Sakiyama, S., & Kuroki, T. (1991). Transcriptional activation of early-response genes by hydrogen peroxide in a mouse osteoblastic cell line. *Eur J Biochem*, *201*(1), 99–106.
193. Thannickal, V. J., Day, R. M., Klinz, S. G., Bastien, M. C., Larios, J. M., & Fanburg, B. L. (2000). Ras-dependent and -independent regulation of reactive oxygen species by mitogenic growth factors and tgf-beta1. *FASEB J*, *14*(12), 1741–8.
194. Kemble, D. J. & Sun, G. (2009). Direct and specific inactivation of protein tyrosine kinases in the src and fgfr families by reversible cysteine oxidation. *Proc Natl Acad Sci U S A*, *106*(13), 5070–5.
195. Taylor, S. S., Knighton, D. R., Zheng, J., Ten Eyck, L. F., & Sowadski, J. M. (1992). Structural framework for the protein kinase family. *Annu Rev Cell Biol*, *8*, 429–62.
196. Kageyama, K., Ihara, Y., Goto, S., Urata, Y., Toda, G., Yano, K., & Kondo, T. (2002). Overexpression of calreticulin modulates protein kinase b/akt signaling to promote apoptosis during cardiac differentiation of cardiomyoblast h9c2 cells. *J Biol Chem*, *277*(22), 19255–64.

197. Seo, J. H., Ahn, Y., Lee, S. R., Yeol Yeo, C., & Chung Hur, K. (2005). The major target of the endogenously generated reactive oxygen species in response to insulin stimulation is phosphatase and tensin homolog and not phosphoinositide-3 kinase (pi-3 kinase) in the pi-3 kinase/akt pathway. *Mol Biol Cell*, *16*(1), 348–57.
198. Gonzalez, E. & McGraw, T. E. (2009a). The akt kinases: isoform specificity in metabolism and cancer. *Cell Cycle*, *8*(16), 2502–8.
199. Chan, T. O., Rittenhouse, S. E., & Tsichlis, P. N. (1999). Akt/pkb and other d3 phosphoinositide-regulated kinases: kinase activation by phosphoinositide-dependent phosphorylation. *Annu Rev Biochem*, *68*, 965–1014.
200. Gonzalez, E. & McGraw, T. E. (2009b). Insulin-modulated akt subcellular localization determines akt isoform-specific signaling. *Proc Natl Acad Sci U S A*, *106*(17), 7004–9.
201. Cho, H., Mu, J., Kim, J. K., Thorvaldsen, J. L., Chu, Q., Crenshaw, 3., E. B., . . . Birnbaum, M. J. (2001). Insulin resistance and a diabetes mellitus-like syndrome in mice lacking the protein kinase akt2 (pkb beta). *Science*, *292*(5522), 1728–31.
202. Cho, H., Thorvaldsen, J. L., Chu, Q., Feng, F., & Birnbaum, M. J. (2001). Akt1/pkbalph is required for normal growth but dispensable for maintenance of glucose homeostasis in mice. *J Biol Chem*, *276*(42), 38349–52.
203. Chen, K., Vita, J. A., Berk, B. C., & Keaney, J., J. F. (2001b). C-jun n-terminal kinase activation by hydrogen peroxide in endothelial cells involves src-dependent epidermal growth factor receptor transactivation. *J Biol Chem*, *276*(19), 16045–50.
204. Engelman, J. A., Luo, J., & Cantley, L. C. (2006). The evolution of phosphatidylinositol 3-kinases as regulators of growth and metabolism. *Nat Rev Genet*, *7*(8), 606–19.
205. Ushio-Fukai, M., Alexander, R. W., Akers, M., Yin, Q., Fujio, Y., Walsh, K., & Griendling, K. K. (1999). Reactive oxygen species mediate the activation of akt/protein kinase b by angiotensin ii in vascular smooth muscle cells. *J Biol Chem*, *274*(32), 22699–704.
206. Shaw, M., Cohen, P., & Alessi, D. R. (1998). The activation of protein kinase b by h2o2 or heat shock is mediated by phosphoinositide 3-kinase and not by mitogen-activated protein kinase-activated protein kinase-2. *Biochem J*, *336* (Pt 1), 241–6.
207. Van der Kaay, J., Beck, M., Gray, A., & Downes, C. P. (1999). Distinct phosphatidylinositol 3-kinase lipid products accumulate upon oxidative and osmotic stress and lead to different cellular responses. *J Biol Chem*, *274*(50), 35963–8.

208. Esposito, F., Chirico, G., Montesano Gesualdi, N., Posadas, I., Ammendola, R., Russo, T., . . . Cimino, F. (2003). Protein kinase b activation by reactive oxygen species is independent of tyrosine kinase receptor phosphorylation and requires src activity. *J Biol Chem*, *278*(23), 20828–34.
209. Lu, Y., Yu, Q., Liu, J. H., Zhang, J., Wang, H., Koul, D., . . . Mills, G. B. (2003). Src family protein-tyrosine kinases alter the function of pten to regulate phosphatidylinositol 3-kinase/akt cascades. *J Biol Chem*, *278*(41), 40057–66.
210. Wang, X., McCullough, K. D., Franke, T. F., & Holbrook, N. J. (2000). Epidermal growth factor receptor-dependent akt activation by oxidative stress enhances cell survival. *J Biol Chem*, *275*(19), 14624–31.
211. Guyton, K. Z., Liu, Y., Gorospe, M., Xu, Q., & Holbrook, N. J. (1996). Activation of mitogen-activated protein kinase by h2o2. role in cell survival following oxidant injury. *J Biol Chem*, *271*(8), 4138–42.
212. Carvalho-Filho, M. A., Ueno, M., Hirabara, S. M., Seabra, A. B., Carnevali, J. B., de Oliveira, M. G., . . . Saad, M. J. (2005). S-nitrosation of the insulin receptor, insulin receptor substrate 1, and protein kinase b/akt: a novel mechanism of insulin resistance. *Diabetes*, *54*(4), 959–67.
213. Yasukawa, T., Tokunaga, E., Ota, H., Sugita, H., Martyn, J. A., & Kaneki, M. (2005). S-nitrosylation-dependent inactivation of akt/protein kinase b in insulin resistance. *J Biol Chem*, *280*(9), 7511–8.
214. Yellaturu, C. R., Bhanoori, M., Neeli, I., & Rao, G. N. (2002). N-ethylmaleimide inhibits platelet-derived growth factor bb-stimulated akt phosphorylation via activation of protein phosphatase 2a. *J Biol Chem*, *277*(42), 40148–55.
215. Huang, X., Begley, M., Morgenstern, K. A., Gu, Y., Rose, P., Zhao, H., & Zhu, X. (2003). Crystal structure of an inactive akt2 kinase domain. *Structure*, *11*(1), 21–30.
216. Murata, H., Ihara, Y., Nakamura, H., Yodoi, J., Sumikawa, K., & Kondo, T. (2003). Glutaredoxin exerts an antiapoptotic effect by regulating the redox state of akt. *J Biol Chem*, *278*(50), 50226–33.
217. Wani, R., Qian, J., Yin, L., Bechtold, E., King, S. B., Poole, L. B., . . . Furdui, C. M. (2011). Isoform-specific regulation of akt by pdgf-induced reactive oxygen species. *Proc Natl Acad Sci U S A*, *108*(26), 10550–5.
218. Chen, Q., Olashaw, N., & Wu, J. (1995). Participation of reactive oxygen species in the lysophosphatidic acid-stimulated mitogen-activated protein kinase kinase activation pathway. *J Biol Chem*, *270*(48), 28499–502.
219. Lo, Y. Y., Wong, J. M., & Cruz, T. F. (1996). Reactive oxygen species mediate cytokine activation of c-jun nh2-terminal kinases. *J Biol Chem*, *271*(26), 15703–7.

220. Kamata, H. [H.], Honda, S., Maeda, S., Chang, L., Hirata, H., & Karin, M. (2005). Reactive oxygen species promote tnfalpha-induced death and sustained jnk activation by inhibiting map kinase phosphatases. *Cell*, *120*(5), 649–61.
221. Ushio-Fukai, M., Alexander, R. W., Akers, M., & Griendling, K. K. (1998). P38 mitogen-activated protein kinase is a critical component of the redox-sensitive signaling pathways activated by angiotensin ii. role in vascular smooth muscle cell hypertrophy. *J Biol Chem*, *273*(24), 15022–9.
222. Roberts, P. J. & Der, C. J. (2007). Targeting the raf-mek-erk mitogen-activated protein kinase cascade for the treatment of cancer. *Oncogene*, *26*(22), 3291–310.
223. Wagner, E. F. & Nebreda, A. R. (2009). Signal integration by jnk and p38 mapk pathways in cancer development. *Nat Rev Cancer*, *9*(8), 537–49.
224. Wang, X., Martindale, J. L., Liu, Y., & Holbrook, N. J. (1998). The cellular response to oxidative stress: influences of mitogen-activated protein kinase signalling pathways on cell survival. *Biochem J*, *333* (Pt 2), 291–300.
225. Lander, H. M., Milbank, A. J., Tauras, J. M., Hajjar, D. P., Hempstead, B. L., Schwartz, G. D., . . . Quilliam, L. A. (1996). Redox regulation of cell signalling. *Nature*, *381*(6581), 380–1.
226. Yoshizumi, M., Abe, J., Haendeler, J., Huang, Q., & Berk, B. C. (2000). Src and cas mediate jnk activation but not erk1/2 and p38 kinases by reactive oxygen species. *J Biol Chem*, *275*(16), 11706–12.
227. Dolfi, F., Garcia-Guzman, M., Ojaniemi, M., Nakamura, H., Matsuda, M., & Vuori, K. (1998). The adaptor protein crk connects multiple cellular stimuli to the jnk signaling pathway. *Proc Natl Acad Sci U S A*, *95*(26), 15394–9.
228. Veal, E. A., Findlay, V. J., Day, A. M., Bozonet, S. M., Evans, J. M., Quinn, J., & Morgan, B. A. (2004). A 2-cys peroxiredoxin regulates peroxide-induced oxidation and activation of a stress-activated map kinase. *Mol Cell*, *15*(1), 129–39.
229. Park, H. S., Huh, S. H., Kim, M. S., Lee, S. H., & Choi, E. J. (2000). Nitric oxide negatively regulates c-jun n-terminal kinase/stress-activated protein kinase by means of s-nitrosylation. *Proc Natl Acad Sci U S A*, *97*(26), 14382–7.
230. Ichijo, H., Nishida, E., Irie, K., ten Dijke, P., Saitoh, M., Moriguchi, T., . . . Gotoh, Y. (1997). Induction of apoptosis by ask1, a mammalian mapkkk that activates sapk/jnk and p38 signaling pathways. *Science*, *275*(5296), 90–4.
231. Saitoh, M., Nishitoh, H., Fujii, M., Takeda, K., Tobiume, K., Sawada, Y., . . . Ichijo, H. (1998). Mammalian thioredoxin is a direct inhibitor of apoptosis signal-regulating kinase (ask) 1. *EMBO J*, *17*(9), 2596–606.

232. Liu, H., Nishitoh, H., Ichijo, H., & Kyriakis, J. M. (2000). Activation of apoptosis signal-regulating kinase 1 (ask1) by tumor necrosis factor receptor-associated factor 2 requires prior dissociation of the ask1 inhibitor thioredoxin. *Mol Cell Biol*, *20*(6), 2198–208.
233. Nadeau, P. J., Charette, S. J., Toledano, M. B., & Landry, J. (2007). Disulfide bond-mediated multimerization of ask1 and its reduction by thioredoxin-1 regulate h(2)o(2)-induced c-jun nh(2)-terminal kinase activation and apoptosis. *Mol Biol Cell*, *18*(10), 3903–13.
234. Nadeau, P. J., Charette, S. J., & Landry, J. (2009). Redox reaction at ask1-cys250 is essential for activation of jnk and induction of apoptosis. *Mol Biol Cell*, *20*(16), 3628–37.
235. Park, H. S., Yu, J. W., Cho, J. H., Kim, M. S., Huh, S. H., Ryoo, K., & Choi, E. J. (2004). Inhibition of apoptosis signal-regulating kinase 1 by nitric oxide through a thiol redox mechanism. *J Biol Chem*, *279*(9), 7584–90.
236. Cross, J. V. & Templeton, D. J. (2004). Oxidative stress inhibits mekk1 by site-specific glutathionylation in the atp-binding domain. *Biochem J*, *381*(Pt 3), 675–83.
237. Diao, Y., Liu, W., Wong, C. C., Wang, X., Lee, K., Cheung, P. Y., . . . Wu, Z. (2010). Oxidation-induced intramolecular disulfide bond inactivates mitogen-activated protein kinase kinase 6 by inhibiting atp binding. *Proc Natl Acad Sci U S A*, *107*(49), 20974–9.
238. Templeton, D. J., Aye, M. S., Rady, J., Xu, F., & Cross, J. V. (2010). Purification of reversibly oxidized proteins (prop) reveals a redox switch controlling p38 map kinase activity. *PLoS One*, *5*(11), e15012.
239. Thomas, S. M. & Brugge, J. S. (1997). Cellular functions regulated by src family kinases. *Annu Rev Cell Dev Biol*, *13*, 513–609.
240. Ma, Y. C. & Huang, X. Y. (2002). Novel regulation and function of src tyrosine kinase. *Cell Mol Life Sci*, *59*(3), 456–62.
241. Yeatman, T. J. (2004). A renaissance for src. *Nat Rev Cancer*, *4*(6), 470–80.
242. Xu, W., Harrison, S. C., & Eck, M. J. (1997). Three-dimensional structure of the tyrosine kinase c-src. *Nature*, *385*(6617), 595–602.
243. Giannoni, E. [E.], Taddei, M. L., & Chiarugi, P. (2010). Src redox regulation: again in the front line. *Free Radic Biol Med*, *49*(4), 516–27.
244. Li, Q., Zhang, Y., Marden, J. J., Banfi, B., & Engelhardt, J. F. (2008). Endosomal nadph oxidase regulates c-src activation following hypoxia/reoxygenation injury. *Biochem J*, *411*(3), 531–41.

245. Krasnowska, E. K., Pittaluga, E., Brunati, A. M., Brunelli, R., Costa, G., De Spirito, M., . . . Parasassi, T. (2008). N-acetyl-l-cysteine fosters inactivation and transfer to endolysosomes of c-src. *Free Radic Biol Med*, *45*(11), 1566–72.
246. Cunnick, J. M., Dorsey, J. F., Standley, T., Turkson, J., Kraker, A. J., Fry, D. W., . . . Wu, J. (1998). Role of tyrosine kinase activity of epidermal growth factor receptor in the lysophosphatidic acid-stimulated mitogen-activated protein kinase pathway. *J Biol Chem*, *273*(23), 14468–14475.
247. Tang, H., Hao, Q., Rutherford, S. A., Low, B., & Zhao, Z. J. (2005). Inactivation of src family tyrosine kinases by reactive oxygen species in vivo. *J Biol Chem*, *280*(25), 23918–23925.
248. Sun, G. & Kemble, D. J. (2009). To c or not to c: direct and indirect redox regulation of src protein tyrosine kinase. *Cell Cycle*, *8*(15), 2353–5.
249. Gianni, D., Bohl, B., Courtneidge, S. A., & Bokoch, G. M. (2008). The involvement of the tyrosine kinase c-src in the regulation of reactive oxygen species generation mediated by nadph oxidase-1. *Mol Biol Cell*, *19*(7), 2984–94.
250. Mehdi, M. Z., Pandey, N. R., Pandey, S. K., & Srivastava, A. K. (2005). H₂O₂-induced phosphorylation of erk1/2 and pkb requires tyrosine kinase activity of insulin receptor and c-src. *Antioxid Redox Signal*, *7*(7-8), 1014–20.
251. Abe, J., Takahashi, M., Ishida, M., Lee, J. D., & Berk, B. C. (1997). C-src is required for oxidative stress-mediated activation of big mitogen-activated protein kinase 1. *J Biol Chem*, *272*(33), 20389–94.
252. Sondhi, D., Xu, W., Songyang, Z., Eck, M. J., & Cole, P. A. (1998). Peptide and protein phosphorylation by protein tyrosine kinase csk: insights into specificity and mechanism. *Biochemistry*, *37*(1), 165–72.
253. Mills, J. E., Whitford, P. C., Shaffer, J., Onuchic, J. N., Adams, J. A., & Jennings, P. A. (2007). A novel disulfide bond in the sh2 domain of the c-terminal src kinase controls catalytic activity. *J Mol Biol*, *365*(5), 1460–8.
254. Levinson, N. M., Seeliger, M. A., Cole, P. A., & Kuriyan, J. (2008). Structural basis for the recognition of c-src by its inactivator csk. *Cell*, *134*(1), 124–34.
255. Akhand, A. A., Pu, M., Senga, T., Kato, M., Suzuki, H., Miyata, T., . . . Nakashima, I. (1999). Nitric oxide controls src kinase activity through a sulfhydryl group modification-mediated tyr-527-independent and tyr-416-linked mechanism. *J Biol Chem*, *274*(36), 25821–6.
256. Rahman, M. A., Senga, T., Ito, S., Hyodo, T., Hasegawa, H., & Hamaguchi, M. (2010). S-nitrosylation at cysteine 498 of c-src tyrosine kinase regulates nitric oxide-mediated cell invasion. *J Biol Chem*, *285*(6), 3806–14.

257. Giannoni, E. [Elisa], Buricchi, F., Raugei, G., Ramponi, G., & Chiarugi, P. (2005). Intracellular reactive oxygen species activate src tyrosine kinase during cell adhesion and anchorage-dependent cell growth. *Mol Cell Biol*, *25*(15), 6391–6403.
258. Yoo, S. K., Starnes, T. W., Deng, Q., & Huttenlocher, A. (2011). Lyn is a redox sensor that mediates leukocyte wound attraction in vivo. *Nature*, *480*(7375), 109–12.
259. Pantano, C., Reynaert, N. L., van der Vliet, A., & Janssen-Heininger, Y. M. (2006). Redox-sensitive kinases of the nuclear factor-kappa b signaling pathway. *Antioxid Redox Signal*, *8*(9-10), 1791–806.
260. Reynaert, N. L., Ckless, K., Korn, S. H., Vos, N., Guala, A. S., Wouters, E. F., . . . Janssen-Heininger, Y. M. (2004). Nitric oxide represses inhibitory kappa b kinase through s-nitrosylation. *Proc Natl Acad Sci U S A*, *101*(24), 8945–50.
261. Kapahi, P., Takahashi, T., Natoli, G., Adams, S. R., Chen, Y., Tsien, R. Y., & Karin, M. (2000). Inhibition of nf-kappa b activation by arsenite through reaction with a critical cysteine in the activation loop of ikappa b kinase. *J Biol Chem*, *275*(46), 36062–6.
262. Korn, S. H., Wouters, E. F., Vos, N., & Janssen-Heininger, Y. M. (2001). Cytokine-induced activation of nuclear factor-kappa b is inhibited by hydrogen peroxide through oxidative inactivation of ikappa b kinase. *J Biol Chem*, *276*(38), 35693–700.
263. Reynaert, N. L., van der Vliet, A., Guala, A. S., McGovern, T., Hristova, M., Pantano, C., . . . Janssen-Heininger, Y. M. (2006). Dynamic redox control of nf-kappa b through glutaredoxin-regulated s-glutathionylation of inhibitory kappa b kinase beta. *Proc Natl Acad Sci U S A*, *103*(35), 13086–91.
264. Jaspers, I., Zhang, W., Fraser, A., Samet, J. M., & Reed, W. (2001). Hydrogen peroxide has opposing effects on ikk activity and ikappabalpha breakdown in airway epithelial cells. *Am J Respir Cell Mol Biol*, *24*(6), 769–77.
265. Kamata, H. [Hideaki], Manabe, T., Oka, S. i., Kamata, K., & Hirata, H. (2002, May). Hydrogen peroxide activates ikappa b kinases through phosphorylation of serine residues in the activation loops. *FEBS Lett*, *519*(1-3), 231–237.
266. Leonberg, A. K. & Chai, Y. C. (2007). The functional role of cysteine residues for c-abl kinase activity. *Mol Cell Biochem*, *304*(1-2), 207–12.
267. Guo, Z., Kozlov, S., Lavin, M. F., Person, M. D., & Paull, T. T. (2010). Atm activation by oxidative stress. *Science*, *330*(6003), 517–21.
268. Guo, Z., Deshpande, R., & Paull, T. T. (2010). Atm activation in the presence of oxidative stress. *Cell Cycle*, *9*(24), 4805–11.

269. Anastasiou, D., Poulgiannis, G., Asara, J. M., Boxer, M. B., Jiang, J. K., Shen, M., . . . Cantley, L. C. (2011). Inhibition of pyruvate kinase m2 by reactive oxygen species contributes to cellular antioxidant responses. *Science*, *334*(6060), 1278–83.
270. Penel, S., Hughes, E., & Doig, A. J. (1999). Side-chain structures in the first turn of the alpha-helix. *J Mol Biol*, *287*(1), 127–43.
271. Anderson, T. A. & Sauer, R. T. (2003). Role of an n(cap) residue in determining the stability and operator-binding affinity of arc repressor. *Biophys Chem*, *100*(1-3), 341–50.
272. Zhang, T., Inesta-Vaquera, F., Niepel, M., Zhang, J., Ficarro, S. B., Machleidt, T., . . . Gray, N. S. (2012). Discovery of potent and selective covalent inhibitors of jnk. *Chem Biol*, *19*(1), 140–54.
273. Kwarcinski, F. E., Fox, C. C., Steffey, M. E., & Soellner, M. B. (2012). Irreversible inhibitors of c-src kinase that target a nonconserved cysteine. *ACS Chem Biol*.
274. Singh, J., Dobrusin, E. M., Fry, D. W., Haske, T., Whitty, A., & McNamara, D. J. (1997). Structure-based design of a potent, selective, and irreversible inhibitor of the catalytic domain of the erbb receptor subfamily of protein tyrosine kinases. *J Med Chem*, *40*(7), 1130–5.
275. Liu, Q., Sabnis, Y., Zhao, Z., Zhang, T., Buhrlage, S. J., Jones, L. H., & Gray, N. S. (2013). Developing irreversible inhibitors of the protein kinase cysteinome. *Chem Biol*, *20*(2), 146–59.
276. Seo, Y. H. & Carroll, K. S. (2009b). Facile synthesis and biological evaluation of a cell-permeable probe to detect redox-regulated proteins. *Bioorg Med Chem Lett*, *19*(2), 356–9.
277. Leonard, S. E., Garcia, F. J., Goodsell, D. S., & Carroll, K. S. (2011b). Redox-based probes (rbps) for protein tyrosine phosphatases. *Angew Chem Int Ed Engl*, *in press*.